AFM Minerals in the Halifax Pluton

by

Yi Ding

Submitted in partial fulfilment of the requirements
for the degree of Master of Science

at

Dalhousie University
Halifax, Nova Scotia
January, 1995

DALHOUSIE UNIVERSITY
DEPARTMENT OF EARTH SCIENCES

The undersigned hereby certify that they have read and recommend to the Faculty of Graduate Studies for acceptance a thesis entitled "AFM Minerals in the Halifax Pluton" by Yi Ding in partial fulfilment of the requirements for the degree of Master of Science.

Dated January 6, 1995

External Examiner: R.P. Raeside

Reader: P.T. Robinson

Supervisory Committee: M.A. MacDonald

Chairman: P.J.C. Ryall

Supervisor: D.B. Clarke

DALHOUSIE UNIVERSITY

DATE: Jan. 6

AUTHOR: Yi Ding

TITLE: AFM Minerals in the Halifax Pluton

DEPARTMENT OR SCHOOL: Earth Sciences

DEGREE: M. Sc. CONVOCATION: May YEAR: 1995

Permission is herewith granted to Dalhousie University to circulate and to have copied for non-commercial purposes, at its discretion, the above title upon the request of individuals or institutions.

To Zhaonai Li
who led me to igneous petrology and
To Barrie Clarke
who introduced me to Canada
and studies on peraluminous granitoid rocks

Contents

LIST OF FIGURES

LIST OF FIGURES (CONTINUED)

LIST OF TABLES

Abstract

The Halifax Pluton is part of the South Mountain Batholith. It consists of six lithologies with various assemblages of AFM minerals: biotite granodiorite and biotite monzogranite contain biotite, and traces of muscovite and cordierite; coarse - grained leucomonzogranite and biotite ± cordierite monzogranite contain biotite, muscovite, cordierite, and garnet; fine - grained leucomonzogranite contains biotite, muscovite, cordierite, garnet, and andalusite; and aplite contains biotite, muscovite, cordierite, and garnet.

All phases of the Halifax Pluton contain magmatic biotite the compositions of which are close to those of biotites from metasedimentary rocks. Magmatic muscovite exists in the Halifax Pluton providing evidence for a magma rich in H_2O and with a high A/CNK to achieve the low solidus temperature for muscovite. Magmatic cordierite is characterised by its euhedral shape, low M/(F+M) (<0.5), Na_2O>1%, and rims rich in the ratio M/(F+M). Both magmatic and metamorphic garnets exist in the Halifax Pluton. Magmatic garnet is euhedral or subhedral, shows reverse zoning, and has no inclusions or reaction rims. Skeletal garnet grains in an aplite provide an "instant picture" of garnet growth. Fine - grained leucomonzogranite contains two types of magmatic andalusite: one mantled by muscovite, and the other as inclusions in K-feldspar.

Variations in transition elements (Fe, Mn, Ti) and Mg form chemical zoning in the biotite, muscovite, cordierite, garnet, and andalusite from the Halifax Pluton. These chemical substitutions are sensitive to changes in environments: temperature, pressure, concentration in melt, oxygen fugacity, and water pressure.

In the AFM diagrams, different slopes or positions of tie-lines joining pairs of AFM minerals may indicate different magmatic environments (T, P, X). The theoretical topologies in P-T space show the order of crystallization of the AFM minerals. Biotite or cordierite was always the first crystallizing mineral. The intersection of the muscovite breakdown curve with the granite solidus determines the minimum pressure (3 - 4.4 kb) for emplacement of the Halifax Pluton.

Abbreviations and Symbols

A	mol (Al_2O_3-CaO-Na_2O-K_2O)
Ab	albite
A/CNK	mol Al_2O_3 /(CaO + Na_2O + K_2O)
An	anorthite
And	andalusite
Ap	apatite
Bt	biotite
Crd	cordierite
F	mol FeO
fO_2	fugacity of oxygen
Grt	garnet
HP	Halifax Pluton
Kfs	Alkali feldspar
L	liquid
M	mol MgO
M/(F+M)	mol MgO/(FeO + MgO)
MB	Musquodoboit Batholith
Ms	muscovite
Or	orthoclase
P	pressure (kbar)
Pl	Plagioclase
Qtz	quartz
SMB	South Mountain Batholith
T	temperature (°C)
Tur	tourmaline
X	composition

Note: mineral abbreviations (Kretz, 1983)

Acknowledgements

I am very grateful to my supervisor, Dr. D. B. Clarke, for his support, help, advice, and suggestions regarding this thesis, and for having helped me and my family to become familiarized with Canada.

I am thankful to Mr. M. A. MacDonald, of my committee, for his critical reading and for having generously supplied me with samples, data, and information in the Halifax Pluton, and for having guided me in the field during the collection of samples that were critical for this thesis. I am also thankful to Dr. R. A. Jamieson, of my committee, for critical reading and for her generous supply of some samples.

I would like to thank my friend, Georges Merinfelds, for his help with various matters. Mr.R.M. MacKay provided expert assistance with the electron microprobe analyses at Dalhousie University. I also thank the staff of the Department of the Earth Sciences for various support. I gratefully acknowledge the support of a Dalhousie University Graduate scholarship from 9.1991 to 8.1993, and of additional support from a NSERC grant to Dr. D. B. Clarke from 9.1993 to 12.1993.

I wish to thank heartily the members of my family here and in China for their moral and financial support.

Chapter 1 Introduction

1.1 Objectives

The South Mountain Batholith (SMB) is a large, peraluminous granitoid intrusion underlying 7300 km^2 in southwestern Nova Scotia. It consists of 13 discrete plutons (MacDonald et al., 1992), of which the Halifax Pluton (HP) forms the eastern end. The SMB and HP contain many minerals characteristic of peraluminous granites (Clarke, 1981; MacDonald & Horne, 1988). Most of these minerals can also be classified as AFM minerals because they can be projected onto the AFM (molecular $(Al_2O_3-3*K_2O)$, FeO, and MgO) diagram (Thompson, 1957).

This study has three objectives:

(1) *to describe occurrences of AFM minerals* in the HP using petrographic, binocular microscopy, Nomarski interference contrast, and backscattered images;

(2) *to detect and quantitatively analyze zoning* and its possible microtopographic features in AFM minerals; and

(3) *to interpret the origins of AFM minerals,* including their zoning, and to synthesize the data into a petrogenetic framework.

1.2 Literature review

1.2.1 *AFM minerals*

A granitic rock is peraluminous if the molar ratio of Al_2O_3 to the sum of CaO, Na_2O and K_2O exceeds unity, i.e., $Al_2O_3/(CaO +$

$Na_2O + K_2O) > 1$. Shand (1927) first proposed this ratio, and many authors adopted it as an important coefficient related to the mineralogy, and possibly to the origin, of peraluminous granites (Barker, 1961; Chappell & White, 1974; Clarke, 1981; Speer, 1984; Zen, 1988). Peraluminous granitic rocks must contain at least one of the characteristic minerals: biotite, muscovite, cordierite, garnet, or the aluminum silicate minerals (Clarke, 1981). The characteristic minerals listed above may be primary igneous phases, but they can also originate from assimilated country rocks, or a restite phase, or can be of hydrothermal origin (Clarke, 1981).

Thompson (1957) simplified the AFMK (molecular Al_2O_3, FeO, MgO, and K_2O) tetrahedral diagram (Fig.1.1a) by projecting all its compositional points, lines, areas, and volumes onto the AFM face (Fig. 1.1b) with muscovite as the projection point. In this AFM diagram, tie lines connect coexisting phases. Abbott & Clarke (1979) presented a number of hypothetical liquidus paths for peraluminous melts, and Clarke (1981) summarized AFM projection for the occurrence of magmatic AFM minerals in peraluminous granites and gave some cotectic paths. Maillet & Clarke (1985) plotted cordierite-biotite pairs from the SMB and surrounding contact metamorphic aureole and found that the orientations of tie lines for mineral pairs from the metamorphic aureole are different from those from granitoid rocks.

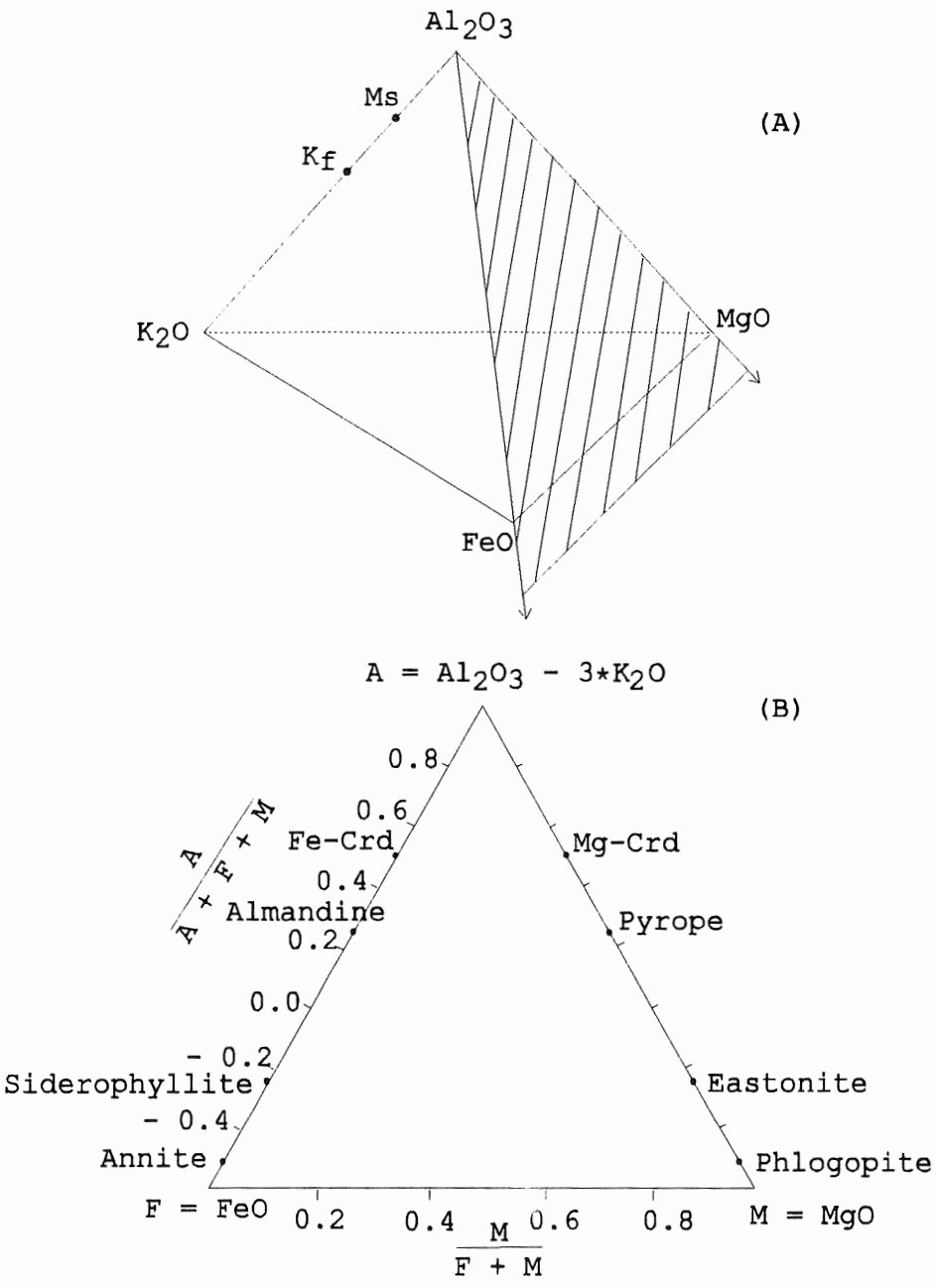

Figure 1.1 Thompson AFM projection. (A) Complete AFMK tetrahedron showing the AFM projection face extended (shaded), and ideal K-feldspar and muscovite projection. (B) AFM projection from muscovite showing projection of composition of aluminous silicates occurring in peraluminous granites (Clarke, 1981).

1.2.2 *General Introduction to Zoning*

Definition of Zoning

In this study, the term zoning refers to spatial differences of composition (systematic variation) in a single AFM crystal phase that can be detected by either general optical techniques or advanced techniques such as backscattered electron imaging and microprobe analysis. The zoning of a magmatic mineral results from its inability to maintain chemical equilibrium with a magma during cooling; the zonation represents a frozen picture of the continuous reaction sequence for that mineral.

Classification of Zoning

This thesis adopts a general zoning classification which is based on zoning pattern. The common type of zoning is concentric zoning which includes normal zoning, reverse zoning, and oscillatory zoning. In normal zoning, the mineral is zoned from a high temperature core composition to a low-temperature rim composition. In reverse zoning, the mineral is zoned from a low-temperature core composition to a high-temperature rim composition. In oscillatory zoning, the mineral composition continuously oscillates between high- and low- temperature compositions from the core to the rim. Figure 1.2 gives some idealized variations for zoning.

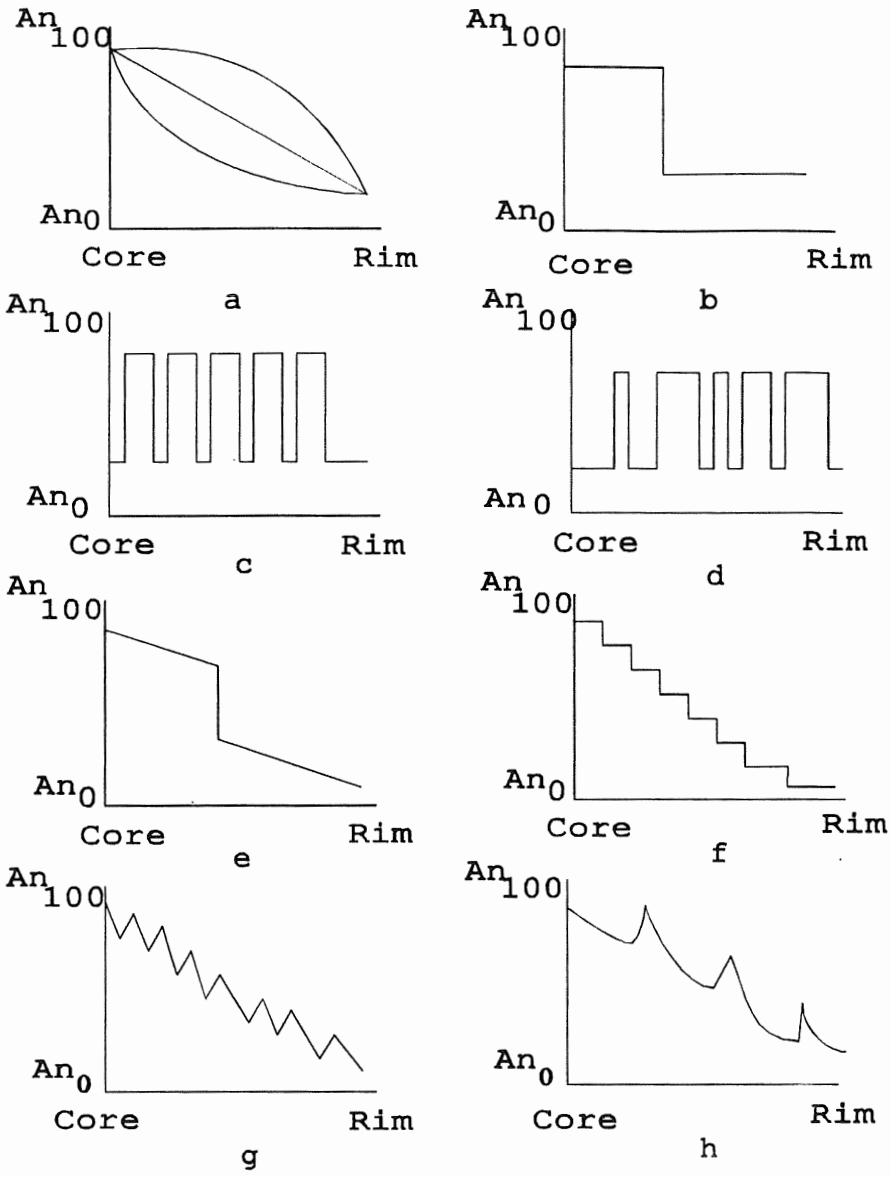

Figure 1.2 Idealized plagioclase zoning patterns.

a. Three continuous normal zonings.
b. Discontinuous normal zoning.
c. Oscillatory, even zoning.
d. Oscillatory, uneven zoning.
e. Combined continuous and discontinuous normal zoning.
f. Step-like, normal zoning.
g. Saw-tooth, oscillatory zoning.
h. Curved saw-tooth, oscillatory zoning.

Origin of Zoning

Early studies on the origin of crystal zoning concentrated mainly on plagioclase. But zoning in ferromagnesian minerals now stimulates considerable interest (Clark et al. 1986: olivine; Dietvorst, 1980, Spry, 1987, Tulloch, 1981: Spinel; Gallagher, 1988: tourmaline; Wass, 1973: pyroxenes). The main reasons for zoning in ferromagnesian minerals are concentration of transitional elements depending on partition among coexisting minerals and partition between matrix and minerals, changes in oxygen fugacity, and water pressure. Zoning in the AFM minerals has not been systematically studied.

The evidence for disequilibrium growth of garnet comes from the observations that: (1) partitioning of Mn between garnet and the matrix phases depends on bulk composition in samples from the same outcrop (Hollister, 1969); (2) partitioning of Mn, Mg, and Fe were observed to depend on metamorphic grade of the sample (Atherton, 1968; Hollister, 1969), i.e., the Mn content decreases and the Fe and Mg contents increase as grade increase in rocks with similar bulk composition; and (3) natural zoning profiles suggest that reverse zoning in garnet, identified by increasing Mn concentra- tion, can occur in the center of crystals (e.g., Hollister, 1969, Fig. 7(a)) and near the end of growth (e.g., Hollister, 1969, p. 2478).

Colours of biotites depend upon their relative contents in iron, magnesium, and titanium (Hall, 1941). In the dyke sample,

green-brown zone (darker than outside the core) corresponds to higher TiO_2 and FeO, and lower MgO. The higher iron content might cause the green colour in the biotite, and this colour difference by elemental effects was already mentioned by Hall (1941) and Kwak (1981).

Czamanske et al. (1983) found zoned biotite (thick light rims in sharp contact with dark cores) from granitic rocks of the Miocene Questra Caldera and demonstrated, on the basis of chemical variations, that zoning resulted from H_2 loss. Loss of water, or abrupt changes in fO_2 affecting Fe^{3+}/Fe^{2+} ratio might account for the central darker zone in the biotite. The quench evidence (described below) supports these interpretations.

Okrush & Evans (1970) showed that the pink cores in andalusite are enriched in Ti, Fe, and Mg relative to the rims, and that the compositional change is abrupt from core to rims.

However, the zoning profiles of the larger andalusite and sillimanite crystals analysed by Yokoi (1983) suggest that much of the central portions of the crystals are either unzoned or have much gentler zoning profiles than the rims of the crystals. There are several possible explanations for this zoning trend: (a) a heterogeneous reaction such as: $Fe_2O_3^{Ilm} + SiO_2^{Qtz} = Fe_2SiO_5^{Sil}$ (Grew, 1980), (b) late-stage diffusion of Fe^{3+} into the rims of the crystals, because of compositional gradient between the crystal and the matrix; and (c) increase in fO_2 during growth of the crystals.

Knowledge of how components partition between phases helps us to understand the origin of zoning. Normal zoning in plagioclase and garnet is simply predicted from the unequal partitioning of components coupled with consequent fractionation of the melt or matrix, regardless of whether the growth rate is controlled by intergranular diffusion or interfacial processes. Partitioning under disequilibrium conditions can cause the composition of a crystal to deviate significantly from the equilibrium composi- tion. Disequilibrium partitioning may cause a crystal composition to change in a manner opposite to the change of the matrix or melt composition caused by fractionation because partitioning is a function of bulk composition as well as temperature and pressure (Loomis, 1983).

For instance, partitioning between plagioclase (Ab and An components) and melt can be expressed by

$$K_{An} = f_{An}\ (T,\ P,\ P_{H2O}\ \text{etc.}) = X^{pl}_{An}/X^{Melt}_{An}$$

$$K_{Ab} = f_{Ab}\ (T,\ P,\ P_{H2O}\ \text{etc.}) = X^{pl}_{Ab}/X^{Melt}_{Ab}$$

Then the distribution coefficient:

$$K_D = K_{An} / K_{Ab} = f_{An} / f_{Ab}$$

At a given T, P and P_{H2O}, the partitioning equations for the distribution of each component between each pair of phases, together with the bulk composition of the system, require that there be a unique composition of each phase in the system.

When the composition imposed on the edge of the crystal by equilibration with other phases differs from the existing composition within the crystal, diffusion can result in zoning around the previous homogeneous crystal. Diffusion controls compositional zoning in two ways:

(1) It tends to eliminate growth zoning that occurred by natural fractionation processes. High diffusion rates may explain the origin of homogeneous crystals. The zoning profiles preserved on the edges of crystals represent the last stage of diffusion that occurred as the rock cooled to temperatures low enough to effectively stop diffusion.

(2) Diffusion creates zoning in a homogeneous crystal during consumption by reaction. This "diffusion zoning" relies for its existence on enough diffusion to propagate inward compositional changes produced on the edge of a crystal, but not enough to homogenize the crystal.

The amount of diffusive transfer (J) of material within a crystal depends on both the diffusion rate (D) and the compositional gradient (∇C) (Loomis, 1983):

$$J = - D\nabla C$$

Diffusion penetration depth (d) is a function of time and temperature for Mn-Fe and Mg-Fe in almandine-rich compositions. Granulite temperature conditions can result in exchange diffusion of Mg and Fe if these temperatures are encountered for millions of years. Contact metamorphic rocks should show diffusion zoning

of garnet if they reached very high temperatures. Manganese zoning should disappear by diffusion at this high temperature. However, rocks at lower temperatures (<550°C) and short times would suffer little diffusion alteration of any growth zoning profiles (Loomis, 1983).

1.3 Methodology

1.3.1 *Conventional optical mineralogy*

The petrographic microscope provides information not only on textures but also on zoning in minerals which may be manifested by color differences and variations in extinction angles.

1.3.2 *Roycroft's method*

Zoning in muscovite has probably been overlooked in many granites because, at normal thin-section thickness (0.03 mm), zoning in white mica is difficult to see (Roycroft, 1989). The Roycroft technique involves using a sharp blade to separate muscovite cleavage flakes up to 0.3 mm thick, to search for zoning of muscovite under a petrographic microscope.

1.3.3 *Nomarski Technique / Etching*

The Nomarski interference contrast technique is used to enhance the visibility of microtopographic relief on the surfaces of etched, polished sections and etched, polished thin sections. Nomarski interference contrast imaging is a useful and inexpensive technique for the investigation of the growth history and subsequent development of minerals in igneous rocks. Although familiar to metallurgists and ceramists, the Normarski

method is relatively unfamiliar to geologists and petrographers. Nomarski interference contrast is a reflected light technique. Polarized light is split by a Wollaston prism (a double-crystal prism) into two beams, which are reflected by the specimen, recombined by the prism, and then passed through a crossed analyzer. Surface irregularities cause phase differences in the reflected wave fronts, producing variations in brightness or color.

Etching of mineral surfaces to enhance and reveal features that are not otherwise visible is a time-honoured, but seldom-used, technique. Several researchers (Anderson, 1983, 1984; Clark et al., 1986; Grossman et al., 1971; Wegner & Christie, 1973) have used it to reveal very subtle zoning microtopography in crystals such as plagioclase, olivine, and clinopyroxene. Differential etching in crystals results from slight compositional variations.

Etching procedures include:

(1) Concentrated hydrochloric acid (45%) is allowed to etch olivine in polished sections or polished thin sections for 10 to 20 minutes, clinopyroxene for 2 to 4 minutes (Clark et al., 1986); concentrated fluoroboric (HBF_4) acid is allowed to etch plagioclase for 30 seconds to 2 minutes (Anderson, 1983); (2) After etching, the acids are neutralized by immersion in a saturated solution of Na_2CO_3; (3) Then the polished surfaces are rinsed with water and dried; (4) The section is finally

carbon-coated (Clark et al., 1986), or vapor-deposit coated with Au-Pd to about 300 Å thickness (Anderson, 1983), to increase its reflectivity and to eliminate internal reflections in the crystals.

1.3.4 *Electron Microprobe*

Electron microprobe analysis is probably the most widely used technique to quantify the compositional zoning in minerals. Microprobe spot analyses were carried out along traverses in crystals of AFM minerals to detect compositional changes from cores to rims.

The need for accurate microprobe analyses of AFM minerals is of great importance in the study of zoning and mineral chemistry. Dunham & Wilkinson (1978) studied microprobe analyses and concluded that for oxides present in amounts greater than 5 wt% (i.e., all major elements) all analyses whether by ED (energy-dispersive) or WD (wavelength-dispersive) analysis, lie within the 6 % error range. They concluded that the ED system compares well with the WD system for accuracy and precision: 68% of the errors lie within ± 2.7% for amounts greater than 1% wt, and ± 2.3% for amounts greater than 5% wt.

The Jeol 733 Superprobe at Dalhousie University produced all mineral analyses used in this thesis. Estimated relative standard deviation is 2 wt% for major elements (person. comm. R.M. MacKay, 1994). For those oxides present in amounts lower than 1 wt%, this thesis adopts the standard deviation based on 10

spot results obtained on a very small area (free from inclusions and less than 10 μm^2) for each mineral. The relative standard deviations were ±5.5% for MgO in garnet, ±3.5% for MnO in cordierite, ±6% and ±5% respectively for TiO_2 and MgO in muscovite, and ±16.6% for FeO in andalusite.

Apart from the precision of microprobe analyses, two other criteria can be helpful in judging if zoning exists: (1) degree of similarity of repeated analyses (replicate microprobe analyses on the same mineral); (2) symmetrical trends of element distributions along transects (such as a plateau pattern in chemical variations) in which microprobe inaccuracy is unlikely.

1.4 Organization

Figure 1.3 summarizes the organization of the thesis. Each box represents a part of thesis work or content.

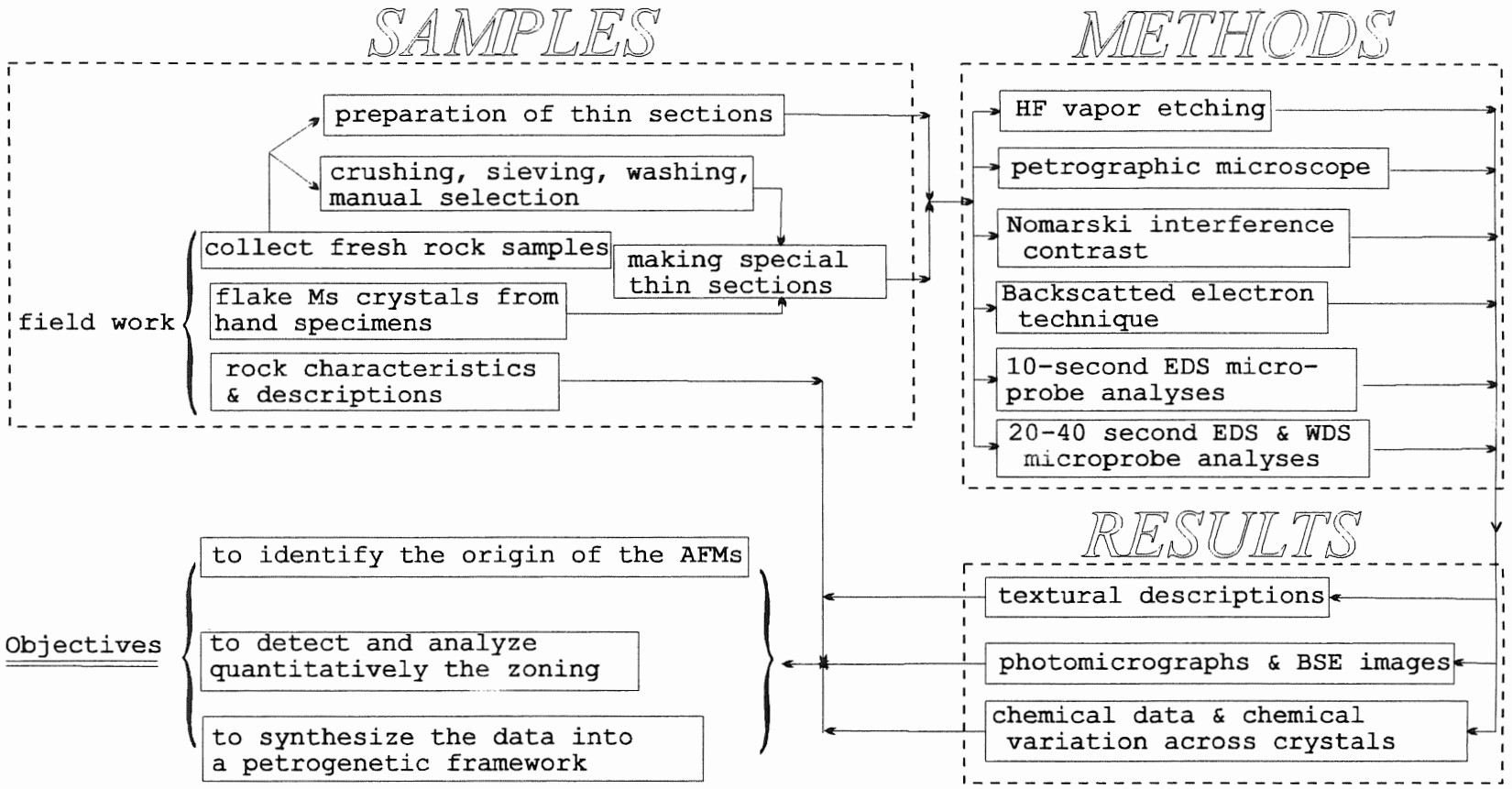

Figure 1.3 Organization flow diagram. Each box represents a part of thesis work or content.

Chapter 2 Petrology and Geochemistry

2.1 The South Mountain Batholith and the Halifax Pluton

The South Mountain Batholith (SMB) is one of the largest peraluminous granitoid bodies in the Appalachian Orogen (Fig. 2.1). Geological and geochemical investigations (Clarke & Halliday, 1980; Clarke & Muecke, 1985; MacDonald et al., 1992; Maillet & Clarke, 1985; McKenzie & Clarke, 1975; Smith, 1974, 1975) over the past two decades have made the SMB well understood. Table 2.1 summarizes its main characteristics. Detailed mapping of the SMB (MacDonald et al., 1992) divides it into 13 plutons which belong to two stages of formation. Stage I Plutons are mostly comprised of biotite granodiorite and biotite monzogranite whereas Stage II Plutons mostly contain muscovite - biotite monzogranite, coarse - and fine - grained leucomonzogranite and leucogranite.

The Halifax Pluton (Fig. 2.2) forms the southeastern end of the SMB and belongs to the Stage II (MacDonald et al. 1992). MacDonald & Horne (1988) mapped the Halifax Pluton in detail and made petrological and geochemical studies on it. They considered that the HP is a discrete plutonic body consisting, from margin to core, of biotite granodiorite (Unit 1), biotite monzogranite (Unit 2), muscovite - biotite ± cordierite leucomonzogranite (Unit 3), biotite ± cordierite monzogranite (Unit 4). Those phases have been intruded by the fine grained leucomonzogranite

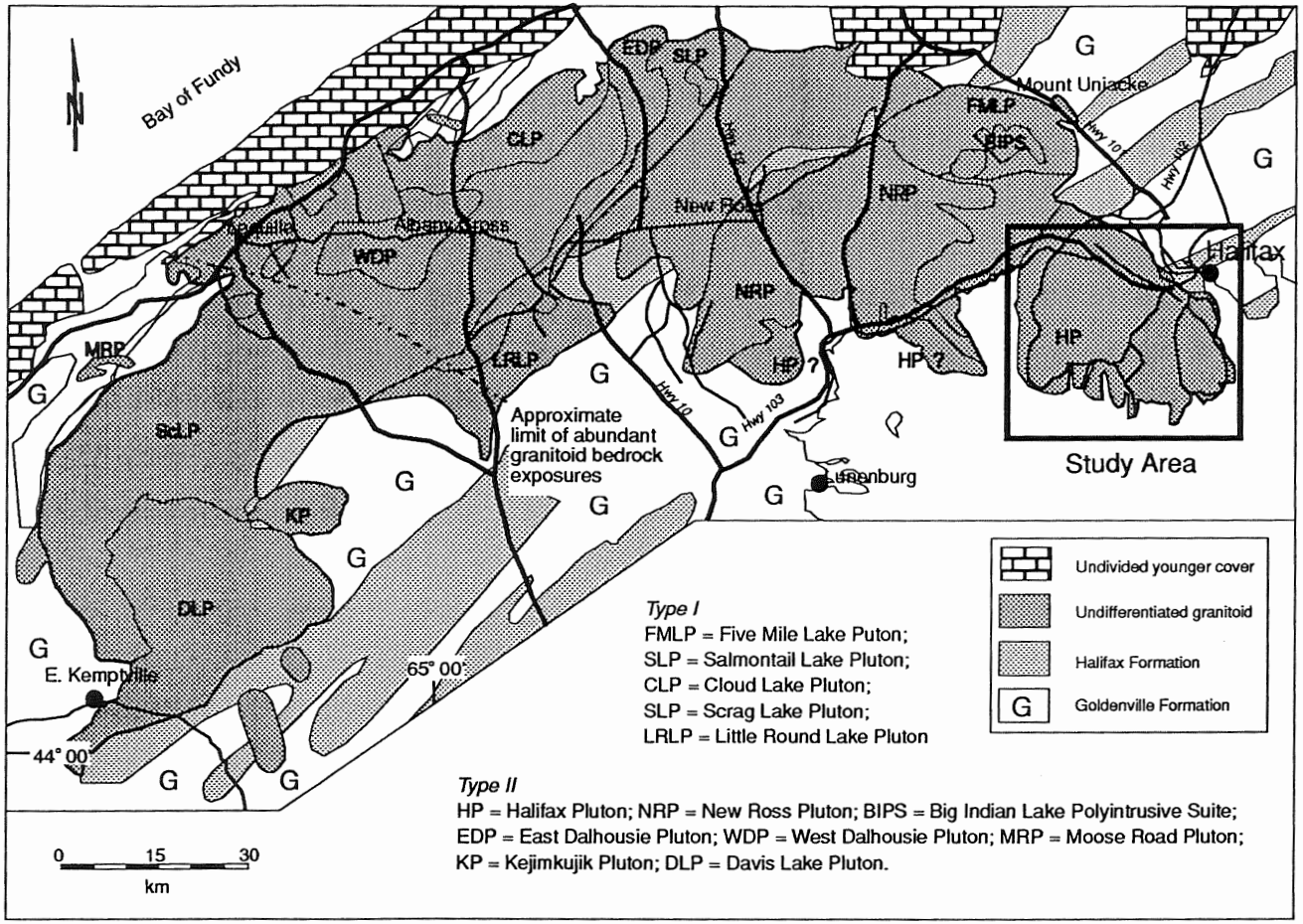

Figure 2.1 The South Mountain Batholith and the study area (after MacDonald et al., 1992).

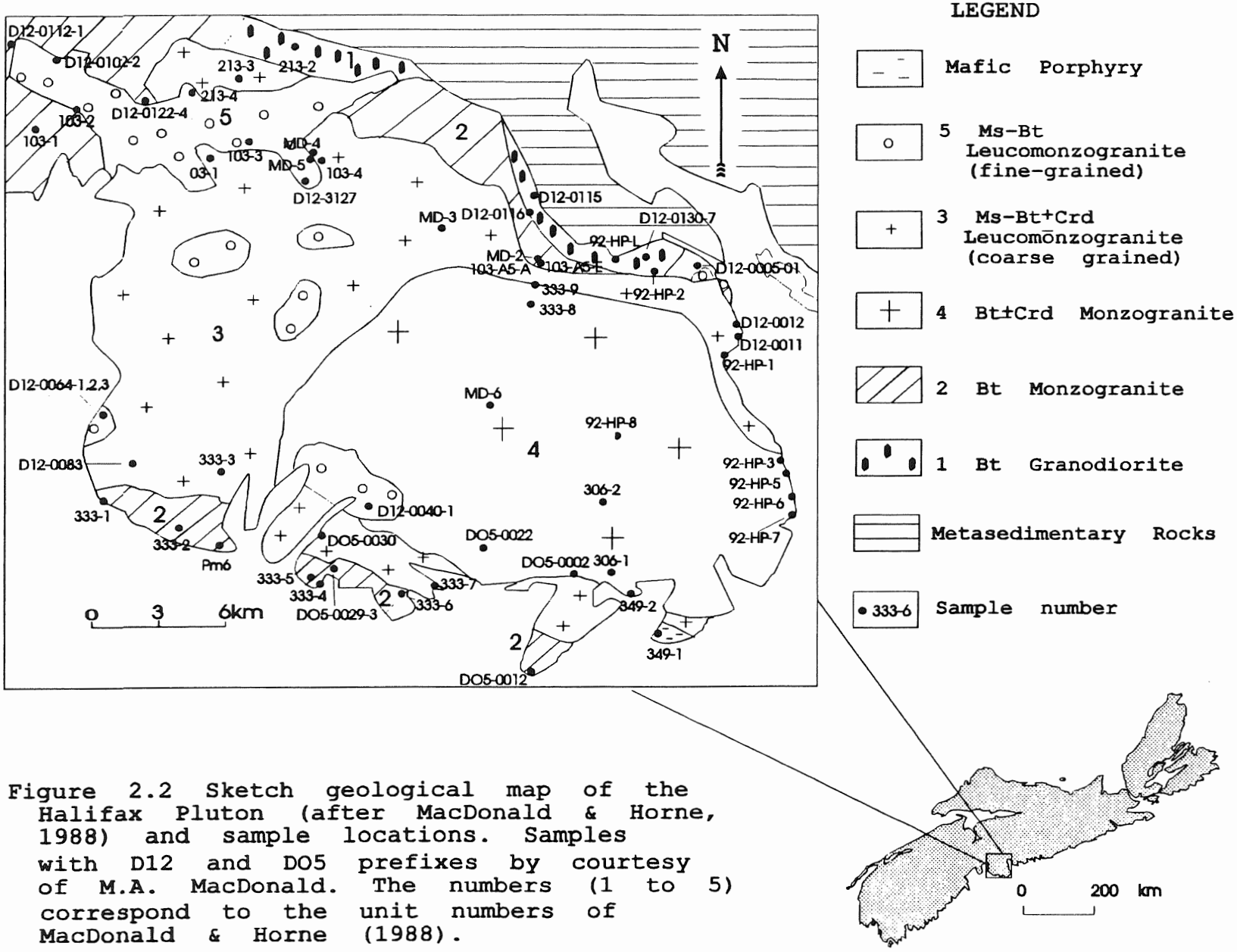

Figure 2.2 Sketch geological map of the Halifax Pluton (after MacDonald & Horne, 1988) and sample locations. Samples with D12 and DO5 prefixes by courtesy of M.A. MacDonald. The numbers (1 to 5) correspond to the unit numbers of MacDonald & Horne (1988).

(Unit 5). In addition, the Halifax Pluton contains many aplite ± pegmatite dykes which intrude all rock units. Several of these dykes intrude an outcrop of biotite monzogranite near Halifax (Fig. 2.3). Several of these dykes were sampled in this study.

Table 2.1 Main characteristics of the SMB

Location	Southwestern Nova Scotia
Area	approximately 7,300 km^2
Rock types	granodiorite - monzogranite - leucomonzogranite - leucogranite - aplite
Ages	Devonian (stratigraphic data); 370 ± 2Ma, (isotopic);
Mineralogy	Characteristic minerals: Bt, Ms, Crd, Grt, And, and Tur
Geochemistry	A/CNK >1; $\delta^{18}O$ = +10 to +12 ‰ SMOW; $(^{87}Sr/^{86}Sr)i$: 0.7076-0.7090; $(\varepsilon^{372\ Ma})_{Nd}$ = -5.2 to -1.4
Mineralization	Polymetallic

References: Clarke, et al. 1988; Clarke & Halliday, 1980; Clarke & Muecke, 1985; MacDonald et al., 1992; Muecke & Chatterjee, 1983.

2.2 Petrology of the HP

The HP has five main rock types or phases. MacDonald & Horne (1988) numbered, based on field observations, the zoned sequence of megacrystic rocks in Units 1-4 from margin to core of the pluton. And a late intrusion to those above phases is Unit 5. MacDonald & Horne (1988) described the petrology and

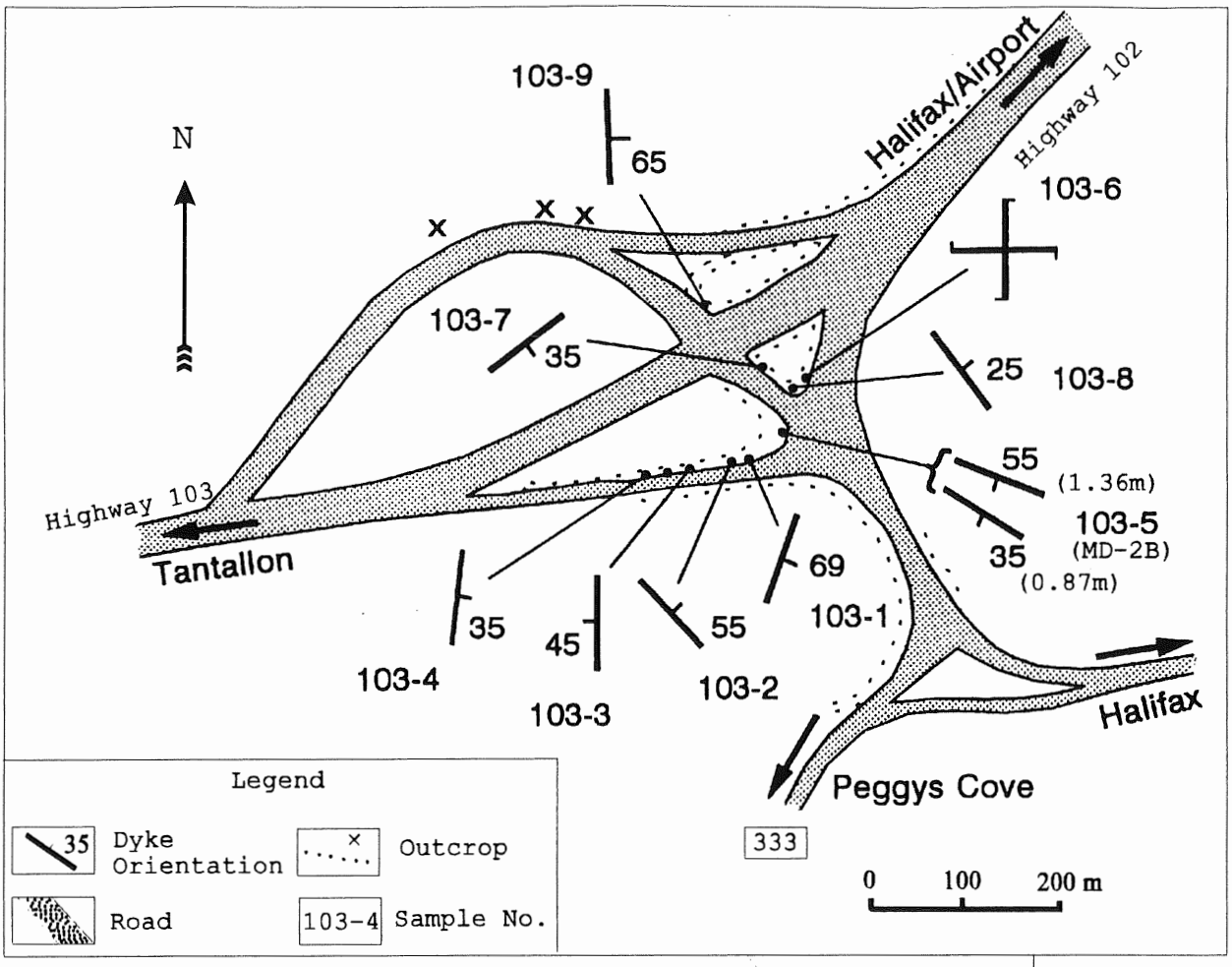

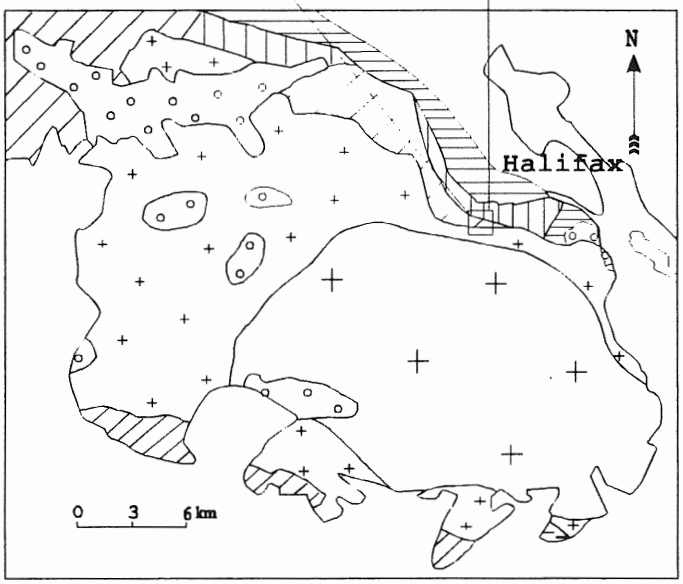

Figure 2.3 Above: sample locations and orientation of the dykes. (Courtesy of M.A. MacDonald, unpublished). The width of these dykes is between 10 cm and 136 cm.

Table 2.2 Main Petrographic Features of the Phases of the Halifax Pluton*

Unit	1	2	3	4	5
Rock	Bt Gd	Bt Mzg	Ms-Bt ± Crd Lmzg	Bt ± Crd Mzg	Ms-Bt Lmzg
Grain Size	fine-medium	medium-coarse	fine-coarse	fine-coarse	fine, medium, coarse
Texture	mega-crystic	mega-crystic	mega-crystic	mega-crystic	equigranular porphyritic megacrystic saccharoidal pegmatitic
Pl	An_{15-33}	An_{11-36}	An_{2-27}	An_{3-30}	An_{1-15}
Bt(%)	12-15	10-12	2-6	8-10	1-4
Ms(%)	trace	trace-<1	1-2, locally 3-4	trace-1, locally 2-3	1-4
Crd(%)	0-trace	0- <1	0->4, avrg 1-2	0-1 up to >4	trace
Grt(%)	trace	trace	trace	trace	trace
And(%)					trace up to 2 locally

* This table cites main results of MacDonald & Horne (1988). Grain Size - fine: < 0.1 cm; medium: 0.1 - 0.5 cm; coarse: > 0.5 cm

Gd = granodiorite
Mzg = monzogranite
Lmzg = leucomonzogranite

geochemistry in detail. Table 2.2 cites their main results. The following paragraphs briefly describe the main characteristics for those phases (mineral modal percentages from MacDonald & Horne, 1988):

Granodiorite (Unit 1), megacrystic, crops out in the northern part of the Halifax Pluton in contact with the Meguma Group Metasedimentary rocks. This unit is the least altered one in the HP and is grey in colour. It contains more biotite (up to 12-15%) than other rocks, traces of muscovite and cordierite, no andalusite or garnet, few alkali - feldspar megacrysts, and shows common zoning in plagioclase.

Biotite monzogranite (Unit 2), megacrystic, occurs in the southern and the northwest parts of the Halifax Pluton. MacDonald & Horne (1988) inferred that these two areas may connect with each other under St. Margaret's Bay. The rocks are usually fresh, medium- to coarse-grained, and contain more feldspar megacrysts and less biotite (10-12%) than biotite granodiorite.

Muscovite - biotite ± cordierite leucomonzogranite (Unit 3), megacrystic, constitutes most of the exposures in the west part of the Halifax Pluton and also forms bands (1-3 km wide) along the northern and southern periphery of the HP, so that it surrounds biotite ± cordierite monzogranite on most sides. In many parts it was intruded by later bodies.

Biotite ± cordierite monzogranite (Unit 4), megacrystic (Kfs up to <15%), is exposed in the east part of the Halifax Pluton. It contains a higher modal percentage of cordierite (0-1, up to 4% in some parts) and less biotite (8-10%) than biotite granodiorite and biotite monzogranite. This unit

contains trace - 1%, with up to 2 - 3% muscovite in some areas. MacDonald et al. (1992) classified this rock into "muscovite - biotite monzogranite".

The transition between muscovite - biotite ± cordierite leucomonzogranite (Unit 3) and biotite ± cordierite monzogranite (Unit 4) is gradational, but can be recognized primarily on the basis of changes in biotite and muscovite abundance. The mineral compositions and textures of these two phases are quite similar. The differences between these phases are: (1) biotite ± cordierite monzogranite contains more biotite (8-10%) than muscovite - biotite ± cordierite leucomonzogranite (2-6%); (2) part of the latter contains more muscovite (3-4%).

Muscovite - biotite leucomonzogranite (Unit 5), equigranular, porphyritic, saccharoidal, is widely distributed in the Halifax Pluton. It mainly appears in the northwest part of the study area, and apparently formed later than any other phase, as shown by its intrusive relationship with other rocks. Relatively abundant muscovite (1-4%, up to 10% in some parts) is characteristic of this rock. It contains few or no megacrysts.

The MgO index (MgO as the abscissa for variation diagrams and the Harker index (SiO_2 as the abscissa) indicate a different order: Unit 1 $\rightarrow$ 2 $\rightarrow$ 4 $\rightarrow$ 3 $\rightarrow$ 5. The use of MgO as an index depends on the fact that cordierite and biotite crystallizing from the magma contain collectively more MgO than the liquid.

MacDonald & Horne (1988) modelled the formation of compositional zonation within the HP. They suggested that the normal phase zonation of granodiorite (Unit 1: MgO = 1.69%) and biotite monzogranite (Unit 2: MgO = 1.4%) is the product of sidewall fractional crystallization. They postulated that reverse zonation in the core (consisting of Unit 3 and Unit 4, the latter is more 'primitive' in major elements, e.g. MgO weight percent and trace elements) could be explained by a mechanism involving magma injection that juxtaposed biotite ± cordierite monzogranite (Unit 4) from lower parts of a zoned chamber with more evolved muscovite - biotite ± cordierite leucomonzogranite (Unit 3) in upper parts of the chamber. Fractional crystallization cannot be used to explain formation of Unit 5, and MacDonald & Horne (1988) suggested that Unit 5 formed from another intrusive pulse.

2.3 Geochemical Characteristics

MacDonald & Horne (1988) analysed many samples from the HP. Table 2.3 gives mean values for the five HP phases. The evolutionary trends in the HP (from high to low MgO values) are characterized by increases of the ratios Mn/(Ca+Mn+Mg), A/CNK (which is here always higher than unity), and A/(A+F+M) and decreases of FeO and TiO_2, and no change of M/(F+M) for the main phases and abrupt change of M/(F+M) between aplite and main phases (Fig. 2.4).

Table 2.3 Mean values of geochemical data for each phase of the HP

Units	1	2	3	4	5	Aplite
Samples analysed	9	9	24	24	24	1
SiO_2	67.75	70.09	72.85	70.94	74.02	75.79
TiO_2	0.58	0.44	0.2	0.39	0.14	0.05
Al_2O_3	15.56	14.9	14.35	14.6	14.18	13.45
FeO	3.66	3	1.84	2.54	1.48	0.84
MnO	0.09	0.08	0.06	0.06	0.05	0.04
MgO	1.69	1.4	0.88	1.23	0.74	0.1
CaO	1.75	1.17	0.68	1.03	0.45	0.48
Na_2O	3.69	3.42	3.46	3.56	3.4	2.71
K_2O	4.02	4.37	4.64	4.47	4.4	5.5
P_2O_5	0.19	0.18	0.22	0.26	0.23	0.15
H_2O	0.68	0.68	0.57	0.68	0.74	0.1
Total	99.66	99.73	99.75	99.76	99.82	99.21
A/CNK	1.14	1.19	1.2	1.16	1.27	1.19
Mn/(Ca+Mn+Mg)	0.02	0.02	0.02	0.02	0.03	0.05
A	0.02	0.02	0.02	0.02	0.03	0.02
M	0.04	0.04	0.02	0.03	0.02	0
F	0.05	0.04	0.03	0.04	0.02	0.01
A+F+M	0.11	0.1	0.07	0.09	0.07	0.04
A/(A+F+M)	0.17	0.24	0.33	0.23	0.43	0.6
M/(A+F+M)	0.37	0.35	0.31	0.35	0.27	0.07
M/(F+M)	0.45	0.45	0.46	0.46	0.47	0.18

Note: original data by courtesy of M.A. MacDonald
Unit 1: Biotite Granodiorite
Unit 2: Biotite Monzogranite
Unit 3: Muscovite - Biotite ± Cordierite Leucomonzogranite
Unit 4: Biotite ± Cordierite Monzogranite
Unit 5: Muscovite - Biotite Leucomonzogranite
$FeO = Fe_2O_3 * 0.89981$

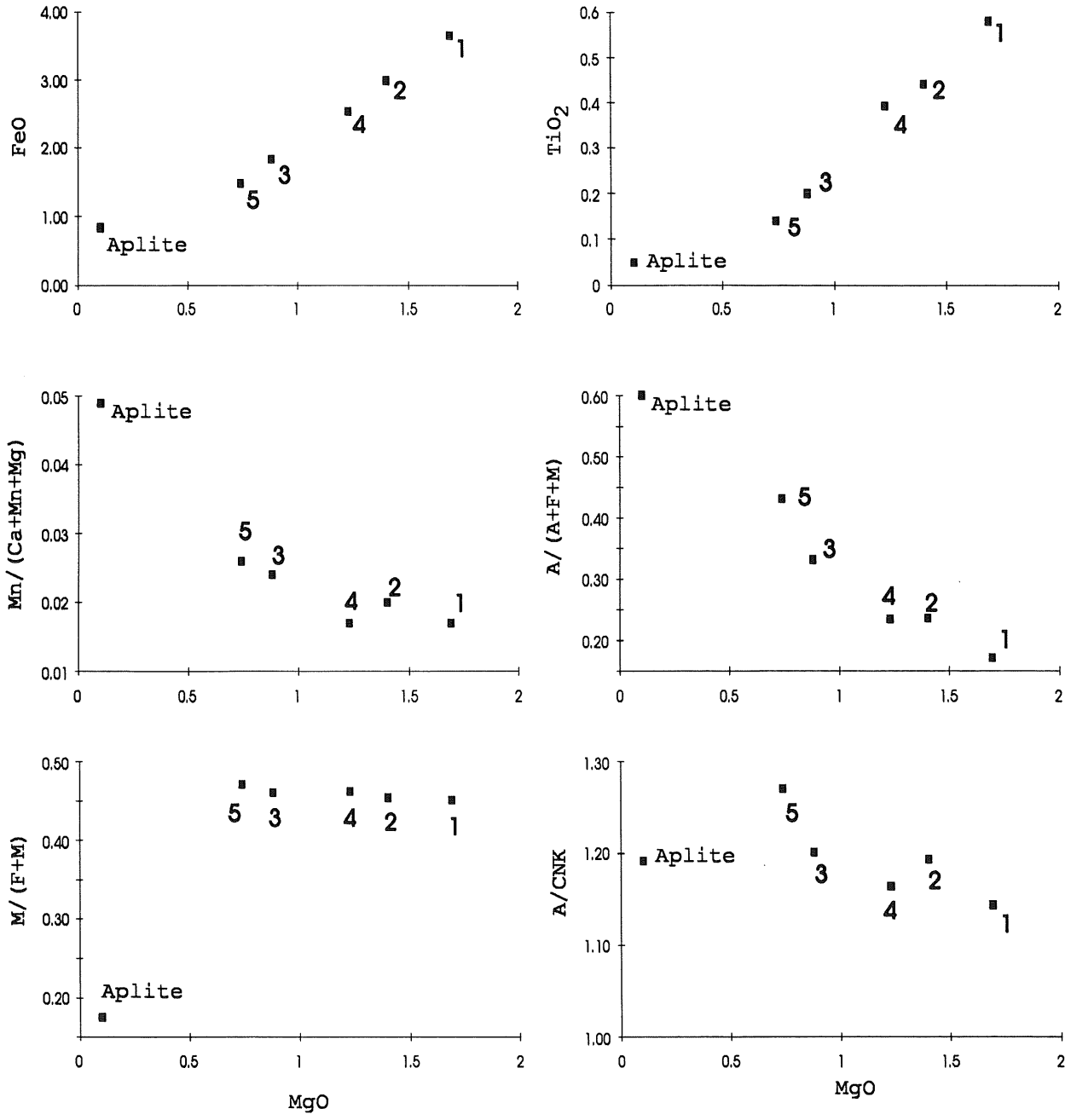

Figure 2.4 Plots of chemical mean data and ratios of the HP phases against MgO, showing, from early (MgO=1.7%) to late (MgO=0.70%) phases, increases of Mn/(Ca+Mn+Mg), A/CNK, A/(A+F+M) and decreases of FeO and TiO_2, M/(F+M) no change for the main phases and abrupt change between aplite and main phases. The numbers in the plots are the unit numbers of MacDonald & Horne (1988).

2.4 Magmatic AFM Minerals

AFM minerals of different origins (primary, xenocrystic, restitic, and metasomatic) may occur in peraluminous granite. The various individual criteria (Table 2.4) used to recognize an igneous origin are not definitive, but in combination they offer compelling reasons to believe a mineral is a magmatic phase in the pluton. The most important criterion is textural evidence, and the other criteria rely on textural recognition of the magmatic phase as a first step.

Table 2.4 Criteria used to recognize magmatic AFM minerals

Texture -grain size comparable to other magmatic minerals -sharp terminations -euhedral to subhedral shape -no reaction or relation textures with other minerals -relatively abundant -the host rock is relatively unaltered
Chemistry -chemical consistency between AFM minerals and the host rocks which relationships indicate their equilibrium -greater content of Ti or Na, depending on different minerals
Mineral Assemblage -the mineral assemblage is indicative of a peraluminous magma composition

Chapter 3 Biotite

3.1 Introduction

This chapter examines the general occurrence, zoning, and chemical characteristics of biotites in igneous rocks. It then reports specific examples of zoned biotites in the Halifax Pluton, and discusses their importance.

Biotite is one species in micas which constitutes an isomorphous group within the phyllosilicates. Two sheets of linked SiO_4 tetrahedra are juxtaposed with the vertices of the tetrahedra pointing inward; these vertices are cross-linked either with Mg, as in phlogopite, or with Al, as in muscovite; hydroxyl groups complete the six-coordination of the Mg or Al.

The general formula for the group:

$W(X,Y)_{2-3}Z_4O_{10}(OH,F)_2$

- W is chiefly K, Na (or may include Ba, Ca, Rb etc.);
- X, Y represent Al, Mg, Fe^{+2}, Fe^{+3}, Li, minor Cr, Mn, Ti;
- Z is Si and Al, may include Be and Fe^{+3}.

The following lists simplified formulas for species in this group:

Muscovite $KAl_2(AlSi_3O_{10})(OH)_2$

Phlogopite $KMg_3(AlSi_3O_{10})(OH,F)_2$

Biotite $K(Mg,Fe)_3(Al,Fe)Si_3O_{10}(OH,F)_2$

Lepidolite $K(Li,Al)_3(Al,Si)_4O_{10}(OH,F)_2$

Glauconite $(K,Na)(Fe,Mg,Al)_2(Si,Al)_4O_{10}(OH)_2$

K in biotite can be replaced in part by Na, Ca, Ba, Rb, or Cs; Mg can be completely replaced by Fe^{+2} in part by Ti and Mn and there is also substitution by Fe^{+3} and Al for Mg and by Al for Si; and OH is replaceable by F. A complete series exists between phlogopite and biotite and their crystal structures are the same.

3.2 Biotite in Igneous rocks

3.2.1 *Biotite Occurrences*

Biotite is the most common AFM mineral in igneous rocks (Clarke, 1981). It is nearly always considered to be a primary mineral, as it is stable over a wide range of P - T conditions (Fig. 3.1). However, biotite may also be mafic remnants derived from the source region (White & Chappell, 1977).

3.2.2 *Review of Biotite Zoning*

Zoning in biotite has not been reported in peraluminous granites, but sector zoning has been found in biotite from many other types of igneous rocks: biotite from granites in south Greenland (Stephenson & Upton, 1982); shonkinite in Katzenbuckel (Yoder & Tilley, 1962); theralites in Taourirt, Morocco (Mokhtari & Velde, 1987); olivine melilitite from Smith - Morehouse Canyon, Utah (Best et al., 1968); and Oka carbonatite (Rimsaite, 1969). Colour zoning may occur in phlogopite as either alternating light and dark bands or as a darker central core (MacKenzie & Guilford, 1980; Phillips & Griffen, 1981). Rimsaite (1969) suggested that

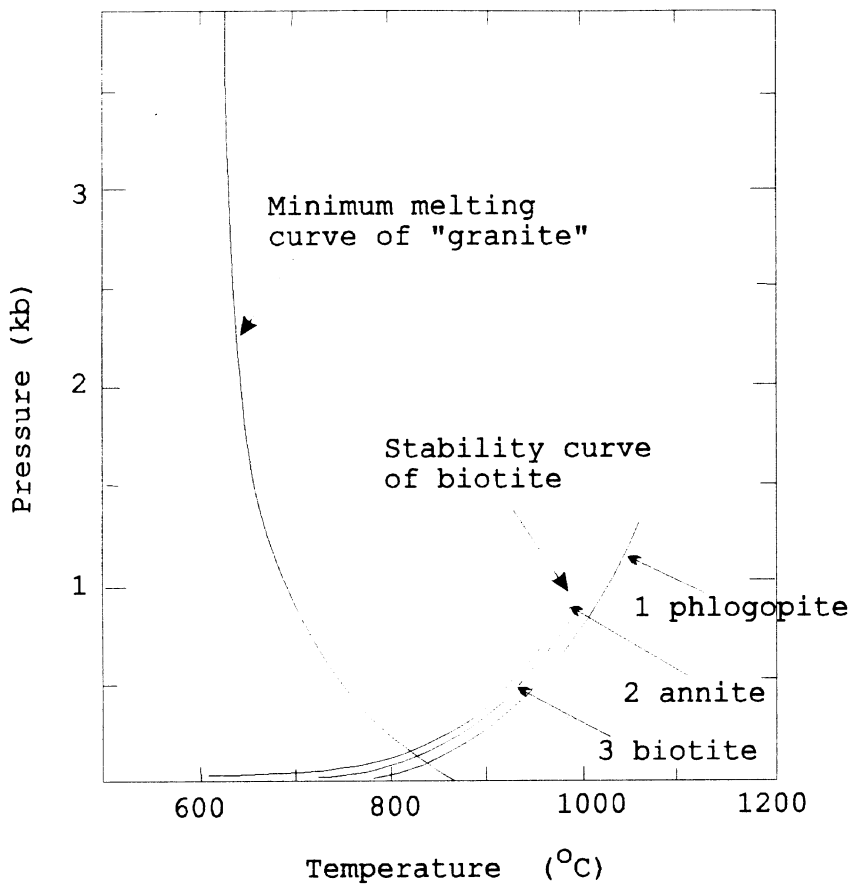

Figure 3.1 Biotite stable region. 1. Phlogopite stability curve from Yoder & Eugster, 1954: phlogopite ↔ forsterite + leucite + orthorhombic $KAlSiO_4$ + vapour; 2. Annite stability curve from Wones et al.,1971: annite ↔ sanidine + magnetite + H_2; 3. Biotite (M/(F+M)=0.6) from Clemens & Wall, 1981: biotite + quartz ↔ orthopyroxene + K-feldspar + vapour; melting curve of "granite" from Tuttle & Bowen, 1958.

the sector-zoned micas resulted from gradual or abrupt compositional changes caused by magma differentiation, or by the starting or stopping of crystallization of other minerals. Biotite, as a solid solution mineral, should be expected to be zoned if conditions in the magmatic environment change during its growth.

3.2.3 *Biotite Chemistry*

Four ideal end-members of "biotite" show complete mutual solid solution. This system is arbitrarily divided into magnesium - rich minerals (M/(F+M) > 2/3), collectively called *phlogopites,* and iron-rich minerals (M/(F+M) < 2/3), collectively called *biotites.* Clarke (1981) concluded that aluminum in both tetrahedral and octahedral positions increases as the coexisting minerals themselves have higher values of A/CNK. Zen (1988) mentioned that biotite from granitic rocks has M/(F+M) ratios around 0.3 - 0.5; it typically shows a persistent A-site alkali deficiency, but excess octahedral and tetrahedral Al. He reported that A/CNK is approximately 1.3 - 1.4 for igneous biotite coexisting with hornblende, but is higher than 1.4 for igneous biotite coexisting with muscovite and other peraluminous minerals.

An early study of the geological occurrence of biotite was the correlation of its chemical composition with different types of host rocks. Vejnar (1971) found that in the series from lherzolite through muscovite - biotite granite, the biotites

increase in Si, Ti, Mg, and Na content and decrease in Al, Fe^{3+}, Fe^{2+}, Mn, Li, and F. Mahood & Hildreth (1983) reported that in the Zaer Pluton (Morocco), when the rock differentiation index increases, the included biotites increased in Rb, Mn, and Al contents, decreased in Mg, Ca, Cr, and Ni contents, and remained unchanged with respect to Si, Ti, K, and Na.

3.3 Biotite in the Halifax Pluton

3.3.1 *Biotite Occurrences*

Biotite is the only ferromagnesian mineral present in all phases of the Halifax Pluton. Its modal abundance is the highest in granodiorite and mafic porphyry (up to 15%) and shows a systematic decrease in modal percent in the HP sequence, down to 1 - 2% in the late - stage phase (MacDonald & Horne, 1988). Most biotites are fresh and appear primary (euhedral or subhedral shapes and size comparable to that of other rock - forming minerals such as quartz and feldspars), and some occur as inclusions in other minerals (Fig. 3.2a,b).

These biotites have two specific characteristics:

(1) normal twins exist in biotite (Fig. 3.2c) from the mafic porphyry. Twinning is rare in biotite, and has not previously been reported from the Halifax Pluton. A crystal relates to its twinned counterpart either by reflection (mirror plane), or by rotation about a line (twin axis). Normal twins have a twin axis normal to the composition plane which is the plane that unites the two individuals (Fig. 3.3).

(2) zircon, monazite, xenotime, ilmenite and apatite, as inclusions or as minerals adjacent to biotite, coexist closely with biotite.

3.3.2 *Biotite Chemistry*

Biotite Chemistry

MacDonald & Horne (1988) noted systematic changes in M/(F+M) of biotite from biotite granodiorite (0.363) to late-stage rocks (0.250 and 0.132). Average biotite analyses for each unit of the Halifax Pluton are projected onto the biotite quadrilateral (Fig. 3.4).

A/CNK and M/(F+M) range from 1.73 to 1.84 and 0.25 to 0.48 respectively, showing that these biotites have much higher A/CNK and lower M/(F+M) values than those of Zen (1988: his higher boundary of 1.4 for A/CNK of igneous biotite coexisting with hornblende, lower boundary of 0.3 for M/(F+M) of igneous biotite from granitic rock), despite the fact that those biotites coexist with few aluminous minerals in the early-stage rocks (biotite: A/CNK = 1.73).

Zoning in Biotites

The scarcity of basal sections of biotite in normal thin sections required preparation of special thin sections (using a sharp blade to separate biotite cleavage flakes to make basal sections) containing complete basal biotite to study its zoning by means of the microprobe.

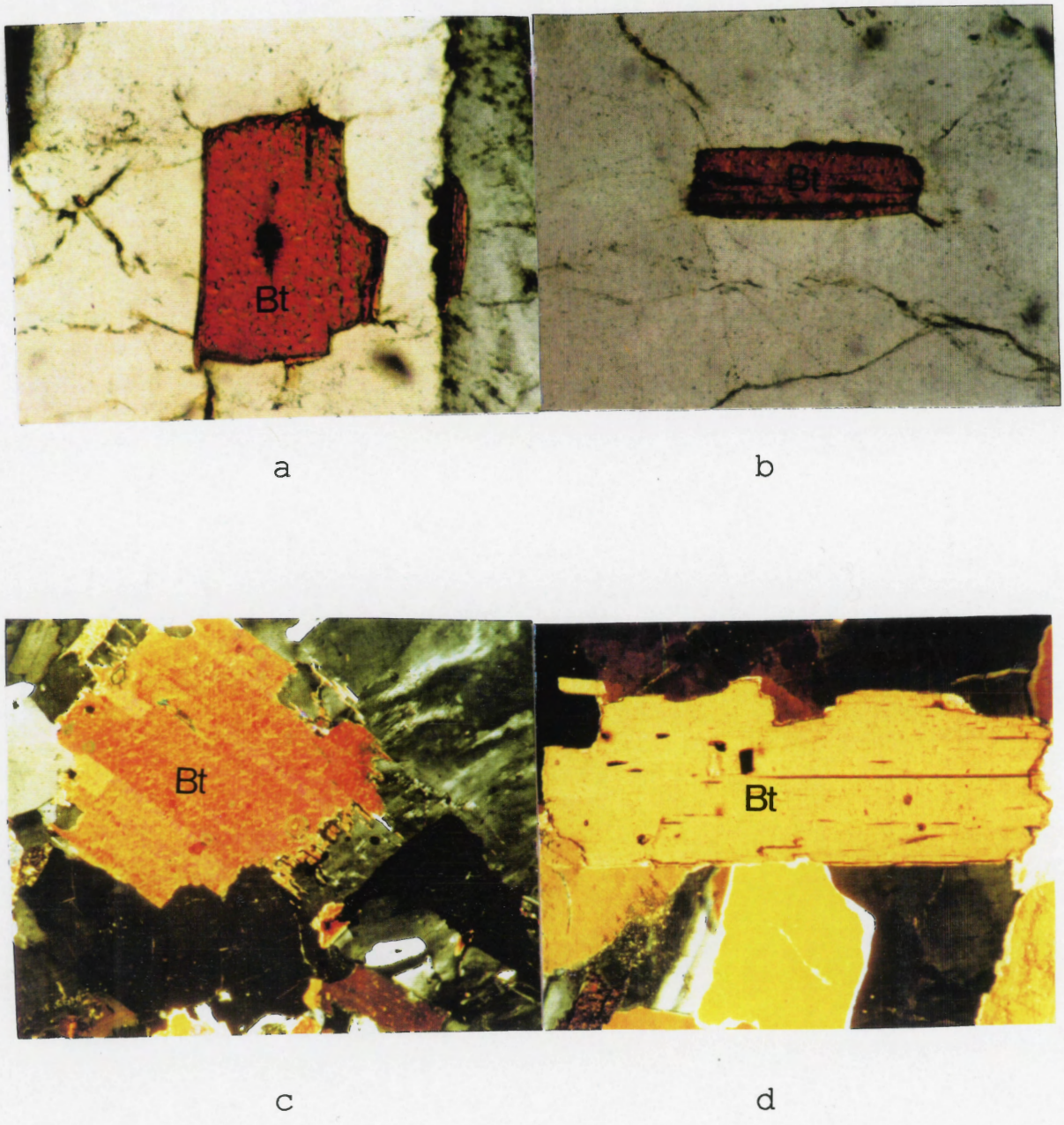

Figure 3.2 Photomicrographs of Biotites from the HP, a-b: euhedral biotite inclusions in Kfs (D12-0130-7, in biotite granodiorite; length for those photos: 1.8mm); c: euhedral biotite with comparable size coexists with quartz and K-feldspar and shows twin structure(DO5-3061 in mafic porphyry; d: 92-HP-12 in muscovite-biotite±cordierite leucomonzogranite; length for those photos: 5.5mm.

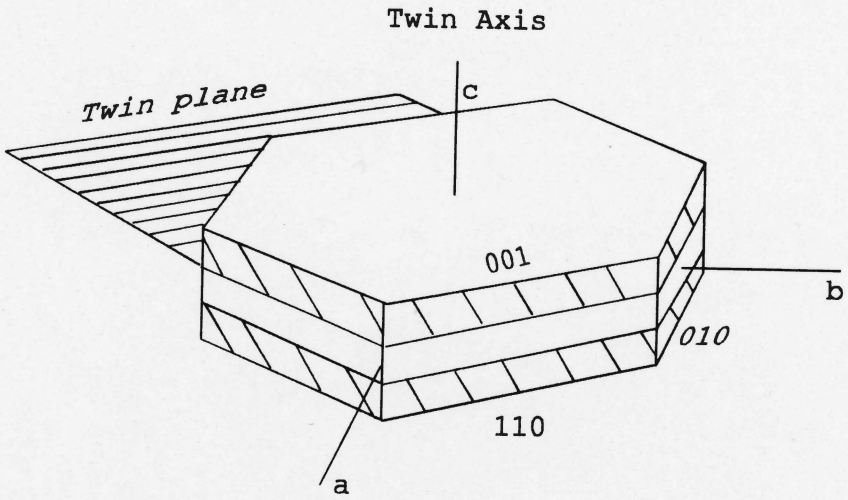

Figure 3.3 Twinning relationships in biotite

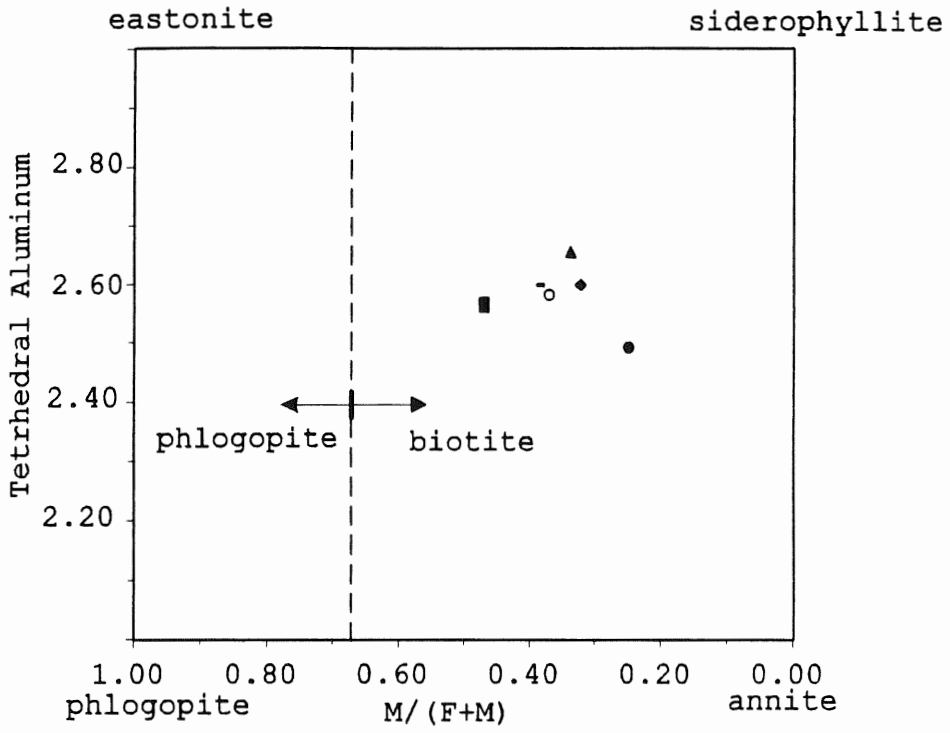

Figure 3.4 Projection of biotites from the HP in the biotite quadrilateral, showing low ratios of M/(F+M) and high tetrahedral aluminum. All plots are mean values of biotite from mafic porphyry ▪, from biotite granodiorite -, from biotite monzogranite ∘ , from biotite ± cordierite monzogranite ▲, from muscovite-biotite ± cordierite leucomonzogranite ◆ , and from muscovite-biotite leucomonzogranite ● .

Biotite crystals are rare and small (<1mm) in the aplite (<0.9%, unpublished data , M.A. MacDonald), and some show optical zoning (Figs. 3.5, 3.6) (Sample No.103-A5-A, 103-A5-E, courtesy of M. MacDonald). Microprobe traverses (Fig. 3.7) across that zoning indicate that: (1) the levels of Fe, Mg, and Ti do not differ between the darker central zone and the outlying area; and (2) Fe, Mg, and Ti display irregular variations across the traverses.

Furthermore sharp zoning exists at rims of the biotite from sample 213-4 of muscovite - biotite ± cordierite leucomonzo-granite (Fig. 3.8). The zoning is only revealed by the outermost rims that are lower in Ti, and higher in Mg and Fe, than the core (Fig. 3.8). The biotite from biotite monzogranite (333-6) has zoning (Fig. 3.9) with the same pattern as in sample 213-4.

3.4 Discussion and Conclusions

3.4.1 *Origins of the Central Darker Zone*

Direct optical recognition of zoning is probably the most convincing method. A central darker zone with clear margins (with rhomb outline) (Figs 3.5, 6) exists in biotites from the aplite. Irregular changes in Fe, Mg, and Ti profiles across those biotites may indicate changes in the levels of those elements in the local magma. However, the profiles reveal that

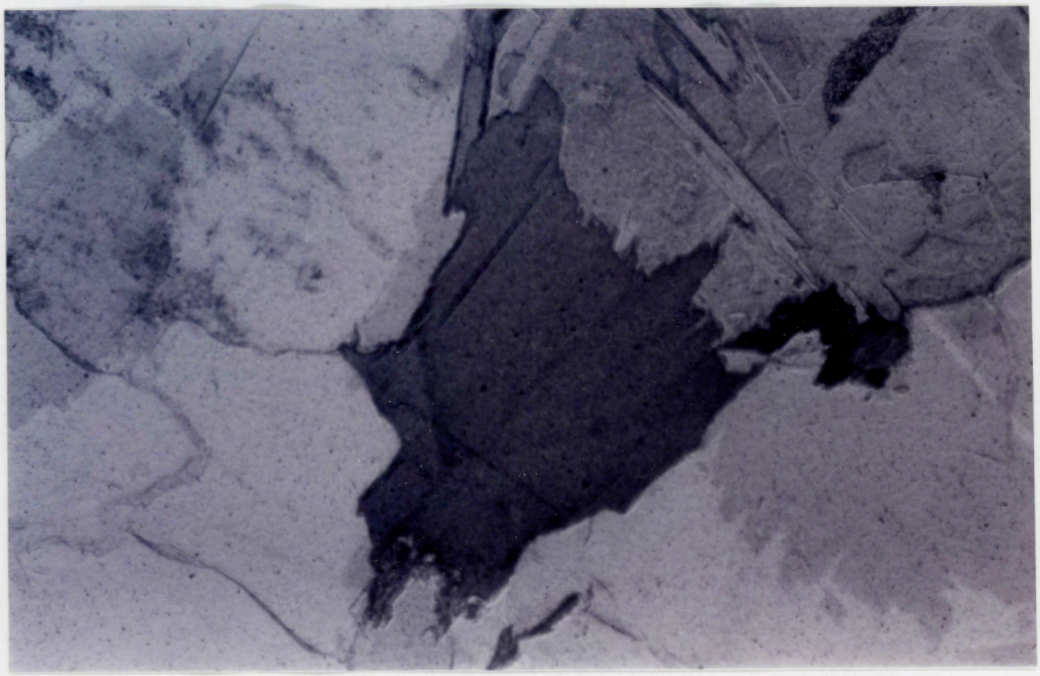

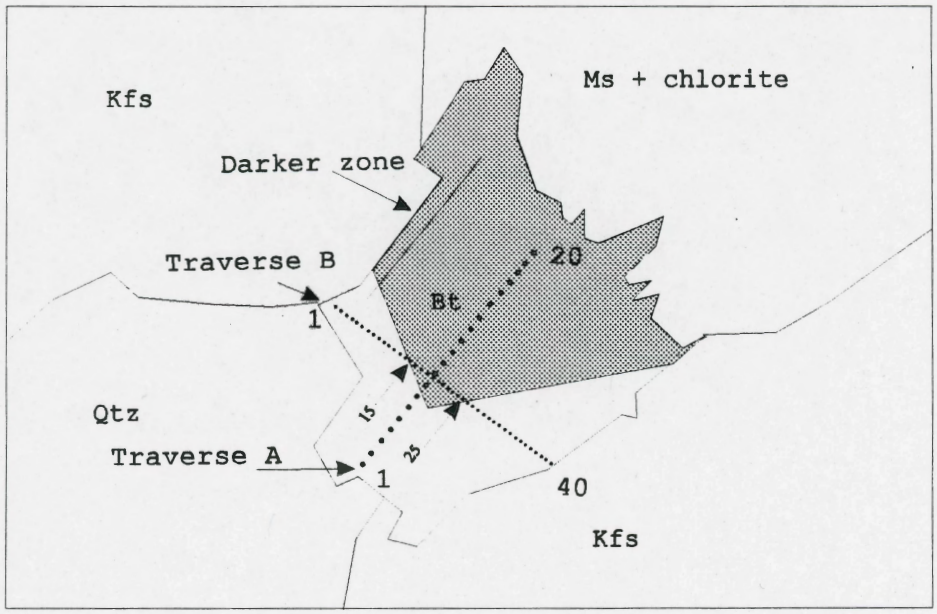

Figure 3.5. Above: photomicrograph of zoned biotite from the aplite (103-A5-A: courtesy of M.MacDonald); below: descriptive sketch of the same biotite, and microprobe traverses; length of the photo is 1.7 mm.

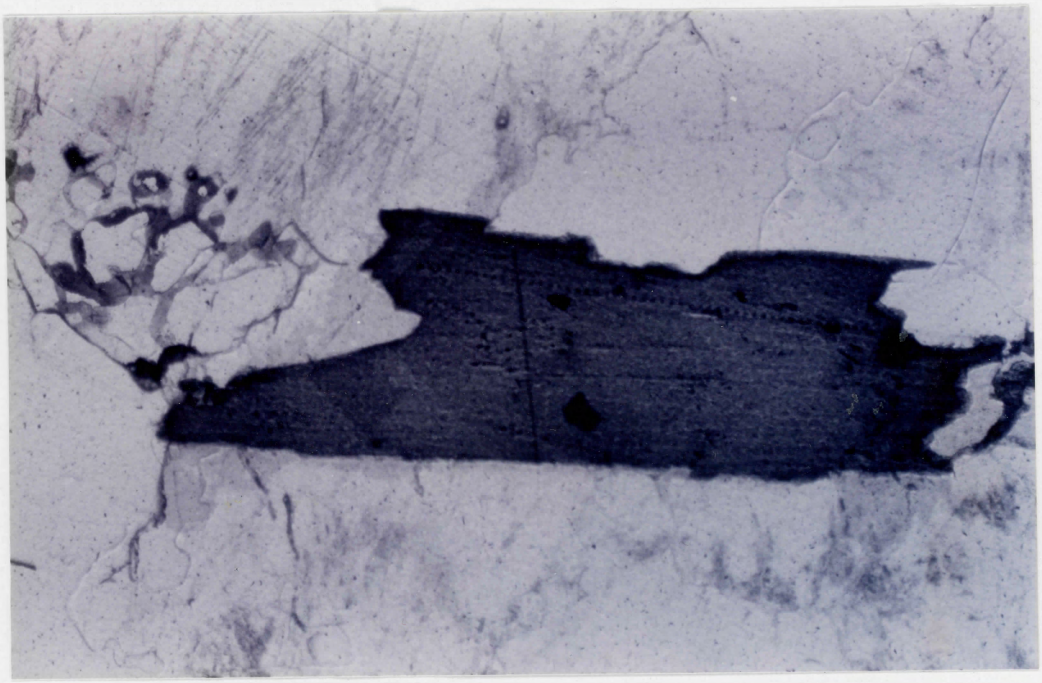

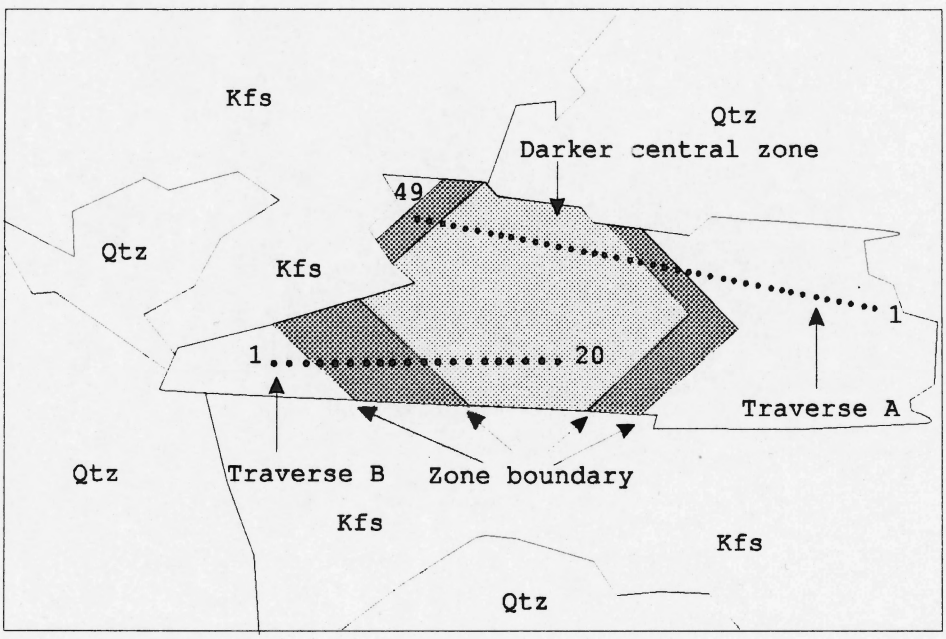

Figure 3.6. Above: photomicrograph of zoned biotite from the aplite (103-A5-E: courtesy of M.MacDonald); below: descriptive sketch that biotite and microprobe traverses; length of the photo is 1.5 mm.

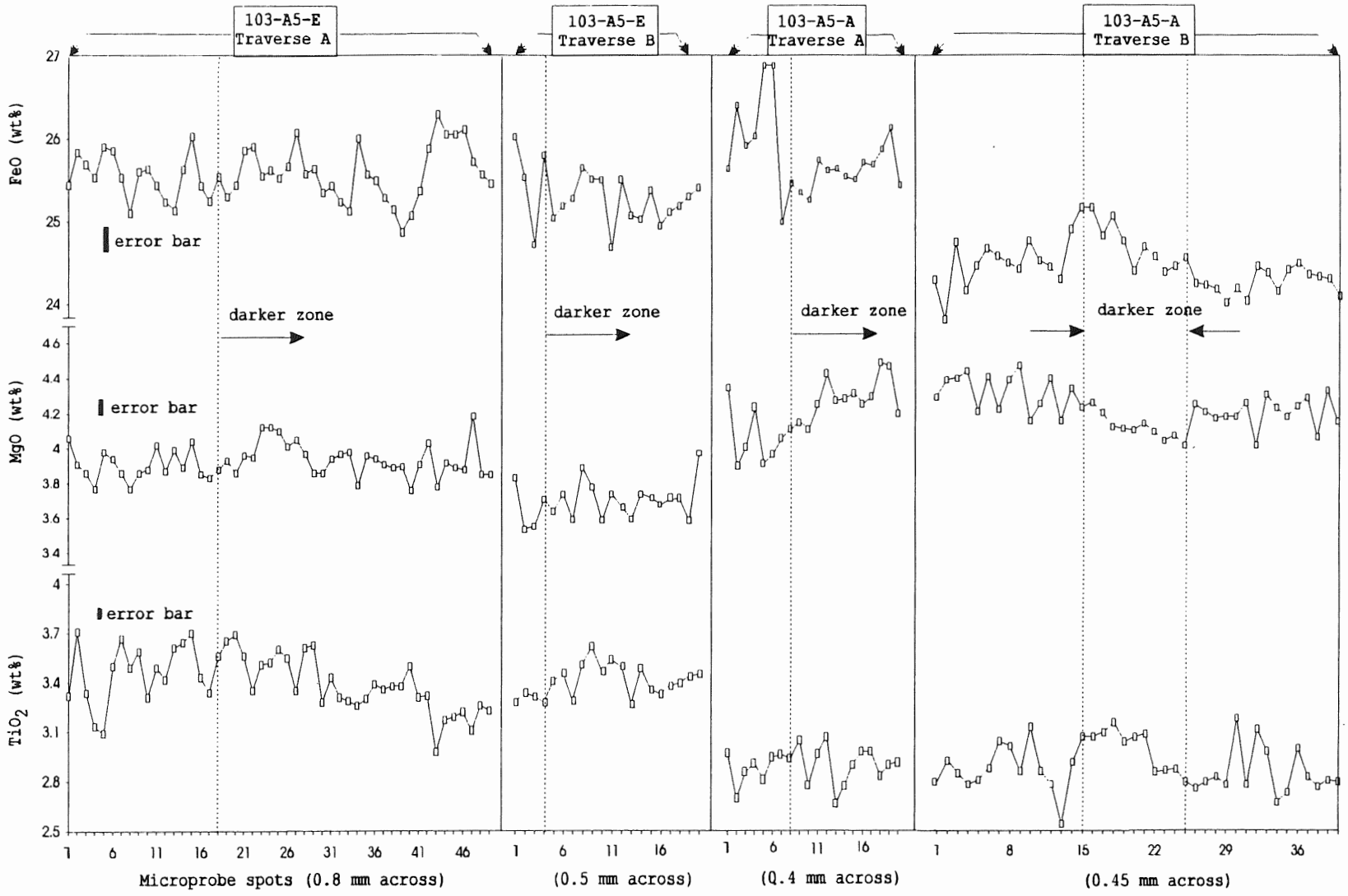

Figure 3.7 Chemical variations across two zoned biotites from samples of the aplite dikes (courtesy of M.MacDonald). See figs. 3.5, 3.6 for crystals and microprobe orientations. Error bars for FeO, MgO, and TiO2 = 0.37, 0.12, and 0.10 respectively.

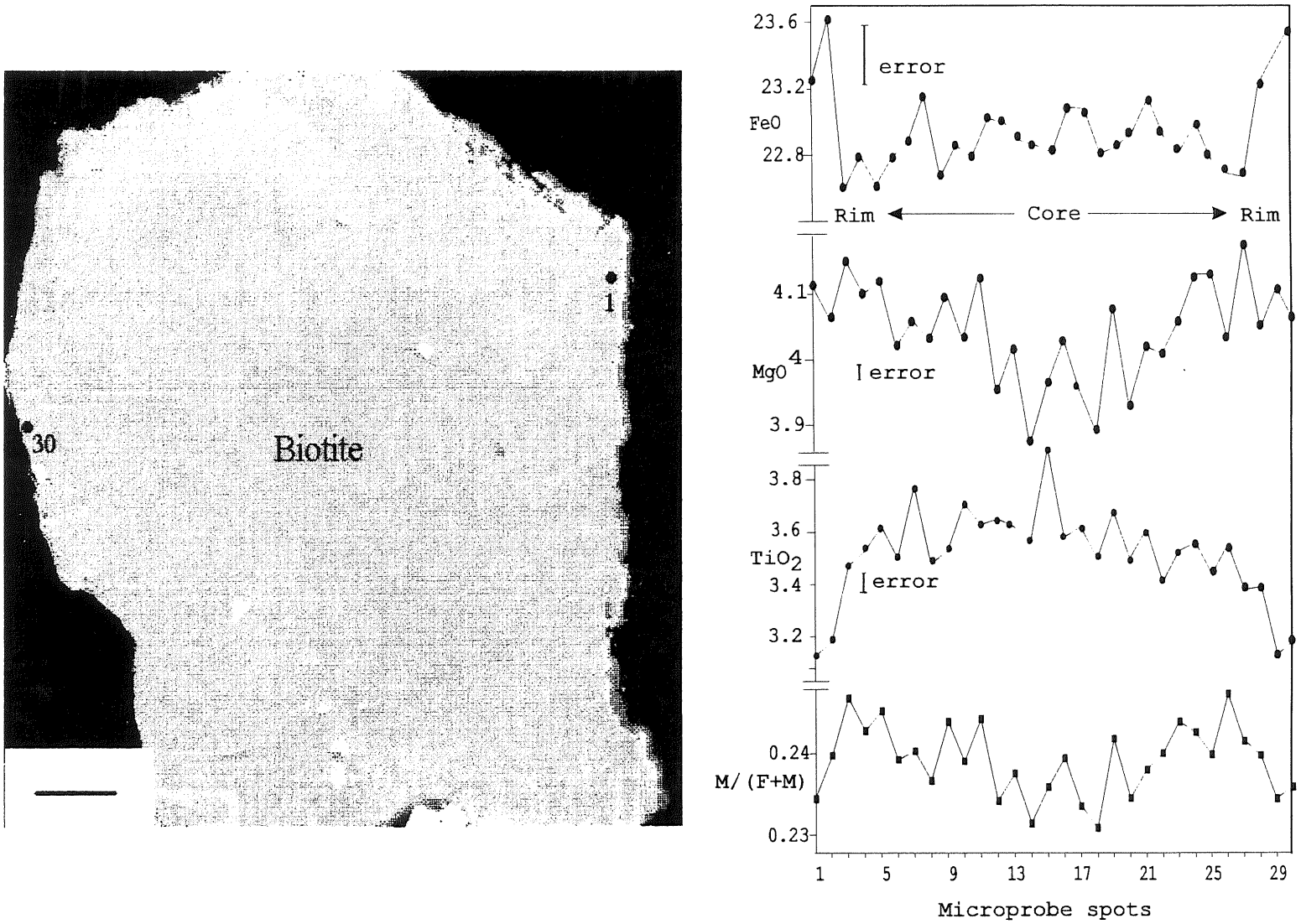

Figure 3.8 BSE image (left: bar scale = 100 um) of the biotite from muscovite-biotite leucomonzogranite (213-4) and its chemical variation traverse (0.95 mm across), showing at outmost rims richer in FeO and poorer in TiO_2 than the core. Error bars = 0.45, 0.02, and 0.03 respectively for FeO, MgO, and TiO2

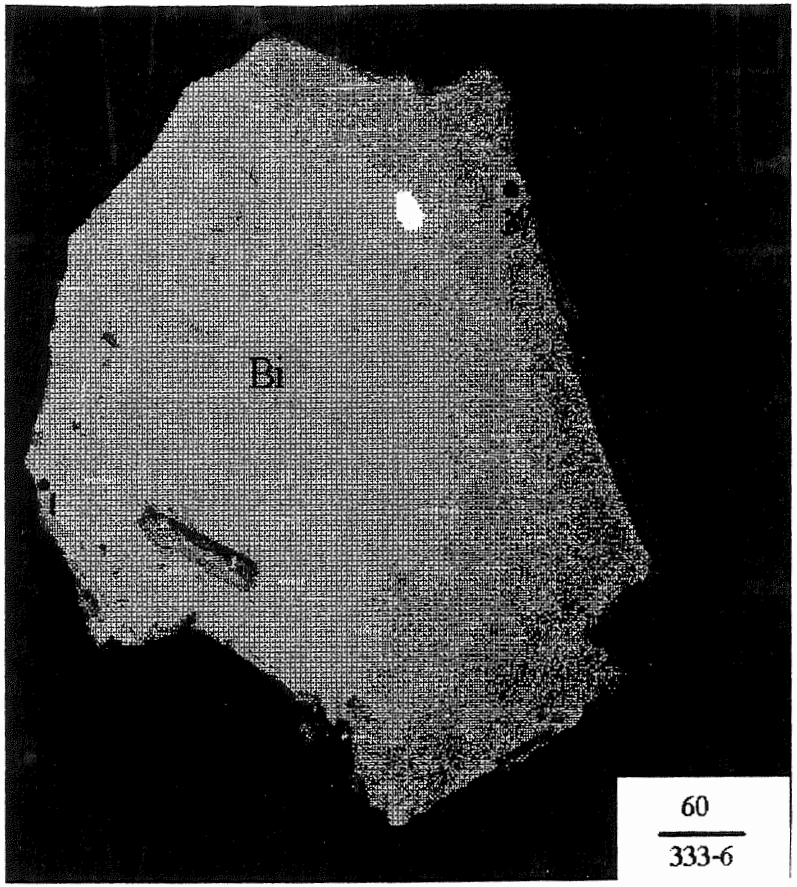

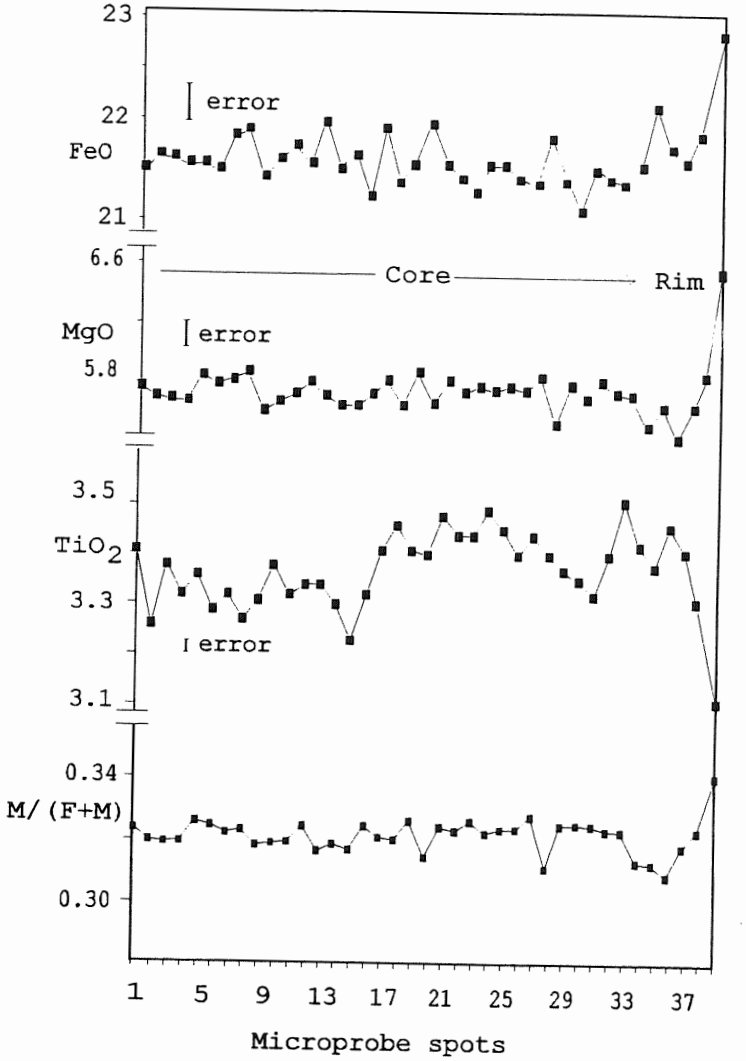

Figure 3.9 BSE image (left: bar scale = 60 um) of a biotite from muscovite-biotite leucomonzogranite (333-6) and its chemical variation traverse (0.51 mm across), showing only outermost rim richer in FeO and MgO and poorer in TiO_2 than the core; error bars = 0.44, 0.03, and 0.03 respectively for FeO, MgO, and TiO2.

these changes do not correspond to the boundaries of the darker zone. Changes in other elements such as Si, Al, Mn, Na, and Ca do not appear to coincide with optical boundaries of the darker central zoning either.

Czamanske et al. (1983) found similar zoned biotite (thick light rims in sharp contact with dark cores) from granitic rocks of the Miocene Questa Caldera and demonstrated, on the basis of chemical variations, that zoning resulted from H_2O loss. Loss of water, or abrupt changes in fO_2 affecting Fe^{3+}/Fe^{2+} ratio might account for the central darker zone in the biotite from the aplite. The quench evidence (described below) supports these interpretations.

Extrusive rocks usually exhibit quenching textures. Quench textures contain skeletal or dendritic or spherulitic crystals in a glassy matrix (e.g., characteristic swallowtail appearance of augite (Cox et al. 1979, Fig. 7.10) and biotite swallowtail shape, Fig. 3.6). Rapid variations in pressure and temperature may result in such textures. Quench texture of the biotite (Figs. 3.5,6, and 10) and quench texture of garnet (see Chapter 6) in the aplite suggest that the aplite magma crystallized rapidly, i.e. an abrupt decrease in temperature and /or pressure. In contrast to the largely subhedral biotite in other phases, biotite crystals in the aplite show extremely elongated shapes, swallow - tail edges, and highly ragged margins (Figs. 3.5,6, and 10).

The studies of Delaney & Pollard (1982) and Petford et al. (1993) suggested that small dikes require rapid rates of emplacement. The differences between the ratios Rb/Sr, Fe/Mg, Na/Ca (= 9, 4.6, 49, respectively) (original data: courtesy of M.A. MacDonald) of the aplite and those (= 1.6, 1.3, 5.3, respectively) of the host - biotite monzogranite indicate that there was an interval of solidification between the host and the guest and further imply the aplite formed in the cooled country rock (the host).

Pressure quenching can result in rapid crystallization (Clarke, 1992) to produce quench textures. There is little doubt that $P_{(total = H2O + CO2 + H2 + ...)}$ of the aplite magma decreased when it moved upward from its origin to the present position. However, neither the total amounts nor the relative proportions of those volatile constituents in the regions of magma generation are precisely known (Burnham, 1979).

3.4.2 *Other Zoning in Biotite*

The zoned biotites from the Halifax Pluton show chemical variations in Ti, Fe, Mg, and M/(F+M). Ti decreases but Mg and Fe increase from core to rims (Figs. 3.8,9). M/(F+M) variation in 213-4 shows a broad W-pattern. This pattern differs from biotites in other igneous rocks in which M/(F+M) decreases from core to rim (Wagner, et al. 1987). However, the sharp compositional zones are characterized by their positions close to the

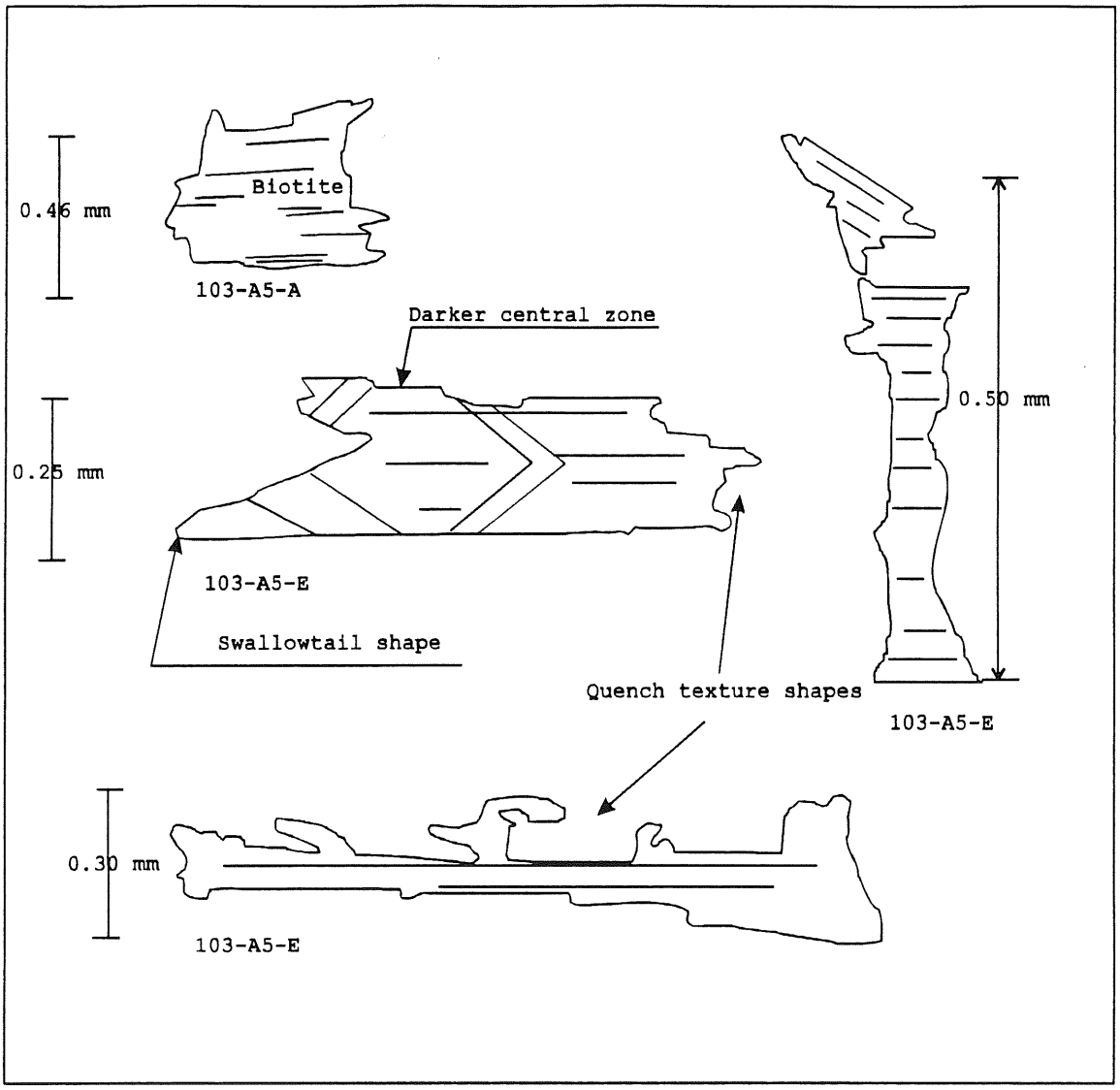

Figure 3.10 Quench texture of biotite from the aplite, showing swallowtail, ragged shapes; see garnet quench texture in Chapter 6 for comparison (samples 103-A5-A, E: courtesy of M. MacDonald).

rims for both samples, meaning that variation occurred only at the last stage of crystal growth. Possible factors influencing this type of crystallization are: bulk composition of the magma, ion diffusion out of or/and into the biotite crystals, and the starting or stopping of crystallization of other minerals which consume the elements from the local magma.

From early to late stages, the HP magma evolved from higher to lower Ti and Fe contents (Fig. 2.4). Ti variation from core to rims in the zoned biotites coincides with those of magmatic evolution from early to late stages. This coincidence may imply that zoning in biotite reflected bulk changes in host melt.

Sharp changes in Mg in the biotites is the reverse of that in magmatic evolution: Mg decreased during the magmatic evolution of the HP. Higher Mg in the rims may be caused by Mg diffusion into the biotites from neighbouring minerals which are richer in Mg than the biotites. Mg ion diffusion would occur from minerals with higher ion contents to minerals with lower amounts. In the local area of the Halifax Pluton, the mineral with higher Mg than the biotites is cordierite. However, cordierite rarely occurs as an adjoining neighbour of biotite, while neighbouring minerals with lower Mg amounts than the biotites, such as alkali-feldspar, plagioclase and quartz, are common.

A possible explanation is that a sudden increase in fO_2 occurred when biotite almost completed crystallization, resulting in more Fe^{+3} and Mg replacement for Fe^{+2} in the X, Y sites or even

more Fe^{+3} replacing Al^{+3} in a tetrahedral site. Diffusion penetration depth is a function of time and temperature. That sharp elemental variation at outermost rims remains is probably because time was limited so that Fe, Mg, Ti could not diffuse inward.

3.5 Summary

Most biotites in all phases of the HP are magmatic. They have euhedral or subhedral shapes as inclusions or individual grains, sizes comparable to those of other rock - forming minerals such as quartz and feldspars, and chemistry consistent with the host rocks. The biotites have high A/CNK (1.73 to 1.84) and low M/(F+M) (0.25 to 0.48).

Zoning in biotite has not previously been reported in peraluminous granites. Loss of water, or abrupt changes in fo_2, in the process of melt moving up and emplacement, may cause the zoning in the biotite of the aplite. Sudden change in fO_2 probably produces the zoning at the outermost rims in biotites from other phases.

Biotites with quench shapes and twinning may exist in the HP and have not been reported for peraluminous granitoid rocks in the literature.

Chapter 4 Muscovite

4.1 Introduction

This chapter explores the general occurrence and zoning of muscovite in igneous rocks, and relates these features to relevant experimental work. It then reports magmatic and secondary forms of muscovite and its zoning in the HP, and discusses their consequences.

The general formula of muscovite is $KAl_2(Si_3AlO_{10})(OH)_2$; K can be replaced by Na, Rb, Cs; OH is replaceable by F. Lithium - free white micas are generally described as solid solutions between the muscovite end member $KAl_2(Si_3AlO_{10})(OH)_2$ and the celadonite end member $K(AlM^{+2})Si_4O_{10}(OH)_2$, with $M^{+2} = Mg^{+2}$, Fe^{+2}, known as the phengitic series. The substitutional mechanism Al^{VI}, $Al^{IV} \Leftrightarrow (M^{+2})^{VI}$, Si^{IV} describes this series. For T > 600°C, the phengitic subsitution becomes negligible (Monier & Robert, 1986).

4.2 Muscovite in Igneous Rocks

4.2.1 *Muscovite Occurrences*

Muscovite is one of the characteristic minerals in peraluminous granites (Clarke, 1981). Miller et al. (1981) stated that muscovite is the most common indicator of "strongly peraluminous" granitoid rocks. Major questions concerning muscovite in igneous rocks are whether it is an igneous or secondary mineral in those rocks, and whether it can be used as an indicator of pressure (Anderson & Rowley, 1981; Charoy, 1986;

Ham & Kontak, 1988; Miller et al., 1981; Monier & Robert, 1986; Speer, 1984; Zen, 1988).

Miller et al. (1981) established textural criteria of magmatic muscovite: coarse grain size comparable to that of other magmatic phases, sharp crystal terminations, subhedral to euhedral forms, and inclusion relationships with other minerals. They also found that the "primary - looking" (magmatic muscovite judged by the textural criteria) muscovites are richer in Ti, Al, and Na and poorer in Mg and Si than the "secondary - looking" muscovites. Large interstitial muscovite crystals in granites may have formed in equilibrium with the liquid, whereas small flakes of muscovite commonly dispersed within feldspar probably crystallized through the leaching of K_2O and SiO_2 from the feldspar at temperatures below that of the granite liquidus (Zen, 1988).

4.2.2 *Muscovite Stability Field*

The pressure and temperature curves of muscovite (Chatterjee & Flux, 1986; Chatterjee & Johannes, 1974) intersect the minimum melting curves of granite (Johannes, 1984; Tuttle & Bowen, 1958) and peraluminous granite (Wyllie, 1977) at a range of temperatures from 635° to 670 °C and pressures from 3 to 4.4 kb (Fig. 4.1). Thus pure end - member muscovite can crystallize from a liquid of granite composition at pressures above 3 to 4.4 kb, but below this pressure it can form only in the solid state.

The above pressure range is contradicted by the evidence of magmatic muscovite in many shallow - level intrusions (Miller et al., 1981; Roycroft, 1991). Primary - looking muscovite is common in granitic rocks which apparently crystallized at depths as shallow as 8 - 9 km (Miller et al., 1981). Zoning in muscovite from the Leinster granite (< 2 kb) (Roycroft, 1991) supports extension of the crystallization field of magmatic muscovite to lower pressures.

4.2.3 *Review of Muscovite Zoning*

Roycroft (1989) first discovered concentrically - zoned muscovite in the peraluminous Leinster Granite, S.E. Ireland. The intrusion is demonstrably emplaced into low - grade rocks (estimated < 2 kb, Roycroft, 1991). The concentric zoning pattern (Roycroft, 1989, 1991) compares well with that in plagioclase. These zoned muscovites also conform to the textural criteria for magmatic muscovite as outlined by Miller et al. (1981), and thus imply that: (1) these muscovites have a history of crystallization from the magma, because they are zoned from cores to rims; and (2) the stability field in the P - T diagram must extend to lower pressure (< 2 kb) given the geological environment (Roycroft, 1991).

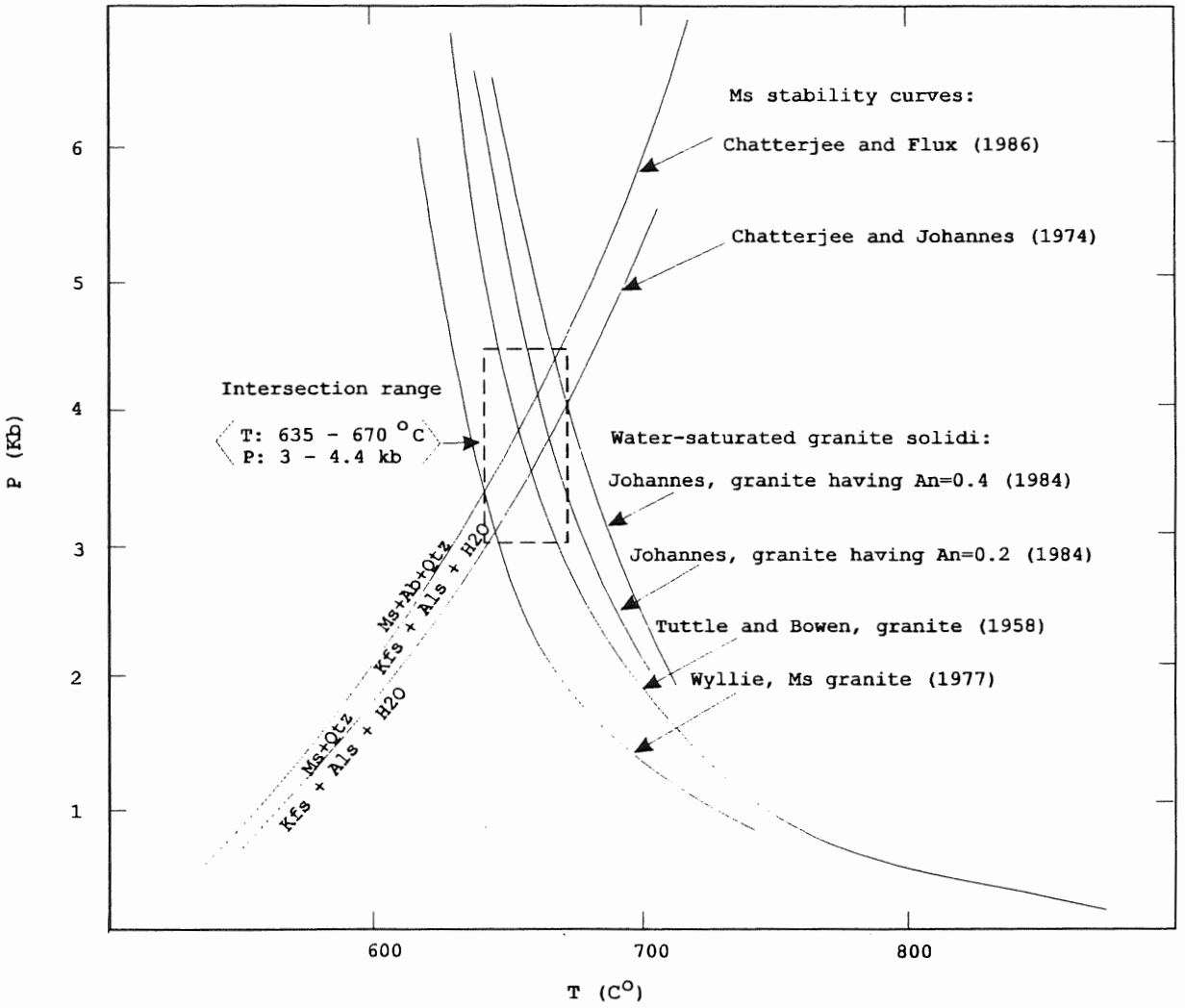

Figure 4.1 Compilation of P-T plots of muscovite equilibrium and granite solidi. Temperature of the intersections range from 635 to 670 °C; pressure from 3 to 4.4 Kb. Special abbreviation used: Als = aluminum silicate polymorph.

4.3 Muscovite in the Halifax Pluton

4.3.1 *Muscovite Occurrences and Zoning*

Fine - grained, and some parts of coarse-grained, muscovite - biotite leucomonzogranite and some parts of muscovite - biotite ± cordierite leucomonzogranite contain up to 10% modal muscovite (MacDonald & Horne, 1988). Other HP rocks include only 1% to traces of muscovite. Large (4 - 10 mm) euhedral muscovite crystals exist in the muscovite - biotite leucomonzogranite. In thin section the muscovite crystals are euhedral or subhedral with clean terminations, are not enclosed in other minerals, and do not enclose other minerals (Figs. 4.2a-b). Also muscovite - biotite ± cordierite leucomonzogranite, muscovite - biotite leucomonzogranite, and other phases contain secondary muscovite (Fig. 4.2c); Table 4.1 compares characteristics of muscovite in the HP with criteria for identification of magmatic muscovite.

Common thin - sectioning techniques seldom preserve good muscovite crystals. Zoning in muscovite is difficult to see in normal thin sections and has probably been overlooked in many peraluminous granites. Primary - looking muscovites from two phases, muscovite - biotite ± cordierite leucomonzogranite and muscovite - biotite leucomonzogranite, were collected to make 'special' thin sections (first by Roycroft's method, then as a polished section) for studying complete zoning patterns in muscovite, because complete (001) faces of muscovite in the normal thin sections are rare. One zoned muscovite crystal from

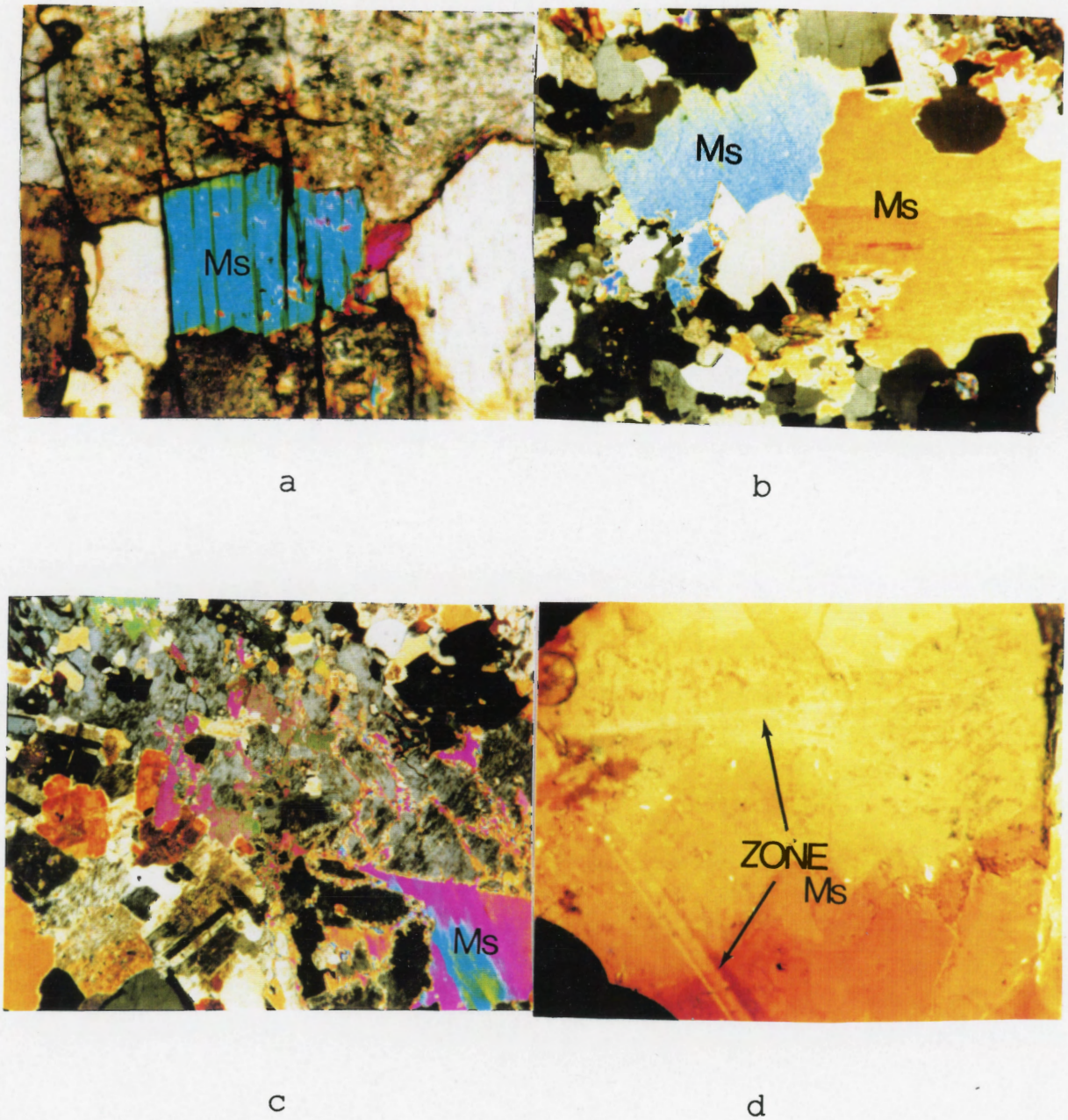

Figure 4.2 Photomicrographs of muscovite from the HP. Length for a-c: 1.3mm, for d: 6.5mm. a: subhedral Ms from Unit 1 (D12-0134-2); b: Ms in Unit 5 (D12-0124-3); c: secondary Ms from Unit 5 (103-3); d: zoned Ms from Unit 3 (MD-4).

Table 4.1 Characteristics of muscovite in the HP and comparison with criteria of magmatic muscovite

Type	Rock	Characteristics of crystals	References
Magmatic	Peraluminous granitoids	Grain size comparable to other magmatic minerals; subhedral to euhedral, with sharp terminations, no reaction - relation textures with other minerals, relatively abundant, absence of inclusions of accessory minerals.	Miller et al. (1981)
Magmatic	Unit 5, some areas of Unit 3 in the HP	Large compared to other rock - forming minerals, high modal percentage (up to 5-8%), euhedral on the outcrops, some euhedral in thin sections; some intergrowths with biotite;	This study
Second-ary	All rocks in the HP	Fine - grained, anhedral, enclosed in other minerals, in cores or along cleavages; cordierite readily altered to Ms + Bt.	This study

muscovite - biotite ± cordierite leucomonzogranite displays zoning (Fig. 4.2d) similar to that observed by Roycroft (1989, 1991).

4.3.2 *Muscovite Chemistry*

Microprobe spot analyses along two traverses in the zoned crystal (Fig. 4.2d) showed compositional changes from core to rims. Figure 4.3 shows sharp decreases in Ti, smooth decrease in Fe and abrupt increase in Mg from core to rims.

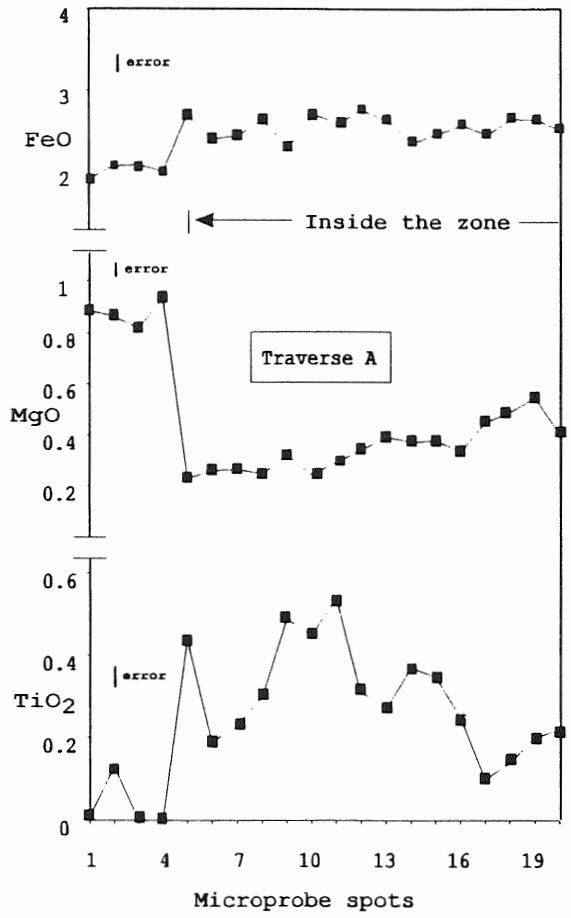

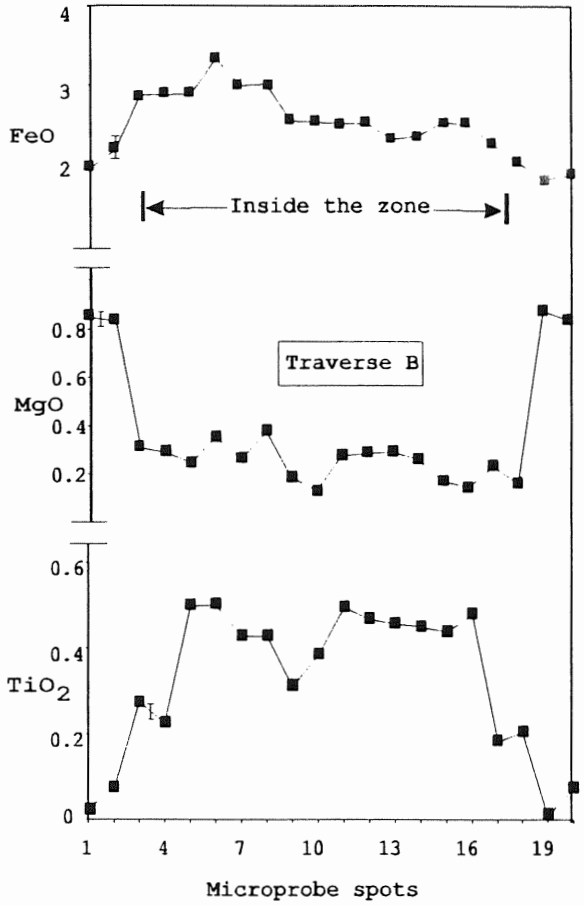

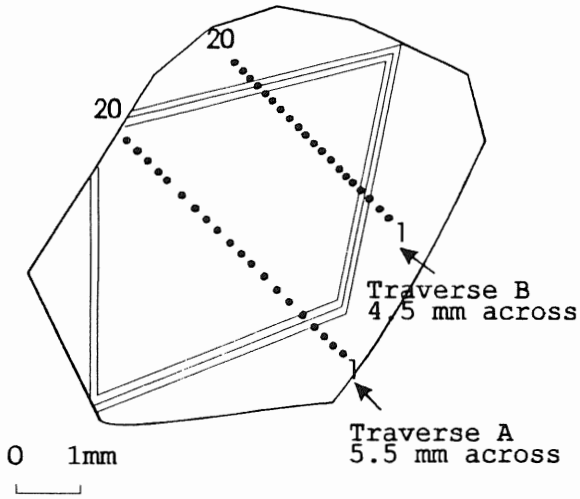

Zoned muscovite from Bt-Crd leucomonzogranite of the HP. The traverses of microprobe analysis spots begin at the the lower right, going from spot 1 to spot 20.

Figure 4.3 Elemental variations across the zoned muscovite from Unit 3 (MD-4), error bars = 0.13, 0.05, and 0.05 respectively for FeO, MgO, and TiO_2. Note that sharp changes in FeO, MgO, and TiO_2 are just outside the zone, and FeO and TiO_2 vary inversely to trends of MgO.

Table 4.2 lists the microprobe results for muscovite from the HP. The muscovite is rich in Al and deficient in Fe compared with muscovite from other granitoid rocks listed in Table 4.3 and formulas differ from the ideal stoichiometry $KAl_3Si_3O_{10}[OH]_2$. Muscovite from the aplite contain lower Ti and higher Si and Al than that from other phases (Table 4.2) and this chemical difference demonstrates consistent relationships between the average composition of muscovite and the whole rocks. Average weight percentages of TiO_2 changes in rocks from 0.44 (wt %) in Unit 2 to 0.05 in the aplite and in the relevant muscovites from 0.45 (wt%) to 0.01; SiO_2 from 70.09 (Unit 2) to 75.79 (aplite) (Table 2.3) in the rocks and from 45.97 to 46.9 in the relevant muscovites. The relationship can also be found in Al, Fe, Mn, and Mg.

4.4 Discussion and Conclusions

4.4.1 *Origins of HP Muscovites*

The texture of the HP primary - looking muscovite crystals (euhedral or subhedral shape, grain size, sharp rims) is probably the strongest evidence for an igneous origin (Miller et al., 1981).

Secondary muscovite prevails in the HP. Secondary muscovite crystals can be recognized by the following features: (1) their enclosure in other minerals; (2)fine - grain size, and (3) anhedral shape. Muscovite in a single granitoid unit (or even in

Table 4.2 Mean muscovite compositions (wt%)

Sno.	Phases	Points	SiO_2	TiO_2	Al_2O_3	FeO	MnO	MgO	Na_2O	K_2O
MD-2B	aplite	20	46.9	0.01	37.06	1.52	0.01	0.57	0.63	9.47
103-3	Unit 5	17	44.75	0.01	33.72	2.76	0.06	0.75	0.93	10.12
103-3	Unit 5	19	44.83	0.18	32.93	2.84	0.09	0.76	0.81	10.02
MD-4	Unit 4	47	45.71	0.15	34.61	2.35	0.03	0.6	0.91	10.08
D12-0011	Unit 4	19	46.08	0.17	34.32	1.82	0.04	1.08	0.68	10.58
DO5-0012	Unit 2	12	45.97	0.45	35.73	1.38	0.01	0.74	0.63	10.29

Table 4.3 Some representative muscovite formulas from four HP phases, and from some igneous muscovites analysed by other workers.

Formulas	References
$K_{0.79}Na_{0.08}Fe_{0.08}Mg_{0.06}Ti_{0.00}Al_{2.86}Si_{3.07}O_{11}$	MD-2B (aplite), this study
$K_{0.89}Na_{0.12}Fe_{0.16}Mg_{0.08}Ti_{0.00}Al_{2.73}Si_{3.08}O_{11}$	103-3 (Unit 5), this study
$K_{0.88}Na_{0.11}Fe_{0.16}Mg_{0.08}Ti_{0.01}Al_{2.69}Si_{3.10}O_{11}$	103-3 (Unit 5), this study
$K_{0.87}Na_{0.12}Fe_{0.13}Mg_{0.06}Ti_{0.01}Al_{2.75}Si_{3.08}O_{11}$	MD-4 (Unit 4), this study
$K_{0.91}Na_{0.09}Fe_{0.10}Mg_{0.11}Ti_{0.01}Al_{2.72}Si_{3.1}O_{11}$	D12-0011 (Unit 4),this study
$K_{0.87}Na_{0.08}Fe_{0.08}Mg_{0.07}Ti_{0.02}Al_{2.80}Si_{3.06}O_{11}$	DO5-0012 (Unit 2),this study
$K_{0.88}Na_{0.09}Fe_{0.23}Mg_{0.06}Ti_{0.03}Al_{2.62}Si_{3.12}O_{11}$	Miller et al.(1980)
$K_{0.93}Na_{0.04}Fe_{0.27}Mg_{0.11}Ti_{0.01}Al_{2.49}Si_{3.19}O_{11}$	Miller & Stoddard (1978)
$K_{0.92}Na_{0.05}Fe_{0.28}Mg_{0.12}Ti_{0.04}Al_{2.46}Si_{3.17}O_{11}$	Sylvester et al. (1978)
$K_{1.03}Na_{0.06}Fe_{0.24}Mg_{0.09}Ti_{0.04}Al_{2.63}Si_{3.05}O_{11}$	Nelson & Sylvester (1971)
$K_{0.92}Na_{0.06}Fe_{0.18}Mg_{0.11}Ti_{0.05}Al_{2.57}Si_{3.13}O_{11}$	Whitney et al. (1976)
$K_{0.96}Na_{0.05}Fe_{0.25}Mg_{0.17}Ti_{0.04}Al_{2.48}Si_{3.14}O_{11}$	Miller & Kish (1980)
$K_{0.94}Na_{0.02}Fe_{0.30}Mg_{0.29}Ti_{0.03}Al_{2.23}Si_{3.26}O_{11}$	Wedemeyer & Spruill (1980)

one single thin section from that unit) can be the product of two different origins. However, in some locations within the HP (Unit 5 and some parts of Unit 3), primary muscovite is dominant relative to secondary muscovite.

4.4.2 *Zoning in Muscovite*

No discussion on the causes of zoning in muscovite exists in the literature. Many factors such as pressure, temperature, composition, and rate of ionic diffusion have been proposed as causes of zoning in various minerals. Abrupt changes in bulk compositions of the melt, in temperature, and in pressure can change the crystallization habit or the element absorption rate of the crystal.

The starting or stopping of crystallization of some minerals can lead to changes in bulk composition of the local melt. In the rock, apatite, cordierite, and biotite are minerals which incorporate Ti, Fe, and Mg, and can change the melt composition in those elements. Cordierite crystallization consumes Mg, hence the completion of that crystallization could lead to changes in the Mg intake into crystallizing muscovite. If biotite and apatite (the latter closely coexists with biotite) began crystallizing during muscovite crystallization and so decreased the local melt content in Ti and Fe, this would decrease the intake of those elements by muscovite. But this process is unlikely given the large P - T stability field for biotite, and its occurrence as inclusions in plagioclase and quartz.

The MgO - rich rims could not have resulted from abrupt rise in temperature because of later intrusive of Unit 5 melt, for the muscovite core grew at high temperature but was poorer in Mg and richer in Ti and Fe than the rims (Fig. 4.3).

Abrupt decreases in Ti and Fe, and an abrupt increase in Mg apparently define zoning in muscovite (Fig. 4.3). The local composition of the melt can change as a result of penetration of foreign melt or liquid rich in Mg and poor in Fe and Ti relative to the muscovite - biotite ± cordierite leucomonzogranite (Unit 4) melt which formed the core of the zoned muscovite. However, this hypothesis is unlikely because there is no physical evidence to show this penetration happened.

4.4.3 *A Pressure Indicator*

Experimental data indicate that the breakdown curves of ideal muscovite and the minimum melting curves for "granite" intersect at 3 - 4.4 kb, i.e.,11.5 - 16.9 km, assuming 10 km = 2.6 kb (Day, 1973; Luth et al., 1964; Miyashiro, 1973; Thompson, 1974). This has prompted some workers to use the presence of "primary - looking" muscovite as an indicator of depth of granite crystallization. But this conclusion contradicts the evidence of magmatic muscovite in many granites formed at shallow levels (≅1 - 2 kb, i.e., 3.8 - 7.7 km) (Zen, 1988). Primary - looking muscovite is not rare in granitic rocks which apparently crystallized at depths as shallow as 8 - 9 km (Miller et al., 1981). The zoning from the core to rims in muscovite proves that

this mineral had a history of crystallization, which zoning indeed indicates that the muscovite nucleated and grew throughout, up to the final stage of magma solidification, at shallow depths (< 2 kb, = 7.7 km, Roycroft, 1989, 1991).

Miller et al. (1981) suggested that high Ti content in muscovite indicates an igneous origin, because it would increase muscovite stability and thus decrease the minimum depth at which it can crystallize from the granitic melt, an idea they later abandoned when they showed experimentally that TiO_2 does not enhance muscovite stability (Miller et al. 1989). In our primary - looking muscovite of muscovite - biotite leucomonzogranite, the Ti concentration approaches zero (Table 4.2). Hence, it is doubtful indeed that high Ti content in muscovite indicates a magmatic origin.

If we consider that the field data indicating a shallow depth of intrusion for many plutons are true, then the following explanation is possible. Magma rich in H_2O and with high A/CNK can have a low muscovite-in curve, thus it may crystallize at lower pressure. Muscovite - biotite leucomonzogranite, containing abundant magmatic muscovite, is characterized by higher A/CNK and H_2O (1.27 and 0.71 wt% respectively) than any other phases in the HP (see Chapter 2). The experiment of Wyllie (1977) demonstrates indeed a lower solidus curve for peraluminous granite than for haplogranite granite (Tuttle & Bowen, 1958; see Figure 4.1).

4.5 Summary

In some locations within the HP (Unit 5, and in some parts of Unit 3), magmatic muscovite is dominant relative to secondary muscovite. Magma rich in H_2O and with high A/CNK can have a low solidus temperature for muscovite.

One muscovite crystal from Unit 3 near the contact between Unit 3 and Unit 5 shows sharp decreases in Ti and Fe and an abrupt increase in Mg from internal zone to external zone. An abrupt change in the composition of local magma may result in the zoning.

Chapter 5 Cordierite

5.1 Introduction

This chapter examines the general occurrences and zoning of cordierite in igneous rocks and relates these features to relevant experimental work. It then reports specific examples of cordierite in the Halifax Pluton, and discusses their importance.

Cordierite is a silicate mineral which contains six - membered rings of linked SiO_4 tetrahedra, with each SiO_4 group sharing two oxygens with adjoining tetrahedra on either side. The formula is $Al_3(Mg,Fe)_2(AlSi_5O_{18})\cdot nH_2O$ which has three Al atoms in six - coordination, the fourth substitutes for one Si in the ring structure, giving an $AlSi_5O_{18}$ group. Water molecules exist within the ring structure. Some substitution of Mg by Fe^{+2} or Mn occurs. Cordierite is commonly altered to some form of mica, chlorite, or talc and is then various shades of grayish - green.

5.2 Cordierite in Igneous Rocks

5.2.1 *Cordierite Occurrences*

Cordierites occur in different igneous rocks, such as pegmatites (Heinrich, 1955), aplites (MacDonald, 1981), and various types of granites (MacDonald, 1981; Morin & Turnock, 1975; Speer, 1981; Taubeneck, 1964). Clarke (1981) and Zen (1988) suggested that cordierite is an indicator of strongly peraluminous granites. White et al. (1986) stated that cordierite is restitic and is one of the important indicators of

S - type granites. Speer (1981) found that magmatic cordierite from granitoid plutons in the southern Appalachians is euhedral and contain high sodium content and that the coexisting biotite has a high aluminum composition compared with biotite in cordierite - free granitoid rocks. A magmatic origin is also the best explanation for the textural features and chemical trends of most of the cordierite from the Strathbogie batholith in Australia (Phillips et al.,1981).

Birch & Gleadow (1974) showed that the small iron - rich cordierite crystals in the Victoria rhyodacites (Australia) were derived from refractory garnet - bearing residues which formed cordierite as the magma intruded to higher crustal levels.

Granitoid rocks indeed contain a great deal of variation in the texture of cordierite. Texturally the cordierite in these rock types is anhedral to euhedral, interstitial or prismatic, 1 mm to 5 cm in diameter, inclusion - rich to inclusion - poor, and fresh to completely replaced by alteration products. Clarke (1994), in a paper on the diversity of cordierites, summarizes cordierite occurrence and its reactions with other minerals, and shows that felsic igneous rocks contain at least five types of cordierites (metamorphic, peritectic magmatic, cotectic magmatic, fluido - magmatic, and metasomatic). Table 5.1 summarizes the characteristics of cordierite types (Clarke, 1994).

Table 5.1 Characteristics of cordierites in felsic igneous rocks (Clarke, 1994)

Origin	*Spatial, Mineralogical, and Textural Characteristics*
Metamorphic (Xenocrystic or restitic)	spatial correlation between cordierite in granites and cordierite in country rocks and/or enclaves; anhedral to euhedral grain shapes; small grain size; in clots with, or with inclusions of, fibrous sillimanite, spinel, foliated biotite; chemical zonation of cordierite (Mg - rich core, Fe - rich discordant rims)
Peritectic Magmatic	most readily identified spatially in leucosomes (and/or melansosomes) of migmatites; early cordierites may have rounded quartz inclusions in core; larger grain size
Cotectic	euhedral grain shapes, few inclusions, grain size compatibility with host rock
Fluido-Magmatic	large grain size; subhedral to euhedral grains associated with aplite - pegmatite contacts, in miarolitic cavities and / or pegmatite cores
Subsolidus Metasomatic	distribution along structural weaknesses in granites; commonly within leucocratic biotite - free haloes; possible pseudographic intergrowths with quartz

Table 5.2 Distinguishing criteria for magmatic and metamorphic cordierites

Origin	*Spatial, Mineralogical, Textural, and Chemical Characteristics*	*References*
Magmatic	euhedral grain shapes, few inclusions, grain size compatibility with host rock; M/(F+M) < 0.5, Na_2O > 1 (wt %); zoning pattern: rims rich in the ratio M/(M+F)	Birch & Gleadow, 1974 Clarke (1994) Flood & Shaw, 1975 Leake, 1960 Maillet, 1984 This study
Metamorphic	spatial correlation between cordierite in granites and cordierite in country rocks and/or enclaves; anhedral to euhedral grain shapes; small grain size; in clots with, or with inclusions of, fibrous sillimanite, spinel, foliated biotite; M/(F+M) > 0.5, Na_2O < 1 (wt %); chemical zonation of cordierite (Mg - rich core, Fe - rich discordant rims)	Clarke (1994) Flood & Shaw, 1975 Leake, 1960 Maillet, 1984 This study

For practical use, Table 5.2 sets up criteria, including spatial, textural, chemical, and zoning characteristics (see the following review of chemical and zoning characteristics of cordierite), for distinguishing between magmatic and metamorphic cordierite.

5.2.2 *Relevant Experiments*

High pressure experimental studies on a pelitic component (Green, 1976) demonstrated that, at temperatures from 850 to 950 °C and pressures below 6 kb, with a water content of 2.5% and a M/(M+F) ratio of 0.3 - 0.4, cordierite is an important residual phase during the partial melting that produces a granitic melt. Cordierite is also in equilibrium with garnet from 6 to 7 kb. From this work, Green (1976) concluded that a suite of cordierite - and garnet - bearing granitic rocks in eastern Australia derived from partial melting of pelitic metasedimentary rocks at depth.

More experimental work (Clemens & Wall, 1981) showed conclusively that, at pressures of 1 - 2 kb, cordierite crystallizes over a wide range of temperature and water contents in the silicate melt. At 5 kb, cordierite crystallizes at low - temperature, near - solidus conditions. According to Clemens & Wall (1981) and Clarke (1981), the overlap of the stability field of cordierite and the stability field of granitic melt indicates a potential primary origin for cordierite. The actual crystallization of cordierite from a peraluminous granitic melt

depends on temperature, pressure, the different compositional variables, and the degree of water saturation of the melt (Clarke, 1994).

5.2.3 *Cordierite Chemistry*

Ideally, the composition of pure magnesium cordierite consists of 13.8% MgO, 34.9% Al_2O_3 and 51.3 % SiO_2, and the composition of pure iron cordierite consists of 22.2 % FeO, 31.5% Al_2O_3 and 46.3% SiO_2. Cordierite occurring in metamorphic rocks is usually richer in Mg than Fe^{2+}, whereas igneous cordierite has been found with up to 15% FeO (Heinrich, 1965).

Small amounts of Fe^{3+}, Mn, Ca, Na, and K are also present in many cordierites (Heinrich, 1965). Cordierite from metamorphic rocks generally contains less than 0.5 wt% Na_2O, whereas cordierites from quartz veins, pegmatites, and granites have a sodium content which ranges from 0.61 to 3.53 wt% (Flood & Shaw, 1975; Leake, 1960).

Magmatic cordierite from pegmatite has a low M/(F+M) ratio of 0.27 and contains 1.08 wt % Na_2O (Maillet, 1984). Cordierite crystals occurring in the Meguma metasedimentary rocks of the contact aureole are small (1 - 3 mm), inclusion - rich, and ovoid. Chemically, they have a high M/(F+M) ratio of 0.58 to 0.62 and lack Na_2O (Maillet, 1984). Birch & Gleadow (1974) reported that magmatic cordierite in the Victoria rhyodacites has a low M/(F+M) ratio ranging from 0.10 to 0.30.

5.2.4 *Review of Cordierite Zoning*

In a review of AFM minerals, Clarke (1981) mentioned that cordierites are usually unzoned or weakly zoned. Zoning in cordierite is unrecognizable by colour or birefringence, but cordierite has potential for zoning, owing to different structural states and ionic substitutions (Phillips & Griffen, 1981). However, only a few authors have reported zoned cordierite. Birch & Gleadow (1974) first reported zoned cordierite phenocrysts (with Mg enrichment and Fe, Mn depletion in margin) in rhyodacites from Australia. The value of M/(M+F) increases from 0.07 at cores to 0.29 at rims. Puziewicz & Johannes (1988), in experiments on water - saturated peraluminous granitic systems, obtained zoned cordierites with magnesium contents increasing towards their margins. The chemical variations of M/(F+M) from core to rims in nine analysed samples fall in a range from 0.37 to 0.79.

5.3 Cordierite in the Halifax Pluton

5.3.1 *Cordierite Occurrences*

Cordierite is unevenly distributed in most rocks of the Halifax Pluton; in parts of muscovite - biotite ± cordierite leucomonzogranite, biotite ± cordierite monzogranite, and the aplite, it may exceed 5% of the mode, forming cordierite - rich sub - zones within the zoned HP (MacDonald & Horne, 1988). In outcrop, cordierite is usually black where fresh and greenish black where replaced by chlorite and muscovite. The aplite

contains fresh cordierite, but in other rocks fresh cordierite is rare.

The crystal size of cordierite in muscovite - biotite ± cordierite leucomonzogranite and biotite ± cordierite monzogranite is different from that in the aplite. Cordierite in the aplite is small (~ 1 mm in diameter), but in muscovite biotite ± cordierite leucomonzogranite and biotite ± cordierite monzogranite cordierite with a short - prism shape can reach 2 cm in length.

In this study two main types (*Type 1:* magmatic and *Type 2:* metamorphic) of cordierites are recognized. *Type 1* has two different textural expressions: *Type 1-A,* euhedral and containing rare inclusions (Fig. 5.1a, b); *Type 1-B*: large grains consisting of an inner euhedral cordierite crystal surrounded by an outer euhedral crystalline cordierite overgrowth. The whole grain contains many inclusions of biotite and quartz, a euhedral cordierite in the centre, and some biotite crystals arranged along the margin of the inner crystal of cordierite (Fig. 5.1c). *Type 2* cordierite is anhedral and has biotite reaction margins (Fig. 5.1d).

5.3.2 *Cordierite Chemistry*

Characteristics

Cordierites from the HP have an M/(F+M) ratio of 0.23 to 0.52 and contain Na_2O from 0.81 to 1.29 wt% (Table 5.3). The

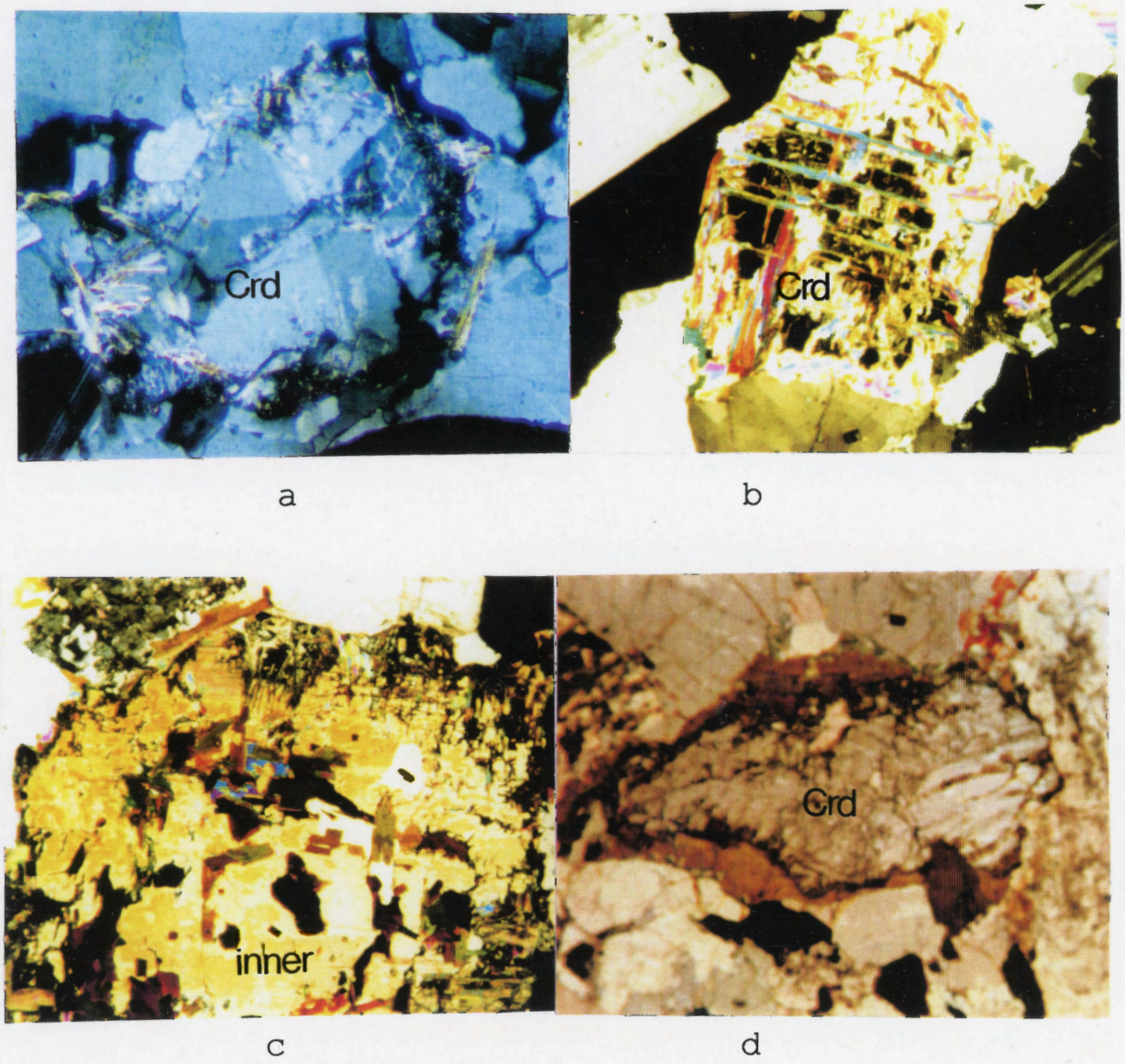

Figure 5.1 Photomicrographs of cordierite from the HP, a: Type 1-A cordierite from the aplite (MD-2B), small and euhedral, showing a sixling twin and fringe - like alteration along crystal rims, length of the photo is 5.2 mm. b: Type 1-A cordierite from biotite ± cordierite monzogranite, subhedral, short prismatic ; length of the photo is 3 mm. Crossed polarizers for both photos. c: Type 1-B cordierite from biotite ± cordierite monzogranite, is large and euhedral and has an inner crystal of euhedral cordierite and contains many biotite, quartz inclusions. Crossed polarizers. Length of the photo is 5.4 mm. d: Type 2 cordierite from biotite ± cordierite monzogranite (DO5-0002) is anhedral and has a biotite reaction rim. Length of the photo is 2.8 mm, plane polarizer.

Na_2O abundance (1.27 - 1.29 wt %) in *Type 1-A* cordierite is high enough to be compared with that in magmatic cordierite as indicated in Table 5.2, and its M/(F+M) ratio ranges from 0.23 to 0.34. *Type 1-B* cordierite has a higher M/(F+M) ratio (0.48) compared to that of above magmatic cordierite, but its Na_2O content (1.26 wt %) is comparable to the standard of magmatic cordierite. *Type-2* cordierite is poor in Na_2O (0.81 wt %) and has a high M/(F+M) ratio (0.52).

Table 5.3 Mean value of cordierites from the HP

Type	Sample	Rock	SiO_2	Al_2O_3	FeO	MnO	MgO	Na_2O	M/(F+M)
Type 1-A	MD-2B	Aplite	47.62	32.3	14.78	1.54	2.46	1.29	0.23
	MD-2B	Aplite	45.06	30.74	13.18	1.13	2.8	1.27	0.34
Type 1-B	306-2	Unit 4	48.15	32.06	10.96	0.75	5.75	1.26	0.48
Type 2	DO5-0002	Unit 4	48.2	32.04	10.37	0.84	6.4	0.81	0.52

Zoning

Microprobe traverses across the centre of two *Type 1* grains show somewhat erratic compositional changes with MgO - rich rims (Figs 5.2, 3). The intersection of sixling twinning in the crystals helps to position microprobe traverses across the centre of cordierite grains.

Microprobe analyses detect three sections (I - III) of chemical variations from core to rims across *Type 1-B* grain (Figure 5.4). Section I: the rims of the outer crystal. They are slightly enriched in M/(M+F) compared to the contacts with inner crystal; Section II: the rims of inner crystal. They

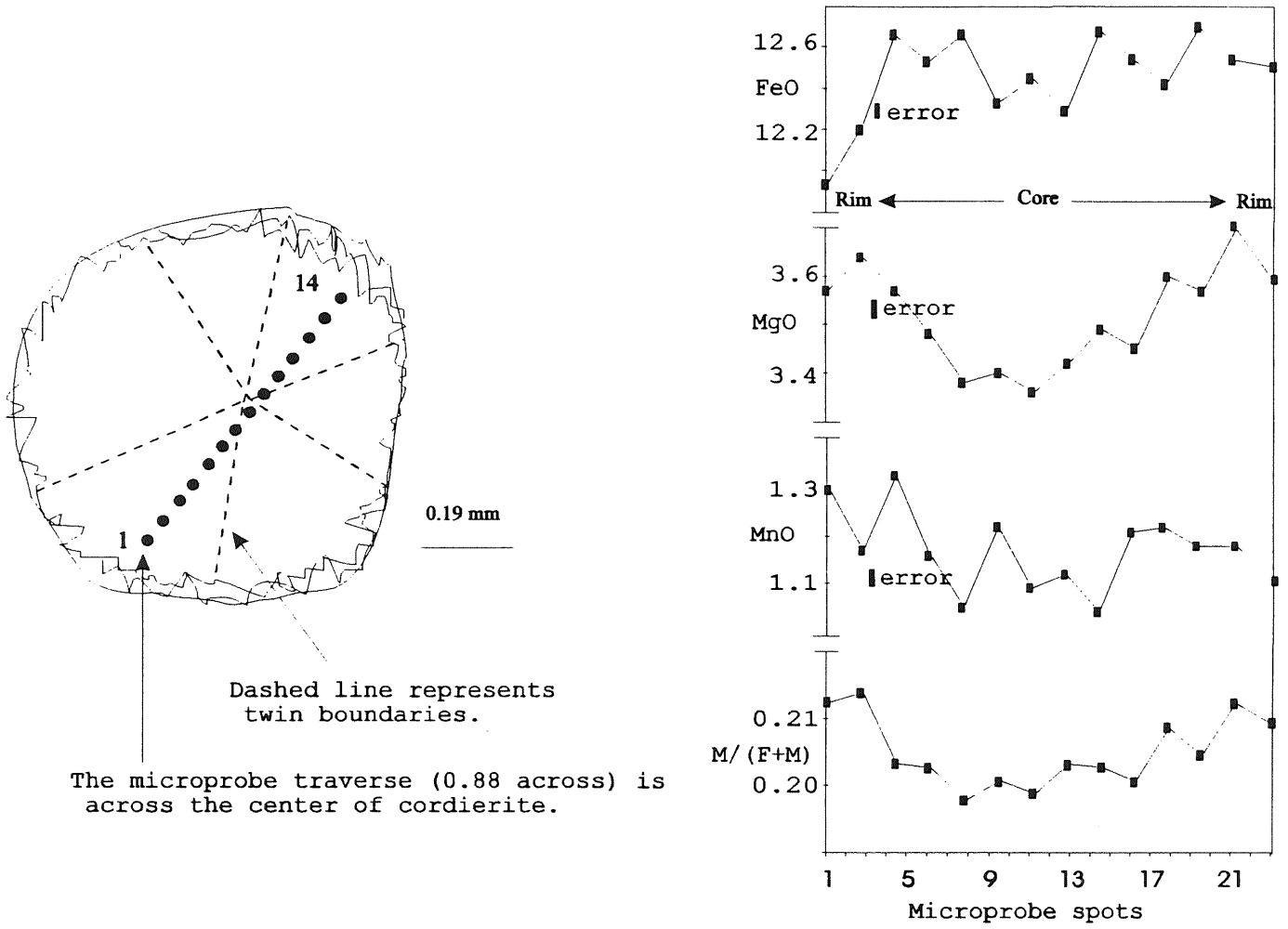

Figure 5.2 Elemental variation across a Type-1A cordierite (left: its crystal outline) from the aplite (MD-2B). Error bars = 0.29, 0.07, 0.04 respectively for FeO, MgO, and MnO. The pattern shows rims rich in MgO and M/(F+M), and rims poor in FeO.

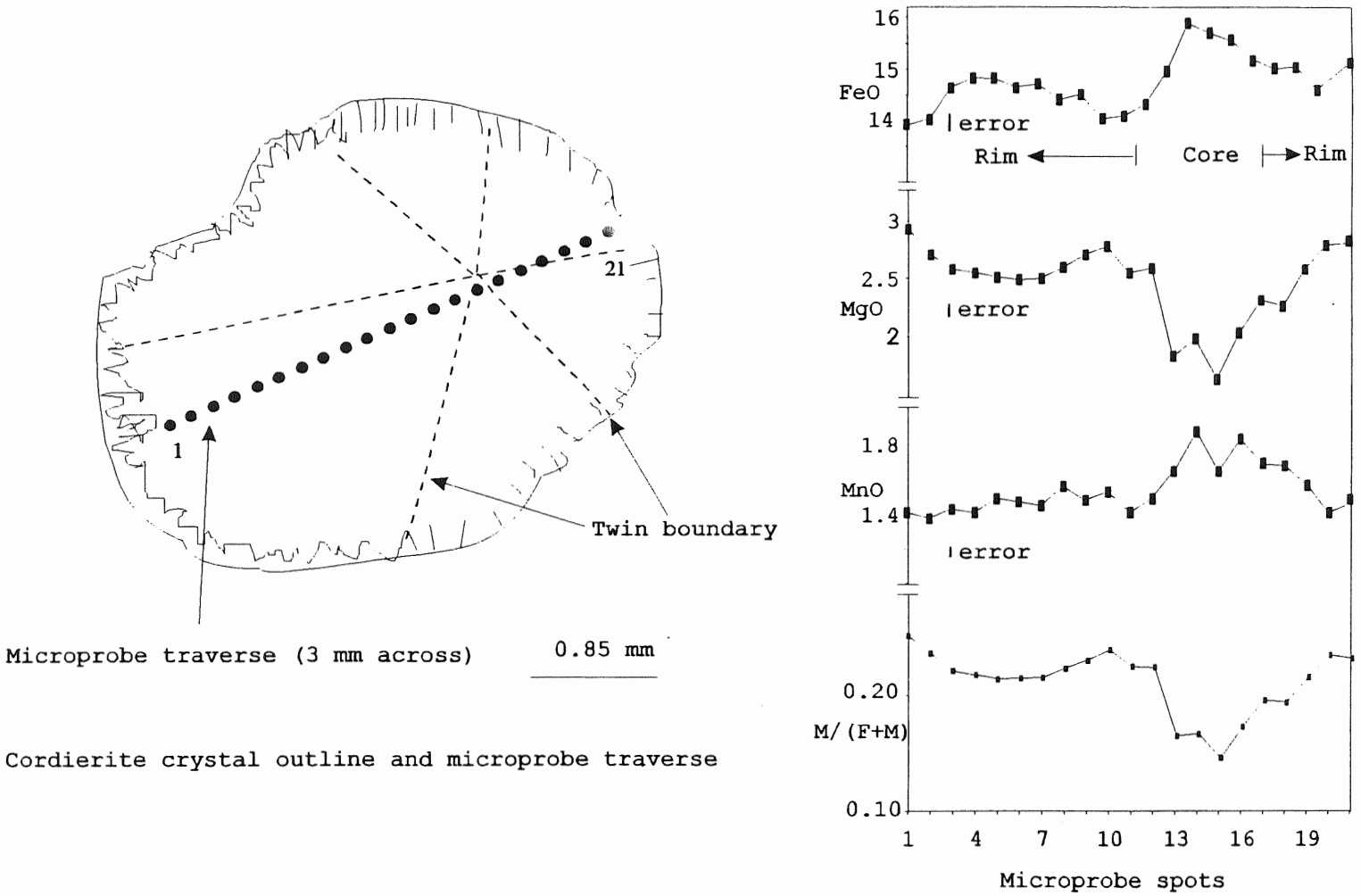

Figure 5.3 Elemental variation across a Type 1-A cordierite crystal from the aplite (MD-2B) (left: outline and microprobe traverse; right: variations). Error bars = 0.29, 0.07, 0.04 respectively for FeO, MgO, and MnO. The rims are richer in M/(F+M) ratio than the core.

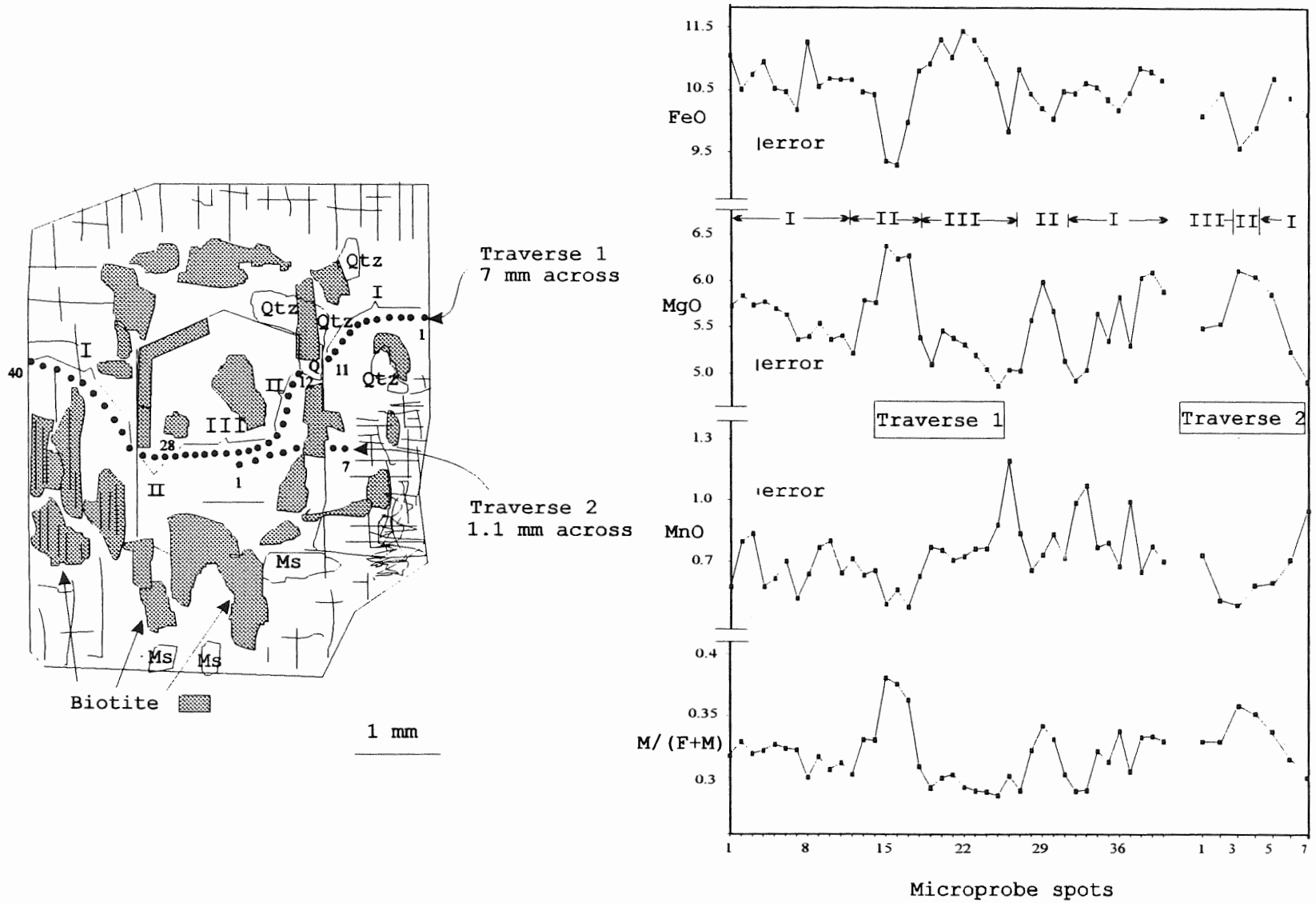

Figure 5.4 Elemental variations along two traverses across a Type-1B cordierite grain from Bt ± Crd monzogranite of the HP. (left: its outline and microprobe traverses). I, II, III denote microprobe sections. Error bars = 0.21, 0.14, and 0.03 respectively for FeO, MgO, and MnO.

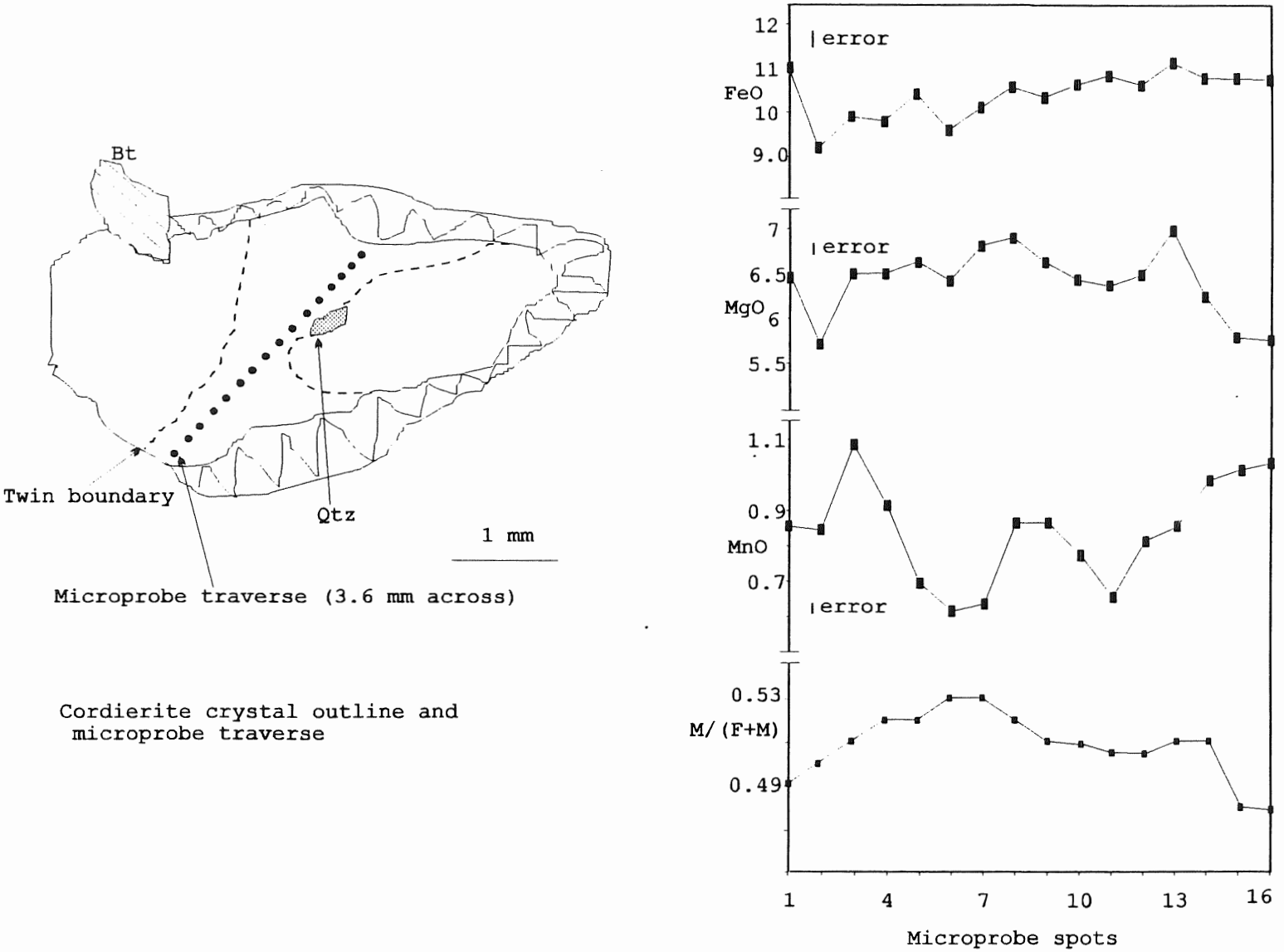

Figure 5.5 Elemental variation across a Type 2 cordierite (left: crystal outline) from Bt ± Crd monzogranite (DO5-0002), showing W-shape pattern for Mn, and rims poor in M/(F+M). Error bars = 0.22, 0.07, and 0.04 respectively for FeO, MgO, and MnO.

are characterized by highest peaks of the ratio M/(M+F); Section III: the core of inner crystal. Its ratio M/(M+F) is lower than the other two sections. Figure 5.5 shows that zoning pattern of *Type-2* cordierite is different from that of *Type 1*, with rims poor in M/(M+F) and with a W - pattern for Mn.

5.4 Discussion and Conclusions

5.4.1 *Origin of Type 1-A Cordierite*

Type 1-A cordierite of the Halifax Pluton has textural features of magmatic cordierite (euhedral or subhedral, with perfect sixling twins, and without inclusions) and M/(F+M) increases towards the rims. Birch & Gleadow (1974) found zoned cordierite phenocrysts in acid lava from Australia, with rims enriched in Mg and depleted in Fe and Mn and they interpreted this zoning pattern as a magmatic type. Puziewicz & Johannes (1988), in their experiments on water - saturated peraluminous granitic systems, obtained zoned cordierites with the ratio M/(F+M) increasing towards their margins.

However, the problem is that the chemical zonation does not match the expected trend of magmatic evolution (MgO increases from early - to late - stage unit, but M/(F+M) does not change; see Table 2.3). This discrepancy may mean that (1) the chemical variation in the cordierite is not the result of magmatic differentiation of the HP; or (2) the chemical variation of the cordierite is the result of magmatic differentiation, but

changing P_{H2O}, temperature, and compositional variations of magma influence the K_D of MgO from core to rim.

Wood (1973) showed that P_{H2O} has an important influence on the partitioning of Fe and Mg between coexisting garnet and cordierite. The relation is such that any decrease in P_{H2O} would lead to crystallization of a more Mg - rich cordierite, such as is observed in the margins of zoned cordierite. The Type 1 cordierite coexists with garnet and two reasons can cause decrease of water pressure: (1) magma crystallization of biotite and (2) the emplacement of magma into the upper crust.

The textural features, the zoning pattern, and chemical characteristics (high Na_2O and low M/(F+M), Table 5.3) indicate that *Type 1-A* cordierite is a magmatic mineral which may have a cotectic crystallization relationship with other rock minerals.

5.4.2 *Origin of Type 1-B Cordierite*

The inner crystal of *Type 1-B* cordierite shows euhedral form against which an array of biotite and quartz grains aligns (Figure 5.4). These textural characteristics suggest that *Type 1-B* cordierite is of magmatic origin. The chemical variation across it appears to be a magmatic zoning pattern (same as in *Type 1-A*) with rims rich in M/(F+M) (Section II). The overgrowth of more cordierite over the inner crystal indicates a complex history of magmatic evolution, with this overgrowth suggesting two stages of crystallization: (1) nucleation and crystallization

from the magma and (2) further growth over the early central crystal.

Both these stages belong to the magmatic evolution, for two reasons: (1) both the inner crystal and overgrowth show trends of M/(F+M) increase (Fig. 5.4: sections I and II of traverse A) from core to rims, the pattern of magmatic cordierite; (2) the "inner" and "outer" crystals intergrew with biotite and quartz. The relationship between cordierite and the coexisting phases can be expressed by the following equation:

$$L \rightarrow Crd + Bt + Qtz + Feldspars$$

5.4.3 *Implication of Chemical Difference*

Type 1 cordierites discussed above are from two different phases of the HP: the aplite and biotite ± cordierite monzogranite. It is interesting that cordierite from aplites is higher in Fe and lower in Mg than cordierite from biotite ± cordierite monzogranite (Table 5.3).

Distribution coefficients (K_D) for Fe and Mg between cordierites and host whole rocks (≅ melt) are very different: $K_D^{FeO} = [10.67/2.95]_{Crd\text{-}Bt\ mz} = 3.6$, $K_D^{FeO} = [13.98/0.93]_{aplite} = 15.03$, $K_D^{MgO} = [6.04/1.28]_{Crd\text{-}Bt\ Mz} = 4.72$, $K_D^{MgO} = [2.63/0.10]_{aplite} = 0.26$. These differences in K_D strongly suggest that cordierite in each aplite crystallized from a different magma pulse which had its own evolutionary history.

MacDonald & Horne (1988) divided the phases of the HP into two sequences (sequence A: biotite granodiorite, biotite monzogranite, biotite±cordierite monzogranite, muscovite - biotite ± cordierite leucomonzogranite; sequence B: muscovite - biotite leucomonzogranite) and suggested that the second sequence might result from a different pulse of magma. The aplite containing *Type 1-A* cordierite is similar to muscovite - biotite leucomonzogranite in texture and colour, and is different from the megacrystic sequence A rocks.

5.4.4 *Origin of Type 2 Cordierite*

Cordierite formed by cotectic crystallization has a euhedral or subhedral outline. *Type-2* cordierite does not have those characteristics, but has an anhedral outline which might have resulted from corrosion by later melt. Microprobe analyses across the centre of the crystal reveal a pattern different from that of magmatic cordierite. The elemental variation shows a W - pattern for Mn and rims poor in Mg, which might have resulted from metamorphic processes (formed the core) plus magma assimilation. The rims rich in MnO in the cordierite may reflect crystalline growth in a magma with increasing Mn/(Ca + Mn + Mg) (Fig. 2.5: the ratio changes from 0.011 to 0.045 from early - to late - stage rocks). This crystallization history of the cordierite is similar to that of garnet with the W - pattern for MnO (Clarke & Rottura, 1994). The zoning pattern of the cordierite and its anhedral form may support the conclusion that

Type-2 cordierite was a metamorphic xenocryst entrained into the magma, which then experienced a short period of magmatic crystallization producing MnO - rich rims.

5.5 Summary

Magmatic cordierite is euhedral or subhedral, shows grain size compatibility with other rock - forming minerals and contains few inclusions. Usually, the ratio M/(F+M) is less than 0.5, Na_2O is greater than 1 (wt %) and rims are higher in the ratio M/(F+M). Magmatic cordierites from the HP have an M/(F+M) ratio of 0.23 to 0.48 and contain Na_2O from 1.26 to 1.29 wt%.

A grain of cordierite consists of an inner euhedral cordierite crystal surrounded by an outer euhedral crystalline cordierite overgrowth. The continuing growth of more cordierite over the early central crystal indicates a complex history of magmatic evolution, with this overgrowth suggesting two crystallization stages which are indicated by the hiatus: (1) nucleation and crystallization from the magma and (2) growth over the early central crystal.

Chapter 6 Garnet

6.1 Introduction

This chapter reviews the general occurrence and zoning of garnet in silicic magmatic rocks and relates these features to relevant experimental work. It then examines specific garnet from the Halifax Pluton and discusses its origin.

Garnet is a nesosilicate consisting of isolated SiO_4^{-4} tetrahedra in the structure. Its general structural formula is $X_3Y_2(SiO_4)_3$, where the X site houses Ca, Mg, Fe^{+2}, or Mn^{+2} and the Y site incorporates Al, Fe^{+3}, and Cr^{+3} . The chemical differences among the main garnet species are reflected by their cations; pyrope, Mg_3Al_2, in which some Ca and Fe^{+2} are usually present; almandine, Fe_3Al_2, in which Fe^{+3} may replace Al and Mg may replace Fe^{+2}; spessartine, Mn_3Al_2, Fe^{+2} usually replaces some Mn^{+2} and Fe^{+3} some Al; grossular, Ca_3Al_2, in which Fe^{+2} replaces Ca, and Fe^{+3} replaces Al; andradite, in which $Ca_3Fe^{+3}_2$, Al may replace Fe^{+3}, Fe^{+2}, Mn^{+2} and Mg may replace Ca; and uvarovite, $Ca_3Cr^{+3}_2$.

6.2 Garnet in Igneous Rocks

6.2.1 *Garnet Occurrences*

Granitoid rocks contain different types of garnets. Garnets in silicic calc - alkaline volcanic and plutonic rocks are typically almandine - and / or spessartine - rich, although the pyrope end - member can be significant. The criteria for establishing a magmatic origin for garnet include: (1) euhedral

or subhedral, inclusion - free crystals (Allan & Clarke, 1981); (2) ragged and surrounded by a rim of quartz which suggests that the garnet has reacted significantly with the melt (Harrison, 1988); (3) compositions of the igneous range (spessartine > 10%) in the Mn - Fe - Mg system (Miller & Stoddard, 1981); and (4) reverse zoning (Mn - poor core and Mn - rich rim, Allan & Clarke, 1981). In metamorphic rocks idioblastic garnets can also exist free of inclusions (Augustithis, 1990: Figs. 40, 118, 119, 174, and 175), and may have reverse zoning (Edmunds & Atherton, 1971; Kretz, 1973). Synthesizing all the evidence is important in judging whether a garnet is of igneous or metamorphic origin.

6.2.2 *Review of Garnet Zoning*

Zoning is a common feature of metamorphic and igneous garnets (Allan & Clarke, 1981; Birch & Gleadow, 1974; Manning, 1983; Wang & Ding, 1990). The zoning in metamorphic garnet is probably caused by changes in growth matrix compositions, which set up concentration gradients at the growing faces of the garnet (Yardley, 1977). Metamorphic garnets can homogenize by cation diffusion at T > 600°C (Yardley, 1977).

The two main types of garnet zoning are reverse and normal. Metamorphic garnets are characterized by normal zoning (rims richer in Fe - Mg and poorer in Ca - Mn), and reverse zoning is characteristic of magmatic garnet (rims richer in Ca - Mn, poorer in Fe - Mg) (Allan & Clarke, 1981). The unusual garnet zoning is caused by assimilation of metamorphic rocks by magma (higher Mn

concentrations in the cores and rims than between the core and rim: Clarke & Rottura, 1994). Many authors have shown that high MnO stabilizes garnets in differentiated magmas (Hall, 1965; Miller & Stoddard, 1981). The regular increase of Mn content from cores to rims of garnets reflects the trend of magma evolution, i.e., corresponding to a progressive increase of the ratio Mn/(Fe+Mg) with differentiation in the magma.

However, zoning in magmatic garnets may be highly complex. Mn - rich cores and unzoned spessartine garnets reflect different crystal growth histories and diverse magmatic conditions (nucleation density, crystal growth rates, ionic diffusion rates). Rims poor in Ca, and M/(F+M) variation from cores to rims, occur in garnets of granites in the Ruby Mountains (Kistler et al. 1981), reflecting control by bulk composition of the melt, and changes of temperature and pressure. Local distribution of unzoned garnets in the Cairngorm granite results from precipitation of a compositionally homogeneous liquid at high temperature (Harrison, 1988).

6.2.3 *Experiments on Garnets*

Experimental work by Green & Ringwood (1986 a, b) showed that almandine garnet occurs as a liquidus or near - liquidus phase in melts of dacite and andesite composition at pressures above 9 kbar. They considered that such melts could have been derived by partial melting of the deep crust and /or the upper mantle at depths greater than 25 km, and also pointed out that

resorbed garnet phenocrysts in some calc - alkaline rocks may provide evidence for a deep origin of their magmas. Using glasses of pelitic composition and natural cordierite - and garnet - bearing granites, Green (1977) showed that Mn stabilizes garnet at lower pressures. He estimated that 20 - 25 mol. % spessartine stabilizes almandine - rich garnets at pressures corresponding to depths of 12 km or less.

6.3 Garnets in the Halifax Pluton

6.3.1 *Garnet Occurrences*

MacDonald & Horne (1988) reported garnets from three units: biotite monzogranite (Unit 2), muscovite - biotite ± cordierite leucomonzogranite (Unit 3), and biotite ± cordierite monzogranite (Unit 4) of the Halifax Pluton. Garnet as an accessory mineral is rare in the thin sections examined. This study recognizes two main types of garnets from Unit 3, Unit 5, and the aplite. Table 6.1 lists the characteristics of those garnets.

The *Type 1* garnet (D12-0083) from Unit 3 is small (1.3 mm across), euhedral, inclusion - free, and has no reaction rims (Fig. 6.1a); the *Type 1* garnet from Unit 5, crushed sample (103-3) is euhedral and inclusion - free (Fig. 6.1b). The aplite (MD-2B) contains many garnets of *Type 1*, (Figs 6.1c) which are skeletal, inclusion - free, small, and without reaction rims. The skeletal garnets have good euhedral outlines (sharp boundaries, no curved edges).

Type 2 garnet (213-3) from Unit 3 is large (6.5 mm across), anhedral, and has reaction rims and many inclusions (Fig. 6.1d).

Table 6.1 Characteristics of two types of garnets from the Halifax Pluton

Type	Hosts	Sample No.	Textural characteristics	Zoning
1	Unit 3	D12-0083	euhedral, no incl., no react. rims, and small	*
1	Unit 5	103-3	euhedral, no incl., no react. rims, and small	reverse
1	Aplite	MD-2B	euhedral, skeletal, no incl., no react. rims, small	normal
2	Unit 3	213-3	anhedral, with incl., react. rims, and large	normal

* no analysis
incl.= inclusions, react.= reaction.

6.3.2 *Zoning in Garnets*

Zoning in the garnets has been examined under the Nomarski microscope, and the microprobe. Optical examination to detect zoning cannot give distinct images as found in plagioclase, because garnet is isotropic.

Compositional zoning exists in all garnets from the Halifax Pluton. *Type 1* garnet from muscovite - biotite leucomonzogranite has Mg - poor and Fe - rich rims, and a U - shape pattern for Mn zoning (Fig. 6.2a). *Type 2* garnet from Bt-Crd leucomonzogranite has Mg - rich but Fe - poor rims, and typical W - shape pattern for Mn zoning (Fig. 6.2b). *Type 1* garnets from the aplite show that those grains analysed have typical or weak W - shape pattern

for Mn, Mg - rich rims, varied (rich in one side of rim, or poor for both rims) patterns for Fe (Fig. 6.3a, b; Fig. 6.4a, b).

6.4 Discussion and Conclusions

6.4.1 *Origins of Type 1 Garnets*

Type 1 garnets from Unit 3 and Unit 5 are interpreted as magmatic type, because they are euhedral, inclusion - free, without reaction rims (Fig. 6.1), and with reverse zoning (Figure 6.2a: *Type 1* garnet from Unit 5). These characteristics can be compared with those of magmatic garnets indicated by Allan & Clarke (1981). The spessartine - rich rims in the garnet possibly reflect crystalline growth in a magma with increasing Mn/(Ca+Mn+Mg) (see Chapter 2: the ratio changes from 0.011 to 0.045 from early - to late - stage phases). Since the other Fe - Mg phases are cordierite and biotite and these phases concentrate Mg, Fe, and not Mn, it is possible that crystallization of these latter minerals caused an increase in Mn/(Ca+Mn+Mg) in the magma.

In general, Green (1977), Leake (1968), Birch & Gleadow (1974), and Miller & Stoddard (1981) have found garnets in equilibrium with silicic liquids to be almandine - rich (60 - 70%) with subordinate spessartine (>10%), pyrope (<8%), and grossular (1-3%). The composition of the *Type 1* garnet from muscovite - biotite leucomonzogranite (Unit 5) (Table 6.2) conforms to that of magmatic garnets, and this garnet has the

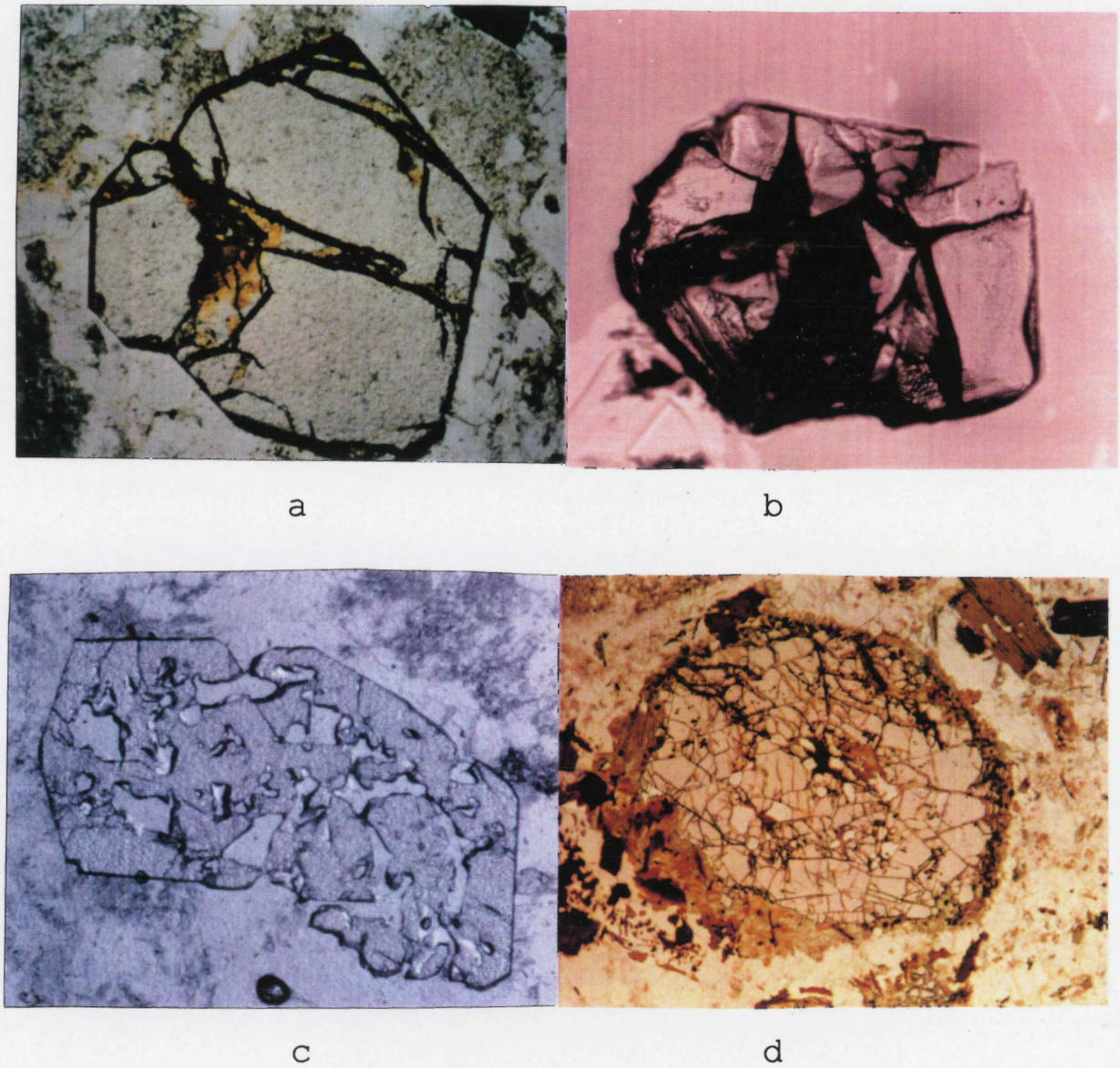

Figure 6.1 Photomicrographs of garnet from the HP, a: *Type 1* garnet from Unit 3 (D12-0083) is euhedral, small, no inclusions, and without reaction rims, (plane polarized light, the long dimension of the photo is 1.9 mm); b: *Type 1* garnet from crushed sample (103-3) of Unit 4, euhedral, small, no inclusions. Plane polarized light and the long dimension of the photo is 1.3 mm. c: *Type 1* garnet crystal (MD-2B) from aplite is skeletal and euhedral. Plane polarizers, long dimension of the photos is 2.2 mm. d: anhedral garnet (*Type 2*) from Unit 3 (213-3), large, many inclusions in it and has reaction rims. Plane polarized light, the long dimension of the photo: 6.2 mm.

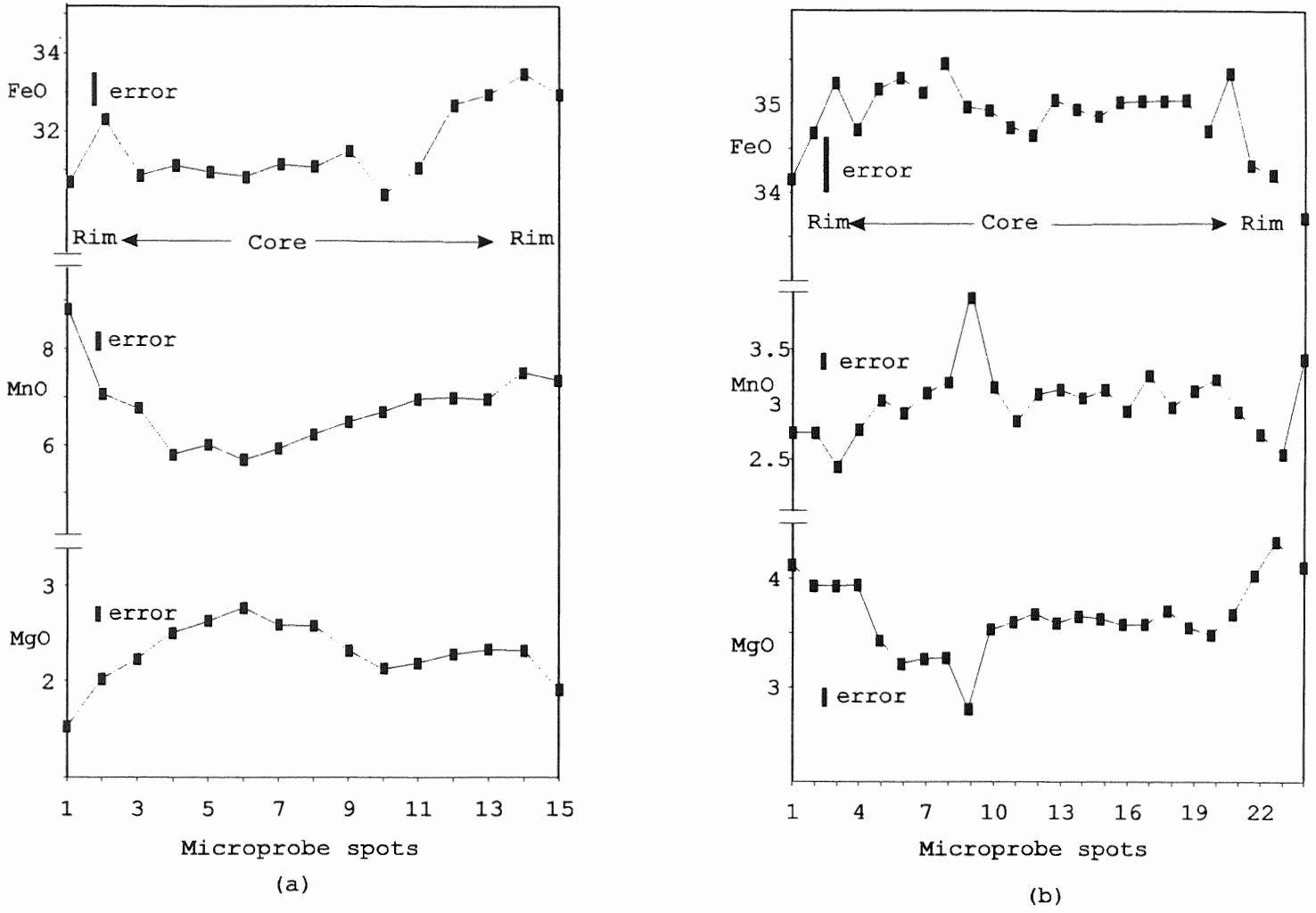

Figure 6.2. The variation of FeO, MnO, and MgO versus distance along traverses (a: 0.66 mm, b: 2.5 mm) of garnets: Type 1 (a:103-3) from Unit 5 shows reverse zoning, error bars = 0.62, 0.14, and 0.05 respectively for FeO, MnO, and MgO; Type 2 (b: 213-3) from Unit 3 displays normal zoning, weak W-pattern for MnO, error bars = 0.69, 0.11 and 0.07 respectively for FeO, MnO, and MgO.

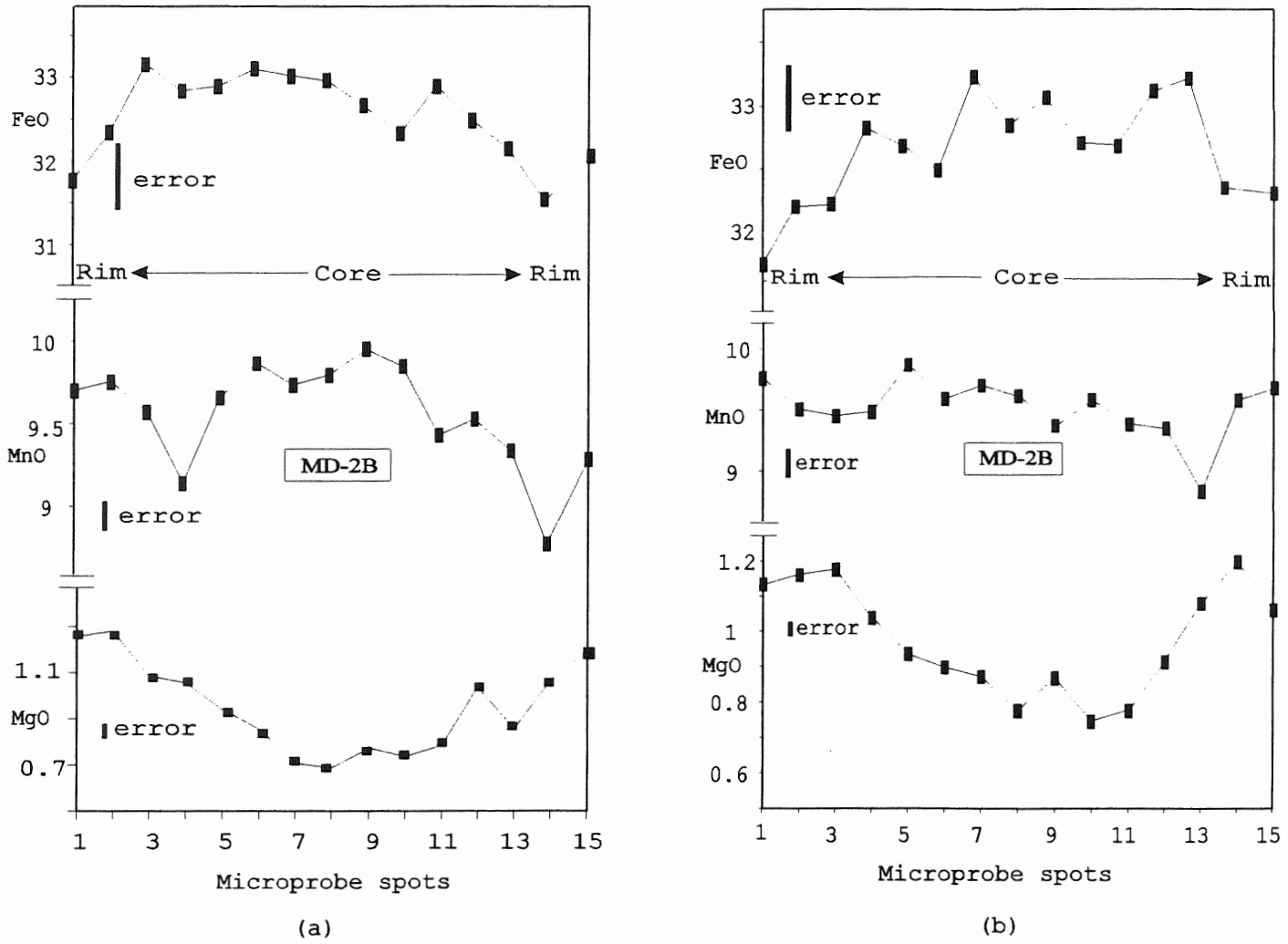

Figure 6.3 Variation of FeO, MnO, and MgO versus distance, along traverses ((a): 2.1 mm across, (b): 2 mm across) of two grains of Type 1 garnet from the aplite (MD-2B), show normal zoning for MgO (a and b), W pattern for MnO (a). Error bars = 0.65, 0.19, and 0.03 respectively for FeO, MnO, and MgO.

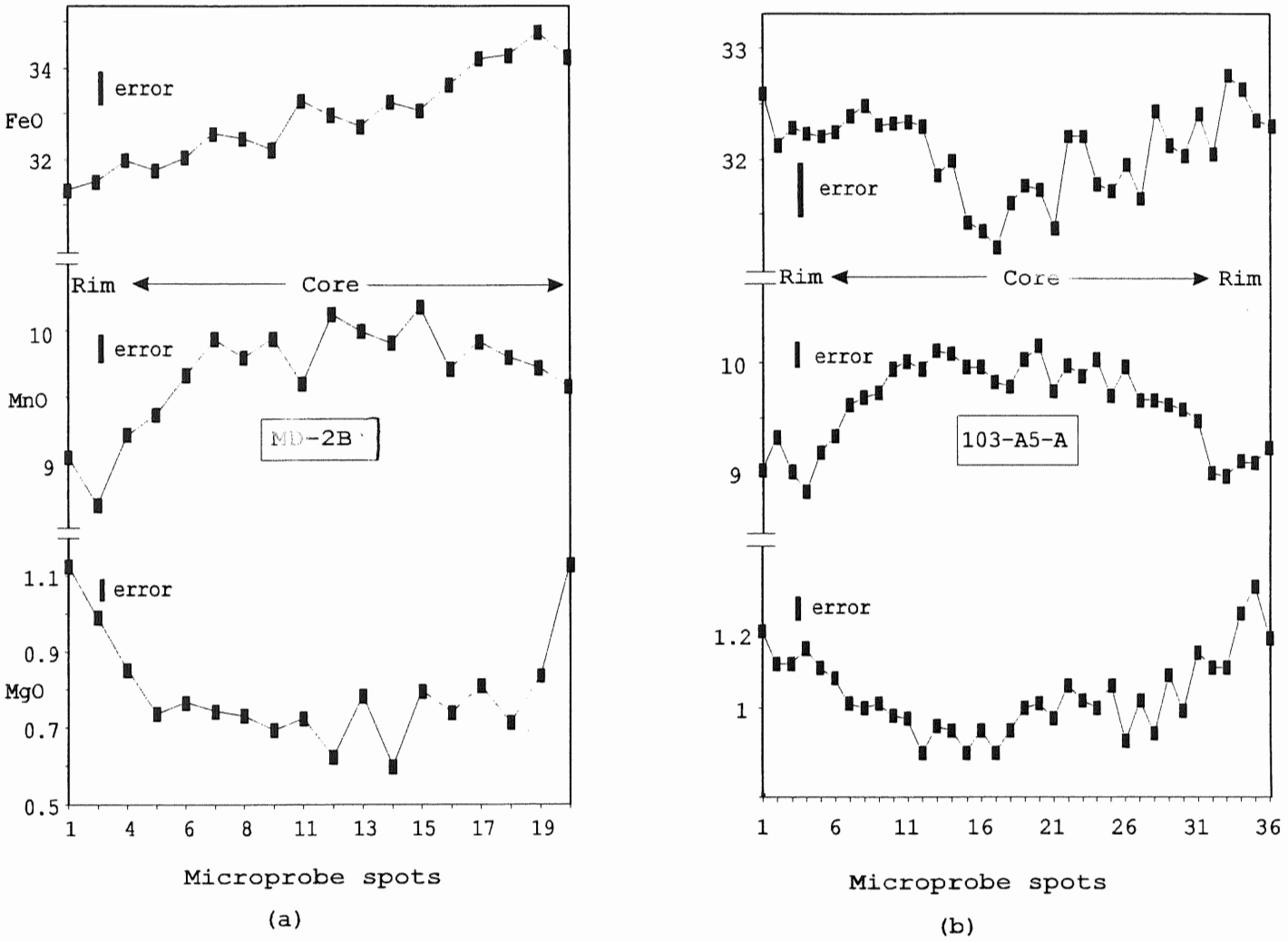

Figure 6.4. Variations of FeO, MnO, and MgO versus distance, along traverses ((a): 2.2 mm across, (b): 2.2 mm across) of two grains of Type 2 garnets from the aplite ((a): MD-2B, (b): 103-A5-A), display normal zoning pattern, and present weak W-shape pattern for MnO. Error bars = 0.65, 0.19, and 0.03 respectively for FeO, MnO, and MgO.

same proportions in its components as the magmatic garnet described by Allan & Clarke (1981).

Table 6.2 Average Microprobe Analyses of the Halifax Pluton Garnets

Type	Hosts	SiO_2	Al_2O_3	FeO	MnO	MgO	CaO	Na_2O	Alm	Sps	Pyr	Grs
1	Ms-Bt Lm	35.55	20.61	31.6	6.75	2.29	0.81	0.2	0.73	0.16	0.09	0.02
2	Bt-Crd Mz	37.16	21.02	34.85	3.02	3.65	0.88	0.22	0.77	0.07	0.14	0.02
1	aplite	35.68	20.46	32.39	9.45	0.98	0.34	0.2	0.73	0.22	0.04	0.01

* For each type of garnet, 15 - 45 microprobe spots were analysed; Lm = leucomonzogranite, Mz = monzogranite, Alm = almandine, Sps = spessartine, Pyr = pyrope, Grs = grossular

6.4.2 *Origin of Type 2 Garnet*

All the evidence from *Type 2* garnet (inclusions, large size (7 mm across), reaction rims, anhedral shape, and normal zoning pattern) points to a metamorphic origin. This garnet is poor in spessartine (7%, Table 6.2) but has a higher pyrope component than *Type 1* from muscovite - biotite leucomonzogranite and *Type 1* from the aplite. It may be a xenocryst because it is associated with xenoliths in the rock. Its W - shape pattern for Mn suggests that it had a different crystallization history from Type 1 garnet and may have partly equilibrated along its rims (i.e., Mn/(Ca + Mn + Mg) increases along the rims) with the melt after being entrained.

6.4.3 *Origin of Type 1 Garnet from the Aplite*

Quench texture

Type 1 garnets from the aplite deserve special discussion. They are small and have euhedral crystal outlines, skeletal shapes, no inclusions, and no reaction rims, but have normal zoning. A conspicuous characteristic of these garnets is that they have embayments and sieve textures which form skeletal shapes (Figs 6.1c). Embayed crystals caused by quenching (such as embayed porphyritic quartz) occur in siliceous volcanic and subvolcanic rocks such as rhyolite, obsidian, quartz - or feldspar - porphyry, and in isolated tuffs (Alling, 1936, p.151, Johannsen, 1939, p.21, Figs. 29, 30, 31, and 39, and MacKenzie & Guilford, 1980, Fig. 70). These crystals characteristically have approximately euhedral outlines. Experimental work by Swanson (1977) showed that with an increase in supercooling, large single crystals give way to an open array of coarse skeletal to dendritic crystals. Another set of cooling experiments, conducted by Lofgren (1973) on plagioclase, showed that the crystals, quenched at intervals of 50°C, quite commonly are initially skeletal, but with continued growth fill in to become tabular (Fig. 6.5). However, embayed crystals resulting from resorption cannot keep their corners and faces intact. Dissolution experiments (Kuo & Kirkpatrick, 1985; Tsuchiyama,

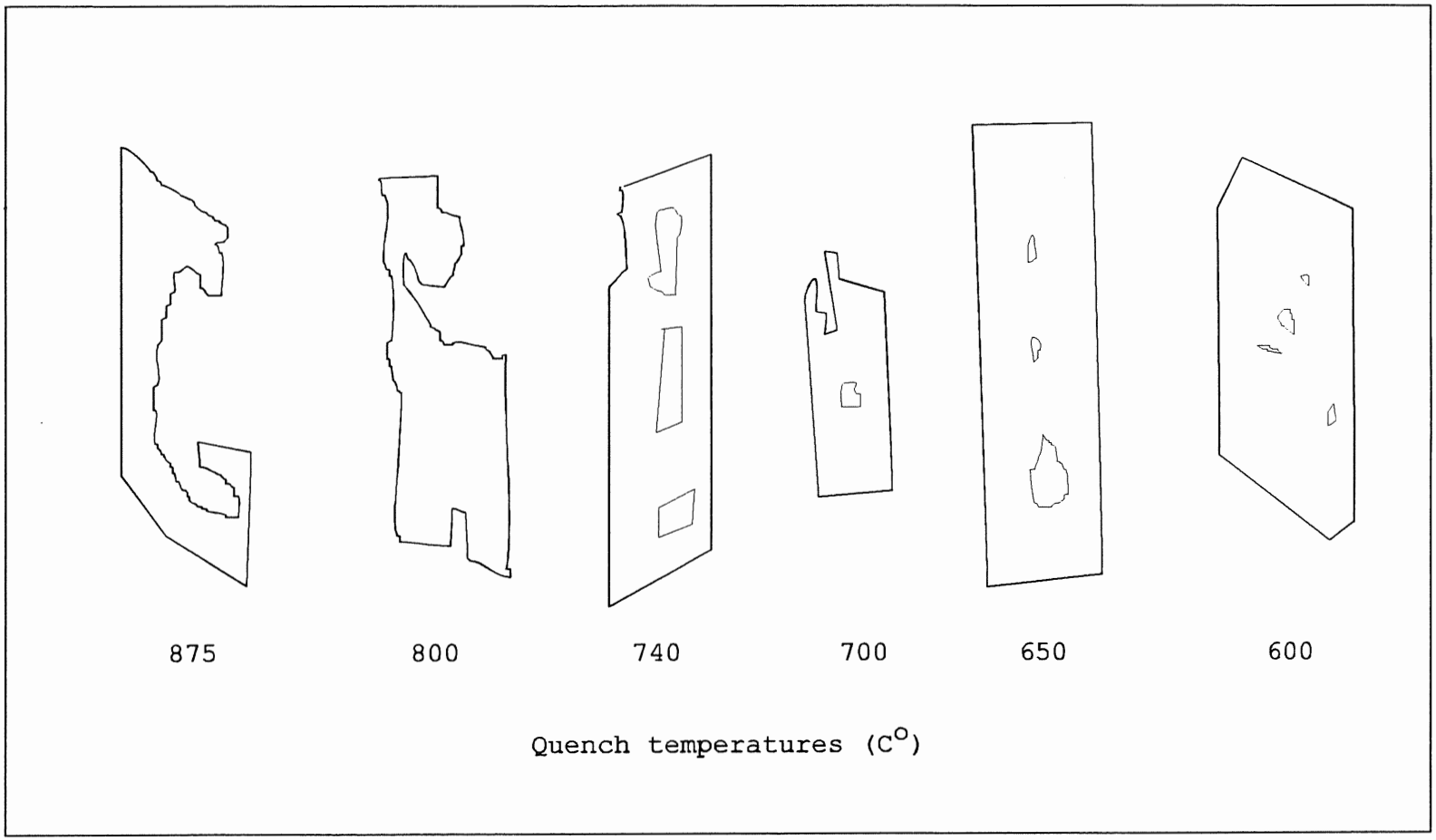

Figure 6.5 Schematic representation of the observed sequence of plagioclase growth forms. The melts were quenched at the temperatures indicated. Skeletal crystals typical of the 875°C quench run must fill in when growth is allowed to proceed to lower temperatures as shown in the 600 °C quench run (Lofgren, 1980).

1985) demonstrate that crystals (quartz and plagioclase), embayed through dissolution have non - faceted outlines, curved sides, and rounded corners. O'Brien et al. (1988) and Stamatelopoulou et al. (1990) reported resorbed phenocrysts, in volcanic rocks, which are characterized by rounded forms and rounded edges.

Implication of quench texture

The euhedral crystal outlines, complete corners, and sieve texture caused by quenching imply that garnet crystals had an equilibrium relationship with the melt for a period of time resulting in nucleation and partial growth, and then had a disequilibrium relationship with the melt to stop growing because of undercooling.

The width of the aplite ranges from 10 to 135 cm. Features of the aplite in the HP, including its sharp contact to the host and different element ratio with the host (see discussion in 3.4.1), imply that it had a short crystallization time after intruding cold, rigid granite rocks.

Normal zoning

If *Type 1* garnet in the aplite is magmatic, it should have had reverse zoning instead of normal zoning according to the proposal of Allan & Clarke (1981). The normal zoning documented in the garnet raises the question about its magmatic or metamorphic origin.

One hypothesis to explain this would be that those garnets were metamorphic minerals entrained in the melt when it

originated. Two points would support this hypothesis: (1) well - developed zoned crystalloblasts and idioblasts can exist free of inclusions (Augustithis, 1990); (2) the *Type 1* garnets are quite similar in molecular formula: $Alm_{0.73}Spss_{0.22}Pyr_{0.04}Grss_{0.01}$ (Table 6.2), to those metamorphic garnets from Whitehead Harbour area (Raeside et al., 1988), but differ, in spessartine and pyrope contents, from other types of garnets from the HP (Figure 6.6), and from magmatic garnets of the South Mountain Batholith, which have generally $Alm_{0.72-0.73}Sps_{0.14-0.15}Pyr_{0.10}Grs_{0.03,}$ (calculated from original data of Allan & Clarke, 1981).

Fine - grained idioblastic garnets exist in metamorphic rocks of the Whitehead Harbour area of the Meguma Group (Raeside et al., 1988); these authors found that in some samples garnets show rims free of inclusions or cores with few inclusions, and most of these garnets have normal zoning, are commonly rich in Mn, with spessartine contents typically 20 - 40 %, grossular contents less than 10 % and the M/(F+M) ratio ranging from 0.046 to 0.159.

However, if the garnets were metamorphic minerals, they should have experienced a process of reaction with or resorption by the aplite magma. The sieve texture present in those garnets could represent a resorption event (Stamatelopoulou et al., 1990), but if resorption by the melt occurred, straight crystal boundaries, clear corners, and euhedral outlines present in those

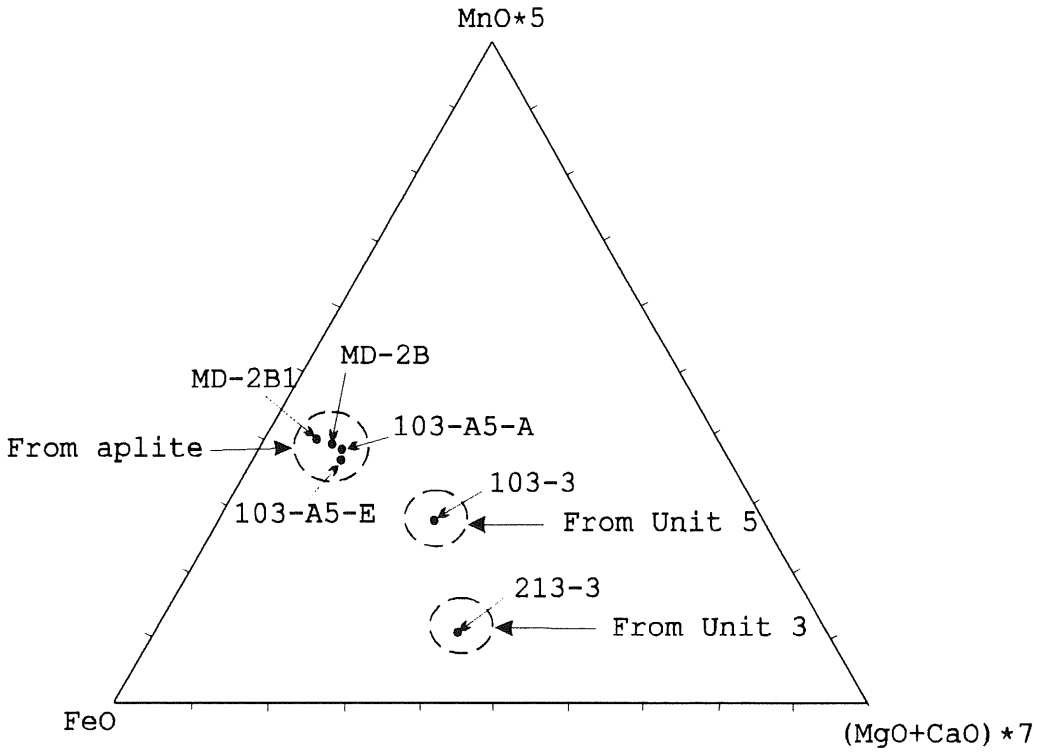

Figure 6.6 Triangular diagram discriminating Type 1 garnet (MD-2B, 103-A5-A,E) from aplite, from Type 1 garnet from Unit 5 (103-3) and Type 2 garnet from Unit 3 (213-3).

garnets should have been eliminated soon after being included in the melt.

Another hypothesis is that the aplite rocks are fractionated from the main sequence of the HP, but those garnets may only have experienced part of the whole differentiation evolution. More likely, the aplite magma represents another magma pulse which is different from the magma of the sequence A. *Type 1* magmatic garnets with normal zoning leave an unsolved problem. In the literature, there has been no report of this nature of magmatic garnets.

6.5 Summary

Two types of garnets, magmatic and metamorphic, exist in the HP. Magmatic garnets are euhedral, inclusion - free, without reaction rims, and with reverse zoning. Metamorphic garnet are anhedral, large size (7 mm across), with reaction rims, inclusions, and normal zoning pattern.

Quench texture for garnets has never been reported in the literature. The garnet from aplite has quench texture characterized by embayments and sieve which form skeletal shapes with wholly or partly their euhedral outlines. The euhedral crystal outlines and complete corners imply that those garnet crystals had an equilibrium relationship with the melt for a period of time resulting in nucleation and partial growth, and then went to a disequilibrium relationship with rapid change in the conditions of melt crystallization, such as supercooling.

Supercooling resulted in skeleton - form garnet with incomplete growth.

The magmatic garnets with quench texture have normal zoning; they should have had reverse zoning instead of normal zoning according to the proposal of Allan & Clarke (1981).

Chapter 7 Andalusite

7.1 Introduction

This chapter examines the general occurrence and zoning of andalusite in igneous rocks, and relates these features to relevant experimental work. It then reports occurrences of andalusite from the Halifax Pluton and andalusite zoning, and discusses their consequences.

Andalusite is one of the aluminum silicate group of minerals which include the three polymorphs of Al_2SiO_5 (andalusite, sillimanite, and kyanite). Its optical properties are summarized in Figure 7.1a. Andalusite consists of edge-shared chains of AlO_6 octahedra that are cross - linked through corner - sharing with double chains which consist of SiO_4 tetrahedra Al in five coordinated trigonal bipyramids (Figure 7.1b). Its general formula is Al_2SiO_5. Al is replaceable by Mn^{+3} and Fe^{+3}.

7.2 Andalusite in Igneous Rocks

7.2.1 *Andalusite Occurrences*

Many peraluminous granitoids have textures suggesting that andalusite was a product of magmatic crystallization (Clarke et al., 1976; Currie & Pajari, 1981; Haslam, 1971; Kerrick & Speer, 1988; Price, 1983). The occurrence of andalusite in volcanic rocks strengthens the case that this mineral may have a magmatic origin (London et al., 1988; Pichavant et al., 1988).

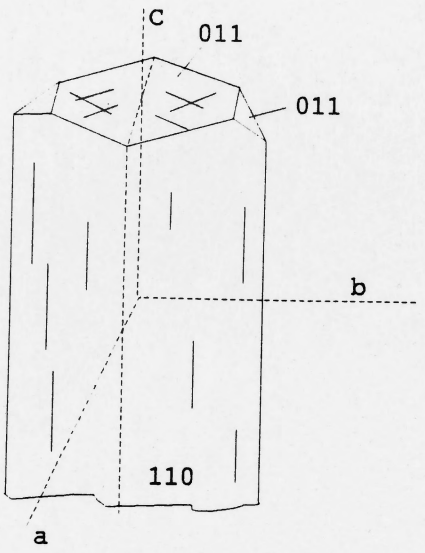

Andalusite, Al_2SiO_5

Crystal system: orthorhombic (-)
Habit: prismatic with nearly square cross sections and many crystals have carbonaceous inclusions
Main optical properties:
high relief (RI: 1.63-1.65)
low birefringence

common pink pleochroism

(a)

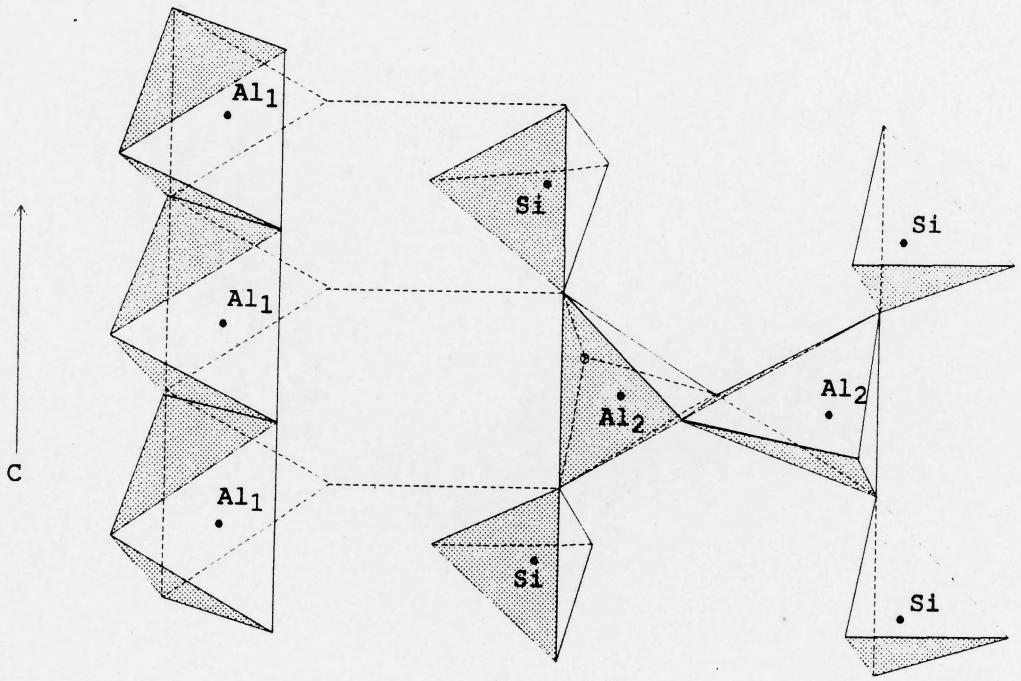

(b)

Figure 7.1 (a) Summary of optical properties of andalusite (RI = refractive indices); (b) the coordination polyhedra projected from the a axis of andalusite (From Papike, 1987).

7.2.2 *Andalusite Stability Fields*

Pressure - temperature diagrams support the existence of a stability field of andalusite + melt. Figure 7.2 shows three determinations of the triple point in the andalusite - sillimanite - kyanite stability diagram: the first from Richardson et al. (1969) with the triple point near 5.5 kbar and 622°C, the second from Holdaway (1971) with the triple point at 3.76 kbar and 510°C, and the third from Pattison (1992) who used entropy and volume data to attain the triple point at 4.5 kbar and 550°C.

With the solidi for metaluminous granodiorites, the Al_2SiO_5 phase equilibrium diagram of Richardson et al. (1969) yields a stability field of andalusite + melt. This has been used as an argument against Holdaway's (1971) phase diagram. In addressing this argument, Holdaway (1971) invoked the expansion of the P - T field of melt by volatiles such as fluorine. Price (1983) concluded that the apparent equilibrium of andalusite with peraluminous melts can be attributed to temperature lowering of the solidus due to elevated boron and fluorine in the melts and / or to expansion of the andalusite P - T stability field by solid solution. Kerrick & Speer (1988) accepted Holdaway's (1971) Al_2SiO_5 phase equilibrium diagram with expansion of the P - T stability field of the melt by F and B.

7.2.3 *Review of Andalusite Zoning*

Andalusite from metamorphic rocks displays two types of zoning: regular concentric zoning, and irregular sector zoning characterized by "patchy" distribution of zones of differing composition. Okrusch & Evans (1970), Plummer (1980), and Grapes (1987) have discussed concentric zoning of andalusite with pink cores and colourless rims. Okrush & Evans (1970) showed that the pink cores are enriched in Ti, Fe, and Mg relative to the rims, and that the compositional change is abrupt from core to rims.

In contrast to that abrupt compositional discontinuity, Yokoi (1983) and Shiba (1988) described andalusite and sillimanite with parabolic zoning profiles of Fe_2O_3 concentrations (higher in the cores). However, the zoning profiles of the larger andalusite and sillimanite crystals analysed by Yokoi suggest that much of the central portions of the crystals are either unzoned or have much gentler zoning profiles than the rims of the crystals. There are several possible explanations for this zoning trend: (a) a heterogeneous reaction such as: $Fe_2O_3^{\ Ilm} + SiO_2^{\ Qtz} = Fe_2SiO_5^{\ Sil}$ (Grew, 1980), (b) late-stage diffusion of Fe^{3+} into the rims of the crystals, because of compositional gradient between the crystal and the matrix; (c) increase in fO_2 during growth of the crystals.

However, andalusite from igneous rocks has rarely revealed any zoning. MacDonald & Merriam (1938) found concentrically zoned andalusite from pegmatite in California, and Burt & Stump

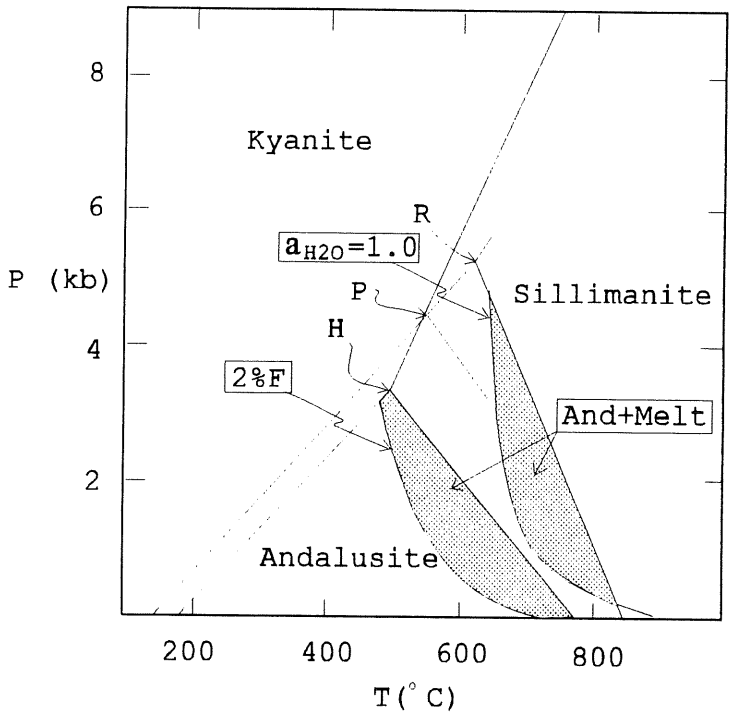

Figure 7.2 Al_2SiO_5 phase equilibrium diagrams of Richardson et al. (1969)(R), Holdaway (1971)(H), and Pattison (1992)(P). The granodiorite solidi with a_{H2O} = 1.0 and with 2 wt% F are from Manning & Pichavant (1983). The shaded areas are the stability fields of andalusite and melt.

(1983) showed a sector - zoned andalusite inclusion within a single crystal of less birefringent andalusite.

7.3 Andalusite in the Halifax Pluton

7.3.1 *Andalusite Occurrences*

In the muscovite - biotite leucomonzogranite of the Halifax Pluton, andalusite exists as an accessory mineral, usually as anhedral crystals (samples D12-0064-2, D12-0064, D12-0005-1, D12-0122-4, D12-0102-2, D12-3127). Sections of these samples were examined under the common microscope, the Nomarski microscope, and some crystals were analysed by the backscattered electron image technique and by microprobe.

The andalusite appears as two types in the late - stage phase: *Type 1* mantled by muscovite (Figure 7.3a), which is similar to one shown by Clarke et al. (1976); and *Type 2* among crystals of alkali-feldspar, and surrounded by quartz (Figure 7.3b). The *Type 2* includes an andalusite crystal containing a small quartz inclusion (Figure 7.3c).

For comparison, I also studied two other andalusites: (1) a pink zoned euhedral crystal (Figure 7.3d, courtesy of Dr. R.A. Jamieson) from a dike in biotite monzogranite at the contact between the SMB and the Halifax Formation at Deep Cove on the Blandford Peninsula in which the andalusite crystals are pink - zoned and surrounded by quartz; (2) a pink zoned euhedral crystal (courtesy of M.A. MacDonald), from a zone of high alumina

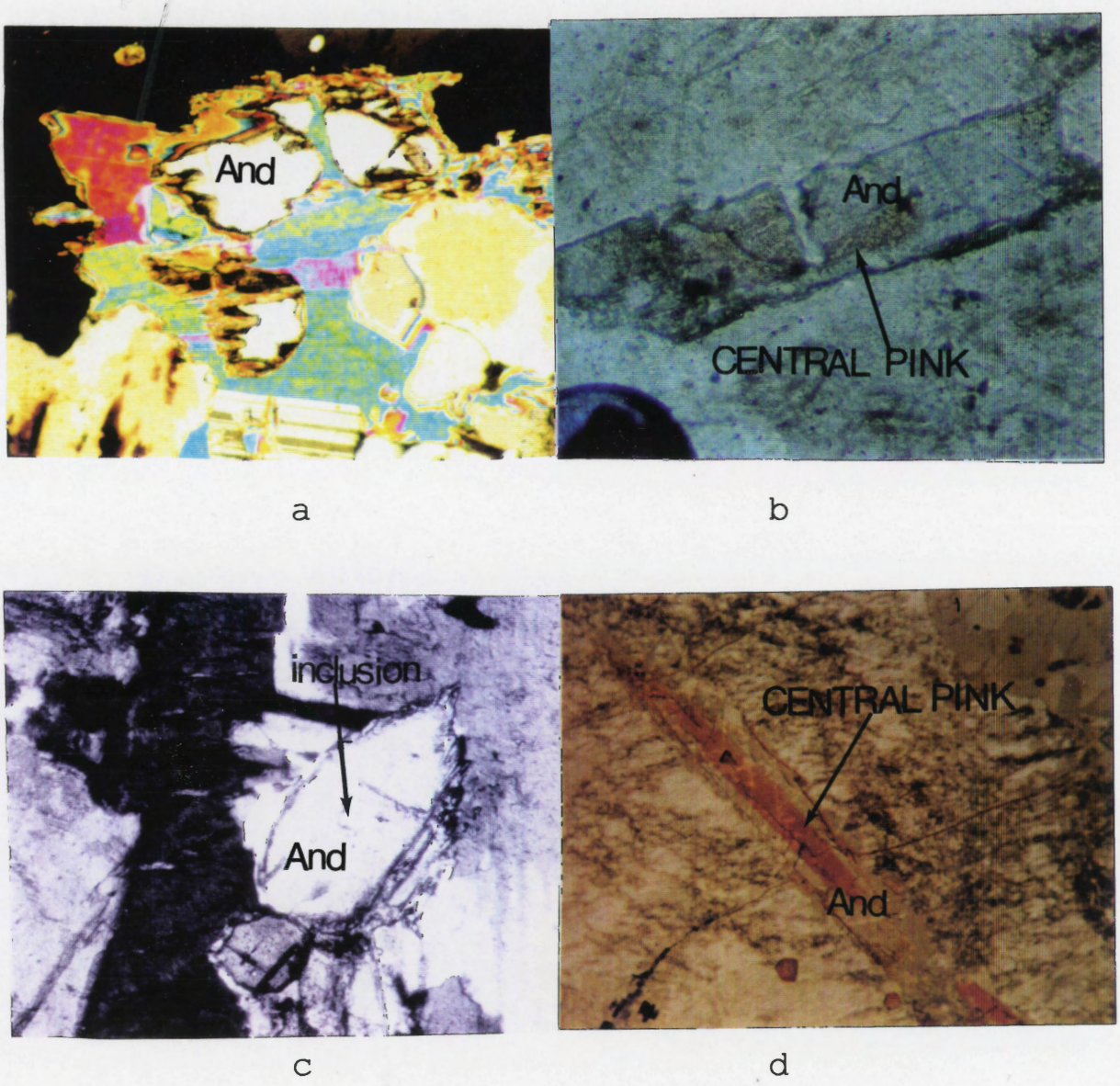

Figure 7.3 Photomicrographs of Andalusite from the HP and the SMB, a: *Type 1* andalusite from Unit 3 (D12-0005-01), mantled by muscovite; long dimension is 1.5 mm; b: *Type 2* andalusite from Unit 5 (D12-0122-4), subhedral, in Kfs, the long dimension is 1.2 mm; c: *Type 2* andalusite from Unit 5 (D12-0122-4), in Kfs and having a quartz inclusion, long dimension of the photo is 1.5 mm; d: andalusite from a dike in biotite monzogranite of the SMB at the contact (MP-5: courtesy of Dr. R.A. Jamieson) between this rock and the Halifax Formation, of the Deep Cove on the Blandford Peninsula, long dimension of the photo is 3.5 mm.

hydrothermal alteration, within granitoid rocks of the Big Indian Polyphase Intrusive suite, characterized by the quartz - absent mineral assemblage andalusite - sillimanite - spinel - muscovite - cordierite - apatite - pyrite (Corey, 1988).

7.3.2 *Zoning in Andalusite*

Two traverses across a *Type 2* andalusite shows Fe variations with a core plateau pattern (Fig. 7.4); the abrupt decreases in Fe from core to rims correspond to the margins of the central pink zone.

A plateau pattern in Fe variation is found not only in a *Type 2* andalusite but also in samples from hydrothermal veins (Fig. 7.5a), and from a dike at the contact between the SMB and country rocks (Fig. 7.5b).

7.4 Discussion and Conclusions

7.4.1 *Causes of Fe-Plateau Zoning Pattern*

The abrupt change in composition shown in Figures 7.4, 5 reflects disequilibrium between the mineral and its growth medium. Abrupt changes in the melt composition, pressure, and temperature may cause this disequilibrium.

Composition

All traverses across andalusites with central pink pleochroism reveal a plateau pattern (Figs. 7.4, 5). Abrupt changing of magmatic composition may result in the sharp change in the plateau pattern of Fe variation when andalusite crystals grow.

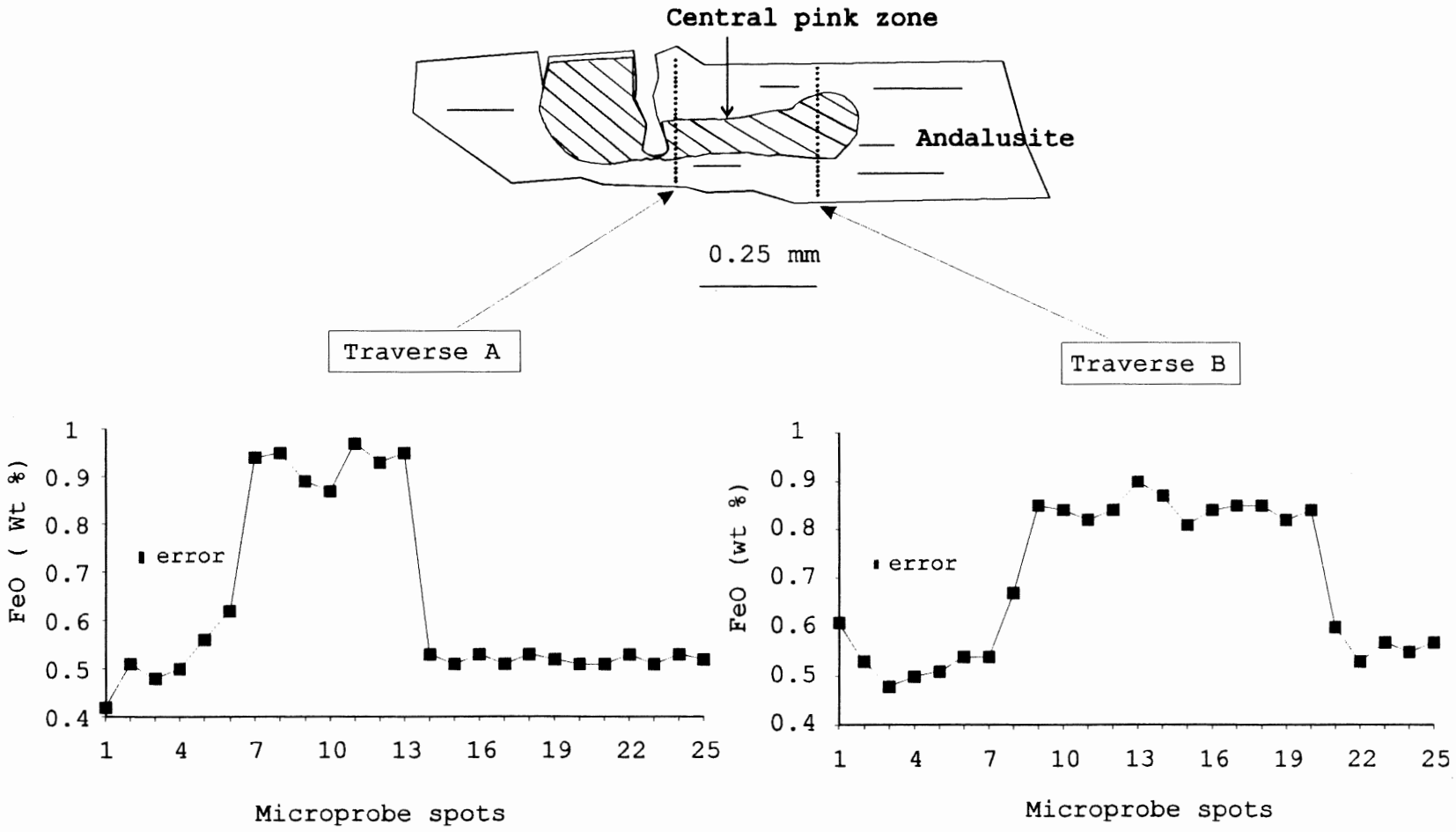

Figure 7.4 FeO variation (error bars = 0.03 wt %) along two traverses (traverse A and B: 0.34 mm across) across the central-pink zoned andalusite from Unit 5 (D12-0122-4), showing that higher FeO part of the crystal corresponds to the pink zone. See the crystal in Fig. 7.3.

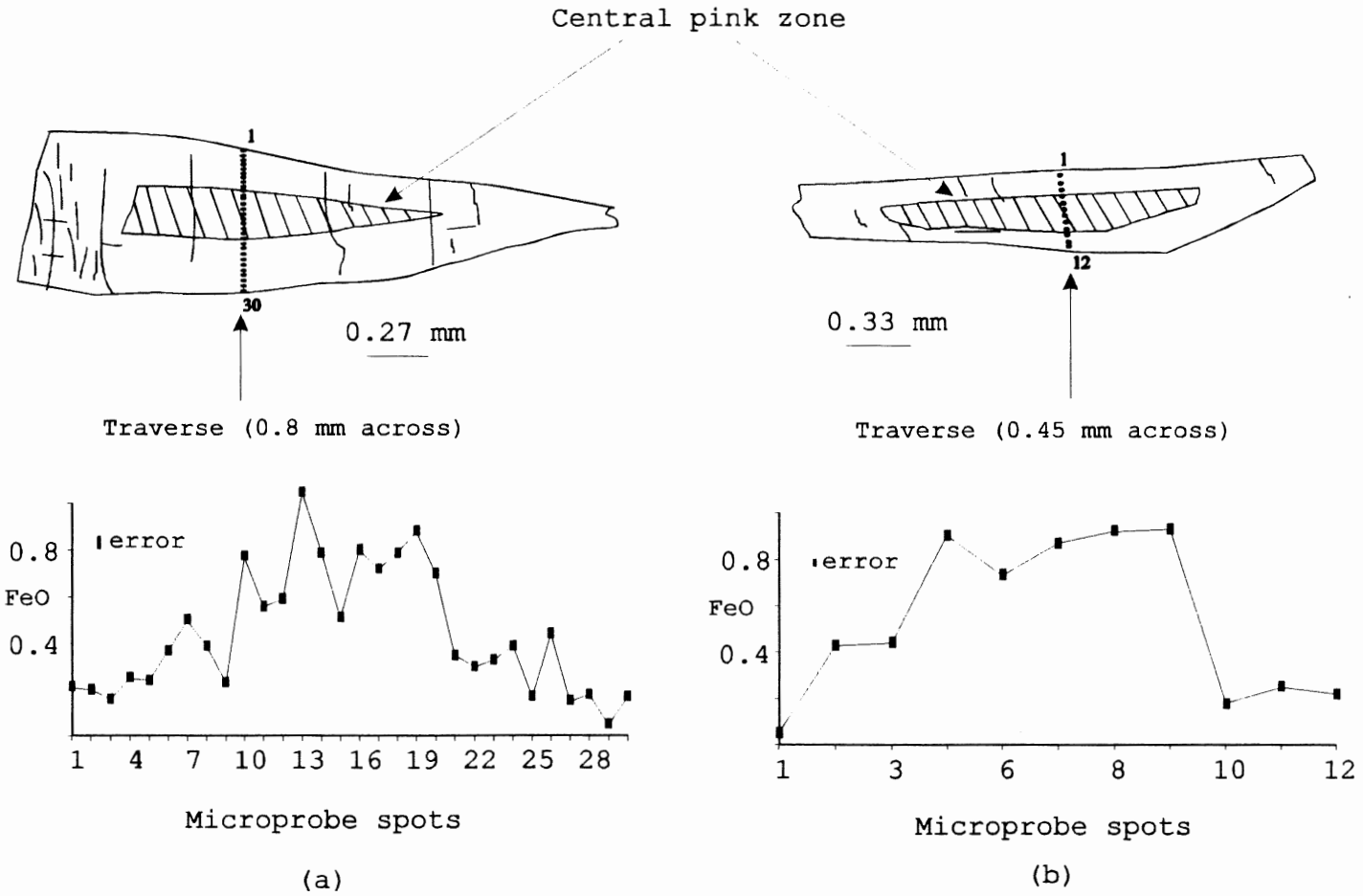

Figure 7.5 FeO variation across andalusites: (a): from hydrothermal zone (2095-07C); (b): from a dike in biotite monzogranite (MP-5) at the contact of the SMB and the Halifax Formation. See their crystals in Figure 7.3.

The plateau pattern of Fe variation shows that Fe intake by andalusite in the earlier stage of magmatic evolution is considerably higher than in the later stage. This can be due to assimilation of country rock during the intrusion of magma. If the assimilated rocks contained less iron than the intruding igneous rocks, the assimilated amount could dilute Fe in the magma. However, assimilation of immediate country rocks (the Halifax Formation) cannot dilute Fe in the magma, because the Halifax Formation contains between 5.43 and 13.44 FeO (weight percent) (Graves & Zentilli, 1988), which is much higher than the South Mountain Batholith (1.24 to 4.07 % FeO).

The starting of crystallization of ferromagnesian minerals such as biotite can result in considerable decrease in Fe in the local melt. The pink - core andalusite may have been growing until biotite became a stable phase. In this case, andalusite formed earlier than biotite, which could be proved by textural evidence, but this textural relationship between andalusite and biotite does not exist in the Halifax Pluton.

Another hypothesis is that the pink core of the andalusite may be a metamorphic 'seed' which was entrained and grew in the magma. The colorless rims formed during a magmatic process. However, metamorphic andalusite in the vicinity of the SMB contact normally has some inclusions.

Those andalusites with the same plateau of zoning may be all of hydrothermal origin, because the andalusite from both the

hydrothermal vein and the dike (weak zone into which hydrothermal liquid penetrated) has this pattern. However, a hydrothermal liquid could not have placed an andalusite seed in K - feldspar in muscovite - biotite leucomonzogranite (Figure 7.3b).

Pressure

Grambling & Williams (1985) suggested that decreasing pressure may result in higher iron intake in andalusite. This conclusion cannot explain the zoning found in our samples, because the andalusite has high - iron core and low - iron rims and this pattern would have formed from low - pressure to high - pressure conditions according to Grambling & Williams (1985). If we assume that the andalusite nucleated at the beginning of crystallization and continued to grow until the emplacement of the magma in the upper crust, the environment of the andalusite changed from a higher pressure to a lower pressure.

Temperature

In a multicomponent silicate liquid the ratio of ferric to ferrous iron is a function of temperature and oxygen fugacity. The relationship between these variables has been calibrated experimentally for a wide range of liquid compositions over a range of temperatures (Sack et al. 1980; Kress & Carmichael, 1988), and can be expressed by the following empirical equation:

$$\ln [X_{Fe_2O_3}/X_{FeO}] = a \ln fO_2 + b/T + c + 4d*(\sum Xi)$$

In this equation:

a, b, c, and d are constants.

It is clear that X_{Fe2O3}/X_{FeO} is proportional to fO_2 and ln fO_2 is proportional to - b/T (i.e.: fO_2 decreases with decreasing temperature as shown in Figure 7.6). Decreasing fO_2 will result in a decrease in the Fe_2O_3/FeO ratio in the melt. Quenching, caused by contact of hot magma with cold country rocks, may result in a rapid decrease in fO_2 in the melt and then the ratio Fe_2O_3/FeO of melt. This may happen in the magma near the contact such as the location of the sample MP-5. Decreasing the unit - cell dimensions (of the AlO_6 octahedra of andalusite) with decrease of temperature (Deer et al., 1982, after Winter & Ghose, 1979) has resulted in larger Fe^{+2} not to fill in. This is probably why a decrease in temperature results in lower iron intake in andalusite. This conclusion considering fO_2 is the same as the studies by Grambling & Williams (1985) who concluded that the ability of andalusite to absorb iron is a function of temperature: an increase in temperature permits greater iron intake by andalusite.

7.4.2 *Andalusite Types*

The textures shown in Figure 7.3 suggest the crystallization history of those andalusites: liquid + andalusite + K-feldspar , and then liquid + muscovite or quartz. An isobaric path (Path A in Figure 7.7) of crystallization might match this procedure. A slow decrease in temperature could lead to andalusite assimilated by the melt completely. Rapid changes in temperature may result

in disequilibrium crystallization to peritectically form muscovite (Clarke, et al. 1976) and quartz.

Quartz may have a cotectic relationship with andalusite, because quartz has a wide P - T stability field. A good example of euhedral andalusite coexisting with large poikilitic quartz has been found in leucosomes of nebulitic migmatites, in the Proterozoic Arunta block of central Australia (Vernon & Collins, 1988). But in our case, a sequential appearance of andalusite followed by muscovite or quartz, as indicated by the texture (Fig. 7.3), clearly suggests that the crystallization procedure represented by Path A in Figure 7.7 has been responsible for the presence of andalusite, muscovite, and quartz. Which mineral (quartz or muscovite) forms a protective mantle may depend upon the composition of the local magma.

7.5 Summary

The andalusite appears as two types in the late - stage phase: andalusite mantled by muscovite and among crystals of K-feldspar. The isobaric path in the andalusite P - T diagram suggests that quartz and muscovite in the protective rims around andalusite are crystallizing products. The abrupt decreases in Fe from core to rims correspond to the margins of the central pink zone. Rapid decreases in temperature and then fo_2 result in lower Fe intake by andalusite, forming the central pink zoning.

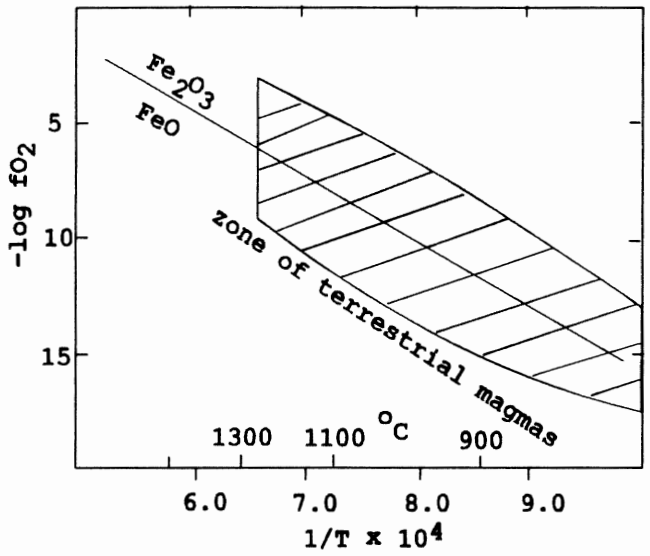

Figure 7.6 Plot of log fO_2 against inverse temperature (K°) for labelled oxidation reactions at 1 bar for pure solids (Carmichael & Ghiorso, 1990), showing fO_2 increases with increasing temperature.

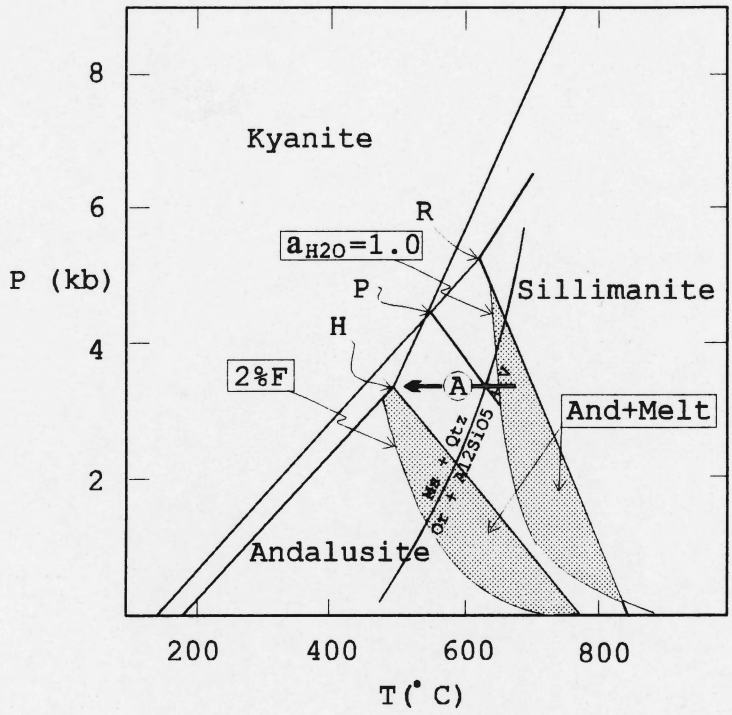

Figure 7.7 Al_2SiO_5 phase equilibrium diagrams of Richardson et al. (1969) (R), Holdaway (1971)(H), and Pattison (1992)(P). The granodiorite solidi with a_{H2O} = 1.0 and with 2 wt%F are from Manning and Pichavant (1983). The shaded areas are the stability fields of andalusite + melt. The muscovite stability curve is from Althaus et al. (1969). A: isobaric path.

Chapter 8 General Discussion

8.1 Introduction

Chapters 3-7 have reviewed AFM minerals in granitoids generally, and have described the occurrence, chemistry, zoning and possible origins for AFM minerals in the Halifax Pluton. This chapter uses AFM diagrams to establish relationships among these minerals, and to make comparisons between AFM mineral pairs from different host phases. This chapter also includes overall evaluations of biotite as an indicator of magmatic evolution, causes of mineral zonings, and additional comments on the aplite.

8.2 AFM Mineral Relationships

8.2.1 *Chemographic Considerations*

Determining sequences of magmatic AFM mineral crystallization reactions in granites relies on observations from different samples and different host phases of composite plutons. AFM diagrams are well suited to show the dependence of the AFM mineral assemblages on the types of peraluminous granitoid rocks (Abbott & Clarke, 1979; Clarke 1981, Maillet & Clarke, 1985; Speer & Becker, 1992). Figure 8.1 shows the tetrahedron Al_2O_3 - FeO - MgO - K_2O, and the plane Al_2O_3 - FeO - MgO (stippled) which extends beyond the tetrahedron. The points Ms and Kfs represent muscovite and K-feldspar, respectively.

Thompson (1957) projected compositions within the tetrahe-

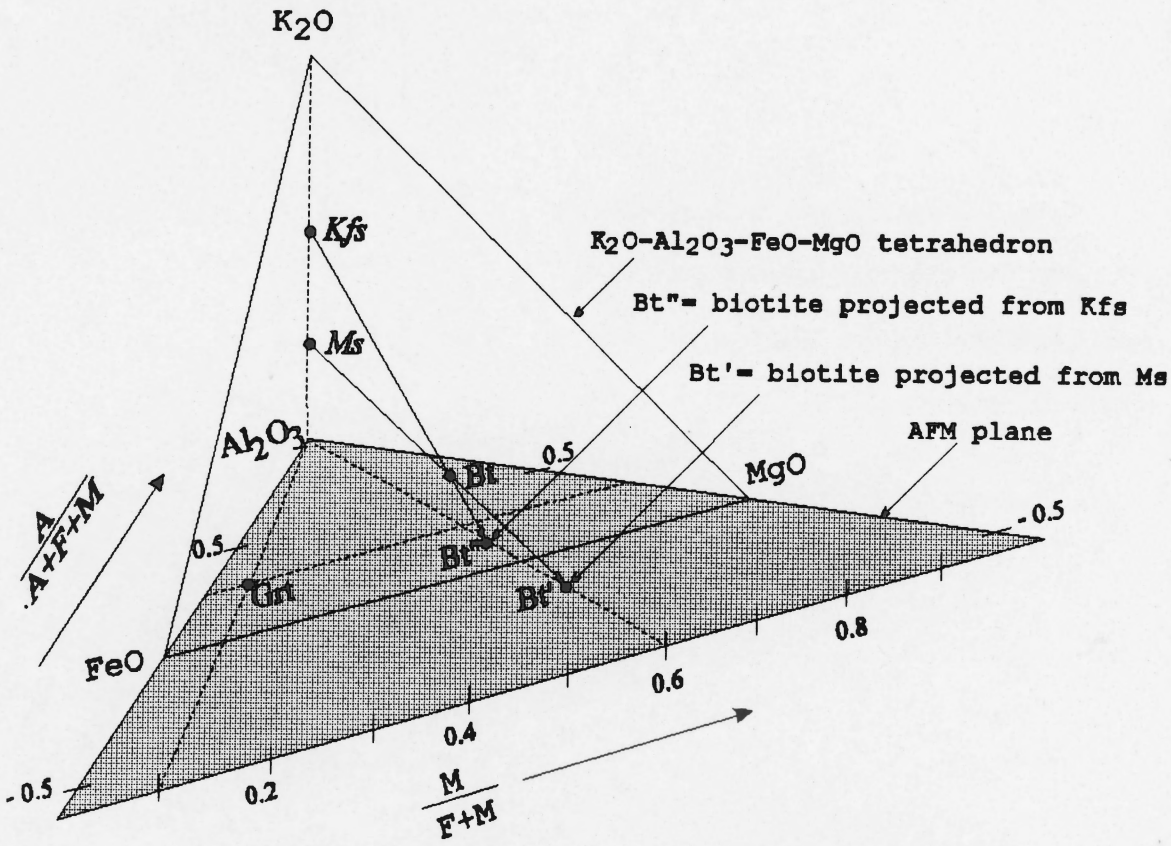

Figure 8.1 The K_2O-Al_2O_3-FeO-MgO tetrahedron and the AFM plane. All points inside the tetrahedron are projected through point Ms or point Kfs onto the AFM plane. For instance, point Bt lies inside the tetrahedron and is projected to Bt' from Ms or to Bt" from Kfs (accordingly A = [Al_2O_3] - [K_2O]). For example, garnet contains no K_2O so that it in the plane remains unchanged. This thesis uses Kfs as a projection point.

dron from Ms onto the AFM plane. Muscovite contains three times as much as $[Al_2O_3]$ as $[K_2O]$ ([ ] designates molecular proportions); this accounts for the expression $A = [Al_2O_3] - 3*[K_2O]$. Barker (1961) constructed an AFM diagram projected from K-feldspar (point Kfs in Fig. 8.1). In his diagram, the value of A is accordingly calculated as: $A = [Al_2O_3] - [K_2O]$. Abbott & Clarke (1979) used an AFM diagram projected from alkali feldspar, plagioclase, and quartz, and for which $A = [Al_2O_3] - [K_2O] - [Na_2O] - [CaO]$.

Magmatic muscovite does not occur in all phases of the Halifax Pluton but alkali feldspar, plagioclase, and quartz coexist with AFM assemblages in every phase. This thesis uses the AFM plane projected from alkali feldspar, (i.e., in which $A = [Al_2O_3] - [K_2O] - [Na_2O] - [CaO]$).

8.2.2 *Coexisting Mineral Assemblages*

AFM assemblages vary in the HP phases:

(1) biotite granodiorite: biotite ± cordierite;

(2) biotite monzogranite: biotite ± cordierite ± garnet;

(3) biotite ± cordierite monzogranite: biotite + cordierite ± garnet;

(4) muscovite - biotite ± cordierite leucomonzogranite: biotite + cordierite, biotite + muscovite (magmatic muscovite in some parts of this phase), biotite ± garnet;

(5) muscovite - biotite leucomonzogranite: biotite + muscovite, biotite ± andalusite, biotite ± garnet;

(6) aplite: biotite + garnet + cordierite + muscovite.

One to five mineral samples have been analysed for each rock phase and 10 to 50 probe points for each of those samples. A representative sample for each AFM mineral has been selected to plot in AFM mineral diagrams and generalized tie-lines connect plotted points which are enclosed with ellipses. Figures 8.2 and 8.3 summarize the relationships of these mineral assemblages. The two parameters A and M/(F+M) equal those in AFM triangular diagram. The different slopes of the tie-lines for the same pair of minerals may reflect different magma compositions, temperatures, or origins such as magmatic or hydrothermal.

Biotite

Biotite inclusions in other rock-forming minerals, its euhedral to subhedral shape, and its similar size to other rock-forming minerals suggest a magmatic origin (see Chapter 3 for details). From biotite granodiorite (Fig. 8.2a, Unit 1) to muscovite - biotite leucomonzogranite (Fig. 8.2f, Unit 5), the M/(F+M) ratios of the biotites decrease except for biotite ± cordierite monzogranite (Unit 4) and the value A remains almost unchanged. MacDonald & Horne (1988) stated that biotite ± cordierite monzogranite (Fig. 8.2c, Unit 4) is more "primitive" than muscovite - biotite ± cordierite leucomonzogranite (Fig. 8.2d, Unit 3). It is true from the M/(F+M) ratio of the biotite that the biotite from Unit 4 has higher M/(F+M) than that from

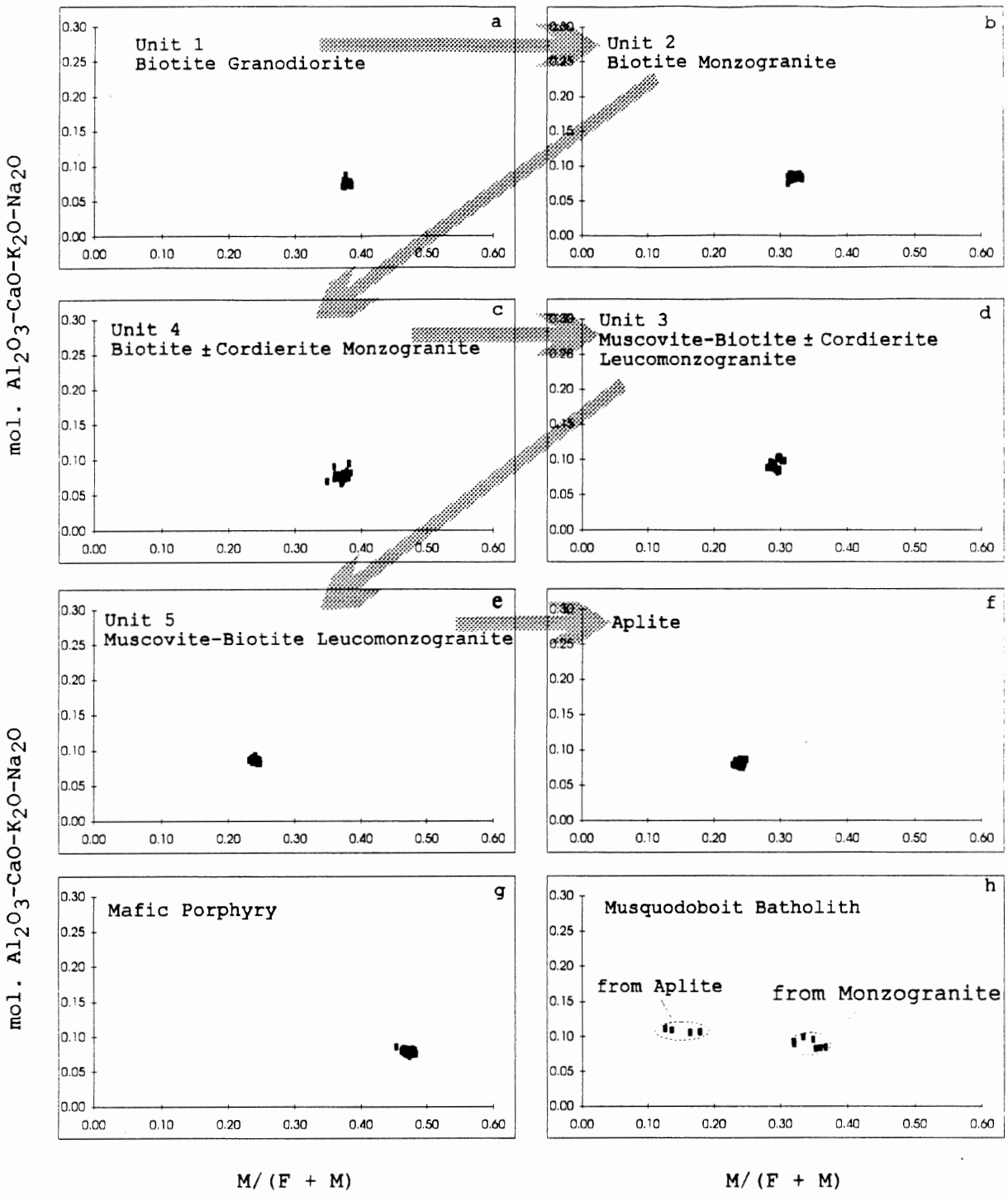
a
Unit 1
Biotite Granodiorite
b
Unit 2
Biotite Monzogranite
c
Unit 4
Biotite ± Cordierite Monzogranite
d
Unit 3
Muscovite-Biotite ± Cordierite
Leucomonzogranite
e
Unit 5
Muscovite-Biotite Leucomonzogranite
f
Aplite
g
Mafic Porphyry
h
Musquodoboit Batholith
from Aplite
from Monzogranite
mol. Al2O3-CaO-K2O-Na2O
mol. Al2O3-CaO-K2O-Na2O
M/(F + M)
M/(F + M)

Figure 8.2

Figure 8.2 AFM plots of the HP biotites projected from Kfs, Qtz, and Pl, from a: Biotite Granodiorite (92-HP-L), b: Biotite Monzogranite (333-6), c: Biotite ± Cordierite Monzogranite (DO5-0002), d: Muscovite - Biotite ± Cordierite Leucomonzogranite (213-3), e: Muscovite - Biotite Leucomonzogranite (213-4), f: Aplite (MD-2B), g: Mafic Porphyry (349-1), h: Aplite and Monzogranite from the Musquodoboit Batholith (MacDonald, 1981). The stippled arrows indicate that MgO in the host rock increases. The contents of biotites (h) from Monzogranite of the Musquodoboit Batholith compare well with those (b,c) from the HP monzogranite.

Cordierite - Biotite Pair

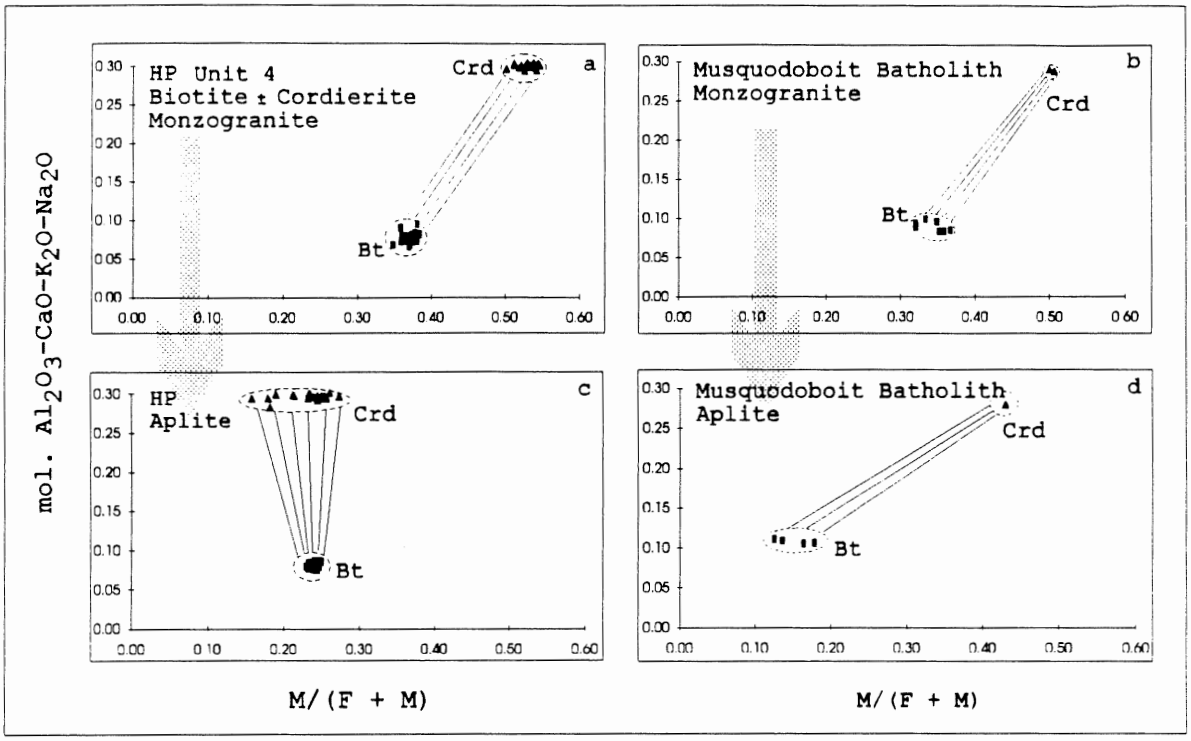

Garnet - Biotite Pair

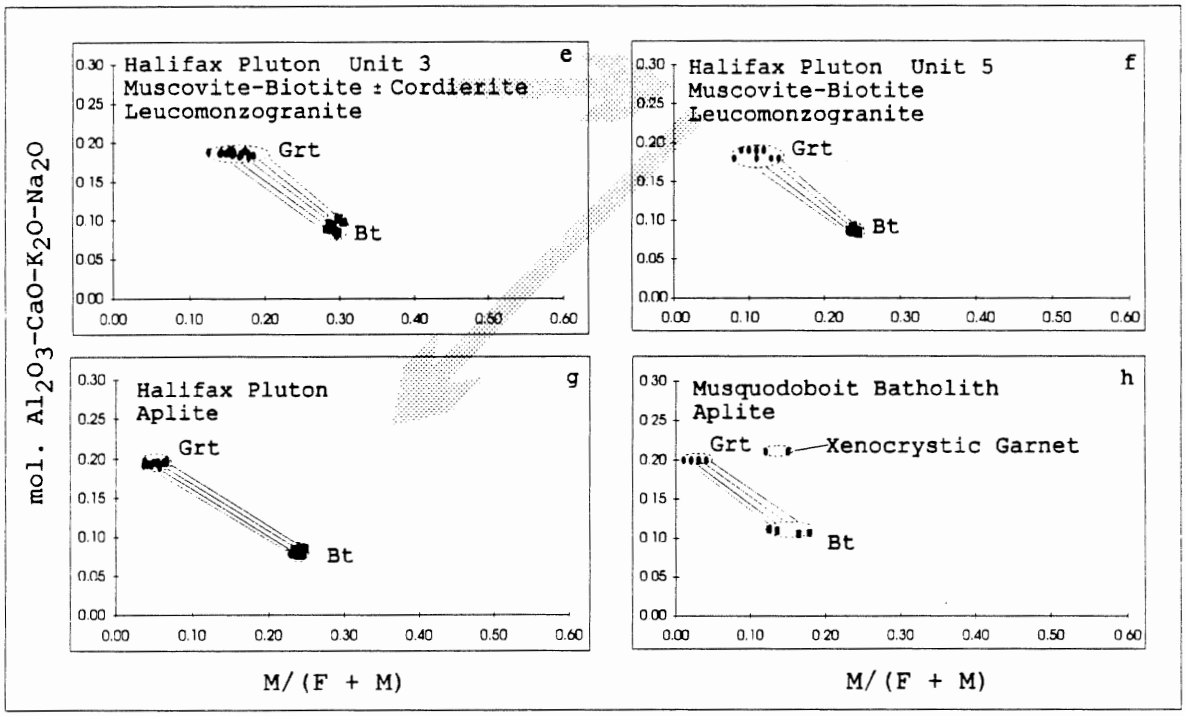

Figure 8.3a-h

Muscovite-Biotite Pair

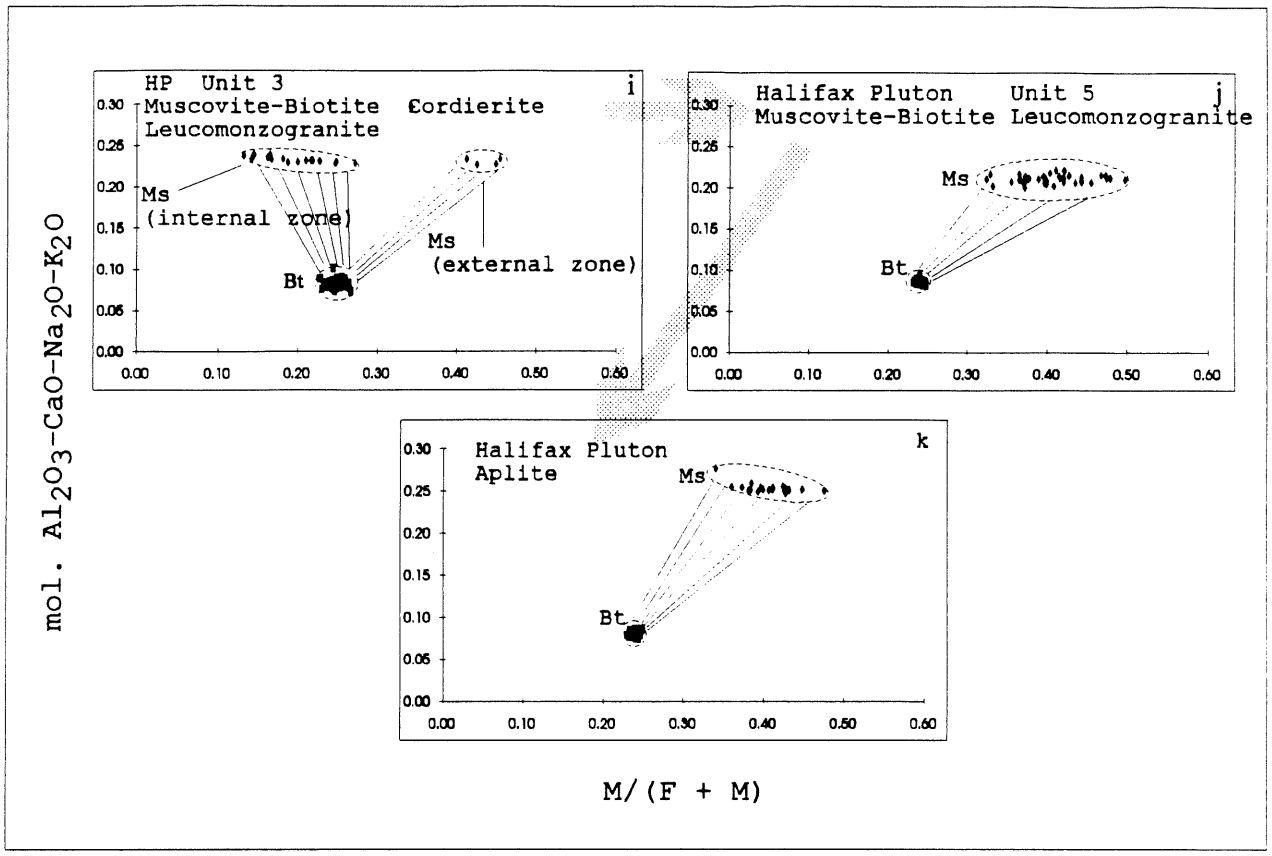

Figure 8.3a-k AFM plots projected from alkali feldspar, quartz, and plagioclase for the pairs of the AFM minerals from the HP and from the Musquodoboit Batholith (MacDonald, 1981). Tie-lines connect coexisting AFM minerals. Different line slopes and different positions of the same pair from different phases may indicate different magma environments. Stippled arrows indicate the HP or Musquodoboit Batholith magmatic trend.

Unit 3. The main trend of decrease in M/(F+M) probably reflects a magmatic differentiation trend. Biotite from monzogranite of the Musquodoboit Batholith (Fig. 8.2h) chemically compares well with that of the HP (Fig. 8.2b-c), but the biotite from aplite of the Musquodoboit Batholith has higher A value and lower M/(F+M) ratio than those of the dikes of this study (compare Fig. 8.2f with Fig. 8.2h).

Cordierite - Biotite pair

Euhedral shapes, even with some corrosion, may be characteristic of magmatic cordierite (Chapter 5). Different slopes for the same pair of AFM minerals (Fig. 8.3) may indicate different magmatic compositions. The slope and position of the pair Crd - Bt from biotite ± cordierite monzogranite (Fig. 8.3a) differ from those from aplite (Fig. 8.3c), which probably reflects not only differences in magmatic compositions, but also in other factors of the magma such as temperature and pressure. The same pair of AFM minerals from monzogranite of the Musquodoboit Batholith, as shown in Fig. 8.3b, has the same slope as that of the HP (Fig. 8.3a), indicating that cordierites and biotites in those two monzogranites, though of different locations, may have approximately the same magmatic environment (T, P, X). However, magmatic environment of the aplite in the Musquodoboit Batholith is either totally different from that of this study, comparing Fig. 8.3c with Fig. 8.3d (different

positions and different slopes), or may indicate different origins for these AFM minerals.

Garnet - Biotite pair

The slopes of tie-lines connecting Grt - Bt pairs from different host rocks are all negative and similar in position and slope (Figs. 8.3e-h), except the minerals (both garnet and biotite) from aplite contain lower M/(F+M) than from muscovite - biotite ± cordierite leucomonzogranite and muscovite - biotite leucomonzogranite. The biotite from aplite of the Musquodoboit Batholith contains lower M/(F+M) than that of this study (Figs. 8.2g, h).

Muscovite - Biotite pair

Figure 8.3i shows the zoned muscovite. The internal zone of this muscovite from muscovite - biotite ± cordierite leucomonzogranite has a lower M/(F+M) ratio (Fig. 8.3i) than the external zone of the same muscovite, which has similar values (A and M/(F+M)) to those of muscovite from muscovite - biotite leucomonzogranite (Fig. 8.3j). Chapter 4 presented some possible reasons for the muscovite zoning, including the possibility that the composition of local melt might have abruptly changed and so promote muscovite zoning. The similar slopes of the tie-lines (compare Fig. 8.3i (external zone) with Fig. 8.3j) may indicate that the changed melt (which formed the external zone of the muscovite) is very similar in compositions to that of muscovite - biotite leucomonzogranite.

8.2.3 *Liquidus Topologies*

Figure 8.4 synthesizes the relationships of all AFM mineral assemblages from the Halifax Pluton and relates them to the theoretical AFM liquidus topology distribution in P - T space (Abbott & Clarke, 1979; Speer, 1987). In the triangular diagrams, tie-lines connect two or three coexisting minerals. A two-phase liquidus boundary separates two primary liquidus fields. If a rock contains three mineral phases and a liquid phase, there must have been either a ternary eutectic or a ternary peritectic formed by those phases.

Methods

Two methods of connecting AFM diagrams of the HP to the theoretical topologies in P - T space are: (1) to constrain pressure for the HP in order to limit predicted liquidus topologies and then to limit appropriate topologies that address mineral assemblages in the HP; or (2) to connect each AFM mineral assemblage diagram to possible theoretical topologies in P - T space and then to find common ones for AFM assemblages of the HP phases to express equilibrium crystallization for those minerals (this second method is as in set theory in statistics: area 1 AND area 2 AND area 3, in which the result is common area of these three areas). McKenzie & Clarke (1975), from field and mineralogical observations near New Ross of the SMB, estimated

pressure condition (a minimum depth of 1.5 - 3 km) and Clarke et al. (1976), from the presence of magmatic andalusite in the SMB, constrained pressure to less than 4 kb for the SMB. This study adopts the second method to avoid possible imprecise pressure estimations.

Biotite granodiorite (Unit 1), biotite monzogranite (Unit 2), muscovite - biotite ± cordierite leucomonzogranite (Unit 3), and biotite ± cordierite monzogranite (Unit 4) all contain euhedral cordierite, which may indicate that cordierite is an early - formed ferromagnesian mineral. The much greater abundance of biotite relative to cordierite in the biotite granodiorite and biotite monzogranite may imply that biotite started to crystallize before cordierite, but modal abundances do not necessarily indicate a crystallization order. However, these textural phenomena indicate that magma began with the reaction: L = Bt or L = Crd. The intergrowth of cordierite with biotite, and biotite alignment along the margin of the inner crystal of cordierite (Fig 5.2b) may be expressed by the next reaction: L = Bt + Crd. For biotite - cordierite pairs only, topologies V - IX in the P - T space can explain their equilibrium relationship (Figs 8.4a-d). The last three rock phases (biotite monzogranite, biotite ± cordierite monzogranite, and muscovite - biotite ± cordierite leucomonzogranite) all contain some trace of garnet but no andalusite (see Chapter 2), which indicates that a liquidus line in the AFM diagram does not reach the andalusite

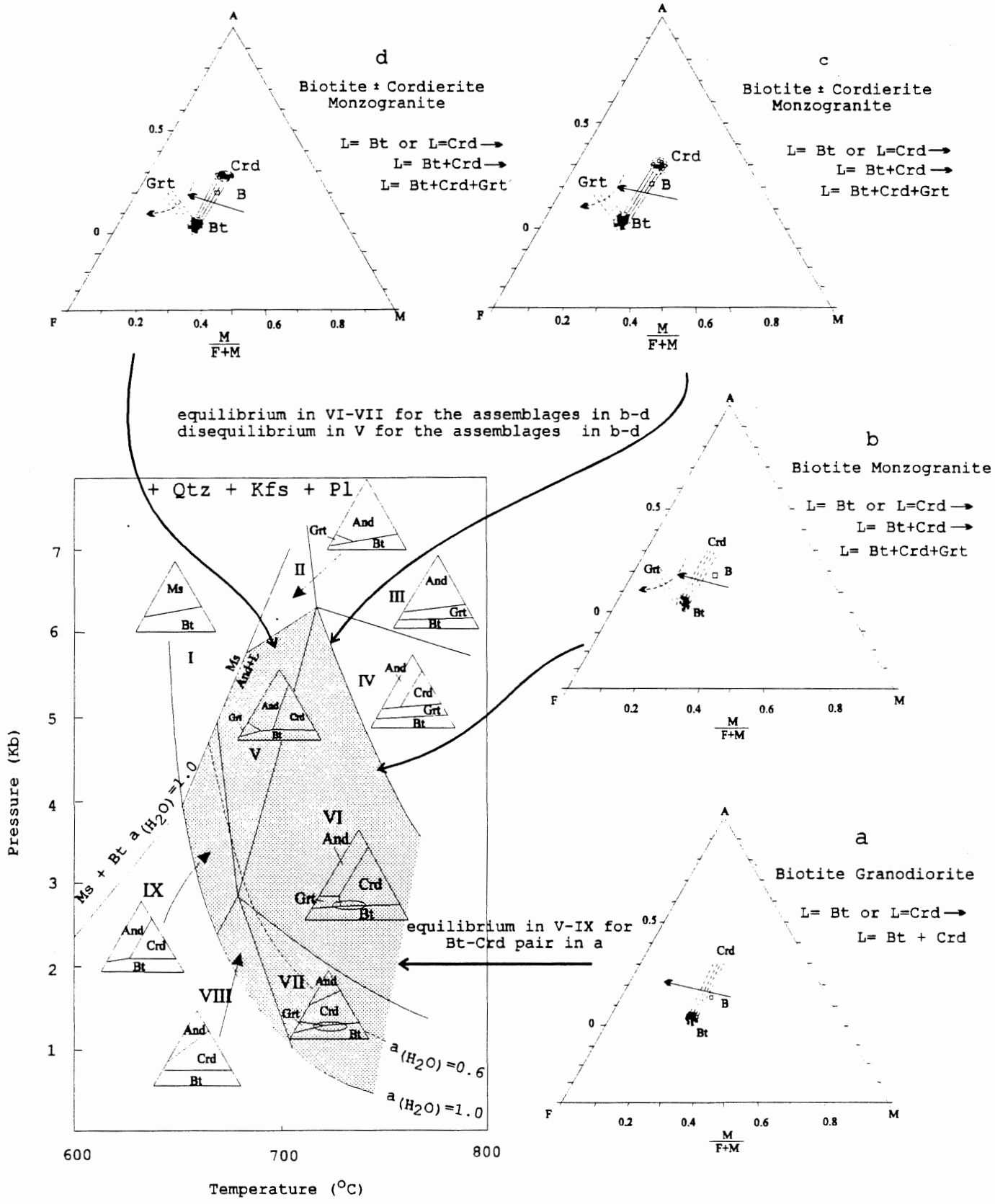
d
Biotite ± Cordierite
Monzogranite
L= Bt or L=Crd
L= Bt+Crd
L= Bt+Crd+Grt
c
Biotite ± Cordierite
Monzogranite
L= Bt or L=Crd
L= Bt+Crd
L= Bt+Crd+Grt
b
Biotite Monzogranite
L= Bt or L=Crd
L= Bt+Crd
L= Bt+Crd+Grt
a
Biotite Granodiorite
L= Bt or L=Crd
L= Bt + Crd
A
F
M
M/(F+M)
Crd
Grt
B
Bt
equilibrium in VI-VII for the assemblages in b-d
disequilibrium in V for the assemblages in b-d
+ Qtz + Kfs + Pl
Ms + Bt a(H2O)=1.0
a(H2O)=0.6
a(H2O)=1.0
equilibrium in V-IX for
Bt-Crd pair in a
Pressure (Kb)
Temperature (°C)
600
700
800

Figure 8.4a-d

Figure 8.4a-d. Regions of distinct AFM liquidus topology in P - T space (compiled from Abbott & Clarke,1979 and Speer, 1987). The AFM liquidus plane is projected from quartz, alkali feldspar, plagioclase (A = [Al_2O_3] - [K_2O] - [Na_2O] - [CaO], F = [FeO], M = [MgO]). The tie-lines connect coexisting AFM minerals. The dash lines connect magmatic minerals which exist in the rocks but no fresh samples are available for analysis. a: biotite and cordierite pair in biotite granodiorite can be illustrated in the topologies V - IX in the P - T space. b-d: the small ellipses in the topologies VI and VII indicate crystallization paths which may explain the biotite - cordierite - garnet assemblage in the biotite monzogranite and biotite ± cordierite monzogranite. The diagrams also include their host bulk composition points (B: open squares).

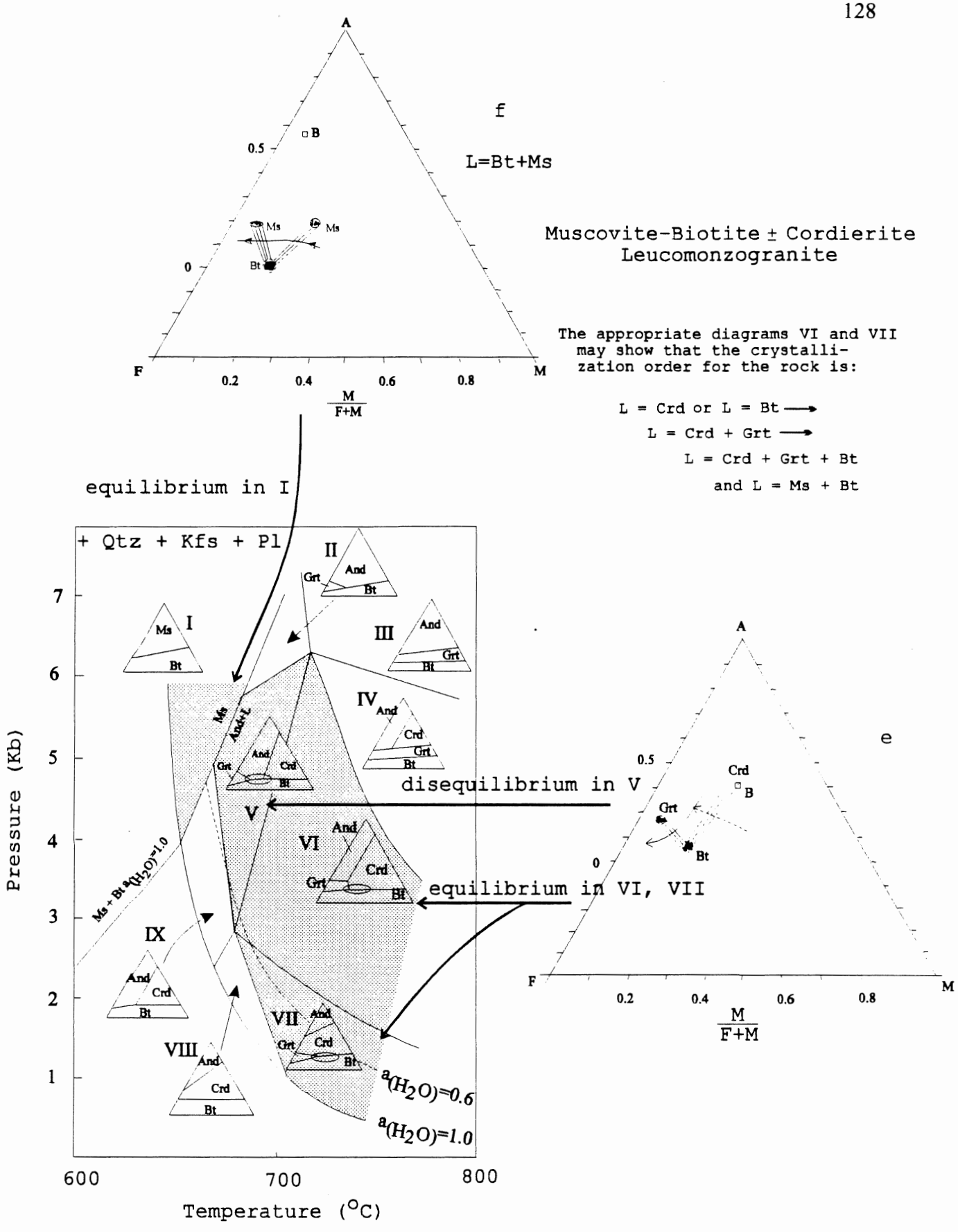
f
L=Bt+Ms
Muscovite-Biotite ± Cordierite
Leucomonzogranite
The appropriate diagrams VI and VII may show that the crystallization order for the rock is:
L = Crd or L = Bt →
L = Crd + Grt →
L = Crd + Grt + Bt
and L = Ms + Bt
equilibrium in I
+ Qtz + Kfs + Pl
disequilibrium in V
equilibrium in VI, VII
e
Pressure (Kb)
Temperature (°C)
M/F+M
Ms + Bt a(H2O)=1.0
a(H2O)=0.6
a(H2O)=1.0

Figure 8.4e-f

Figure 8.4e-f. Regions of distinct AFM liquidus topology in P - T space (compiled from Abbott & Clarke,1979 and Speer, 1987). The AFM liquidus plane is projected from quartz, alkali feldspar, plagioclase (A = [Al_2O_3] - [K_2O] - [Na_2O] - [CaO], F = [FeO], M = [MgO]). The tie-lines connect coexisting AFM minerals. The dash lines connect magmatic minerals which exist in the rocks but no fresh samples are available for analysis. e: the appropriate topologies VI and VII may explain the assemblage: biotite - cordierite - garnet in muscovite - biotite ± cordierite leucomonzogranite; the topology V shows disequilibrium condition for the assemblage. f: the topology I indicates crystallization path for the muscovite - biotite pair in muscovite - biotite ± cordierite leucomonzogranite. The diagrams also include their host bulk composition points (B: open squares).

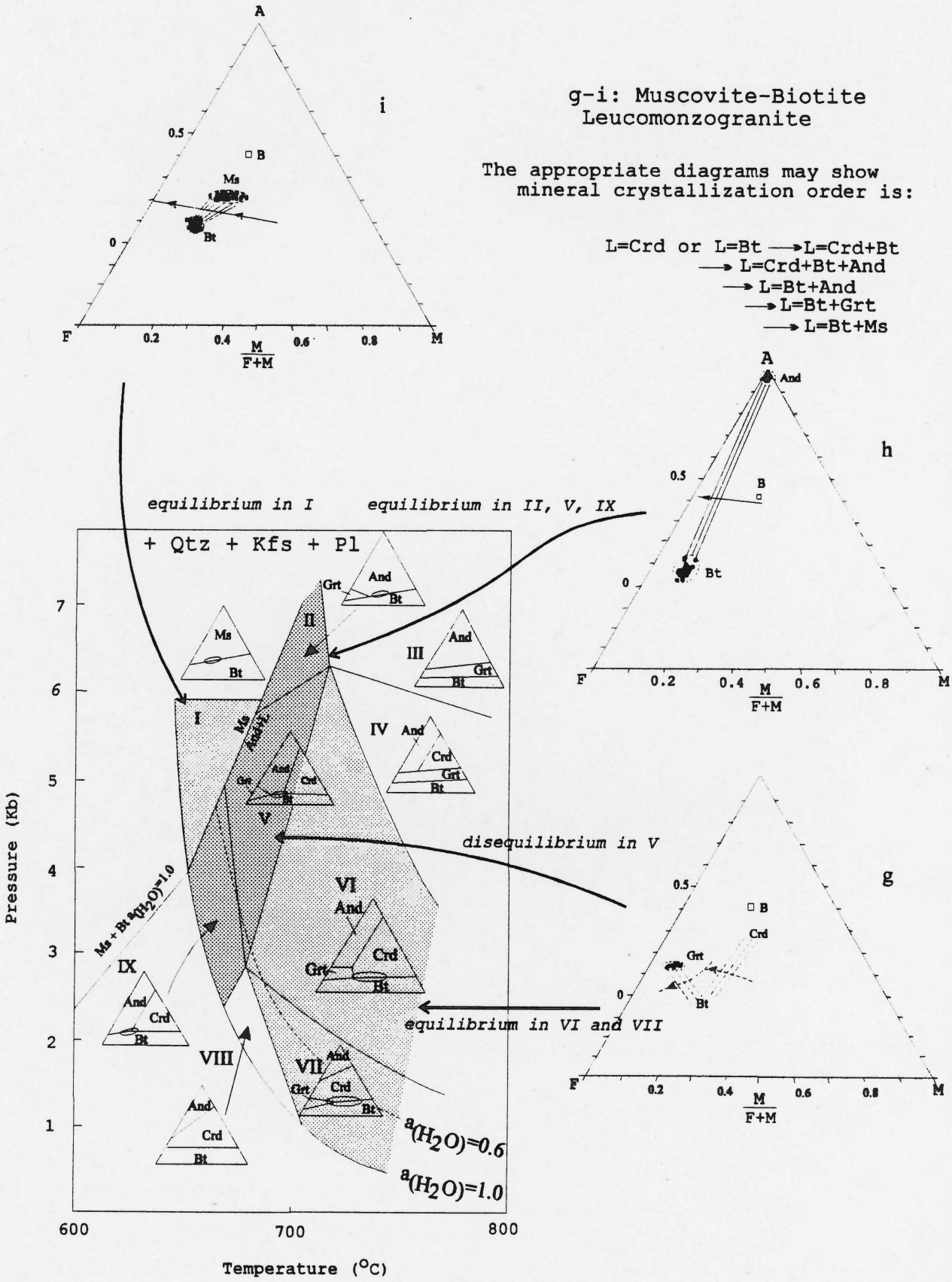
g-i: Muscovite-Biotite Leucomonzogranite
The appropriate diagrams may show mineral crystallization order is:
L=Crd or L=Bt → L=Crd+Bt
→ L=Crd+Bt+And
→ L=Bt+And
→ L=Bt+Grt
→ L=Bt+Ms
i
h
g
equilibrium in I
equilibrium in II, V, IX
disequilibrium in V
equilibrium in VI and VII
+ Qtz + Kfs + Pl
Pressure (Kb)
Temperature (°C)
$a(H_2O)=0.6$
$a(H_2O)=1.0$
$Ms + Bt\ a(H_2O)=1.0$
F
M
F+M

Figure 8.4g-i

Figure 8.4g-i. Regions of distinct AFM liquidus topology in P - T space (compiled from Abbott & Clarke,1979 and Speer, 1987). The AFM liquidus plane is projected from quartz, alkali feldspar, plagioclase (A = [Al_2O_3] - [K_2O] - [Na_2O] - [CaO], F = [FeO], M = [MgO]). The tie-lines connect coexisting AFM minerals. The dash lines connect magmatic minerals which exist in the rocks but no fresh samples are available for analysis. g: the appropriate topologies VI and VII may explain the assemblage: biotite - cordierite - garnet in muscovite - biotite ± cordierite leucomonzogranite. The small ellipses in the topologies VI and VII indicate crystallization paths; h: The small ellipses of the topologies II, V, and IX (dark area) in the P - T space can illustrate the pair of biotite and andalusite in the rock but these topologies make disequilibrium condition for the assemblage in the diagram g; i: the topology I shows crystallization path for the muscovite - biotite pair in muscovite - biotite leucomonzogranite. The diagrams include their host bulk composition points (B: open squares).

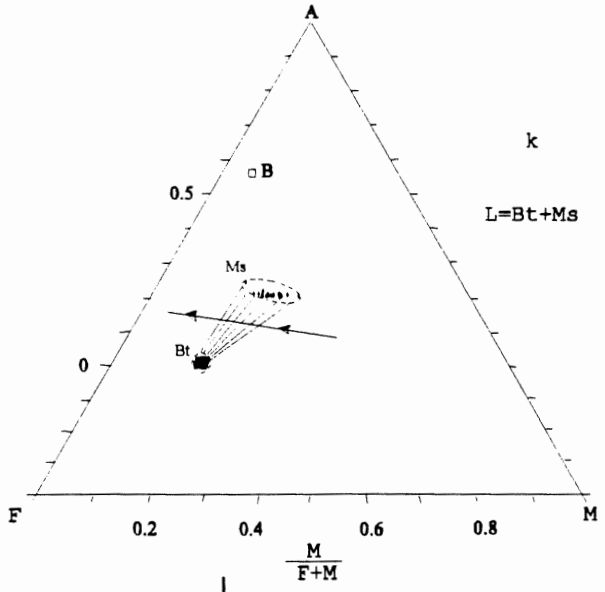

Aplite

The appropriate diagrams VI and VII may show that mineral crystallization order for aplite will be:

L = Crd →

L = Crd + Grt →

L = Crd + Grt + Bt →

L + Crd = Grt + Bt

and L = Ms + Bt

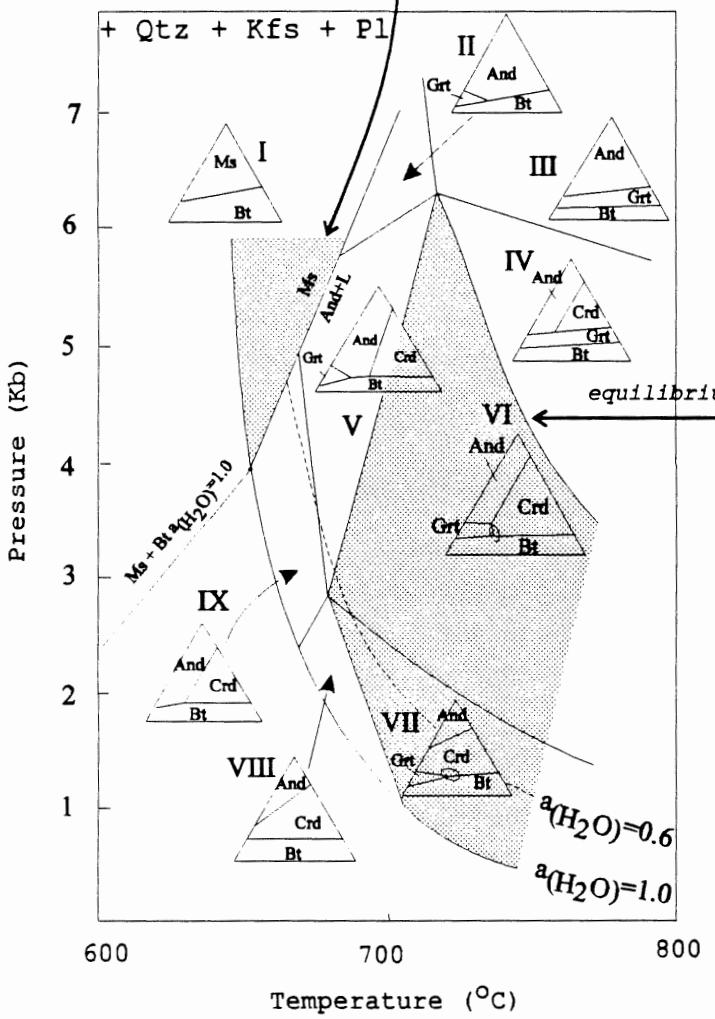

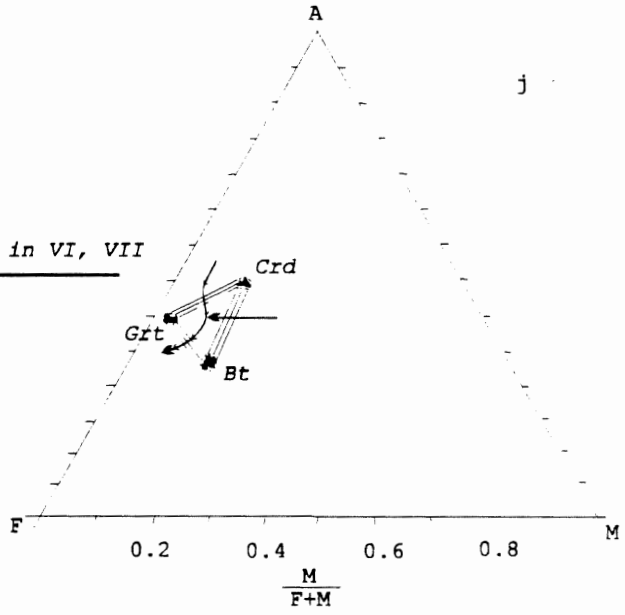

Figure 8.4j-k

Figure 8.4j-k. Regions of distinct AFM liquidus topology in P - T space (compiled from Abbott & Clarke,1979 and Speer, 1987). The AFM liquidus plane is projected from quartz, alkali feldspar, plagioclase (A = [Al_2O_3] - [K_2O] - [Na_2O] - [CaO], F = [FeO], M = [MgO]). The tie-lines connect coexisting AFM minerals. j: the appropriate topologies VI and VII may explain the assemblage: biotite - cordierite - garnet in the aplite but the crystallization path may be different from muscovite - biotite ± cordierite leucomonzogranite. The small ellipses in the topologies VI and VII indicate crystallization paths; k: the topology I shows crystallization path for the muscovite - biotite pair in the aplite. The diagrams include their host bulk composition points (B: open squares).

field. The AFM reaction order for those three phases would be L = Bt or L = Crd, → L = Bt + Crd, → L = Bt + Crd + Grt, which equilibrium relationship can be expressed by the topologies VI and VII in the P - T space. The origin of muscovite in some parts of muscovite - biotite ± cordierite leucomonzogranite may be the final stage. Decreasing temperature and increasing water pressure would allow the appearance of the muscovite field in the AFM topology and the crystallization reaction L = Bt + Ms (Fig. 8.4f) (Abbott, 1985; Speer, 1987).

Muscovite - biotite leucomonzogranite contains biotite, muscovite, cordierite, and andalusite (Figs. 8.4g-i). Common andalusite without garnet in this rock differs in its liquidus reaction from other rocks. The topologies V - IX in Figure 8.4 may describe the liquidus trend: L = Crd or L = Bt → L = Bt + Crd. The topologies II, V, and IX can illustrate equilibrium relationship between biotite and andalusite: L = Bt + Crd + And, and L + Crd = Bt + And, finally L = Bt + Ms (topology I).

The topology for the aplite may be the same as for muscovite - biotite ± cordierite leucomonzogranite (Fig. 8.4j, k), because the aplite contains the same mineral assemblage as this rock: Crd, Grt, Bt, and Ms. The texture (corroded cordierite) in the aplite shows that cordierite completed its crystallization but biotite and garnet did not finish crystallization because of quenching. However, the aplite contains many magmatic garnet

grains whereas muscovite - biotite ± cordierite leucomonzogranite only contains traces of garnet. Then, the AFM diagrams may be same (i.e., topologies VI and VII), but the reaction order may be different (different part of crystallization line): L = Crd → L = Crd + Grt → L = Crd + Grt + Bt → L + Crd = Grt + Bt, finally L = Ms + Bt (topology I).

Summary

Figures 8.4a-k connect each AFM mineral assemblage diagrams to possible theoretical topologies in P - T space. Figure 8.5 adopts the method as in set theory of probability theory (e.g.: area 1 AND area 2 AND area 3, in which the result is common area of these three areas) to further summarize AFM diagrams for each rocks of the HP to select common areas in the P - T space to express rock P - T condition for the whole Halifax Pluton. The final P - T space indicates variation of magma P - T conditions, corresponding 5kb and 650 - 750°C.

The pressure estimated is higher than the estimations for the SMB (Clarke, et al. 1976; McKenzie & Clarke, 1975) and contrast to others (2-4 Kb: Miller, et al. 1981; Roycroft, 1991). However, if the topology IX (which looks like a curb the arrow has to overpass in Figure 8.5) is included to explain the coexisting relationship between biotite and cordierite or andalusite, the corresponding pressure will be 4kb (Figure 8.6). In addition, the P - T curves of muscovite (Chatterjee & Flux,

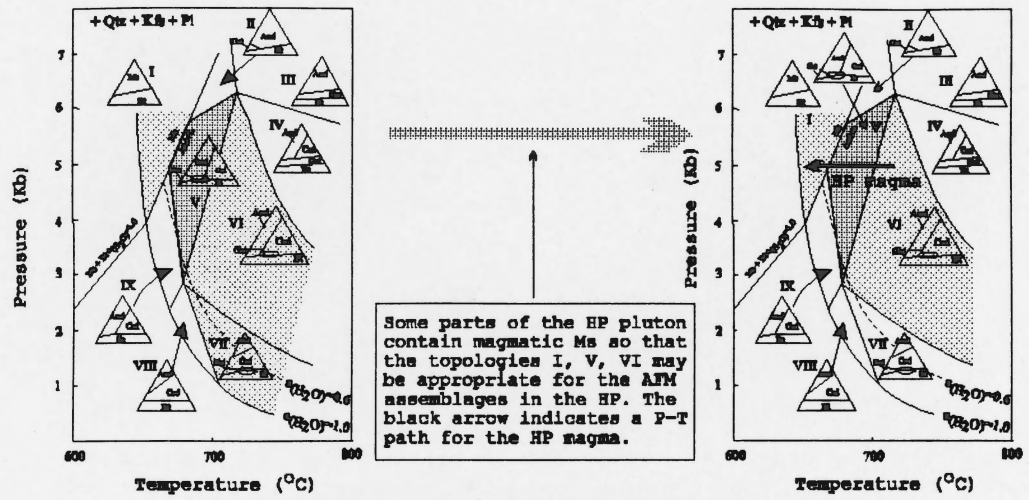
+Qtz+Kfs+Pl
Pressure (Kb)
Temperature (°C)
HP magma
Some parts of the HP pluton contain magmatic Ms so that the topologies I, V, VI may be appropriate for the AFM assemblages in the HP. The black arrow indicates a P-T path for the HP magma.

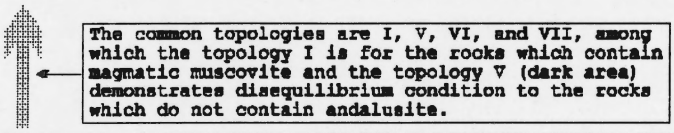
The common topologies are I, V, VI, and VII, among which the topology I is for the rocks which contain magmatic muscovite and the topology V (dark area) demonstrates disequilibrium condition to the rocks which do not contain andalusite.

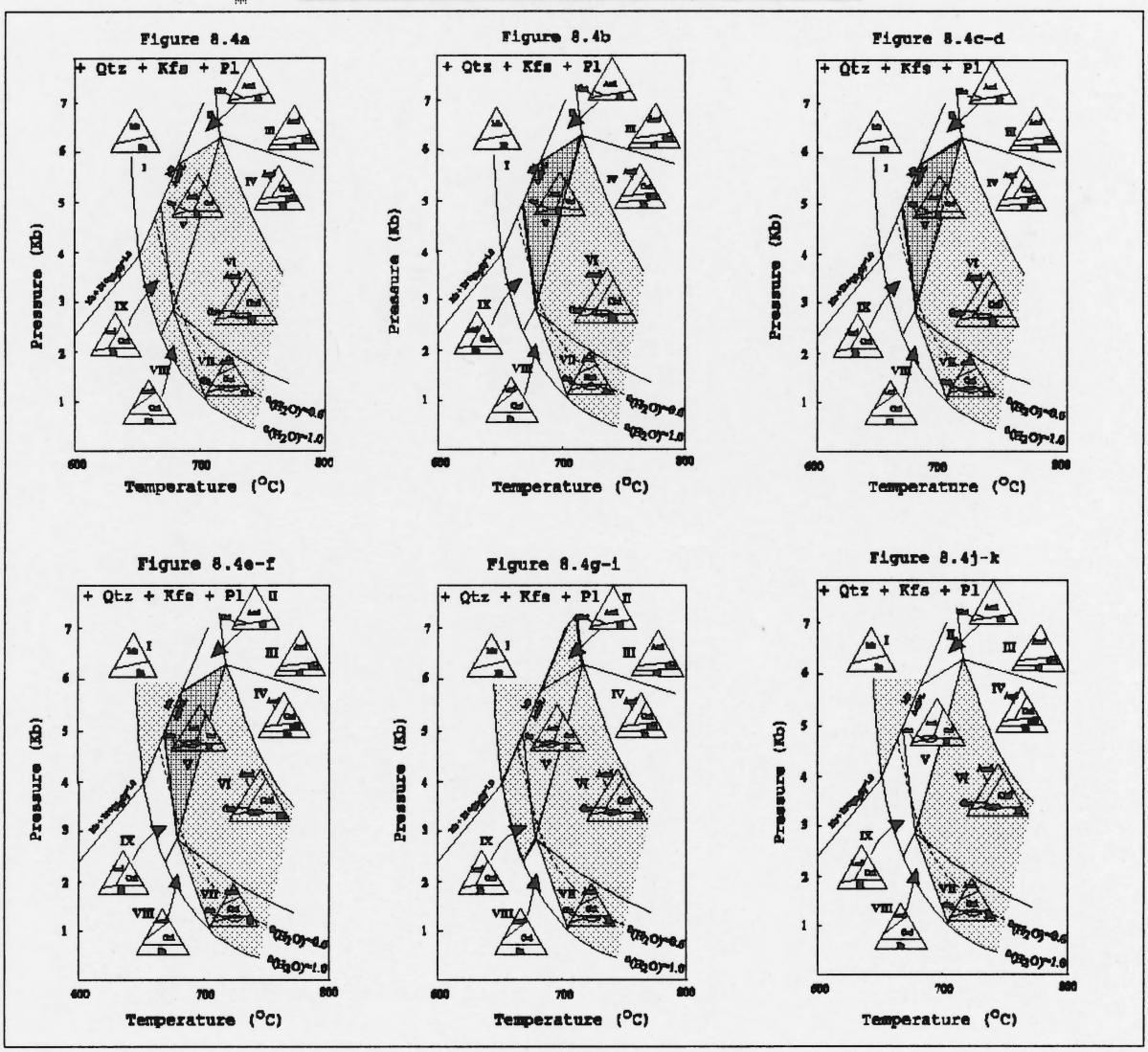
Figure 8.4a
Figure 8.4b
Figure 8.4c-d
Figure 8.4e-f
Figure 8.4g-i
Figure 8.4j-k
+ Qtz + Kfs + Pl
Pressure (Kb)
Temperature (°C)

Figure 8.5

Figure 8.5 Summarized AFM topologies in the P - T space. Stippled areas and diagrams are selected for each rock of the HP (see previous text paragraphs for details). The common topologies are V and VI, and I for the muscovite - contained rocks. The dark stippled area shows disequilibrium condition to the rocks which do not contain andalusite. A black arrow in the final P - T space may indicate variation of magma P - T conditions, corresponding 5kb and 650 - 750°C.

1986; Chatterjee & Johannes, 1974) intersect the minimum melting curves of granite (Johannes, 1984; Tuttle & Bowen, 1958) and peraluminous granite (Wyllie, 1977) at a range of temperatures from 635° to 670 °C and pressures from 3 to 4.4 kb (see Fig. 4.1). And if both F and B are present in the melt, the solidus temperature will be reduced (Figure 8.6) (Manning & Pichavant, 1983).

8.3 Reason For Zonings in the AFM Minerals

Zonings exist in the AFM minerals in the HP. The reasons for those zonings have been discussed individually in chapters 3 - 7. Overall, variations in transitional elements (Fe, Mn, Ti) and Mg form those chemical zonings. Substitutions of an transitional ion or ionic group for another ion or ionic group are sensitive images of change of environments: temperature, pressure, concentration of melt, oxygen fugacity, and water pressure. Fe valences may be the most sensitive to changes in oxygen fugacity, resulting in more or less Fe intake of minerals because of different sizes of Fe ion according to different valences. In these cases, Mn, Ti and Mg elements will have had to reciprocally fill into the crystal structure.

8.4 Biotite - an indicator of peraluminous granitoid origin

MacDonald & Horne (1988) reported that, in the HP, biotite varies in modal abundance from 12 - 15% in the early - phase rocks to 0 - 5 % in the late - phase rocks. Biotite is one of the magmatic mineral phases in peraluminous granite. Zen (1989)

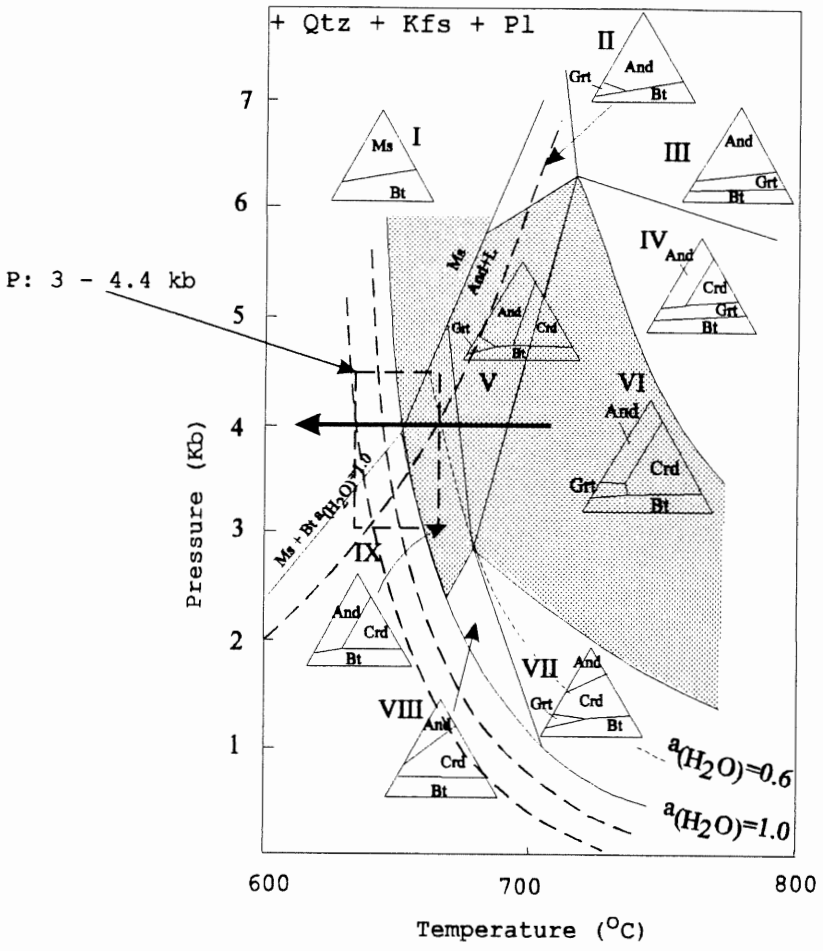

Figure 8.6 The selected common areas which include the topology IX indicate the corresponding pressure is 4 kb (arrow). In addition, the P - T curves of muscovite (Chatterjee & Flux, 1986; Chatterjee & Johannes, 1974) intersect the minimum melting curves of granite (Johannes, 1984; Tuttle & Bowen, 1958) and peraluminous granite (Wyllie, 1977) at a range of temperatures from 635° to 670 °C and pressures from 3 to 4.4 kb (dashed square and also see Figure 4.1 in details). And if both F and B are present in the melt, the granite solidus temperature will be reduced (Manning & Pichavant, 1983).

noted that the magmatic biotites in the SMB exist as equigranular grains with other magmatic minerals and as interstitial grains. In the HP, biotite ranges from euhedral inclusions in other minerals, to equigranular with other magmatic minerals, to smaller ones occurring in intergranular spaces. These variable occurrences are related to the wide P - T stability region (Fig. 3.1) of biotite which permits it to crystallize over the whole magma evolution. Predicted AFM diagrams (in P - T space in Fig. 8.4) have biotite as the first or second crystallizing mineral.

Early - crystallized phases of the HP, such as biotite granodiorite and biotite monzogranite, are more primitive than later phases such as muscovite - biotite leucomonzogranite. The compositional similarity between magmatic biotites from those early - crystallized phases of the HP and biotites from sedimentary rocks and metasedimentary rocks (Fig. 8.7), may indicate that the biotite crystallized from a source, the composition of which is close to metasedimentary rocks.

8.5 A Unique Aplite

The studied aplite intrudes biotite monzogranite (location in Fig. 2.3) and contains a rare assemblage of four different AFM minerals: Bt, Ms, Crd and Grt. The bulk composition of this aplite indicates that the liquid may fall in the Fe - cordierite area but close to garnet area in the AFM plane (see Fig. 8.4g and text for sequence). The quench textures shown by the biotite (extremely elongated shapes and swallowtail edges, see Fig. 3.10)

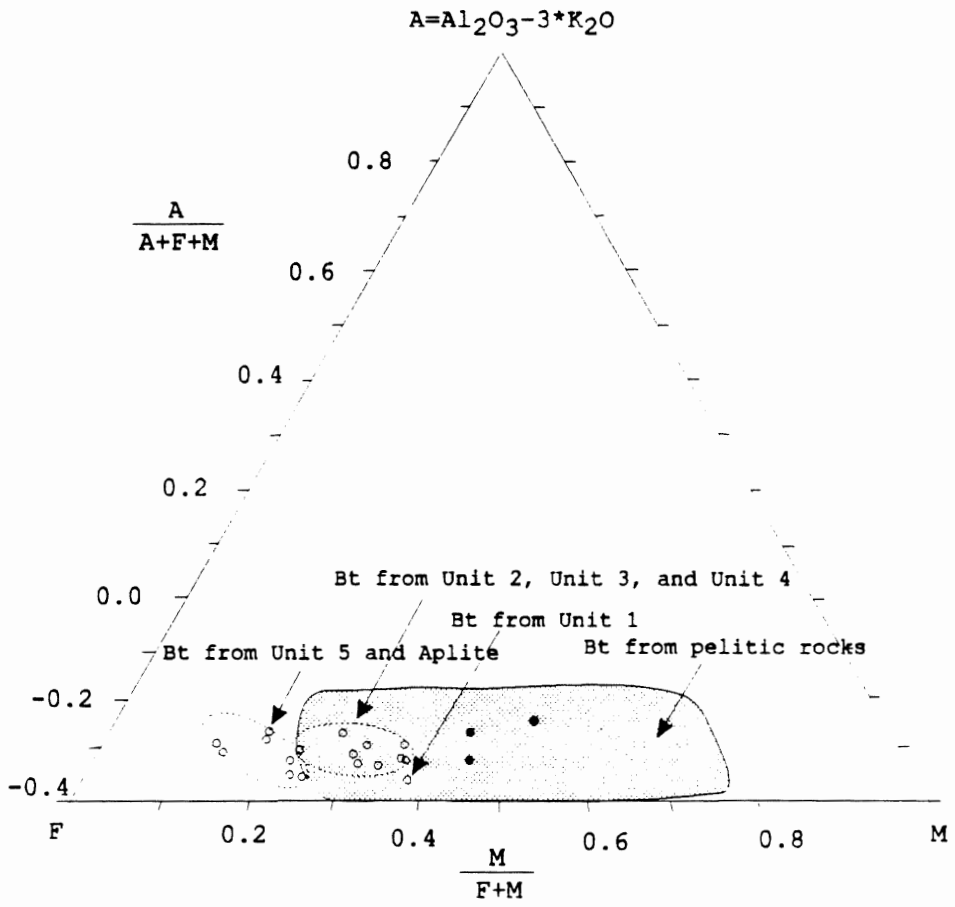

Figure 8.7 AFM projection from muscovite showing plotted positions of biotites from different phases of the HP; stippled area shows the composition range of biotite occurring in pelitic rocks (Best, 1982); solid cycles are biotite from Lower Paleozoic Meguma Group of the Beaver Dam area (Kontak & Smith, 1993).

and the garnet (skeletal, see Figs. 6.1c) in the aplite prove that the aplite magma crystallized rapidly, i.e. with an abrupt decrease in temperature and/or pressure.

The studies of Delaney & Pollard (1982) and Petford et al. (1993) suggest that small dikes require rapid rates of emplacement. Because of the size of the HP dike (width is less than 148 cm), it may have crystallized quickly. Two lines of evidence may support the hypothesis that the biotite monzogranite host had been cool when the hot aplite magma intruded: (1) sharp contacts between the aplite and the host; (2) the ratios Rb/Sr, Fe/Mg, Na/Ca (= 9, 4.6, 49 respectively) (M.A. MacDonald's unpublished data) of the aplite differ from those (= 1.6, 1.3, 5.3 respectively) of the host (biotite monzogranite). Those lines of evidence support idea that the aplite may represent a different magma pulse (Clemens & Mawer, 1992; Takada, 1990; Weertman, 1971, 1980).

The quenched aplite provides a good, static picture of crystallization sequence of peraluminous granite magma in the HP. As discussed in Section 8.1 (see Figs 8.1j, k and text), the magma had probably already crystallized cordierite and had just begun to crystallize garnet and biotite when it underwent quenching. The result is a rare disequilibrium assemblage of cordierite, garnet, biotite, and muscovite.

8.6 Summary

Different slopes or positions of the same pair AFM minerals in the AFM diagrams may indicate different magmatic environments (T, P, X). The theoretical topologies in P - T space can illustrate the AFM mineral crystallization order for each phase of the HP. The pressure estimated from the summarized AFM topologies is 4 kb for the SMB. The pressure may be lower, for the P - T curves of muscovite intersect the minimum melting curves of granite at lower pressure. The transitional elements (Fe, Mn, Ti) are sensitive to change of environments: temperature, pressure, concentration of melt, oxygen fugacity, and water pressure, resulting in the zonings. The compositional information of the magmatic biotites may help to study the pluton source. The quenched aplite provides a good, static picture of crystallization sequence of peraluminous granite magma in the HP and it is worth further studying.

Chapter 9 Summary of Results

9.1 Summary List of Main Results

1. Biotite is an indicator of peraluminous granitoid origin

Most of the biotite present in all phases of the HP is magmatic. The compositional similarity between magmatic biotite from those early - crystallized phases of the HP and biotites from metasedimentary and sedimentary rocks may indicate that those biotites crystallized from the magma compositions which are close to metasedimentary and sedimentary rocks.

2. Biotites from the HP have high A/CNK and low M/(F+M)

The biotites have A/CNK and M/(F+M), ranging from 1.73 to 1.84 and 0.25 to 0.48, respectively, showing that these biotites have much higher A/CNK and lower M/(F+M) values than those of Zen (1988: his higher boundary of 1.4 for A/CNK of igneous biotite coexisting with hornblende, lower boundary of 0.3 for M/(F+M) of igneous biotite from granitic rock). The A/CNK of igneous biotite follows the peraluminosity of the rock.

3. Zoning in biotite

Zoning in biotite has not previously been reported in peraluminous granites. The biotite from the aplite of the HP shows optical zoning which might be caused by loss of water, or abrupt changes in fO_2. Chemical zoning of the biotite from Unit 3 is seen only at the outermost rims with lower Ti, and higher Mg and

Fe, than the core. Sudden change in fO_2 probably produced the zoning at the outermost rims in the biotite.

4. Twinning

Twinning is rare in biotites but exists in the biotite from the mafic porphyry. It probably exists in other plutons but has not yet been recognized.

5. Quench texture of the biotite

Biotite crystals in the aplite show extremely elongated shapes, swallowtail edges, and highly ragged margins which may result from an abrupt decrease in temperature and /or pressure.

6. Chemical consistency between the muscovite and the host

The muscovites from the HP are rich in Al and deficient in Fe compared with muscovites from other granotoid rocks. The chemical compositions of muscovites demonstrates consistent relationships between the average composition (Si and Ti) of the muscovite and of the host.

7. Zoning in muscovite

One muscovite crystal from Unit 3 near the contact between Unit 3 and Unit 5 shows sharp decreases in TiO_2 and FeO and an abrupt increase in Mg from the internal zone to the external zone. Abrupt change in the composition of local magma with regards to penetration along the contact of later melt may result in the zoning.

8. Magmatic muscovite

Magmatic muscovite exists in the HP. In some locations within the HP (muscovite - biotite leucomonzogranite, and in some parts of muscovite - biotite ± cordierite leucomonzogranite), primary muscovite is dominant relative to secondary muscovite. Magma rich in H_2O and with high A/CNK can have a low solidus temperature for muscovite.

9. Magmatic cordierite

Magmatic cordierite is euhedral, shows grain size compatibility with other rock - forming minerals and contains few inclusions. Usually, the ratio M/(F+M) is less than 0.5, Na_2O is greater than 1 wt % and rims higher in the ratio M/(F+M). Magmatic cordierites from the HP have an M/(F+M) ratio of 0.23 to 0.48 and contain Na_2O from 1.26 to 1.29 wt%.

10. An interesting cordierite

A grain of cordierite consists of an inner euhedral cordierite crystal surrounded by an outer euhedral crystalline cordierite overgrowth. The continuing growth of more cordierite over the early central crystal indicates a complex history of magmatic evolution, with this overgrowth suggesting two crystallization stages which are indicated by the hiatus: (1) nucleation and crystallization from the magma and (2) growth over the early central crystal.

11. Magmatic and metamorphic garnet

Two types of garnet, magmatic and metamorphic, exist in the HP. Magmatic garnet is euhedral, inclusion-free, without reaction rims, and with reverse zoning. Metamorphic garnet is anhedral, large size (7 mm across), with reaction rims, inclusions, and normal zoning pattern. Synthesizing all the evidence is important in judging whether a garnet is of igneous or metamorphic origin.

12. Quench texture of garnets

Crystals with quench texture occur in siliceous volcanics and subvolcanic rocks such as rhyolite, obsidian, quartz - or feldspar - porphyry, also in isolated tuffs. Those crystals are usually plagioclase, quartz, pyroxene, and olivine and quench texture has never been recognized for garnets. Garnet from the aplite has a quench texture characterised by embayments and sieve texture which forms skeletal shapes with partly euhedral outlines. The euhedral crystal outlines and complete corners imply that those garnet crystals had an equilibrium relationship with the melt for a period of time resulting in nucleation and partial growth, and then went to a disequilibrium relationship with rapid change in the conditions of melt crystallization, such as supercooling. Supercooling resulted in skeleton - form garnet with incomplete growth.

13. Magmatic garnet with normal zoning

The magmatic garnets with quench texture have normal zoning; they should have had reverse zoning instead of normal zoning according to the proposal of Allan & Clarke (1981).

14. Two types of andalusite and cause of central pink zoning

The andalusite appears as two types in the late - stage phase: andalusite mantled by muscovite and among crystals of alkali feldspar. The abrupt decreases in Fe from core to rims correspond to the margins of the central pink zone. Rapid decreases in temperature and then fo_2 result in lower Fe intake by andalusite, forming central pink zoning.

15. A unique aplite

The studied aplite contains one rare assemblage of four different AFM minerals: Bt, Ms, Crd and Grt. Quench textures shown by the biotite and the garnet in the aplite prove that the aplite magma crystallized rapidly.

16. Information from AFM diagrams

AFM diagrams are well suited to show the dependence of the AFM mineral assemblages on the types of peraluminous granitoid rocks. Different slopes or positions of the same pair AFM minerals may indicate different magmatic environment (T, P, X, see Chapter 8).

17. Mineral crystallization order

The theoretical topologies in P - T space may illustrate AFM mineral crystallization order for each phase of the HP:

Unit 1: L = Bt or L = Crd, → L = Bt + Crd;

Unit 2, 3, 4: L = Bt or L = Crd, → L = Bt + Crd, → L = Bt + Crd + Grt and L = Bt + Ms (for some parts);

Unit 5: L = Crd or L = Bt → L = Bt + Crd → L = Bt + Crd + And, or L + Crd = Bt + And → L = Bt + Ms;

Aplite: L = Crd → L = Crd + Grt → L = Crd + Grt + Bt → L + Crd = Grt + Bt → L = Ms + Bt.

Appendix 1 Comments on the Methods

This study uses conventional optical mineralogy, Roycroft's technique, etching / Nomarski technique, electron microprobe, and backscattered image technique to detect zoning in the AFM minerals. Roycroft's technique is efficient to prepare mica samples to detect zoning by petrographic microscope and electron microprobe.

Concentrated hydrochloric acid is allowed to etch biotite, cordierite, and garnet in polished thin sections for 2 to 17 minutes. Then the etched samples are observed with Nomarski and petrographic microscopes. Fresh cordierite samples are rare in the Halifax Pluton, and HF readily destroys cordierite before any possible microtopography may appear. Etched garnet reveals zoning poorly. These observations may indicate that etching is suitable only for those minerals in which: 1) zoning is caused by variation of main cations whose physical natures are highly contrasted (e.g., Ca and Na in plagioclase); 2) zoned minerals are hard enough to withstand etching; and 3) samples are fresh enough to avoid "fog" occurring when etching.

Practically and economically to detect any possible zoning in a mineral, first use optical methods which include conventional petrographic microscope, Roycroft's technique, etching / Nomarski, and then electron microprobe and back - scattered image technique. The back - scattered technique is better than optical methods for very small minerals (less than 0.5mm across).

Appendix 2 Microprobe Analyses

(data as obtained directly from electron microprobe)

Biotite from Mafic Porphyry (Unit 7: 349-1)

Point	SiO2	TiO2	Al2O3	FeO	MnO	MgO	Na2O	K2O	Total	A/CNK	M/(F+M)
1	36.19	3.10	19.34	18.25	0.46	8.90	0.25	9.57	96.05	1.80	0.46
2	36.18	3.16	19.26	18.04	0.41	9.01	0.28	9.72	96.06	1.75	0.47
3	35.68	3.14	18.90	18.10	0.48	8.92	0.25	9.60	95.08	1.75	0.47
4	35.73	3.26	18.96	18.15	0.54	8.90	0.36	9.60	95.49	1.73	0.47
5	35.21	3.17	18.85	18.03	0.45	8.85	0.31	9.44	94.32	1.76	0.47
6	35.67	3.12	18.80	17.86	0.32	8.95	0.22	9.60	94.56	1.75	0.47
7	35.59	2.91	18.57	18.60	0.44	9.13	0.30	9.57	95.13	1.71	0.47
8	35.64	3.04	18.99	18.06	0.45	8.96	0.14	9.50	94.78	1.81	0.47
9	35.70	2.91	18.78	17.70	0.55	9.13	0.29	9.27	94.34	1.79	0.48
10	35.57	2.81	18.88	17.58	0.61	9.03	0.24	9.25	93.98	1.81	0.48
11	35.44	2.93	18.82	17.96	0.59	9.09	0.38	9.36	94.57	1.75	0.47
12	35.55	3.01	18.72	17.83	0.54	8.87	0.20	9.38	94.10	1.79	0.47
13	35.50	2.90	18.71	17.66	0.62	9.24	0.34	9.59	94.57	1.71	0.48
14	35.77	2.90	18.85	17.86	0.41	9.08	0.22	9.46	94.54	1.78	0.48
15	35.18	3.00	18.50	17.53	0.44	9.03	0.30	9.57	93.55	1.71	0.48
16	35.32	2.88	18.35	17.88	0.50	9.02	0.27	9.75	93.98	1.67	0.47
17	34.74	2.95	18.45	18.43	0.33	8.93	0.25	8.95	93.05	1.83	0.46
18	35.78	2.94	19.00	18.26	0.33	9.19	0.16	9.64	95.29	1.78	0.47
19	35.84	2.94	19.14	18.66	0.44	9.10	0.24	9.79	96.14	1.74	0.46
20	35.78	2.87	18.83	18.23	0.40	8.93	0.25	9.73	95.02	1.72	0.47
21	34.92	2.68	18.64	18.98	0.30	8.86	0.22	8.84	93.43	1.88	0.45
22	35.79	2.83	18.60	18.15	0.20	8.83	0.19	9.55	94.15	1.75	0.46
23	35.53	3.01	18.49	17.79	0.46	8.96	0.21	9.64	94.08	1.72	0.47
24	35.62	3.20	18.95	18.60	0.29	8.93	0.25	9.64	95.47	1.75	0.46
25	35.69	2.80	19.04	17.68	0.43	9.18	0.37	9.57	94.74	1.74	0.48
26	35.82	2.88	18.86	17.67	0.46	9.19	0.27	9.47	94.63	1.76	0.48
27	35.32	3.03	18.42	17.81	0.51	8.83	0.47	9.31	93.70	1.70	0.47

28	35.63	2.82	18.68	17.99	0.46	9.02	0.37	9.34	94.31	1.74	0.47
29	35.15	2.70	18.61	17.80	0.39	8.96	0.45	9.44	93.50	1.70	0.47
30	35.06	2.68	18.57	18.02	0.58	8.80	0.19	9.39	93.28	1.77	0.47
T/30	35.55	2.95	18.79	18.04	0.45	8.99	0.27	9.48	94.53	1.76	0.47

Biotite from Unit 1(92-HP-L)

Point	SiO2	TiO2	Al2O3	FeO	MnO	MgO	Na2O	K2O	Total	A/CNK	M/(F+M)
1	34.51	4.14	18.24	20.11	0.41	6.71	0.19	9.05	93.37	1.80	0.37
2	34.10	3.88	18.01	20.10	0.29	6.79	0.24	9.35	92.78	1.71	0.38
3	33.82	3.61	19.12	19.93	0.41	6.75	0.29	9.09	93.04	1.85	0.38
4	33.84	3.95	17.97	20.16	0.48	7.04	0.34	8.85	92.63	1.77	0.38
5	33.83	3.75	18.08	19.96	0.33	6.76	0.31	9.17	92.19	1.73	0.38
6	34.14	3.73	17.85	19.94	0.29	6.77	0.20	9.11	92.02	1.75	0.38
7	34.00	3.71	17.81	20.26	0.41	6.97	0.27	9.12	92.57	1.73	0.38
8	33.77	3.61	17.74	20.62	0.51	6.93	0.41	9.20	92.80	1.67	0.37
9	33.38	3.62	17.85	20.06	0.29	7.04	0.32	9.13	91.68	1.72	0.38
10	33.51	3.58	17.64	20.35	0.24	6.74	0.30	9.19	91.55	1.69	0.37
11	33.90	3.63	17.65	20.10	0.31	7.04	0.37	8.97	91.97	1.71	0.38
12	34.11	3.61	17.97	20.62	0.31	7.11	0.33	9.28	93.33	1.70	0.38
13	33.93	3.38	18.30	20.36	0.46	7.01	0.21	9.28	92.93	1.76	0.38
14	34.01	3.33	18.49	20.10	0.32	6.90	0.37	9.23	92.74	1.74	0.38
T/14	33.92	3.68	18.05	20.19	0.36	6.90	0.30	9.14	92.54	1.74	0.38

Biotite from Unit 2 (333-2)

Points	SiO2	TiO2	Al2O3	FeO	MnO	MgO	Na2O	K2O	Total	A/CNK	M/(F+M)
1	35.27	3.73	18.46	20.84	0.54	6.87	0.39	9.08	95.18	1.76	0.37
2	35.17	3.77	18.30	20.85	0.51	6.77	0.30	9.16	94.84	1.76	0.37
3	35.04	3.74	18.05	20.59	0.29	6.58	0.28	9.15	93.73	1.74	0.36
4	35.10	3.73	18.31	20.64	0.38	6.65	0.24	9.20	94.26	1.77	0.36
5	35.06	3.57	18.26	21.19	0.47	6.78	0.42	9.22	94.96	1.71	0.36
6	35.19	3.91	18.36	20.73	0.42	6.83	0.28	9.09	94.82	1.78	0.37

7	35.74	3.70	18.49	20.81	0.46	6.78	0.25	9.32	95.55	1.76	0.37
8	35.26	3.69	18.27	20.92	0.39	6.81	0.25	9.26	94.86	1.75	0.37
9	34.73	3.53	18.24	20.90	0.52	6.97	0.28	9.05	94.22	1.78	0.37
10	34.35	3.34	18.42	21.18	0.40	7.14	0.20	8.94	93.98	1.84	0.38
T/10	35.09	3.67	18.32	20.87	0.44	6.82	0.29	9.15	94.64	1.77	0.37

Biotite from Unit 3 (333-7)

Points	SiO2	TiO2	Al2O3	FeO	MnO	MgO	Na2O	K2O	Total	A/CNK	M/(F+M)
1	34.95	3.42	19.19	21.73	0.55	5.86	0.27	9.27	95.25	1.83	0.32
2	34.63	3.61	19.00	21.53	0.28	5.81	0.35	9.28	94.48	1.79	0.32
3	34.51	3.27	18.74	21.95	0.39	5.61	0.29	9.12	93.87	1.81	0.31
4	34.51	3.46	19.04	21.28	0.50	5.88	0.39	9.38	94.43	1.76	0.33
5	34.29	3.38	18.58	20.98	0.53	5.83	0.44	9.17	93.21	1.75	0.33
6	34.36	3.31	18.62	21.61	0.39	5.73	0.39	8.97	93.39	1.80	0.32
T/7	34.54	3.41	18.86	21.51	0.44	5.79	0.36	9.20	94.11	1.79	0.32

Biotite from Unit 4 (333-8)

Points	SiO2	TiO2	Al2O3	FeO	MnO	MgO	Na2O	K2O	Total	A/CNK	M/(F+M)
1	34.81	3.45	19.28	22.12	0.31	5.80	0.41	9.06	95.22	1.84	0.32
2	35.09	3.68	19.55	22.04	0.00	6.81	0.46	9.22	96.84	1.82	0.36
T/2	34.95	3.57	19.42	22.08	0.16	6.31	0.44	9.14	96.03	1.83	0.34

Biotite from Unit 2 (333-6)

Points	SiO2	TiO2	Al2O3	FeO	MnO	MgO	Na2O	K2O	Total	A/CNK	M/(F+M)
1	34.53	3.90	18.68	22.05	0.38	5.91	0.27	8.65	94.37	1.91	0.32
2	34.92	3.84	18.90	21.86	0.31	6.03	0.42	8.90	95.18	1.83	0.33
3	35.01	3.95	18.90	22.15	0.50	6.18	0.26	9.15	96.10	1.83	0.33
4	35.22	3.65	19.18	22.05	0.35	6.08	0.34	8.99	95.85	1.86	0.33
5	34.59	3.91	18.65	21.94	0.42	5.89	0.25	8.86	94.50	1.86	0.32
6	34.66	3.70	18.85	22.00	0.31	6.03	0.35	8.97	94.87	1.83	0.33
7	35.04	3.82	18.96	22.76	0.32	5.92	0.27	8.86	95.95	1.89	0.32

8	34.96	3.80	18.84	22.31	0.47	6.09	0.23	8.90	95.59	1.88	0.33
9	34.82	3.74	18.60	21.94	0.33	5.99	0.36	8.80	94.58	1.84	0.33
10	34.58	3.93	18.33	21.79	0.27	5.99	0.27	8.80	93.97	1.84	0.33
11	35.04	3.85	18.71	21.77	0.34	6.08	0.49	8.97	95.25	1.78	0.33
12	33.66	3.86	17.87	21.78	0.51	5.56	0.35	9.00	92.59	1.73	0.31
13	34.90	3.85	18.83	21.75	0.44	6.05	0.38	8.90	95.10	1.84	0.33
14	34.89	4.06	18.54	22.45	0.30	5.97	0.16	8.83	95.20	1.89	0.32
15	34.65	3.83	18.96	22.02	0.34	6.05	0.35	8.84	95.05	1.87	0.33
16	34.85	3.78	18.57	21.83	0.50	6.07	0.38	8.82	94.80	1.83	0.33
17	34.68	3.81	18.93	22.26	0.30	5.96	0.31	8.98	95.24	1.85	0.32
18	34.70	3.77	18.95	21.96	0.37	5.97	0.36	8.88	94.95	1.86	0.33
19	34.43	4.10	18.64	22.16	0.37	5.83	0.34	8.90	94.76	1.83	0.32
20	34.61	3.86	18.63	22.33	0.36	6.00	0.34	8.92	95.04	1.82	0.32
21	34.39	3.95	18.80	22.41	0.36	5.94	0.26	8.90	95.01	1.87	0.32
22	34.56	4.09	18.42	22.12	0.47	5.74	0.24	8.86	94.49	1.85	0.32
23	34.18	3.90	18.42	21.71	0.47	5.77	0.31	8.69	93.44	1.86	0.32
24	34.58	3.95	18.68	22.41	0.43	6.00	0.39	8.79	95.23	1.84	0.32
25	34.54	3.90	18.43	21.85	0.23	5.65	0.19	8.43	93.23	1.95	0.32
26	34.32	4.52	18.03	21.61	0.25	5.51	0.26	8.27	92.77	1.92	0.31
27	34.35	3.92	18.41	21.93	0.32	5.84	0.30	8.80	93.88	1.84	0.32
28	34.36	4.04	18.41	22.11	0.30	5.76	0.36	8.99	94.32	1.79	0.32
29	34.34	3.89	18.35	22.33	0.32	5.97	0.36	8.87	94.41	1.80	0.32
30	35.03	3.94	19.08	21.94	0.39	6.01	0.35	9.17	95.91	1.82	0.33
T/30	34.65	3.90	18.65	22.05	0.37	5.93	0.32	8.86	94.72	1.85	0.32

Biotite from Unit 5 (103-2)

Point	SiO2	TiO2	Al2O3	FeO	MnO	MgO	Na2O	K2O	Total	A/CNK	M/(F+M)
1	36.13	4.82	19.19	21.86	0.49	4.01	0.29	9.13	95.92	1.85	0.25
2	36.28	4.51	19.12	22.04	0.46	4.03	0.30	9.24	96.00	1.82	0.25
3	35.90	4.43	18.91	22.04	0.55	4.29	0.43	9.36	95.90	1.75	0.26
4	35.86	4.53	19.01	21.88	0.65	4.40	0.38	9.27	96.00	1.78	0.26

5	36.04	4.51	18.57	22.48	0.71	4.09	0.31	9.15	95.86	1.78	0.24
6	35.90	4.39	19.06	22.06	0.67	4.42	0.37	9.07	95.94	1.83	0.26
7	35.91	4.51	18.75	22.39	0.54	4.35	0.32	9.22	96.00	1.79	0.26
8	36.30	4.17	19.07	22.19	0.39	4.38	0.24	9.18	95.92	1.85	0.26
9	35.93	4.13	18.82	22.64	0.58	4.35	0.23	9.22	95.89	1.82	0.26
10	36.12	4.23	19.11	22.24	0.53	4.43	0.22	9.13	96.00	1.87	0.26
11	35.73	4.28	19.02	22.26	0.61	4.49	0.41	9.10	95.91	1.81	0.26
12	36.13	4.03	19.03	22.36	0.53	4.26	0.39	9.27	96.00	1.78	0.25
13	35.53	4.19	18.93	22.47	0.59	4.53	0.51	9.26	96.00	1.74	0.26
14	36.02	3.92	18.69	22.70	0.59	4.42	0.29	9.29	95.92	1.77	0.26
15	35.79	3.81	18.80	22.83	0.54	4.35	0.36	9.51	96.00	1.73	0.25
16	35.89	4.01	19.10	22.31	0.62	4.36	0.34	9.29	95.91	1.80	0.26
17	35.74	4.08	18.97	22.60	0.57	4.33	0.21	9.37	95.88	1.81	0.25
18	35.61	3.91	18.98	22.55	0.66	4.31	0.34	9.58	95.93	1.74	0.25
19	35.83	3.73	19.16	22.85	0.66	4.17	0.18	9.32	95.90	1.85	0.25
20	35.77	3.80	19.25	22.51	0.52	4.43	0.36	9.26	95.89	1.81	0.26
21	35.80	3.46	19.25	22.86	0.52	4.33	0.34	9.34	95.90	1.80	0.25
22	35.76	3.77	19.23	22.63	0.47	4.47	0.31	9.36	96.00	1.81	0.26
23	35.85	3.61	19.22	22.73	0.47	4.31	0.24	9.26	95.68	1.85	0.25
24	35.91	3.58	19.22	22.48	0.44	4.51	0.41	9.33	95.89	1.78	0.26
25	35.66	3.76	19.00	22.89	0.57	4.50	0.30	9.24	95.93	1.81	0.26
26	36.09	3.75	19.07	22.23	0.62	4.66	0.29	9.30	96.00	1.81	0.27
27	35.87	3.55	19.12	22.82	0.63	4.50	0.29	9.23	96.00	1.83	0.26
28	35.87	3.59	19.14	22.43	0.50	4.53	0.44	9.41	95.91	1.75	0.26
29	36.32	3.73	19.42	21.93	0.45	4.61	0.43	9.11	96.00	1.84	0.27
T/29	35.92	4.03	19.04	22.42	0.56	4.37	0.33	9.27	95.93	1.80	0.26

Biotite from Unit 5 (213-4)

Point	SiO2	TiO2	Al2O3	FeO	MnO	MgO	Na2O	K2O	Total	A/CNK	M/(F+M)
1	35.26	3.12	19.12	23.62	1.01	4.06	0.32	9.34	95.92	1.80	0.23
2	35.83	3.13	19.61	23.23	0.84	4.11	0.10	9.18	96.03	1.94	0.24

3	36.09	3.47	19.10	22.59	0.87	4.15	0.30	9.09	95.66	1.85	0.25
4	36.28	3.53	19.01	22.80	0.64	4.10	0.42	9.23	96.00	1.78	0.24
5	36.18	3.62	19.12	22.62	0.89	4.12	0.30	9.14	96.00	1.84	0.25
6	36.03	3.50	19.22	22.79	0.93	4.02	0.27	9.24	96.00	1.84	0.24
7	35.98	3.77	18.99	22.88	0.93	4.06	0.28	9.04	95.92	1.85	0.24
8	35.78	3.48	19.25	23.16	0.76	4.03	0.35	9.08	95.89	1.85	0.24
9	36.25	3.53	19.28	22.67	0.74	4.10	0.35	9.08	96.00	1.85	0.24
10	36.00	3.71	19.03	22.86	0.83	4.03	0.30	9.14	95.90	1.83	0.24
11	35.77	3.63	19.18	22.79	0.88	4.13	0.31	9.23	95.91	1.83	0.24
12	35.74	3.65	19.24	23.02	0.90	3.95	0.36	9.14	96.00	1.84	0.23
13	35.73	3.62	19.21	23.00	0.85	4.02	0.26	9.22	95.92	1.85	0.24
14	35.94	3.56	19.29	22.89	0.88	3.87	0.39	9.19	96.00	1.82	0.23
15	35.87	3.92	19.07	22.86	0.74	3.96	0.33	9.26	96.00	1.81	0.24
16	35.89	3.58	18.95	22.82	0.80	4.03	0.20	9.33	95.60	1.82	0.24
17	35.90	3.62	19.25	23.09	0.76	3.95	0.29	9.14	96.00	1.86	0.23
18	35.81	3.50	19.24	23.08	0.90	3.89	0.28	9.29	96.00	1.83	0.23
19	35.73	3.68	19.38	22.81	0.79	4.08	0.33	9.13	95.92	1.86	0.24
20	35.65	3.50	19.40	22.85	0.82	3.93	0.35	9.36	95.85	1.81	0.23
21	35.53	3.61	19.35	22.94	0.98	4.02	0.42	9.15	96.00	1.83	0.24
22	35.75	3.53	19.15	22.91	0.91	4.06	0.34	9.28	95.93	1.81	0.24
23	35.88	3.56	19.22	22.83	0.81	4.13	0.35	9.11	95.88	1.84	0.24
24	35.85	3.44	19.08	22.99	0.91	4.13	0.31	9.21	95.93	1.82	0.24
25	36.05	3.55	19.28	22.77	0.74	4.03	0.23	9.35	96.00	1.84	0.24
26	35.89	3.38	19.14	22.69	0.93	4.18	0.37	9.43	96.00	1.77	0.25
27	36.14	3.39	19.17	22.67	0.83	4.05	0.30	9.36	95.92	1.80	0.24
28	35.83	3.13	19.61	23.23	0.84	4.11	0.10	9.18	96.03	1.94	0.24
29	35.26	3.18	19.12	23.62	1.01	4.06	0.32	9.34	95.92	1.80	0.23
30	35.89	3.41	19.47	23.15	0.72	4.01	0.23	9.13	96.00	1.90	0.24
T/30	35.86	3.51	19.22	22.94	0.85	4.05	0.30	9.21	95.94	1.84	0.24

Biotite from Aplite (103-A5-E: Taverse A)

Point	SiO2	TiO2	Al2O3	FeO	MnO	MgO	Na2O	K2O	Total	A	M/(F+M)
1	35.18	3.32	20.27	25.44	0.35	4.06	0.34	8.87	97.83	0.10	0.22
2	35.41	3.71	20.55	25.84	0.35	3.91	0.27	9.50	99.54	0.10	0.21
3	34.66	3.34	20.16	25.69	0.49	3.86	0.32	9.13	97.65	0.10	0.21
4	34.11	3.13	19.72	25.53	0.44	3.77	0.36	8.22	95.28	0.10	0.21
5	34.42	3.09	20.34	25.91	0.42	3.98	0.36	8.05	96.57	0.11	0.21
6	35.12	3.50	20.13	25.86	0.40	3.94	0.49	9.20	98.64	0.09	0.21
7	34.67	3.67	20.24	25.53	0.43	3.86	0.29	9.45	98.14	0.09	0.21
8	35.03	3.49	20.22	25.10	0.34	3.77	0.37	9.48	97.80	0.09	0.21
9	35.05	3.59	20.11	25.60	0.42	3.86	0.29	9.52	98.44	0.09	0.21
10	35.28	3.31	20.54	25.64	0.38	3.88	0.26	9.44	98.73	0.10	0.21
11	35.09	3.49	20.12	25.44	0.48	4.02	0.37	9.39	98.40	0.09	0.22
12	35.22	3.42	20.22	25.24	0.31	3.87	0.38	9.56	98.22	0.09	0.21
13	34.84	3.61	20.53	25.14	0.45	3.99	0.40	9.65	98.61	0.09	0.22
14	35.02	3.64	20.08	25.63	0.44	3.89	0.33	9.48	98.51	0.09	0.21
15	35.10	3.70	20.34	26.03	0.47	4.04	0.32	9.11	99.11	0.10	0.22
16	35.17	3.43	20.08	25.43	0.44	3.85	0.36	9.35	98.11	0.09	0.21
17	35.41	3.34	20.34	25.25	0.35	3.83	0.22	9.57	98.31	0.09	0.21
18	35.49	3.56	20.22	25.54	0.26	3.88	0.33	9.55	98.83	0.09	0.21
19	35.64	3.65	20.51	25.30	0.28	3.93	0.36	9.48	99.15	0.09	0.22
20	35.36	3.69	20.19	25.44	0.27	3.86	0.33	9.55	98.69	0.09	0.21
21	35.40	3.56	20.35	25.86	0.45	3.96	0.44	9.37	99.39	0.09	0.21
22	35.21	3.35	20.44	25.91	0.32	3.95	0.45	9.11	98.74	0.10	0.21
23	34.73	3.51	20.08	25.55	0.52	4.12	0.44	8.49	97.44	0.10	0.22
24	35.22	3.52	20.40	25.62	0.43	4.12	0.51	9.03	98.85	0.10	0.22
25	35.48	3.60	20.48	25.52	0.40	4.10	0.44	9.22	99.24	0.10	0.22
26	35.23	3.55	20.57	25.67	0.40	4.01	0.40	8.94	98.77	0.10	0.22
27	35.21	3.35	20.66	26.08	0.35	4.05	0.34	9.09	99.13	0.10	0.22
28	35.29	3.61	20.47	25.58	0.34	3.97	0.33	9.14	98.73	0.10	0.22
29	35.49	3.63	20.70	25.64	0.31	3.86	0.39	9.22	99.24	0.10	0.21

30	35.29	3.28	20.38	25.35	0.39	3.86	0.38	9.40	98.33	0.09	0.21
31	35.61	3.43	20.56	25.43	0.35	3.94	0.30	9.37	98.99	0.10	0.22
32	34.95	3.31	20.49	25.24	0.47	3.97	0.36	9.37	98.16	0.10	0.22
33	35.34	3.29	20.26	25.13	0.51	3.98	0.36	9.16	98.03	0.10	0.22
34	35.22	3.26	20.41	26.01	0.44	3.79	0.38	9.02	98.53	0.10	0.21
35	34.91	3.30	20.35	25.57	0.33	3.96	0.44	9.07	97.93	0.10	0.22
36	35.24	3.39	20.54	25.50	0.31	3.94	0.36	9.53	98.81	0.09	0.22
37	35.07	3.36	20.29	25.29	0.55	3.91	0.34	9.37	98.18	0.09	0.22
38	34.83	3.38	20.19	25.15	0.34	3.89	0.30	9.48	97.56	0.09	0.22
39	34.76	3.38	20.07	24.87	0.41	3.90	0.31	9.55	97.25	0.09	0.22
40	35.08	3.50	20.27	25.08	0.36	3.76	0.36	9.41	97.82	0.09	0.21
41	34.54	3.31	19.96	25.37	0.47	3.91	0.35	9.41	97.32	0.09	0.22
42	35.14	3.32	20.42	25.88	0.27	4.03	0.37	9.22	98.65	0.10	0.22
43	34.31	2.98	19.79	26.30	0.33	3.78	0.29	7.36	95.14	0.11	0.20
44	34.10	3.17	19.74	26.05	0.42	3.92	0.47	7.46	95.33	0.11	0.21
45	34.41	3.19	19.98	26.05	0.43	3.89	0.46	8.12	96.53	0.10	0.21
46	34.58	3.22	20.47	26.11	0.51	3.88	0.20	9.01	97.98	0.10	0.21
47	34.78	3.11	20.55	25.72	0.35	4.19	0.42	9.26	98.38	0.10	0.22
48	34.55	3.26	20.13	25.57	0.44	3.85	0.39	9.43	97.62	0.09	0.21
49	34.83	3.23	20.11	25.46	0.45	3.85	0.22	9.20	97.35	0.10	0.21
T/49	34.98	3.40	20.27	25.65	0.39	3.94	0.36	9.07	98.06	0.10	0.21

Biotite from Aplite (103-A5 A: Traverse B)

Point	SiO2	TiO2	Al2O3	FeO	MnO	MgO	Na2O	K2O	Total	A	M/(F+M)
1	34.13	2.81	20.12	24.31	0.47	4.32	0.27	9.60	96.03	0.09	0.24
2	34.50	2.94	19.82	23.83	0.66	4.42	0.32	9.33	95.82	0.09	0.25
3	34.32	2.86	20.00	24.77	0.65	4.43	0.37	9.41	96.81	0.09	0.24
4	33.94	2.79	19.97	24.19	0.83	4.47	0.43	9.45	96.07	0.09	0.25
5	34.42	2.82	20.19	24.48	0.66	4.24	0.32	9.60	96.73	0.09	0.24
6	34.51	2.89	19.89	24.69	0.68	4.44	0.35	9.43	96.88	0.09	0.24
7	33.74	3.06	19.35	24.60	0.90	4.25	0.32	9.23	95.45	0.09	0.24

8	33.68	3.03	19.33	24.52	0.74	4.42	0.28	9.12	95.12	0.09	0.24
9	34.11	2.87	19.81	24.44	0.68	4.50	0.41	9.09	95.91	0.09	0.25
10	32.92	3.15	19.11	24.79	0.59	4.18	0.46	9.16	94.36	0.08	0.23
11	34.14	2.87	19.47	24.55	0.62	4.28	0.40	9.24	95.57	0.09	0.24
12	34.22	2.79	19.45	24.47	0.66	4.43	0.32	9.39	95.73	0.09	0.24
13	34.49	2.54	19.91	24.32	0.64	4.18	0.36	8.74	95.18	0.10	0.23
14	33.59	2.93	19.18	24.93	0.60	4.37	0.32	9.38	95.30	0.08	0.24
15	33.36	3.09	19.29	25.20	0.82	4.26	0.15	9.42	95.59	0.09	0.23
16	33.43	3.09	19.36	25.20	0.65	4.29	0.32	9.52	95.86	0.08	0.23
17	33.39	3.12	19.39	24.85	0.65	4.23	0.34	9.48	95.45	0.08	0.23
18	33.16	3.18	19.21	25.09	0.73	4.15	0.34	9.40	95.26	0.08	0.23
19	33.68	3.06	19.24	24.79	0.67	4.14	0.32	9.52	95.42	0.08	0.23
20	33.53	3.09	19.29	24.42	0.68	4.13	0.24	9.45	94.83	0.09	0.23
21	33.01	3.11	19.45	24.72	0.62	4.17	0.24	9.17	94.49	0.09	0.23
22	33.12	2.87	19.35	24.60	0.61	4.12	0.28	9.23	94.18	0.09	0.23
23	33.11	2.88	19.18	24.41	0.51	4.07	0.32	9.22	93.70	0.09	0.23
24	33.13	2.89	19.30	24.48	0.60	4.10	0.32	9.40	94.22	0.08	0.23
25	33.17	2.81	19.26	24.59	0.42	4.04	0.29	9.42	94.00	0.08	0.23
26	32.89	2.77	18.79	24.28	0.70	4.28	0.37	9.22	93.30	0.08	0.24
27	32.96	2.81	19.13	24.26	0.71	4.24	0.27	9.29	93.67	0.08	0.24
28	32.97	2.84	19.20	24.21	0.70	4.20	0.37	9.29	93.78	0.08	0.24
29	33.38	2.79	19.38	24.04	0.45	4.21	0.40	8.98	93.63	0.09	0.24
30	33.26	3.21	19.36	24.22	0.65	4.21	0.45	9.34	94.70	0.08	0.24
31	33.36	2.79	19.20	24.06	0.59	4.29	0.38	9.44	94.11	0.08	0.24
32	32.93	3.14	19.13	24.48	0.54	4.04	0.31	9.39	93.96	0.08	0.23
33	33.30	3.00	19.28	24.40	0.61	4.34	0.35	9.32	94.60	0.08	0.24
34	33.40	2.68	19.44	24.18	0.69	4.26	0.45	9.54	94.64	0.08	0.24
35	33.38	2.74	19.12	24.44	0.62	4.21	0.34	9.42	94.27	0.08	0.23
36	33.32	3.02	19.06	24.52	0.58	4.27	0.39	9.37	94.53	0.08	0.24
37	32.84	2.84	19.08	24.39	0.61	4.32	0.39	9.48	93.95	0.08	0.24
38	32.88	2.78	18.83	24.36	0.67	4.09	0.40	9.31	93.32	0.08	0.23

39	33.03	2.82	19.07	24.33	0.67	4.36	0.40	9.29	93.97	0.08	0.24
40	32.55	2.81	18.74	24.13	0.71	4.18	0.45	9.17	92.74	0.08	0.24
T/40	33.49	2.90	19.35	24.53	0.64	4.26	0.35	9.32	94.84	0.09	0.24

Muscovite from Unit 3 (MD-4, traverse 1)

Point	SiO2	TiO2	Al2O3	FeO	MnO	MgO	Na2O	K2O	Total	A	M/(F+M)
1	45.90	0.01	35.21	1.92	0.07	0.88	0.80	9.86	94.67	0.23	0.45
2	45.98	0.13	34.91	2.07	0.14	0.86	0.79	9.69	94.57	0.23	0.43
3	45.94	0.00	35.17	2.08	0.06	0.82	0.80	9.30	94.18	0.23	0.41
4	46.18	0.00	35.42	2.01	0.02	0.94	0.77	9.54	94.87	0.23	0.45
5	45.18	0.44	35.58	2.70	0.00	0.23	0.83	9.22	94.17	0.24	0.13
6	45.55	0.19	35.76	2.40	0.05	0.26	0.88	9.44	94.53	0.24	0.16
7	45.49	0.23	35.58	2.44	0.07	0.27	0.74	9.27	94.08	0.24	0.16
8	45.75	0.30	35.58	2.64	0.04	0.25	0.74	9.29	94.57	0.24	0.14
9	45.37	0.49	34.88	2.30	0.00	0.32	0.87	9.24	93.48	0.23	0.20
10	45.54	0.45	35.20	2.70	0.11	0.25	0.73	9.45	94.42	0.23	0.14
11	45.50	0.54	35.35	2.60	0.13	0.29	0.90	9.32	94.63	0.23	0.17
12	45.85	0.31	35.40	2.75	0.08	0.34	0.82	9.43	94.97	0.23	0.18
13	45.66	0.27	35.42	2.63	0.00	0.39	0.89	9.50	94.75	0.23	0.21
14	45.48	0.37	35.22	2.36	0.05	0.37	0.83	9.42	94.09	0.23	0.22
15	45.54	0.35	35.21	2.46	0.01	0.38	0.81	9.40	94.16	0.23	0.22
16	45.77	0.25	34.91	2.57	0.03	0.33	0.77	9.47	94.10	0.23	0.19
17	45.93	0.10	35.01	2.46	0.19	0.45	0.89	9.50	94.52	0.23	0.25
18	45.71	0.14	35.04	2.65	0.04	0.49	0.90	9.32	94.29	0.23	0.25
19	45.92	0.20	34.89	2.63	0.00	0.55	0.76	9.55	94.50	0.23	0.27
20	46.25	0.22	35.14	2.49	0.07	0.41	0.85	9.35	94.78	0.23	0.23
T/20	45.72	0.25	35.24	2.44	0.06	0.45	0.82	9.43	94.42	0.23	0.25

Muscovite from Unit 3 (MD-4, traverse 2)

Point	SiO2	TiO2	Al2O3	FeO	MnO	MgO	Na2O	K2O	Total	A	M/(F+M)
1	46.21	0.00	35.47	2.14	0.00	0.76	0.78	9.42	94.79	0.24	0.39
2	45.12	0.40	35.38	2.65	0.00	0.24	0.81	9.13	93.73	0.24	0.14

3	46.18	0.27	35.73	2.57	0.03	0.29	0.63	9.06	94.76	0.24	0.17
4	45.81	0.50	35.82	2.44	0.16	0.19	0.82	9.05	94.78	0.24	0.12
5	45.62	0.09	35.88	2.46	0.00	0.11	0.90	9.22	94.28	0.24	0.07
T/5	45.79	0.25	35.66	2.45	0.04	0.32	0.79	9.18	94.47	0.24	0.19

Muscovite from Unit 5 (213-4)

Point	SiO2	TiO2	Al2O3	FeO	MnO	MgO	Na2O	K2O	Total	A	M/(F+M)
1	44.95	0.41	32.76	2.29	-0.02	0.76	0.44	10.69	92.28	0.20	0.37
2	45.29	0.21	34.04	2.27	0.00	0.84	0.90	10.16	93.50	0.21	0.40
3	45.39	0.51	34.12	2.12	0.06	0.86	0.93	10.07	94.00	0.21	0.42
4	45.28	0.53	33.99	2.27	0.13	0.61	0.95	10.09	93.72	0.21	0.32
5	45.00	0.56	33.53	2.05	0.07	0.91	0.80	9.68	92.52	0.21	0.44
6	44.89	0.82	33.81	2.26	0.01	0.90	0.72	10.13	93.54	0.21	0.42
7	45.38	0.26	34.17	2.51	0.02	0.69	0.68	10.08	93.51	0.22	0.33
8	45.37	0.58	34.23	1.96	0.09	0.80	0.81	9.60	93.36	0.22	0.42
9	45.02	0.45	34.26	1.87	0.16	0.94	0.80	10.22	93.56	0.21	0.47
10	46.36	0.35	33.62	2.02	-0.04	0.90	0.40	10.89	94.19	0.21	0.44
11	45.16	0.25	34.29	2.13	0.14	0.78	0.87	10.22	93.46	0.21	0.39
12	45.73	0.39	34.03	1.93	0.13	0.71	1.03	10.40	94.56	0.21	0.40
13	45.43	0.46	34.71	2.33	-0.05	0.91	0.51	10.35	94.69	0.22	0.41
14	44.70	0.68	33.93	2.34	0.39	0.78	0.79	9.98	93.58	0.21	0.37
15	45.67	0.56	34.36	2.64	0.03	0.85	0.90	9.92	94.91	0.22	0.36
16	45.57	0.28	34.13	2.80	0.16	1.00	0.78	10.45	94.73	0.21	0.39
17	46.01	0.04	33.98	2.35	-0.01	1.21	0.96	9.98	94.48	0.21	0.48
18	45.26	0.15	33.89	1.77	0.07	0.98	0.76	10.34	93.01	0.21	0.50
19	45.39	0.21	34.61	2.22	0.08	1.09	0.81	10.40	94.52	0.22	0.47
20	44.66	0.01	33.43	1.99	-0.12	0.81	0.49	10.17	91.56	0.21	0.42
21	45.43	0.23	34.09	2.11	0.17	0.88	0.52	10.46	93.50	0.21	0.43
22	44.90	0.26	33.52	2.35	-0.07	0.89	0.63	9.42	91.71	0.22	0.40
23	46.17	-0.12	34.20	2.57	0.13	1.02	0.86	10.17	94.98	0.21	0.41
24	45.14	0.03	33.71	2.44	0.26	0.83	0.84	9.93	92.88	0.21	0.38

25	45.75	0.21	33.61	2.68	0.22	0.88	0.92	10.21	94.06	0.21	0.37
26	45.24	0.25	33.29	2.94	-0.11	0.98	0.72	9.96	93.14	0.21	0.37
27	44.56	0.20	33.73	2.30	0.04	0.71	0.76	10.35	92.40	0.21	0.35
28	44.84	0.27	32.98	2.31	0.10	0.86	0.68	10.17	91.83	0.20	0.40
29	44.75	0.17	33.18	2.19	0.04	0.61	0.93	10.11	91.77	0.20	0.33
30	45.23	0.16	33.95	2.15	0.18	0.80	1.04	10.04	93.21	0.21	0.40
31	45.15	0.29	33.38	2.51	0.02	0.97	0.87	10.45	93.34	0.20	0.41
32	45.55	-0.09	33.85	1.86	0.00	0.94	0.67	10.28	93.15	0.21	0.47
33	44.53	0.33	33.93	2.34	-0.11	1.04	0.89	10.24	92.96	0.21	0.44
34	45.47	0.21	33.48	2.16	-0.03	0.70	0.72	9.75	92.27	0.21	0.37
35	44.66	0.54	33.43	1.99	0.26	0.81	0.52	10.59	92.55	0.21	0.42
36	45.64	0.31	33.61	2.27	0.21	1.06	0.96	10.12	93.67	0.21	0.45
37	44.98	0.14	33.37	2.27	-0.12	0.98	0.76	10.23	92.60	0.21	0.43
38	45.32	0.35	33.43	2.42	-0.10	0.78	0.84	9.84	93.18	0.21	0.36
T/38	45.26	0.30	33.81	2.26	0.06	0.87	0.77	10.16	93.34	0.21	0.41

Muscovite from Unit 5 (103-3)

Point	SiO2	TiO2	Al2O3	FeO	MnO	MgO	Na2O	K2O	Total	A	M/(F+M)
1	44.09	0.19	33.93	2.45	0.01	0.77	0.89	10.36	92.49	0.21	0.36
2	44.03	0.06	33.38	2.91	0.07	0.83	0.94	9.99	92.08	0.21	0.34
3	44.65	-0.03	34.56	2.62	-0.11	0.82	0.77	10.22	93.64	0.22	0.36
4	44.86	-0.05	34.05	2.72	0.02	0.86	0.87	10.36	93.72	0.21	0.36
5	45.31	-0.12	34.10	3.11	0.09	0.90	1.18	10.45	95.36	0.20	0.34
6	44.33	-0.04	33.29	2.77	0.27	0.65	0.92	10.04	91.99	0.21	0.29
7	44.98	-0.01	33.06	2.90	0.27	0.47	0.77	10.23	92.42	0.20	0.22
8	44.39	0.09	33.22	2.78	0.05	0.67	1.10	10.02	92.19	0.20	0.30
9	45.92	0.07	33.67	2.98	0.27	0.76	1.07	10.27	94.66	0.20	0.31
10	44.75	0.15	33.74	2.69	0.07	0.91	0.79	9.80	92.68	0.21	0.38
11	44.93	-0.05	33.63	3.14	-0.08	0.56	0.76	9.92	92.95	0.21	0.24
12	44.41	-0.18	33.92	2.38	0.05	0.47	1.19	9.92	92.29	0.21	0.26
13	45.00	-0.04	33.57	2.38	0.00	0.71	0.85	10.05	92.57	0.21	0.35

14	44.63	0.13	33.59	2.66	0.24	0.74	1.12	9.97	92.83	0.21	0.33
15	44.40	-0.02	33.92	2.77	-0.18	0.73	1.13	10.21	93.15	0.21	0.32
16	45.25	-0.01	34.11	2.92	-0.12	0.96	0.77	9.99	93.98	0.22	0.37
17	44.83	0.08	33.43	2.76	0.11	0.87	0.69	10.30	92.89	0.21	0.36
T/17	44.75	0.01	33.72	2.76	0.06	0.75	0.93	10.12	93.05	0.21	0.33

Muscovite from Unit 5 (103-3)

Point	SiO2	TiO2	Al2O3	FeO	MnO	MgO	Na2O	K2O	Total	A	M/(F+M)
1	44.72	0.06	33.25	2.49	0.17	0.53	0.81	10.09	92.18	0.21	0.27
2	44.65	-0.10	33.46	2.42	-0.11	0.65	1.00	10.38	92.56	0.20	0.32
3	44.73	0.45	33.32	2.41	0.19	0.74	1.07	9.83	92.56	0.21	0.35
4	45.06	0.32	33.14	2.72	-0.07	0.68	0.70	10.12	92.42	0.21	0.31
5	44.81	0.22	32.65	2.95	0.11	0.60	0.52	10.18	91.72	0.20	0.27
6	44.81	0.39	33.28	2.69	0.14	0.68	0.66	10.36	92.86	0.21	0.31
7	45.30	0.22	33.18	2.58	-0.12	0.57	0.75	10.17	92.55	0.21	0.28
8	44.84	0.18	32.21	2.98	0.20	0.81	0.84	10.20	92.17	0.19	0.33
9	45.21	0.22	32.33	3.13	0.03	0.85	0.82	9.80	92.28	0.20	0.33
10	45.23	0.32	32.51	2.91	0.23	0.80	0.75	10.07	92.80	0.20	0.33
11	44.31	0.13	32.61	2.99	0.03	0.82	1.10	9.86	92.01	0.20	0.33
12	44.93	0.27	32.77	2.77	0.00	0.70	0.64	9.87	91.68	0.21	0.31
13	45.16	-0.09	32.32	2.65	0.31	0.69	0.57	10.04	91.43	0.20	0.32
14	44.70	0.25	32.55	2.84	-0.09	0.65	0.75	9.98	91.47	0.20	0.29
15	45.05	0.09	33.31	3.04	0.16	1.08	0.64	10.23	93.34	0.21	0.39
16	44.81	0.20	32.99	3.70	0.01	0.72	0.83	9.82	92.86	0.21	0.26
17	45.06	0.08	33.49	2.77	0.15	1.03	0.84	9.91	93.10	0.21	0.40
18	44.43	0.22	33.46	3.09	0.31	0.84	1.11	9.76	92.97	0.21	0.33
19	44.02	0.06	32.89	2.84	0.14	0.92	1.04	9.76	92.03	0.20	0.37
T/19	44.83	0.18	32.93	2.84	0.09	0.76	0.81	10.02	92.37	0.20	0.32

Muscovite from Aplite (MD-2B)

Point	SiO2	TiO2	Al2O3	FeO	MnO	MgO	Na2O	K2O	Total	A	M/(F+M)
1	46.29	0.00	36.85	1.46	0.01	0.46	0.63	9.32	95.01	0.25	0.36
2	46.81	0.00	36.81	1.25	0.07	0.46	0.63	9.22	95.25	0.25	0.40
3	46.70	0.00	37.51	1.14	0.03	0.38	0.86	9.36	95.98	0.25	0.37
4	46.55	0.00	36.74	1.34	0.00	0.57	0.71	9.28	95.20	0.25	0.43
5	46.10	0.00	36.92	2.63	0.10	0.76	0.52	7.31	94.36	0.28	0.34
6	46.75	0.00	36.85	1.56	0.03	0.58	0.67	9.33	95.76	0.25	0.40
7	46.92	0.00	37.23	1.38	-0.02	0.57	0.66	9.33	96.06	0.26	0.42
8	46.95	0.00	37.07	1.26	0.07	0.64	0.78	9.55	96.32	0.25	0.48
9	47.22	0.00	37.19	1.48	0.06	0.58	0.78	9.33	96.64	0.25	0.41
10	47.31	0.00	37.12	1.65	0.00	0.69	0.66	9.51	96.94	0.25	0.43
11	46.73	0.00	36.85	1.78	0.03	0.62	0.80	9.21	96.02	0.25	0.38
12	46.64	0.00	36.93	1.79	0.02	0.70	0.68	9.40	96.16	0.25	0.41
13	46.80	0.00	36.88	1.89	-0.08	0.66	0.66	9.46	96.26	0.25	0.38
14	46.87	0.00	36.75	1.65	-0.02	0.69	0.72	9.63	96.29	0.25	0.43
15	47.19	0.16	37.19	1.32	0.01	0.60	0.53	9.89	96.73	0.25	0.45
16	47.26	0.00	36.99	1.30	-0.01	0.50	0.48	9.84	96.36	0.25	0.41
17	47.28	0.00	37.50	1.34	-0.04	0.47	0.38	9.68	96.62	0.26	0.38
18	47.30	0.00	37.39	1.25	-0.04	0.52	0.50	10.29	97.20	0.25	0.43
19	47.07	0.00	37.13	1.38	0.05	0.50	0.31	10.41	96.86	0.25	0.39
20	47.20	0.09	37.29	1.48	-0.01	0.51	0.63	10.01	97.11	0.25	0.38
T/20	46.90	0.01	37.06	1.52	0.01	0.57	0.63	9.47	96.16	0.25	0.40

Cordierite from Unit 4 (DO5-0002), Type-2 in this study

Point	SiO2	Al2O3	FeO	MnO	MgO	Na2O	Total	A	M/(F+M)
1	48.22	32.12	10.99	0.85	6.46	0.63	99.27	0.30	0.51
2	48.48	32.10	9.15	0.84	5.70	1.28	97.55	0.29	0.53
3	48.43	32.23	9.86	1.08	6.48	1.12	99.20	0.30	0.54
4	48.31	31.96	9.77	0.91	6.49	1.10	98.54	0.30	0.54
5	48.32	31.86	10.39	0.69	6.62	0.76	98.64	0.30	0.53
6	48.34	32.06	9.56	0.61	6.41	0.61	97.59	0.30	0.54

7	48.55	32.19	10.08	0.63	6.80	0.83	99.08	0.30	0.55
8	48.52	32.24	10.54	0.86	6.89	0.65	99.70	0.31	0.54
9	48.01	32.03	10.31	0.86	6.61	0.82	98.64	0.30	0.53
10	48.14	32.10	10.00	0.75	6.05	1.04	98.08	0.30	0.52
11	48.24	32.34	10.80	0.65	6.35	0.97	99.35	0.30	0.51
12	48.18	31.93	10.59	0.81	6.47	0.71	98.69	0.30	0.52
13	48.13	32.13	11.09	0.85	6.97	0.73	99.90	0.30	0.53
14	48.30	32.21	10.75	0.98	6.78	0.62	99.64	0.31	0.53
15	47.15	31.26	10.74	0.87	6.06	0.59	96.67	0.30	0.50
16	47.95	31.90	10.72	0.71	6.56	0.71	98.55	0.30	0.52
T/16	48.20	32.04	10.33	0.83	6.48	0.82	98.70	0.30	0.53

Cordierite from Aplite (MD-2B), Type 1-A in this study

Point	SiO2	Al2O3	FeO	MnO	MgO	Na2O	Total	A	M/(F+M)
1	47.88	32.48	13.94	1.41	2.93	1.35	99.99	0.30	0.27
2	48.15	32.27	14.06	1.38	2.71	1.42	99.99	0.29	0.26
3	47.56	32.40	14.68	1.43	2.58	1.35	100.00	0.30	0.24
4	47.35	32.58	14.86	1.41	2.55	1.26	100.01	0.30	0.23
5	47.93	32.03	14.85	1.49	2.51	1.19	100.00	0.30	0.23
6	47.59	32.45	14.68	1.47	2.49	1.33	100.01	0.30	0.23
7	47.51	32.57	14.74	1.45	2.50	1.22	99.99	0.30	0.23
8	47.54	32.49	14.44	1.56	2.60	1.36	99.99	0.30	0.24
9	47.76	32.29	14.54	1.48	2.71	1.22	100.00	0.30	0.25
10	48.27	32.35	14.07	1.53	2.78	1.01	100.01	0.30	0.26
11	48.00	32.56	14.12	1.41	2.55	1.36	100.00	0.30	0.24
12	47.85	32.21	14.35	1.49	2.59	1.51	100.00	0.29	0.24
13	47.34	32.62	15.00	1.65	1.83	1.56	100.00	0.29	0.18
14	46.68	31.77	15.91	1.87	1.98	1.79	100.00	0.28	0.18
15	47.46	32.16	15.72	1.65	1.64	1.37	100.00	0.29	0.16
16	47.32	32.21	15.58	1.83	2.03	1.03	100.00	0.30	0.19
17	47.21	32.34	15.21	1.69	2.31	1.25	100.01	0.30	0.21

24	48.13	32.70	11.00	0.77	5.05	1.17	98.82	0.30	0.45
25	48.34	32.68	10.61	0.88	4.86	1.35	98.72	0.30	0.45
26	48.40	32.81	9.85	1.19	5.04	1.68	98.97	0.29	0.48
27	48.27	32.51	10.84	0.84	5.03	1.17	98.66	0.30	0.45
28	48.42	32.49	10.46	0.66	5.57	1.05	98.65	0.30	0.49
29	49.14	33.06	10.22	0.73	5.99	1.07	100.21	0.31	0.51
30	48.77	32.95	10.05	0.83	5.67	1.25	99.52	0.30	0.50
31	48.71	32.82	10.49	0.72	5.14	1.51	99.39	0.30	0.47
32	48.21	32.41	10.46	0.99	4.93	1.28	98.28	0.30	0.46
33	48.42	32.71	10.62	1.07	5.04	1.34	99.20	0.30	0.46
34	48.38	32.64	10.56	0.77	5.66	0.98	98.99	0.30	0.49
35	48.50	32.76	10.36	0.80	5.35	1.12	98.89	0.30	0.48
36	48.71	32.69	10.20	0.68	5.83	0.92	99.03	0.31	0.50
37	48.52	32.56	10.47	1.00	5.31	1.25	99.11	0.30	0.47
38	48.61	32.46	10.86	0.65	6.04	0.68	99.30	0.31	0.50
39	48.81	32.62	10.81	0.78	6.10	0.85	99.97	0.31	0.50
40	48.41	32.50	10.67	0.71	5.89	0.97	99.15	0.30	0.50
T/40	48.53	32.66	10.58	0.74	5.54	1.11	99.16	0.30	0.48

Cordierite from Unit 4 (306-2, traverse 2), Type 1-B in this study

Point	SiO2	Al2O3	FeO	MnO	MgO	Na2O	Total	A	M/(F+M)
1	48.17	32.59	10.01	0.78	5.73	1.17	98.45	0.30	0.50
2	48.84	32.67	10.25	0.53	5.79	1.21	99.29	0.30	0.50
3	48.88	33.37	9.49	0.51	6.93	0.91	100.09	0.31	0.57
4	48.99	33.08	9.66	0.59	6.73	0.82	99.87	0.31	0.55
5	48.97	33.02	10.43	0.60	6.40	0.86	100.28	0.31	0.52
6	48.60	32.90	10.20	0.69	5.40	1.26	99.05	0.30	0.49
7	48.44	32.60	10.10	1.07	4.98	1.62	98.81	0.29	0.47
T/7	48.56	32.69	10.50	0.73	5.61	1.11	99.20	0.30	0.49

Cordierite from the aplite (MD-2B), Type 1-A in this study

Point	SiO2	Al2O3	FeO	MnO	MgO	Na2O	Total	A	M/(F+M)
1	47.21	31.32	11.93	1.30	3.57	1.12	96.45	0.29	0.35
2	46.34	31.22	12.20	1.17	3.64	1.08	95.65	0.29	0.35
3	46.60	31.24	12.66	1.33	3.57	1.11	96.51	0.29	0.33
4	46.56	31.05	12.53	1.16	3.48	1.03	95.81	0.29	0.33
5	46.29	31.06	12.66	1.05	3.38	1.04	95.48	0.29	0.32
6	46.88	30.94	12.33	1.22	3.40	1.03	95.80	0.29	0.33
7	46.57	30.90	12.45	1.09	3.36	0.98	95.35	0.29	0.32
8	46.70	31.13	12.29	1.12	3.42	0.87	95.53	0.29	0.33
9	46.90	31.30	12.68	1.04	3.49	1.03	96.44	0.29	0.33
10	46.87	31.16	12.54	1.21	3.45	0.91	96.14	0.29	0.33
11	46.73	30.96	12.42	1.22	3.60	1.16	96.09	0.28	0.34
12	46.40	30.95	12.70	1.18	3.57	0.96	95.76	0.29	0.33
13	46.71	31.17	12.54	1.18	3.70	0.94	96.24	0.29	0.34
14	46.61	31.05	12.49	1.10	3.60	1.04	95.89	0.29	0.34
T/14	46.67	31.10	12.46	1.17	3.52	1.02	95.94	0.29	0.33

Cordierite from Aplite (103-A5-D), Type 1-A in this study

Point	SiO2	Al2O3	FeO	MnO	MgO	Na2O	Total	A	M/(F+M)
1	45.71	30.98	13.48	1.22	2.89	1.29	95.57	0.28	0.28
2	45.27	30.76	13.90	1.22	2.84	1.21	95.20	0.28	0.27
3	45.86	31.03	13.69	1.16	2.97	1.25	95.96	0.28	0.28
4	45.32	30.63	10.83	0.75	2.42	0.86	90.81	0.29	0.28
5	45.37	31.00	13.40	1.12	2.85	1.28	95.02	0.28	0.27
6	45.13	30.82	13.22	1.14	2.85	1.36	94.52	0.28	0.28
7	45.60	30.78	13.15	1.38	2.92	1.52	95.35	0.28	0.28
8	45.50	30.73	13.51	1.31	2.87	1.39	95.31	0.28	0.27
9	45.41	30.58	12.94	1.40	2.81	1.35	94.49	0.28	0.28

10	45.55	30.87	13.43	1.14	2.77	1.38	95.14	0.28	0.27
11	45.07	30.67	13.31	1.06	2.78	1.37	94.26	0.28	0.27
12	44.92	30.67	13.29	1.18	3.03	1.33	94.42	0.28	0.29
13	40.30	29.79	12.99	0.66	2.28	0.59	86.61	0.28	0.24
14	45.87	31.09	13.35	1.10	2.87	1.59	95.87	0.28	0.28
T/14	45.06	30.74	13.18	1.13	2.80	1.27	94.18	0.28	0.27

Cordierite from monzogranite of the MB (MacDonald, 1981)

Sno.	SiO2	Al2O3	FeO	MnO	MgO	Na2O	Total	A	M/(F+M)
48	48.18	32.30	10.23	0.64	5.69	1.61	98.65	0.29	0.50
22	48.31	32.20	9.99	0.69	5.51	1.77	98.47	0.29	0.50
22	49.60	32.67	10.38	0.79	5.71	1.86	101.01	0.29	0.50
91	48.22	31.73	9.71	0.27	6.71	0.43	97.07	0.30	0.55
85	47.70	31.94	9.31	2.71	3.89	2.12	97.67	0.28	0.43

Sno. 48, 22 are from Monzogranite, Sno.85 Aplite, Sno.91 pelitic hornfels

Garnet from Aplite (MD-2B1)

Points	SiO2	Al2O3	FeO	MnO	MgO	CaO	Na2O	Total	A	M/(M+F)
1	35.07	20.04	31.34	9.04	1.13	0.32	0.18	97.12	0.19	0.06
2	35.23	20.02	31.52	8.68	0.99	0.22	0.25	96.90	0.19	0.05
3	35.36	20.35	31.98	9.21	0.85	0.26	0.17	98.18	0.19	0.05
4	35.53	20.04	31.77	9.37	0.74	0.25	0.21	97.91	0.19	0.04
5	35.44	20.25	32.04	9.66	0.77	0.35	0.23	98.75	0.19	0.04
6	35.86	20.55	32.57	9.93	0.74	0.29	0.25	100.20	0.19	0.04
7	36.28	20.50	32.47	9.80	0.73	0.31	0.17	100.30	0.19	0.04
8	36.19	20.94	32.22	9.94	0.69	0.25	0.19	100.40	0.20	0.04
T/8	35.62	20.34	31.99	9.45	0.83	0.28	0.21	98.72	0.19	0.04

Garnet from Aplite (MD-2B2)

Points	SiO2	Al2O3	FeO	MnO	MgO	CaO	Na2O	Total	A	M/(M+F)
1	35.39	20.89	31.78	9.71	1.26	0.20	0.11	99.33	0.20	0.07
2	35.54	20.74	32.34	9.76	1.28	0.29	0.15	100.10	0.20	0.07

3	35.64	20.95	33.16	9.58	1.08	0.32	0.23	101.00	0.20	0.05
4	35.76	20.86	32.85	9.14	1.05	0.20	0.28	100.10	0.20	0.05
5	35.51	20.71	32.90	9.66	0.94	0.29	0.13	100.10	0.20	0.05
6	35.70	20.64	33.10	9.87	0.85	0.34	0.16	100.70	0.19	0.04
7	35.73	20.85	33.02	9.74	0.71	0.23	0.17	100.40	0.20	0.04
8	35.49	20.60	32.97	9.80	0.69	0.28	0.32	100.10	0.19	0.04
9	35.41	20.69	32.66	9.95	0.77	0.31	0.22	100.00	0.19	0.04
10	35.40	20.44	32.33	9.85	0.73	0.19	0.14	99.08	0.19	0.04
11	35.37	20.60	32.90	9.43	0.78	0.31	0.23	99.62	0.19	0.04
12	35.17	20.86	32.50	9.53	1.04	0.32	0.31	99.73	0.19	0.05
13	35.21	20.51	32.16	9.34	0.86	0.39	0.16	98.63	0.19	0.05
14	35.50	20.50	31.54	8.77	1.06	0.58	0.10	98.06	0.19	0.06
15	35.24	20.95	31.93	9.27	1.19	0.46	0.08	99.14	0.20	0.06
T/15	35.47	20.72	32.54	9.56	0.95	0.31	0.19	99.74	0.19	0.05

Garnet from Aplite (MD-2B3)

Points	SiO2	Al2O3	FeO	MnO	MgO	CaO	Na2O	Total	A	M/(M+F)
1	35.37	20.61	31.74	9.77	1.13	0.45	0.28	99.34	0.19	0.06
2	35.80	20.50	32.19	9.51	1.16	0.37	0.23	99.77	0.19	0.06
3	35.11	20.67	32.22	9.46	1.18	0.37	0.25	99.26	0.19	0.06
4	35.46	20.54	32.83	9.49	1.04	0.34	0.22	99.92	0.19	0.05
5	35.50	20.52	32.69	9.87	0.93	0.34	0.13	99.98	0.19	0.05
6	35.39	20.29	32.49	9.60	0.90	0.21	0.19	99.07	0.19	0.05
7	35.45	20.84	33.23	9.71	0.87	0.28	0.30	100.70	0.19	0.04
8	35.52	20.71	32.86	9.62	0.78	0.26	0.13	99.88	0.20	0.04
9	35.61	20.66	33.07	9.38	0.87	0.33	0.16	100.10	0.19	0.04
10	35.15	20.61	32.72	9.59	0.75	0.31	0.15	99.27	0.19	0.04
11	35.54	20.54	32.69	9.39	0.78	0.31	0.23	99.49	0.19	0.04
12	34.66	20.53	33.12	9.36	0.91	0.36	0.20	99.15	0.19	0.05
13	35.83	20.62	33.22	8.84	1.08	0.30	0.11	100.00	0.20	0.05
14	35.74	20.87	32.36	9.59	1.20	0.37	0.09	100.20	0.20	0.06

15	36.01	20.92	32.33	9.68	1.06	0.49	0.23	100.70	0.19	0.06
T/15	35.48	20.63	32.65	9.52	0.98	0.34	0.19	99.79	0.19	0.05

Garnet from Unit 5 (103-3)

Points	SiO2	Al2O3	FeO	MnO	MgO	CaO	Na2O	Total	A	M/(M+F)
1	35.26	20.45	30.69	8.83	1.53	0.75	0.18	97.70	0.18	0.08
2	35.51	20.62	32.29	7.06	2.02	0.79	0.18	98.47	0.19	0.10
3	34.26	20.02	30.87	6.77	2.23	0.79	0.12	95.08	0.18	0.11
4	35.40	20.44	31.12	5.81	2.51	0.71	0.18	96.18	0.18	0.13
5	35.35	20.50	30.95	6.01	2.63	0.88	0.17	96.49	0.18	0.13
6	35.05	20.59	30.84	5.69	2.77	0.77	0.32	96.03	0.18	0.14
7	35.61	20.50	31.15	5.92	2.59	0.81	0.20	96.78	0.18	0.13
8	35.53	20.44	31.08	6.22	2.58	0.79	0.30	96.93	0.18	0.13
9	35.85	20.74	31.50	6.48	2.32	0.76	0.24	97.88	0.19	0.12
10	34.87	20.31	30.37	6.69	2.13	0.91	0.23	95.53	0.18	0.11
11	35.56	20.50	31.06	6.96	2.19	0.83	0.15	97.25	0.18	0.11
12	36.14	21.01	32.69	6.99	2.28	0.76	0.16	100.00	0.19	0.11
13	36.07	20.82	32.95	6.95	2.33	0.89	0.26	100.30	0.18	0.11
14	36.25	21.19	33.47	7.52	2.32	0.83	0.23	101.80	0.19	0.11
15	36.51	21.04	32.96	7.35	1.91	0.85	0.11	100.70	0.19	0.09
T/15	35.55	20.61	31.60	6.75	2.29	0.81	0.20	97.81	0.18	0.11

Garnet from Unit 3 (213-3)

Points	SiO2	Al2O3	FeO	MnO	MgO	CaO	Na2O	Total	A	M/(M+F)
1	37.26	21.22	34.15	2.74	4.13	0.97	0.25	100.70	0.19	0.18
2	37.13	20.94	34.67	2.74	3.94	0.94	0.25	100.60	0.18	0.17
3	37.38	20.74	35.25	2.43	3.93	0.92	0.31	101.00	0.18	0.17
4	37.46	21.22	34.71	2.77	3.94	0.89	0.34	101.30	0.19	0.17
5	37.04	21.08	35.17	3.04	3.44	0.89	0.27	100.90	0.19	0.15
6	37.01	20.95	35.29	2.93	3.22	0.87	0.21	100.50	0.19	0.14
7	37.05	21.18	35.14	3.11	3.26	0.88	0.23	100.90	0.19	0.14

8	37.40	21.00	35.45	3.20	3.27	0.86	0.24	101.40	0.19	0.14
9	36.90	21.08	34.97	4.02	2.81	0.83	0.23	100.80	0.19	0.13
10	36.99	20.99	34.93	3.15	3.53	0.83	0.24	100.70	0.19	0.15
11	37.20	21.03	34.75	2.84	3.60	0.73	0.15	100.30	0.19	0.16
12	36.76	21.01	34.64	3.09	3.68	0.85	0.30	100.30	0.19	0.16
13	37.00	21.00	35.05	3.13	3.59	0.80	0.14	100.70	0.19	0.15
14	36.82	20.94	34.95	3.06	3.66	0.79	0.15	100.40	0.19	0.16
15	36.84	20.79	34.86	3.13	3.64	0.89	0.27	100.40	0.18	0.16
16	37.29	21.02	35.02	2.95	3.58	0.84	0.12	100.80	0.19	0.15
17	37.10	21.15	35.04	3.27	3.58	0.78	0.18	101.10	0.19	0.15
18	37.35	21.05	35.04	2.98	3.71	0.82	0.23	101.20	0.19	0.16
19	37.38	21.07	35.05	3.13	3.55	0.85	0.25	101.30	0.19	0.15
20	37.08	21.09	34.70	3.23	3.48	0.83	0.19	100.60	0.19	0.15
21	37.41	21.00	35.35	2.93	3.68	0.80	0.26	101.40	0.19	0.16
22	37.35	21.27	34.32	2.73	4.03	0.93	0.10	100.70	0.19	0.17
23	37.45	20.82	34.20	2.54	4.34	1.00	0.15	100.50	0.18	0.18
24	37.10	20.91	33.77	3.41	4.10	1.22	0.17	100.70	0.18	0.18
T/24	37.16	21.02	34.85	3.02	3.65	0.88	0.22	100.80	0.19	0.16

Garnet from the Musquodoboit Batholith

Sno.	SiO2	Al2O3	FeO	MnO	MgO	CaO	Na2O	Total	A	M/(M+F)
41	35.85	20.51	27.80	16.22	0.72	0.16	0.00	101.26	0.20	0.04
41	35.68	20.52	28.34	15.78	0.72	0.18	0.00	101.22	0.20	0.04
70	35.40	20.38	32.16	11.79	0.39	0.13	0.00	100.25	0.20	0.02
82	35.12	20.17	28.28	16.30	0.13	0.08	0.00	100.08	0.20	0.01
108	36.17	20.77	26.25	18.54	0.52	0.15	0.00	102.40	0.20	0.03
56	36.77	21.12	37.55	4.80	3.80	1.43	0.00	105.47	0.21	0.15
96	36.32	21.09	33.32	7.04	2.65	0.80	0.00	101.22	0.21	0.12

Sno 41--Sno.108 are garnets from aplites and Sno.56 and 96 are xenocrystic garnets.

Andalusite from Unit 5 (D12-0122-4: Traverse A)

Point	SiO2	TiO2	Al2O3	FeO	MnO	MgO	CaO	Na2O	K2O	P2O5	Total
1	36.56	0.03	63.01	0.42	-0.05	0.20	0.05	0.04	0.04	-0.11	100.44
2	36.69	0.08	62.83	0.51	0.06	0.13	0.04	0.11	-0.03	-0.07	100.03
3	36.85	0.13	62.77	0.48	0.08	0.08	0.03	0.07	-0.01	-0.03	100.11
4	36.63	-0.02	62.76	0.50	-0.07	0.02	-0.04	0.02	-0.02	-0.05	99.89
5	36.98	0.05	63.01	0.56	0.06	0.11	-0.01	0.07	0.09	0.15	100.63
6	36.66	-0.02	62.93	0.62	-0.17	0.10	0.07	0.01	-0.02	0.04	100.21
7	36.84	0.10	62.63	0.94	0.08	0.10	0.00	-0.01	-0.02	-0.03	100.41
8	36.28	0.09	62.00	0.95	0.02	0.11	0.05	0.12	0.06	0.17	99.23
9	36.67	0.03	62.34	0.89	-0.12	0.15	0.06	0.05	-0.05	-0.10	100.05
10	36.50	0.06	62.48	0.87	0.07	0.10	0.04	0.01	0.01	0.04	99.85
11	36.22	-0.06	62.16	0.97	-0.06	0.05	0.03	-0.02	-0.04	0.02	99.35
12	36.51	0.08	62.46	0.93	0.02	0.07	0.02	-0.06	-0.02	-0.03	99.90
13	36.58	-0.05	62.31	0.95	0.00	0.01	0.00	0.04	0.02	0.10	99.85
14	36.51	0.14	62.99	0.53	0.00	0.08	-0.01	0.02	0.03	0.05	100.03
15	36.86	-0.01	62.88	0.51	0.10	0.04	0.01	0.05	-0.01	0.16	100.26
16	36.91	0.03	63.22	0.53	0.10	0.09	-0.05	0.06	0.07	-0.10	100.73
17	36.65	0.07	62.96	0.51	0.07	0.10	-0.03	0.10	0.04	0.02	100.12
18	36.53	0.05	62.89	0.53	0.07	0.04	0.01	0.03	0.00	0.19	100.13
19	36.59	0.02	62.99	0.52	-0.07	0.04	0.01	0.03	0.04	0.05	100.10
20	36.71	0.11	63.09	0.51	-0.02	0.16	0.03	0.04	0.01	-0.04	100.46
21	36.73	0.04	63.07	0.51	0.04	0.07	0.01	0.06	0.00	-0.03	100.32
22	36.49	0.11	62.73	0.53	-0.04	0.05	-0.03	0.01	-0.01	0.01	99.75
23	36.63	0.10	62.94	0.51	-0.05	0.08	-0.01	0.08	0.03	0.08	100.08
24	36.58	0.10	62.68	0.53	-0.02	0.02	-0.03	0.07	0.01	-0.06	99.79
25	36.08	0.04	62.44	0.52	0.10	0.06	0.06	0.02	0.01	-0.06	99.04
T/25	36.61	0.05	62.74	0.63	0.01	0.08	0.01	0.04	0.01	0.01	100.03

Andalusite from Unit 5 (D12-0122-4, Traverse B)

Point	SiO2	TiO2	Al2O3	FeO	MnO	MgO	CaO	Na2O	K2O	P2O5	Total
1	37.24	0.02	60.81	0.61	-0.03	0.16	0.07	0.01	0.05	-0.03	98.88
2	36.61	0.05	63.08	0.53	-0.01	0.08	-0.02	0.02	0.04	-0.08	100.21
3	35.80	-0.03	61.51	0.48	-0.07	0.11	-0.03	0.02	0.01	0.03	97.79
4	35.77	0.13	61.63	0.50	0.08	0.06	0.09	0.02	-0.04	-0.07	97.98
5	36.25	0.02	62.19	0.51	0.03	0.09	0.00	0.08	0.02	-0.03	98.95
6	36.16	0.07	62.65	0.54	0.01	0.21	-0.02	-0.03	-0.04	0.09	99.81
7	36.52	0.06	62.43	0.54	0.09	0.08	0.02	0.01	-0.02	-0.04	99.50
8	35.14	0.02	59.83	0.67	0.03	0.12	0.04	-0.02	0.03	-0.01	95.64
9	37.43	0.13	57.10	0.85	0.02	0.49	0.15	0.21	0.18	0.11	97.22
10	36.61	0.11	62.47	0.84	-0.03	0.17	0.04	0.10	-0.03	-0.02	100.08
11	36.33	0.07	62.38	0.82	0.05	0.05	-0.05	0.00	0.03	-0.08	99.53
12	36.13	-0.04	61.99	0.84	-0.03	0.02	-0.01	-0.07	0.00	0.08	98.95
13	36.28	0.00	62.23	0.90	0.01	0.08	0.00	0.05	0.03	-0.03	99.41
14	36.27	-0.03	62.22	0.87	-0.02	0.05	0.00	0.04	0.02	0.06	99.36
15	36.40	0.09	61.94	0.81	-0.08	0.02	0.02	0.07	0.04	0.03	99.15
16	36.47	0.09	62.27	0.84	0.00	0.06	0.02	-0.06	0.08	-0.09	99.66
17	36.13	0.04	62.37	0.85	-0.06	0.06	-0.01	0.08	0.07	0.12	99.43
18	36.26	0.13	62.19	0.85	0.00	0.10	0.04	0.02	-0.02	0.08	99.30
19	36.58	-0.03	62.22	0.82	0.01	0.09	-0.02	0.05	0.04	0.02	99.62
20	36.37	0.08	62.40	0.84	0.04	0.02	-0.01	0.04	-0.02	0.15	99.62
21	36.42	0.04	62.44	0.60	-0.04	0.07	0.02	0.07	-0.01	-0.02	99.46
22	36.46	0.01	63.36	0.53	-0.05	0.13	0.00	0.13	-0.02	-0.04	100.48
23	36.45	0.10	62.88	0.57	-0.04	0.15	-0.01	0.09	0.04	-0.01	100.05
24	36.64	-0.06	62.89	0.55	-0.02	0.07	0.03	0.03	-0.04	0.11	100.08
25	36.57	-0.09	62.99	0.57	0.07	0.05	-0.04	-0.03	-0.01	0.04	100.13
T/25	36.37	0.04	62.02	0.72	0.00	0.10	0.01	0.04	0.02	0.02	99.21

Andalusite from a hydrothermal zone of granitoid rocks (2095-07C)

Point	SiO2	TiO2	Al2O3	FeO	MnO	MgO	CaO	Na2O	K2O	P2O5	Total
1	35.78	0.06	62.53	0.21	-0.14	-0.30	0.04	-0.07	-0.01	-0.15	98.31
2	36.03	0.01	62.75	0.20	-0.02	-0.13	-0.03	-0.04	-0.06	0.00	98.78
3	36.42	0.09	63.67	0.16	0.11	0.00	-0.02	-0.02	0.0[illegible]	0.12	100.08
4	36.68	0.12	63.27	0.25	-0.17	0.09	0.00	-0.11	-0.03	-0.15	99.95
5	36.20	0.34	63.84	0.24	0.00	0.33	0.01	0.16	0.05	0.09	100.50
6	36.51	-0.10	63.33	0.37	-0.01	-0.05	0.00	-0.21	0.00	-0.15	99.84
7	36.30	0.01	63.08	0.50	0.02	0.07	0.05	0.03	0.08	-0.03	99.88
8	35.79	0.02	63.13	0.39	-0.16	0.20	0.03	0.06	-0.07	0.11	99.30
9	36.78	0.18	63.64	0.23	0.16	0.26	0.07	0.00	-0.01	-0.04	100.42
10	36.23	-0.02	62.48	0.77	-0.02	0.15	-0.08	0.05	-0.07	0.04	99.48
11	36.56	0.13	61.67	0.56	0.02	0.18	0.13	0.04	0.05	0.23	98.79
12	36.01	0.29	62.19	0.59	0.16	0.14	0.02	-0.20	0.09	0.03	98.79
13	36.70	0.15	62.54	1.05	-0.04	0.27	0.01	0.19	0.07	0.26	100.29
14	36.78	0.08	63.88	0.79	-0.05	0.18	-0.02	-0.04	-0.09	0.23	101.44
15	36.75	0.08	62.15	0.51	0.01	-0.18	0.00	0.00	0.05	0.44	99.85
16	36.99	0.18	63.34	0.80	0.19	0.17	-0.02	0.11	-0.01	0.13	101.13
17	36.78	0.03	62.23	0.72	-0.29	0.14	-0.11	0.01	0.20	0.33	100.27
18	35.99	0.15	61.76	0.79	-0.06	0.16	0.08	0.05	0.03	0.21	98.55
19	35.87	0.09	62.14	0.88	0.10	0.25	0.01	0.04	-0.16	-0.03	98.90
20	36.24	0.36	63.32	0.70	-0.28	0.26	-0.03	0.00	0.04	0.13	100.62
21	35.65	0.09	62.56	0.35	-0.19	-0.01	0.01	0.10	-0.04	0.09	98.21
22	36.54	-0.12	63.76	0.30	0.28	0.00	0.04	0.21	0.09	-0.16	100.30
23	36.50	0.22	63.51	0.33	0.03	0.00	-0.01	0.07	0.05	-0.10	100.01
24	36.62	0.19	63.99	0.39	0.10	0.12	0.05	0.07	-0.02	-0.11	100.99
25	37.13	0.34	63.72	0.17	-0.05	0.09	0.12	0.00	-0.04	-0.02	101.19
26	36.62	0.20	63.64	0.44	-0.01	-0.16	0.08	0.12	-0.01	0.01	100.70
27	36.57	0.06	63.28	0.15	-0.07	-0.08	-0.05	0.05	-0.06	-0.09	99.85
28	36.95	0.10	63.73	0.18	0.14	0.05	0.11	0.17	-0.03	0.06	100.68
29	36.26	0.14	63.31	0.05	0.08	-0.11	0.05	0.02	0.08	0.11	99.57

30	36.69	0.14	64.14	0.17	-0.22	-0.14	-0.03	-0.04	-0.02	0.10	100.83
T/30	36.43	0.12	63.09	0.44	-0.01	0.07	0.02	0.03	0.01	0.06	99.92

Andalusite from biotite monzogranite at the contact, see text for the location (MP-5)

Point	SiO2	TiO2	Al2O3	FeO	MnO	MgO	CaO	Na2O	K2O	P2O5	Total
1	36.22	0.17	63.09	0.05	-0.21	0.24	0.06	0.08	-0.03	-0.13	99.30
2	36.06	0.12	63.63	0.43	0.02	0.13	-0.05	0.12	-0.06	0.02	100.63
3	36.36	0.24	61.96	0.44	-0.12	0.03	-0.04	0.00	-0.03	-0.12	98.77
4	35.87	-0.03	62.38	0.90	0.10	0.16	0.06	-0.04	-0.02	-0.01	99.15
6	36.47	0.06	62.59	0.73	0.01	0.16	-0.05	0.13	0.05	0.02	99.78
7	35.92	0.09	61.64	0.87	0.03	-0.03	0.01	0.08	0.03	-0.05	98.43
8	36.02	-0.15	62.30	0.92	0.01	0.14	-0.11	-0.09	-0.04	0.16	99.25
9	35.87	0.07	61.96	0.93	-0.06	0.04	-0.08	-0.02	-0.04	0.09	98.77
10	36.09	-0.17	62.76	0.18	-0.07	0.12	0.05	-0.01	-0.09	0.08	98.84
11	35.91	0.05	62.74	0.25	-0.02	0.06	-0.04	0.11	0.14	0.01	98.79
12	36.40	0.04	62.65	0.22	0.15	-0.04	0.06	-0.05	0.06	-0.17	99.05
T/11	36.11	0.04	62.52	0.54	-0.01	0.09	-0.01	0.03	0.00	-0.01	99.16

References

Abbott, R.N., Jr. 1985. Muscovite-bearing granites in the AFM liquidus projection. Can.Mineral. **23**: 553-561.

Abbott, R.N., Jr. & Clarke, D.B. 1979. Hypothetical liquidus relationships in the subsystem Al_2O_3 - FeO - MgO projected from quartz, alkali feldspar and plagioclase for $a_{(H2O)} \leq 1$. Can. Mineral. **17**: 549-560.

Allan, B.D. & Clarke, D.B. 1981. Occurrence and origin of garnets in the South Mountain Batholith, Nova Scotia. Can. Mineral. **19**: 19-24.

Alling, A.L. 1936. Interpretive petrology. McGraw-Hill, New York.

Althaus, E., Karotke, E., Nitsch, K.B., & Winkler, H.G.F. 1970. An experimental re-examination of the upper stability limit of muscovite plus quartz. Neues Jahrb. Mineral. Monatsh. 325-336.

Anderson, A.T., Jr. 1983. Oscillatory zoning of plagioclase: Nomarski interference contrast microscopy of etched sections. Am. Miner. **68**: 125-129.

Anderson, A.T., Jr. 1984. Probable relations between plagioclase zoning and magma dynamics, Fuego Volcano, Guatemala. Am. Miner. **69**: 660-676.

Anderson, J.L. & Rowley, M.C. 1981. Synkinematic intrusion of peraluminous and associated metaluminous granitic magmas, Whipple Mountains, California. Can. Mineral. **19**: 83-101.

Augustithis, S.S. 1990. Atlas of metamorphic metasomatic textures and processes. Elsevier Science Publishers B.V. pp. 44-53, 46, and 102.

Barker, F. 1961. Phase relations in cordierite-garnet-bearing Kinsman quartz monzonite and the enclosing schist, Lovewell Mountain quadrangle, New Hampshire. Am. Mineral. **46**: 1166-1176.

Best, B.G., Henage, L.F., & Adams, J.A.S. 1968. Mica peridotite, wyomingite, and associated potassic igneous rocks in Northeastern Utah. Am. Mineral. **53**: 1041-1048.

Best, M.G. 1982. Igneous and metamorphic petrology, p.404. W.H. Freeman and Company.

Birch, W.P. & Gleadow, T.W. 1974. The genesis of garnets and cordierite in acid volcanic rocks: evidence from the Cerberean Cauldron, Central Victoria, Australia. Contr. Mineral. Petrol. **45**: 1-3.

Burnham, C.W. 1979. The importance of volatile constituents. In The evolution of the igneous rocks: fiftieth anniversary perspectives. Ed. Yoder, H.S., Jr. Princeton University Press.

Burt, D.M. & Stump, E. 1983. Mineralogical investigation of andalusite-rich pegmatites from Szabo Bluff, Scott Glacier area. Antarctic J. US, **18**: 49-52.

Carmichael, I.S.E. & Ghiorso, M.S. 1990. The effect of oxygen fugacity on the redox state of natural liquids and their crystallizing phases. In Modern methods of igneous petrology: understanding magmatic processes; Reviews in mineralogy **24**: 196.

Cashman, K.V. 1990. Textural constraints on the kinetics of crystallization of igneous rocks. In Modern methods of igneous petrology: understanding magmatic processes. Eds: Nicholls, J. & Russell, J.K. Reviews in mineralogy, **24**: 259-314.

Chappell, B.W. & White, A.J.R. 1974. Two contrasting granite types. Pacific Geology, **8**: 173-174.

Charoy, B. 1986. The genesis of the Cornubian batholith (south-west England): the example of the Carnmenellis pluton. J. Petrol. **27**: 571-604.

Chatterjee, N.D. & Flux, S. 1986. Thermodynamic mixing properties of mucovite-paragonite crystalline solutions at high

temperatures and pressures, and their geological applications. J. Petrol. **27**: 677-693.

Chatterjee, N.D. & Johannes, W. 1974. Thermal stability and standard thermodynamic properties of synthetic $2M_1$-muscovite, $KAl_2[AlSi_3O_{10}(OH)_2]$. Contrib. Mineral. Petrol. **48**: 89-114.

Clark, A.H., Pearce, T.H., Roeder, P.L. & Wolfson, I. 1986. Oscillatory zoning and other microstructures in magmatic olivine and augite: Nomarski interference contrast observations on etched polished surfaces. Am. Miner. **71**: 734-741.

Clarke, D.B. 1981. The mineralogy of peraluminous granites: a review. Can. Mineral. **19**: 3-17.

Clarke, D.B. 1992. Granitoid rocks, (p. 135-136). "Topics in the Earth Sciences" series, editor: T.H. van Andel. Chapman & Hall, London.

Clarke, D.B. 1994. Cordierite in felsic igneous rocks: a synthesis. Mineral. Mag. (in press).

Clarke, D.B. & Halliday, A.N. 1980. Strontium isotope geology of the South Mountain Batholith, Nova Scotia. Geochim. Cosmo. Acta. **44**: 1045-1058.

Clarke, D.B., Halliday, A.N, & Hamilton, P.J. 1988. Neodymium and strontium isotopic constraints on the origin of the peraluminous granitoids of the South Mountain Batholith, Nova Scotia, Canada. Chem. Geol. **73**: 15-24.

Clarke, D.B., McKenzie, C.B., Muecke, G.K., & Richardson, S.W. 1976. Magmatic andalusite from the South Mountain batholith, Nova Scotia. Contrib. Mineral. Petrol. **56**: 279-287.

Clarke, D.B. & Muecke, G.K. 1985. Review of the petrochemistry and origin of the South Mountain Batholith and associated plutons, Nova Scotia, Canada. *In* High heat production

granite, hydrothermal circulation and ore genesis. Institute of Mining and Metallurgy, London, pp. 41-54.

Clarke, D.B. & Rottura, A. 1994. Garnet-forming and garnet-eliminating reactions in a quartz diorite intrusion at Capo Vaticano, Calabria, Southern Italy. The Can. Mineral. **32:** 623-635.

Clemens, J.D. & Mawer, C.K. 1992. Granitic magma transport by fracture propagation. Tectonophysics, 204: 339-360.

Clemens, J.D. & Wall, V.J. 1981. Origin & crystallization of some peraluminous (S-type) granitic magmas. Can. Mineral. **19:** 111-131.

Corey, M.C. 1988. An occurrence of metasomatic aluminosilicates related to high alumina hydrothermal alteration within the South Mountain Batholith, Nova Scotia. Maritime Sediments and Atlantic Geology. **24**: 83-95.

Cox, K.G., Bell, J.D., & Pankhurst, R.J. 1979. The interpretation of igneous rocks, P.190-191. George Allen & Unwin (Publishers) Ltd., London.

Currie, K.L. & Pajari, G.E. 1981. Anatectic peraluminous granites from the Carmanville area, Northeastern Newfoundland. Can. Mineral. **19:** 147-161.

Czamanske, G.K., Lipman, P.W., & Calk, L.C. 1983. Acmite, arfvedsonite, & biotite in granitic rocks from the Miocene Questa Caldera, NM. Abstracts with Programs, GSA **15**: 380.

Day, H.W. 1973. The high temperature stability of muscovite plus quartz. Amer. Miner. **58**: 255-262.

Deer, W.A., Howie, R.A., and Zussman, J. 1982. Othosilicates, 761 p. Published in the USA by Halsted Press, a Division of John Wiley & Sons, Inc. New York.

Delaney, P.T. & Pollard, D.D. 1982. Solidification of basaltic magma during flow in a dike. Amer. J. Sci. **282**: 856-885.

Dietvorst, E.J.L. 1980. Biotite breakdown and the formation of gahnite in metapelitic rocks from Kemio, southwest Finland. Contr. Mineral. Petrol. **75**: 327-337.

Dunham, A.C. & Wilkinson, F.C.F. 1978. Accuracy, precision and detection limits of energy-dispersive electron-microprobe analyses of silicates. X-ray Spectrometry, **7**: 50-56.

Edmunds, W. M. & Atherton, M.P. 1971. Polymetamorphic evolution of garnet in the Fanad aureole, Donegal, Eire. Lithos, **4**: 147-161.

Flood, R.H. & Shaw, S.E., 1975. A cordierite-bearing granite suite from the New England batholith, N.S.W., Australia. Contr. Mineral. Petrol. **52**: 157-164.

Gallagher, V. 1988. Coupled substitutions in schorl-dravite tourmaline new evidence from SE Ireland. Mineral. Mag. **52**: 637-650.

Grambling, J.A.& Williams, M.L. 1985. The effects of Fe^{3+} and Mn^{3+} on aluminum silicate phase relationships in north central New Mexico, USA. Journal of Petrology, **26**: 324-354.

Grapes, R.H. 1987. Composition and melting relationships of andalusite in a schist xenolith, Wehr Volcano, East Eifel. N.Jahrb. Mineral. Monatsh. **12**: 550-556.

Graves, M.C. & Zentilli, M. 1988. The lithochemistry of metal-enriched coticules in the Goldenville-Halifax transition zone of the Meguma Group, Nova Scotia. *In* Current Research, Part B, Geological Survey of Canada, Paper 88-1B, p. 251-161.

Green, T.H. 1976. Experimental generation of cordierite- and garnet-bearing granitic liquids from a pelitic composition. Geology, **4**: 85-88.

Green, T.H. 1977. Garnets in silicic liquids and its possible use as a P-T indicator. Contr. Mineral. Petrol. **65**: 59-67.

Green, T.H. & Ringwood, A.E. 1968a. Origin of garnet phenocrysts in calc-alkaline rocks. Contrib. Mineral. and Petrol. **18**: 163-164.

Green, T.H. & Ringwood, A.E. 1968b. Genesis of the calc-alkaline igneous rock suite. Contr. Mineral. Petrol. **18**: 105-62.

Grew, E.S. 1980. Sillimanite and ilmenite from high-grade metamorphic rocks of Antarctica and other areas. J. Petrol. **21**: 39-68.

Grossman, J.J., Ryan, J.A., Mukherjee, N.R., & Wegner, M.W. 1971. Microchemical, microphysical, and adhesive properties of lunar material, II. Proceedings of the 2nd lunar Science Conference. **3**: 2153-2164.

Hall, A. 1965. The origin of accessory garnet in the Donegal granite. Mineral. Mag. **35**: 628-633.

Ham, L.J. & Kontak, D.J. 1988. A textural and chemical study of white mica in the South Mountain batholith, Nova Scotia: primary versus secondary origin. Mar. Sed. Atl. Geo. **24**: 111-121.

Harrison, T.N. 1988. Magmatic garnets in the Cairngorm granite, Scotland. Mineral. Mag. **52**: 659-667.

Haslam, H.W. 1971. Andalusite in the Mullach nan Coirean granite, Inverness-shire. Geol. Mag. **108**: 97-102.

Heinrich, E.W. 1955. Cordierite in pegmatite near Micanite, Colorado. Am. Mineral., **35**: 174-184.

Heinrich, E.W. 1965. Microscopic identification of minerals, McGraw-Hill, New York, 177-183.

Holdaway, M.J. 1971. Stability of andalusite and the aluminium silicate phase diagram. Am. J.Sci. **271**: 97-131.

Humchison, C.S. 1974. Laboratory handbook of petrographic techniques, John Wiley & Sons Inc.

Johannes, W. 1984. Beginning of melting in the granite system Qz-Or-Ab-An-H2O. Contrib. Mineral. Petrol. **86**: 264-273.

Johannsen, A. 1939. Descriptive petrography of the igneous rocks, v.1, U. Chicago Press.

Kerrick, D.M. & Speer, J.A. 1988. The role of minor element solid solution on the andalusite-sillimanite equilibrium in metapelites and peraluminous granitoids. Am. J. Sci. **288**:152- 192.

Kistler, R.W., Ghent, E.D., & O'Neil, J.R. 1981. Petrogenesis of garnet two-mica granites in the Ruby Mountains, Nevada. J. Geophy. Res. **86**: 10591-10606.

Kontak, D.J. & Smith, P. 1993. A metaturbidite-hosted lode gold deposit: the Beaver Dam deposit, Nova Scotia. I. vein paragenesis and mineral chemistry. Can. Mineral. **31**: 471-522.

Kress, V.C., & Carmichael, I.S.E. 1988. Stoichiometry of the iron oxidation reaction in silicate melts. Am.Mineral. **73**: 1267-1274.

Kretz, R. 1973. Kinetics of the crystallization of garnet at two localities near Yellowknife. Can. Mineral **12**: 1-20.

Kretz, R. 1983. Symbols for rock-forming minerals. Ame. Mineral. **68**: 277-279.

Kuo, L.C. and Kirkpatrick, R.J. 1985. Kinetics of crystal dissolution in the system diopside-forsterite-silica. Ame. J. Sci. **285**: 51-90.

Kwak, T.A.P. 1981. Sector-zoned annite phlogopite micas from the Mt. Lindsay Sn-W-F(-Be) deposit, Tasmania, Australia. Can. Mineral. **19**: 643-650.

Leake, B.E. 1960. Compilation of chemical analyses and physical constants of natural cordierites. Am. Mineral. **45**: 282-298.

Leake, B.E. 1968. Zoned garnets from the Galway granite and its aplites. Earth Planet. Sci. Lett. **3**: 311-316.

Lofgren, G.E. 1973. Experimental crystallization of synthetic plagioclase at prescribed cooling rates. EOS Trans. AGU, **54**: 482.

London, D., Hervig, R.L., & Morgan, G.B. 1988. Melt-vapor solubilities and elemental partitioning in peraluminous granite-pegmatite systems: experimental results with Macusani glass at 200 MPa. Contrib. Mineral. Petrol. **99**: 502-516.

Loomis, Timothy P. 1983. Compositional Zoning of Crystals: A Record of Growth and Reaction History. In Kinetics and Equilibrium in Mineral Reactions, Edited by S.K. Saxena. Springer-Verlag, NY.

Luth, W.C., Jahns, R. H. & Tuttle, O.F. 1964. The granite system at pressures of 4 to 10 kilobars. J. Geophys. Res. **69:** 759-773.

MacDonald, G.A. & Merriam, R. 1938. Andalusite in pegmatite from Fresno County, California. Am. Mineral. **23:** 588-549.

MacDonald, M. A. 1981. The mineralogy, petrology and geochemistry of the Musquodoboit batholith. MSc. Thesis, Dalhousie University, Halifax, N.S.

MacDonald, M.A. & Horne, R.J. 1988. Petrology of the zoned, peraluminous Halifax Pluton, South-Central Nova Scotia. Marit. Sed. and Atl. Geo. **24:** 33-45.

MacDonald, M.A., Horne, R.J., Corey, M.C., & Ham, L.J. 1992. An overview of recent bedrock mapping and follow-up petrological studies of the South Mountain Batholith, southwestern Nova Scotia, Canada. Atl. Geol. **28**: 7-28.

MacKenzie, W.S. & Guilford, C. 1980. Atlas of rock-forming minerals in thin section. Halsted Press, a Division of John Wiley & Sons, Inc.

Mahood, G. & Hildreth, W. 1983. Large partition coefficients for trace elements in high silica rhyolites. Geochim. Cosmochim. Acta **47**: 11-30.

Maillet, L. 1984. The origin and occurrence of cordierite in the South Mountain Batholith. BSc thesis, Dalhousie University, Halifax, N.S.

Maillet, L.A. & Clarke, D.B. 1985. Cordierite in the peraluminous granites of the Meguma Zone, Nova Scotia, Canada. Min. Mag. **49**: 695-702.

Manning, D.A.C. 1983. Chemical variation in garnets from aplites and pegmatites, peninsular Thailand. Mineral. Mag. **47**: 353-358.

Manning, D.A.C., & Pichavant, M. 1983. The role of fluorine and boron in the generation of granitic melts. In: Atherton, M.P., and Gribble, C.D. (eds), Migmatites, Melting and Metamorphism, Shiva Publishing Ltd., Nantwich, England p.94-109.

McKenzie, C.B. & Clarke, D.B. 1975. Petrology of the South Mountain Batholith, Nova Scotia. Can. J. Earth Sci. **12**: 1209-1218.

Miller, C.F. & Kish, S.A. 1980. Peraluminous trondhjemite, Whiteside pluton, North Carolina. Geol. Soc. Amer. Abstr. Programs. **12**: 201.

Miller, C.F. & Stoddard, E.F. 1978. Origin of garnet in granitic rocks; an example of the role of Mn from the Old Woman-Piute range, California. Can. Mineral. Assoc. Can. Abstr. Prog. **3**: 456.

Miller, C.F. & Stoddard, E.F. 1981. The role of manganese in the paragenesis of magmatic garnet: an example from the Old Woman-Piute Range, California. J. Geol. **89**: 233-246.

Miller, C.F., Rapp, R.P., & Watson, E.B. 1989. Controls of muscovite stability and composition at 8kb: an experimental study. Geol. Soc. Amer. Abst. with Progr., GSA. **21**: 238-239.

Miller, C. F., Sparkes, A.K., Stoddard, E.F., Hoisch, T.D. & Hurst, R.W. 1980. Old Woman-Piute Range plutonic complex, southeastern California. Geol. Soc. Amer. Abstr. with Programs. **12**: 141.

Miller, C.F., Stoddard, E.F., Bradfish, L.J. & Dollase, W.A. 1981. Composition of plutonic muscovite: genetic implications. Can. Mineral. **19**: 25-34.

Miyashiro, A. 1973. Metamorphism and metamorphic belts. George Allen & Unwin Ltd., London.

Mokhtari, A. & Velde, D. 1987. Sector-zoned kaersutite in camptonites from Morocco. Mineral. Mag. **51**: 151-156.

Monier, G. & Robert, J.L.1986. Muscovite solid solutions in the system K_2O-MgO-FeO-Al_2O_3-SiO_2-H_2O: an experimental study at 2 kbar P_{H2O} and comparison with natural Li-free white micas. Mineral. Mag. **50**: 257-66.

Morin, J.A. & Turnock, A.C. 1975. The clotty granite at Perrault Falls, Ontario, Canada. Can. Mineral. **13**: 352-357.

Muecke, G.K. & Chatterjee, A.K. 1983. Lithogeochemistry as an indicator of uranium and tin mineralization, South Mountain Batholith, Nova Scotia, Canada. J. Geoche. Expl. **19**: 589-594

Nelson, C.A. & Sylvester, A.G. 1971. Wall rock decarbonation and forcible emplacement of Birch Creek pluton, southern White Mountains, California. Geol. Soc. Amer. Bull. **82**: 2891-2904.

O'Brien, H.E., Irving, A.J., and McCallum, I.S. 1988. Complex zoning and resorption of phenocrysts in mixed potassic mafic magmas of the Highwood Mountains, Montana. Ame. Miner. **73**: 1007-1024.

Okrusch, M. & Evans, B.W. 1970. Minor element relationships in coexisting andalusite and sillimanite. Lithos, **3**: 261-268.

Papike, J.J. 1987. Chemistry of the rock-forming silicates: ortho, ring, and single-chain structures. Rev. Geophysics. **25**: 1483-1526.

Pattison, D.R.M. 1992. Stability of andalusite and sillimanite and the Al_2SiO_5 triple point; constraints from the Ballachulish aureole, Scotland. J. of Geol. **100**: 423-446.

Petford, N., Kerr, R.C., Lister, J.R. 1993. Dike transport of granitoid magmas. Geology, **21**: 845-848.

Phillips, G.N., Wall, V.J. & Clemens, J.D. 1981. Petrology of the Strathbogie Batholith: a cordierite-bearing granite. Can. Mineral. **19**: 47-63.

Phillips, W.R. & Griffen, D.T. 1981. Optical mineralogy. W.H. Freeman and Company, San Francisco. p.169.

Pichavant, M., Kontak, D.J., Valencia H. J., & Clark, A.H. 1988. The Miocene-Pliocene Macusani Volcanics, SE Peru I. Mineralogy and magmatic evolution of a two-mica aluminosilicate-bearing ignimbrite suite. Contrib. Mineral. Petrol. **100:** 300-324.

Plummer, C.C. 1980. Dynamothermal contact metamorphism superposed on regional metamorphism in the pelitic rocks of the Chiwaukum Mountains area, Washington Cascades. Bull. Geol. Soc. Am., Part II, **91:** 1627-1668.

Price, R.C. 1983. Geochemistry of a peraluminous granitoid suite from north-eastern Victoria, south-eastern Australia. Geochim Cosmochim. Acta, **47:** 31-42.

Puziewicz, J. & Johannes, W. 1988. Phase equilibria and compositions of Fe-Mg-Al minerals and melts in water-saturated peraluminous granitic systems. Contr. Mineral. Petrol. **100:** 156-168.

Raeside, R.P., Hill, J.D. and Eddy, B.G. 1988. Metamorphism of Meguma Group metasedimentary rocks, Whitehead Harbour Area, Guysborough County, Nova Scotia. Marit. Sed. and Atlan. Geol. **24:** 1-9.

Richardson, S.W., Gilbert, M.C., & Bell, P.M. 1969. Experimental determination of kyanite-andalusite and andalusite-sillimanite equilibria: the aluminium silicate triple point. Am. J.Sci., **267:** 259-272.

Rimsaite, J. 1969. Evolution of zoned micas & associated silicates in the Oka Carbonatite. Contr. Mineral. Petrol. **23**: 340-360.

Roycroft, P. 1989. Zoned muscovite from the Leinster Granite, S.E. Ireland. Mineral. Mag. **53**: 663-665.

Roycroft, P. 1991. Magmatically zoned muscovite from the peraluminous two-mica granites of the Leinster batholith, southeast Ireland. Geology, **19**: 437-440.

Sack, R.O., Carmichael, I.S.E. Rivers, M.L., & Ghiorso, M.S. 1980. Ferric-ferrous equilibria in natural silicate liquids at 1 bar. Contrib. Mineral. Petrol., **75**: 369-376.

Shand, S.J. 1927. Eruptive rocks. J. Wiley & Sons, New York.

Shiba, M. 1988. Metamorphic evolution of the southern part of the Hidaka belt, Hokkaido, Japan. J. Metamorphic Geol. **6**: 273-296.

Smith, T.E. 1974. The geochemistry of the granitic rocks of Halifax County, Nova Scotia. Can. J. Earth Sci. **11**: 650-656.

Smith, T.E. 1975. Layered granitic rocks at Chebucto Head, Halifax County, Nova Scotia. Can. J. Earth Sci. **12**: 456-463.

Speer, J.A. 1981. Petrology of cordierite- and almandine-bearing granitoid plutons of the southern Appalachian Piedmont, U.S.A. Can. Mineral. **19**: 35-46.

Speer, J.A. 1984. Micas in igneous rocks. Mineral. Soc. Am. Rev. Mineral. **13**: 299-356.

Speer, J.A. 1987. Evolution of magmatic AFM mineral assemblages in granitoid rocks: The hornblende + melt = biotite reaction in the Liberty Hill pluton, South Carolina. Ame. Mineral. **72**: 863-878.

Speer, J.A.& Becker, S.W. 1992. Evolution of magmatic and subsolidus AFM mineral assemblages in granitoid rocks: biotite, muscovite, and garnet in the Cuffytown Creek pluton, South Carolina. Amer. Mineral. **77**: 821-833.

Spry, P.G. 1987. Compositional zoning in zincian spinel. Can. Mineral. **25**: 97-104.

Stamatelopoulou, S.K., Vlassopoulos, D., Pearce, T.H., Rice, C. 1990. The record of magma chamber processes in plagioclase phenocrysts at Thera Volcano, Aegean volcanic arc, Greece. Contr. Miner. Petrol. **104**: 73-84.

Stephenson, D. & Upton, B.G.J. 1982. Ferromagnesian silicates in a differentiated alkaline complex, Kungnat Fjeld, South Greenland. Mineral. Mag. **46**: 283-300.

Swanson, S.E. 1977. Relation of nucleation and crystal-growth rate to the development of granitic textures. Ame. Mineral. **62**: 966-978.

Sylvester, A.G., Oertel, G., Nelson, C.A. & Christie, J.M. 1978. Papoose Flat pluton: a granitic blister in the Inyo Mountains, California. Geol. Soc. Amer. Bull. **89**: 1205-1219.

Takada, A., 1990. Experimental study on propagation of liquid-filled crack in gelatin: Shape and velocity in hydrostatic stress condition. J. of Geophy. Res. **B95**: 8471-8481.

Taubeneck, W. H. 1964. Cornucopia Stock, Wallowa Mountains, Northeastern Oregon: field relationships. Bull. Geol. Soc. Am. **75**: 1093-1116.

Thompson, A.B. 1974. Calculation of muscovite-paragonite-alkali feldspar phase relations. Contr. Miner. Petrol. **44**: 173-194.

Thompson, J.B. 1957. The graphical analysis of mineral assemblages in pelitic schists. Am. Miner. **42**: 842 - 858.

Tsuchiyama, A. 1985. Plagioclase dissolution experiments. Contr. Miner. Petrol. **89**: 1-16.

Tulloch, A.J. 1981. Gahnite and columbite in an alkali-feldspar granite from New Zealand. Mineral. Mag. **44**: 275-278.

Tuttle, O.F. & Bowen, N.L. 1958. Origin of granite in the light of experimental studies in the system $NaAlSi_3O_8$ - $KAlSi_3O_8$ - H_2O. Geol. Soc. Am. Mem. **74**: 153.

Vejnar, Z. 1971. Trioctahedral micas of west Bohemian pluton & their petrogenetic significance. Krystalinikum **7**: 149-164.

Vernon, R.H. & Collins, W.J. 1988. Igneous microstructures in migmatites. Geology, **16**: 1126-1129.

Wagner, C. Velde, D., & Mokhtari, A. 1987. Sector-zoned phlogopites in igneous rocks. Contrib. Mineral. Petrol. **96**: 186-191.

Wang, S.C. and Ding, Y. 1990. The discovery of garnet from calc-alkaline volcanic rocks of western Qinling and its geological significance. Acta Petrologica et Mineralogica, **9**: 13-20.

Wass, S.Y. 1973. The origin and petrogenetic significance of hour-glass zoning in titaniferous clinopyroxenes. Mineral. Mag. **39**: 133-137.

Wedemeyer, R.C. & Spruill, R.K. 1980. Geochemistry and geochronology of Sims granite, eastern Carolina State Belt, North Carolina. Geol. Soc. Amer. Abstr. Programs. **12**: 211.

Weertman, J., 1971. Theory of water filled crevasses in glaciers applied to vertical magma transport beneath ocean ridges. J. of Geophy. Res. **B76**: 1171-1183.

Weertman, J., 1980. The stopping of a rising, liquid-filled crack in the earth's crust by a freely slipping horizontal joint. J. of Geophy. Res. **B85**: 967-976.

Wegner, M.W. & Christie, J.M. 1973. Preferential chemical etching of terrestrial and lunar olivines. Contr. Miner. Petr. **43**: 195-212.

White, A.J.R. & Chappell, B.W. 1977. Ultrametamorphism and granitoid genesis. Tectonophys. **43**: 7-22.

White, A.J.R., Clemens, J.D., Holloway, J.R., Silver, L.T., & Chappell, B.W., 1986. S-type granites and their probable absence in southwestern North America. Geology, **14**: 115-118.

Whitney, J.A., Jones, L.M. & Walker, R.L. 1976. Age and origin of the Stone Mountain granite, Lithonia district, Georgia. Geo. Soc. Amer. Bull. **87**: 1067-1077.

Winter, J.K. and Ghose, S.,1979. Thermal expansion and high-temperature crystal chemistry of the Al_2SiO_5 polymorphs. Amer. Min., **64**: 573-586.

Wones, D.R., Burns, R.G., & Carroll, B.M. 1971. Stability & properties of synthetic annite. Ame. Geophy. Union Trans. **52**: 369-370.

Wood, B.J. 1973. Fe^{2+} - Mg^{2+} partition between coexisting cordierite and garnet: a discussion of the experimental data. Contr. Mineral. Petrol. **40**: 253-258.

Wyllie, P.J. 1977. Crustal anatexis: an experimental review. Tectonophysics, **43**: 41-71.

Yardley, B.W.D. 1977. An empirical study of diffusion in garnets. Am. Miner. **62**: 793-800.

Yoder, H.S. & Eugster, H.P. 1954. Phlogopite synthesis & stability range. Geochim. Cosmo. Acta **6**: 157-185.

Yoder, H.S. Jr. & Tilley, C.E. 1962. Origin of basalt magmas: an experimental study of natural & synthetic rock systems. J. Petrol. **3**: 342-532. **16**: 21-51.

Yokoi, K. 1983. Fe_2O_3 content of co-existing andalusite and sillimanite in the Ryoke metamorphic rocks occurring in the Hiraoka-Kadoya area, central Japan. J. Japanese Assoc. Mineral. Petrol. Econ. Geol. **78**: 246-254.

Zen, E-An. 1988. Phase relations of peraluminous granitic rocks and their petrogenetic implications. Ann. Rev. Earth Planet. Sci. **16**: 21-51.

Zen, E-An. 1989. Wet and dry AFM mineral assemblages of strongly peraluminous granites. EOS, Trans. Am. Geophys. Union. **70**: 109.